AICT 2011

The Seventh Advanced International Conference on Telecommunications

March 20-25, 2011

St. Maarten, The Netherlands Antilles

AICT 2011 Editors

Mariusz Glabowski, Poznan University of Technology, Poland

Djafar K. Mynbaev, New York City College of Technology - Brooklyn, USA

AICT 2011

Foreword

The Seventh Advanced International Conference on Telecommunications (AICT 2011) held on March 20-25, 2011 in St. Maarten, The Netherlands Antilles, covered a variety of challenging telecommunication topics ranging from background fields like signals, traffic, coding, communication basics up to large communication systems and networks, fixed, mobile and integrated, etc. Applications, services, system and network management issues also received significant attention.

We are witnessing many technological paradigm shifts imposed by the complexity induced by the notions of fully shared resources, cooperative work, and resource availability. P2P, GRID, Clusters, Web Services, Delay Tolerant Networks, Service/Resource identification and localization illustrate aspects where some components and/or services expose features that are neither stable nor fully guaranteed. Examples of technologies exposing similar behavior are WiFi, WiMax, WideBand, UWB, ZigBee, MBWA and others.

Management aspects related to autonomic and adaptive management includes the entire arsenal of self-ilities. Autonomic Computing, On-Demand Networks and Utility Computing together with Adaptive Management and Self-Management Applications collocating with classical networks management represent other categories of behavior dealing with the paradigm of partial and intermittent resources.

E-learning refers to on-line learning delivered over the World Wide Web via the public Internet or the private, corporate intranet. The conference considered how, when and where e-learning helps to solve the training needs, what the challenges of creating and managing vast amounts of e-learning are, how the upcoming IT technologies influence e-learning and how the Web based educational materials should be developed to meet the demands of the long-life, motivated and very often self-directed students.

The conference also addressed teletraffic modeling and management. It covered traffic theory, traffic control and QoS, performance evaluation methods, network design and optimization of wired and wireless networks, and simulation methodology for communication networks.

We take this opportunity to thank all the members of the AICT 2011 Technical Program Committee as well as the numerous reviewers. The creation of such a broad and high-quality conference program would not have been possible without their involvement. We also kindly thank all the authors who dedicated much of their time and efforts to contribute to the AICT 2011. We truly believe that, thanks to all these efforts, the final conference program consists of top quality contributions.

This event could also not have been a reality without the support of many individuals, organizations, and sponsors. We are grateful to the members of the AICT 2011 organizing committee for their help in handling the logistics and for their work to make this professional meeting a success.

We hope that AICT 2011 was a successful international forum for the exchange of ideas and results between academia and industry and for the promotion of progress in telecommunications.

We are convinced that the participants found the event useful and communications very open. The beautiful places of St. Maarten surely provided a pleasant environment during the conference and we hope you had a chance to visit the surroundings.

AICT 2011 Chairs

Tulin Atmaca, Telecom SudParis, France
Eugen Borcoci, University Politehncia Bucharest, Romania
Michael D. Logothetis, University of Patras, Greece
Paul J. Geraci, Technology Survey Group, USA
Herwig Mannaert, University of Antwerp, Belgium
Javier Del Ser Lorente, TECNALIA-Telecom - Bizkaia, Spain
Reijo Savola, VTT Technical Research Centre of Finland - Oulu, Finland
Michel Marot, Telecom SudParis, France
Michael Massoth, Hochschule Darmstadt, Germany
Mariusz Glabowski, Poznan University of Technology, Poland
Djafar K. Mynbaev, New York City College of Technology - Brooklyn, USA
Harald Øverby, Norwegian University of Science and Technology - Gløshaugen, Norway

AICT 2011

Committee

AICT Advisory Chairs

Tulin Atmaca, Telecom SudParis, France
Eugen Borcoci, University Politehncia Bucharest, Romania
Michael D. Logothetis, University of Patras, Greece
Paul J. Geraci, Technology Survey Group, USA
Herwig Mannaert, University of Antwerp, Belgium
Javier Del Ser Lorente, TECNALIA-Telecom - Bizkaia, Spain
Reijo Savola, VTT Technical Research Centre of Finland - Oulu, Finland

Special Area Chairs

TELET
Mariusz Glabowski, Poznan University of Technology, Poland

Ad hoc, autonomic and sensor networks
Michel Marot, Telecom SudParis, France
Michael Massoth, Hochschule Darmstadt, Germany

Optical
Djafar K. Mynbaev, New York City College of Technology - Brooklyn, USA
Harald Øverby, Norwegian University of Science and Technology - Gløshaugen, Norway

AICT 2011 Technical Program Committee

Fatma Abdelkefi, High School of Communications of Tunis - SUPCOM, Tunisia
Atiq Ahmed, Troyes University of Technology, France
Muayad Al-Janabi, Newcastle University - Newcastle upon Tyne, UK
Sabapathy Ananthi, University of Madras - Chennai, India
Pedro A. Aranda Gutiérrez, University of Paderborn, Germany
Loredana Arienzo, Joint Research Centre - European Commission - Ispra, Italy
Andres Arjona, Nokia Siemens Networks, Japan
Miguel Arjona Ramirez, São Paulo University, Brasil
Nils Aschenbruck, University of Bonn, Germany
Marco Aurélio Spohn, Federal University of Campina Grande, Brazil
Ilija Basicevic, University of Novi Sad, Serbia
Carlos Becker Westphall, Federal University of Santa Catarina, Brazil
Ilham Benyahia, Université du Québec en Outaouais, Canada
Francisco Bernardo, Universitat Politécnica de Catalunya, Spain
Indayara Bertoldi Martins, UNICAMP, Brazil
Eugen Borcoci, University "Politehnica" of Bucharest (UPB), Romania
Sylvia Borissova Encheva, Stord/Haugesund University College - Haugesund, Norway
Christos Bouras, University of Patras, Greece

Julien Broisin, Université Paul Sabatier, Toulouse III, France
Tijani Chahed, Telecom SudParis, France
Hakima Chaouchi, Telecom SudParis, France
Sungsoo Choi, Korea Electrotechnology Research Institute (KERI), Korea
Carlos Colman Meixner, National University of Asuncion, Paraguay
Todor Cooklev, Indiana-Purdue University - Fort Wayne, USA
Valentin Cristea, University Politehnica of Bucharest, Romania
Carlton Davis, École Polytechnique de Montréal, Canada
Peter Deussen, Fraunhofer Research Institute for Open Communication Systems - Berlin, Germany
Serge Fdida, University Pierre and Marie Curie / CNRS - Paris, France
Mário F. S. Ferreira, University of Aveiro, Portugal
Pedro Fortuna, University of Porto, Porutgal
Lídia Galdino, Universidade Estadual de Campinas, Brazil
Alex Galis, University College London, UK
Wolfgang Gentzsch, DEISA & OGF, Germany
Christos K. Georgiadis, University of Macedonia - Thessaloniki, Greece
Paul J. Geraci, Technology Survey Group, USA
Lei Guo, Northeastern University, China
Mannaert Herwig, University of Antwerp, Belgium
Muhammad Ali Imran, University of Surrey - Guildford, UK
Sripimanwat Keattisak, National Science and Technology Development Agency (NSTDA), Thailand
Santhi Kumaran, Kigali Institute of Science and Technology (KIST), Rwanda
Frank Li, University of Agder, Norway
Jia-Chin Lin, National Central University, Taiwan, ROC
Diogo Lobata Acatauassú Nunes, Federal University of Pará - Belém, Brazil
Renata Lopes Rosa, University of São Paulo (USP), Brazil
Zoubir Mammeri, IRIT - Toulouse, France
Mário Marques Freire, University of Beira Interior, Portugal
Michael Massoth, Hochschule Darmstadt, Germany
Bertrand Mathieu, Orange Labs - Lannion, France
Carmo Medeiros, University of Algarve, Portugal
Natarajan Meghanathan, Jackson State University, USA
Ioannis Moscholios, University of Peloponnese - Tripolis Greece
Masayuki Murata, Osaka University, Japan
Djafar K. Mynbaev, New York City College of Technology - Brooklyn, USA
Nokolai Nefedov, Nokia Research Center, Switzerland
Bernhard Neumair, Karlsruhe Institute of Technology (KIT), Germany
Petros Nicopolitidis, Aristotle University of Thessaloniki, Greece
Serban Obreja, University “Politehnica” Bucharest, Romania
Niyazi Odabasioglu, Istanbul University, Turkey
George Oikonomou, Loughborough University, UK
Masaya Okada, Shizuoka University, Japan
Sema Oktug, Istanbul Technical University, Turkey
Cristina Oprea, Politehnica University of Bucharest, Romania
Harald Øverby, Norwegian University of Science and Technology - Gløshaugen, Norway
Constantin Paleologu, University Politehnica of Bucharest, Romania
Andreas Papazois, Research Academic Computer Technology Institute, Greece
Claunir Pavan, Institute of Telecommunications / University of Aveiro, Portugal

Maciej Piechowiak, Kazimierz Wielki University - Bydgoszcz, Poland
Adrian Popescu, Blekinge Institute of Technology - Karlskrona, Sweden
Tarek Saadawi, City University of New York, USA
Reijo Savola, VTT Technical Research Centre of Finland - Oulu, Finland
Thomas Schmidt, FHTW - Berlin, Germany
Sergei Semenov, Nokia Corporation, Finland
Sandra Sendra Compte, University Polytechnic of Valencia, Spain
Shinji Shimojo, NICT, Japan
Shabnam Sodagari, The Pennsylvania State University - University Park, USA
Tomohiko Taniguchi, Fujitsu Laboratories Limited, Japan
Richard Trefler, University of Waterloo, Canada
Theo Tryfonas, University of Bristol, UK
Charalampos Tsimenidis, University of Newcastle Upon Tyne, UK
Kenneth Turner, The University of Stirling, Scotland
Kazuya Tsukamoto, Kyushu Institute of Technology, Japan
Doru Ursutiu, University "Transilvania" of Brasov, Romania
Guillaume Valadon, French Network and Information and Security Agency, France
John Vardakas, University of Patras, Greece
Dimitris Vasiliadis, University of Peloponnese Greece
Calin Vladeanu, University Politehnica of Bucharest, Romania
Lusheng Wang, INSA-Lyon, France
Bernd E. Wolfinger, University of Hamburg, Germany
Qin Xin, Simula Research Laboratory, Norway
Vladimir S. Zaborovsky, Technical University - Saint-Petersburg, Russia
Halim Zaim, Istanbul University, Turkey
Bruno B. Zarpelão, UNICAMP, Brazil
Giannis Zaoudis, CTI, Greece
Demóstenes Zegarra Rodríguez, Nokia Technology Institute, Brazil
Rong Zhao, Detecon International GmbH - Bonn, Germany
Martin Zimmermann, Hochschule Offenburg - Gengenbach, Germany
Piotr Zwierzykowski, Poznan University of Technology, Poland

TELET Track

Tulin Atmaca, TELECOM SudParis, France
Denis Collange, Orange Labs - Sophia Antipolis, France
Sebastià Galmés, Universitat de les Illes Balears (UIB), Spain
Marc Gilg, University of Haute Alsace, France
Mariusz Glabowski , Poznan University of Technology, Poland
Vic Grout, Glyndŵr University - Wrexham, UK
Ilias Iliadis, IBM Zurich Research Laboratory, Switzerland
Lucian Ioan, University: "Politehnica" of Bucharest (UPB), Romania
Michael D. Logothetis, University of Patras, Greece
Bernhard Neumair, Karlsruhe Institute of Technology (KIT), Germany
Grazziela Niculescu, ”Politehnica” University of Bucharest, Romania
John Vardakas, University of Patras, Greece

Cognitive Radio Track

Anwer Al-Dulaimi, Brunel University, UK
Carlos Becker Westphall, Federal University of Santa Catarina, Brazil
Derya Cavdar, Bogazici University - Istanbul, Turkey
Ziad Khalaf, SUPELEC/SCEE, France
Insoo Koo, University of Ulsan, Korea
Thomas D. Lagkas, University of Western Macedonia - Thessaloniki, Greece
Jia-Chin Lin, National Central University, Taiwan, R.O.C.
Markus Mueck, Infineon Technologies AG, Germany
Amor Nafkha, SUPELEC, France
Homayoun Nikookar, Delft University of Technology, The Netherlands
Dominique Noguet, CEA-LETI/MINATEC - Grenoble, France
Sema Oktug, Istanbul Technical University, Turkey
Jordi Pérez Romero, Universitat Politecnica de Catalunya (UPC) - Barcelona, Spain
Neeli R. Prasad, Aalborg University, Denmark
Tobias Renk, Universitaet Karlsruhe-Institut fuer Nachrichtentechnik, Germany
Masahiro Umehira, Ibaraki University, Japan
Liaoyuan Zeng, University of Limerick, Republic of Ireland

ELETE Track

Philip L. Balcaen, University of British Columbia Okanagan - Kelowna, Canada
Joan Ballantine, University of Ulster - Newtownabbey, UK
Katie Goeman, Hogeschool-Universiteit Brussel, Belgium
Michail Kalogiannakis, University Paris 5 - Rene Descartes, France
Charalampos Karagiannidis, University of Thessaly - Volos, Greece
Cerstin Mahlow, University of Applied Sciences Northwestern Switzerland, Switzerland
Amjad Mahmood, University of Bahrain, Kingdom of Bahrain
Antonio Navarro Martín, Universidad Complutense de Madrid, Spain
Jari Palomäki, Tampere University of Technology - Pori, Finland
Andreas Papasalouros, University of the Aegean - Samos, Greece
David Pheanis, Arizona State University, USA
Michael Piotrowski, University of Zurich, Switzerland
Danguole Rutkauskiene, Kaunas University of Technology, Lithuania
Tomas Sabaliauskas, Vytautas Magnus University - Kaunas, Lithuania
Demetrios G Sampson, University of Piraeus / CERTH, Greece
Jeanne Schreurs, Universiteit Hasselt, Belgium
Thrasyvoulos Tsiatsos, Aristotle University of Thessaloniki, Greece
Benno Volk, E-Learning Center (ELC) / University of Zurich, Switzerland
Amali Weerasinghe, University of Canterbury, New Zealand
Steve Wheeler, University of Plymouth, UK
Mudasser F. Wyne, National University - San Diego, USA

Ad Hoc, autonomic and sensor networks Track

Mahdi Aiash, Middlesex University - London, UK
Eugen Borcoci, University "Politehnica" of Bucharest (UPB), Romania
Chérif Diallo, Telecom SudParis, France

Anna Förster, Università della Svizzera Italiana - Lugano, Switzerland
Ashish Gupta, Telecom SudParis-Evry, France
Feng Cheng Lee, Nanyang Technological University, Singapore
Michel Marot, Telecom SudParis, France
Bruno Filipe Marques, Polytechnic Institute of Viseu, Portugal
Eric Renault, Telecom SudParis, France

OPTICAL Track

Muayad Al-Janabi, Newcastle University - Newcastle upon Tyne, UK
Djafar K. Mynbaev, New York City College of Technology - Brooklyn, USA
Harald Øverby Norwegian University of Science and Technology - Gløshaugen, Norway
John Vardakas University of Patras, Greece

Copyright Information

For your reference, this is the text governing the copyright release for material published by IARIA.

The copyright release is a transfer of publication rights, which allows IARIA and its partners to drive the dissemination of the published material. This allows IARIA to give articles increased visibility via distribution, inclusion in libraries, and arrangements for submission to indexes.

I, the undersigned, declare that the article is original, and that I represent the authors of this article in the copyright release matters. If this work has been done as work-for-hire, I have obtained all necessary clearances to execute a copyright release. I hereby irrevocably transfer exclusive copyright for this material to IARIA. I give IARIA permission or reproduce the work in any media format such as, but not limited to, print, digital, or electronic. I give IARIA permission to distribute the materials without restriction to any institutions or individuals. I give IARIA permission to submit the work for inclusion in article repositories as IARIA sees fit.

I, the undersigned, declare that to the best of my knowledge, the article is does not contain libelous or otherwise unlawful contents or invading the right of privacy or infringing on a proprietary right.

Following the copyright release, any circulated version of the article must bear the copyright notice and any header and footer information that IARIA applies to the published article.

IARIA grants royalty-free permission to the authors to disseminate the work, under the above provisions, for any academic, commercial, or industrial use. IARIA grants royalty-free permission to any individuals or institutions to make the article available electronically, online, or in print.

IARIA acknowledges that rights to any algorithm, process, procedure, apparatus, or articles of manufacture remain with the authors and their employers.

I, the undersigned, understand that IARIA will not be liable, in contract, tort (including, without limitation, negligence), pre-contract or other representations (other than fraudulent misrepresentations) or otherwise in connection with the publication of my work.

Exception to the above is made for work-for-hire performed while employed by the government. In that case, copyright to the material remains with the said government. The rightful owners (authors and government entity) grant unlimited and unrestricted permission to IARIA, IARIA's contractors, and IARIA's partners to further distribute the work.

Table of Contents

Time Domain Analysis of Propagation Channels in Tunnels

Concepcion Garcia-Pardo, J. Molina-Garcia-Pardo
Information Technologies and Commun. Dept.
Technical Univ. of Cartagena
Cartagena, Spain
[conchi.gpardo; josemaria.molina]@upct.es

Martine Lienard, Pierre Degauque
IEMN/TELICE
University of Lille
Villeneuve d Ascq, France
[martine.lienard; pierre.degauque]@univ-lille1.fr

***Abstract*—Extensive measurement campaigns have been carried out in a road tunnel in a frequency band extending from 2.8 to 5 GHz. From the experimental results, a time domain analysis is performed to study small scale fading, time dispersion of the ultra wide band pulse and correlation between signals received at different locations.**

Keywords- tunnel; impulse response; UWB; delay spread; direction of arrival; correlation.

I. INTRODUCTION

There is now an increased interest for ensuring high bit rate communication and localization in tunnels. As an example, for automatic underground subways, a train to track link allows increasing the performances of maintenance and control-command techniques. Similarly, video surveillance, voice communication and wireless sensor monitoring are of great importance in underground mines. A large number of papers have thus already been published in the literature for studying the narrow band and wide band channel characteristics.

For mine tunnels, the variation of path loss as a function of frequency from 2 GHz to 5 GHz was studied in [1] and a frequency-domain autoregressive model was developed. Various communication links were also considered including both Line-of-Sight (LOS) and non-LOS scenarios [2].

In case of road or railway tunnels, path loss and probability distribution with respect to fading widths deduced from measurements at 2 GHz were detailed in [3], while the effects of pedestrians and vehicles in different road tunnels are studied in [4]. A wideband directional measurement campaign conducted inside an arched highway tunnel is described in [5]. Using a channel sounder centered at 5.2 GHz with a bandwidth of 100 MHz, the spatio-temporal characteristics of the received propagation paths are estimated by means of a super-resolution estimation algorithm. Lastly, for a road tunnel, many papers deal with channel characterization for predicting the performance of a Multiple-Input Multiple-Output (MIMO) link, without or with polarization diversity [6].

The objective of this contribution is to extend these previous experimental works for studying the time domain channel response for ultra wide band (UWB) applications. Frequency domain measurements have thus been carried out in a straight road tunnel, and in a band extending from 2.8 GHz to 5 GHz. Time domain analysis was then performed through Fourier Transform.

This paper is organized as follows: Section II briefly recalls the methodology of the measurement campaigns while Section III presents results on the mean path loss, small scale fading and delay spread. An analysis of the waveform of the received signal as a function of the distance between the transmitter and the receiver is detailed in Section IV and the correlation between signals received at different positions is also studied.

II. DESCRIPTION OF THE MEASUREMENT CAMPAIGN

Measurements took place in a straight arched tunnel, 3 km long. Its transverse section was semicircular and the diameter of the cylindrical part was 8.6 m. The maximum height was 6.1 m at the center of the tunnel. The tunnel was nearly free of obstacles like road signs, lamps, cables, etc. Furthermore the roughness of the walls was rather small, on the order of few cm. The tunnel was closed to traffic and consequently, the channel can be considered as stationary during the experiments. The transmitting (Tx) and receiving (Rx) antennas were wideband conical antennas, their gain being nearly flat in the bandwidth of interest.

Both Tx and Rx antennas were mounted on a rail, put at 1 m above ground and allowing their displacement, controlled by a step by step motor, on a maximum distance of 33 cm. During this measurement campaign, these rails were put perpendicular to the tunnel axis. The spatial step in this transverse plane was 3 cm, corresponding to half a wavelength at 5 GHz. This leads, for each axial distance D between Tx and Rx and for each frequency, to a set of 144 values of the channel transfer function H. The axial step was chosen to be equal to 4 m when 50 m < D < 202 m and to 6 m when 202 m < D < 500 m. Tx and Rx were not moving during measurements and thus the Doppler effect was avoided.

The channel sounder was based on a vector network analyzer (VNA). The Rx antenna was directly connected to one port of the VNA using a low attenuation coaxial cable and a 30 dB low-noise amplifier. To be able to make measurements up to 500 m, the signal of the Tx port of the VNA was converted into an optical signal, which was sent through fibre optics. The frequency step is 1.37 MHz from 2.8 to 5 GHz, leading to 1601 frequency points.

More details concerning the utilized system and experimental aspects of this study can be found in [7]. One can also mention that for this type of channel, the main contribution at large distance comes from multiple reflections of rays impinging the tunnel walls under a

 ISBN: 978-1-61208-123-6

grazing angle of incidence. Furthermore path loss strongly decreases for frequencies such that the transverse dimensions of the tunnel are much larger than the wavelength λ. However, when the roughness of the walls becomes on the order of λ, diffusion effect may counterbalance this decrease of path loss.

III. MEAN PATH LOSS, SMALL SCALE FADING AND DELAY SPREAD

In narrow band communication systems, path loss is frequency and distance dependent, while small scale fading is due to constructive and destructive interference of all possible paths between Tx and Rx. For UWB signals the most important characteristics are related to the variation of the energy of the pulse and not of its individual spectral components. Table 1 gives the value of the path loss defined as the value of the received power averaged over the whole frequency band, and normalized to the transmitted power.

TABLE I. MEAN PATH LOSS

Distance (m)	100	200	300	400	500
Path loss (dB)	82	83.1	84.2	85.5	86

We clearly see the guiding effect of the tunnel, the additional attenuation between 100 m and 500 m being only 4 dB.

To determine the characteristics of the small-scale fading, we consider a rectangular grid containing successive Rx positions. The width of the grid, i.e., its dimension along the transverse axis is equal to 33 cm and corresponds to the maximum displacement of the antenna in the transverse plane. Along the tunnel axis, we consider 3 successive distances as shown in Figure 1. Thus the length of the grid is either 8 m or 12 m depending if the distance *D* between Tx and Rx is smaller or larger than 200 m, as explained in Section I.

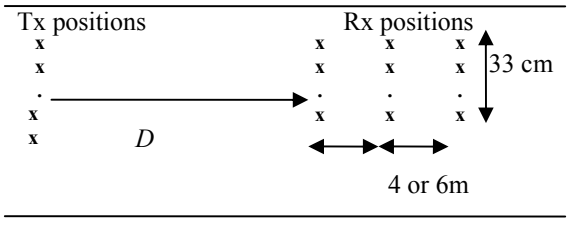

Figure 1. Successive positions of the Tx and Rx antennas. The transverse dimension of the tunnel is 8.6 m. The antennas are situated in the middle of one lane of this 2-lane tunnel.

The standard deviation ("*std*") of the path loss in the rectangular grid, normalized to its average value in this grid, was calculated for successive values of *D* varying between 50 m and 480 m and by also considering the 12 possible positions of the Tx antenna in the transverse plane of the tunnel. Curve in Figure 2 shows that *std* does not vary appreciably with the distance and remains on the order of 15%. This means that there is almost no fading as a result of interference and this is the same conclusion as in the case of propagation in typical in-building environment [8], [9], [10].

The time domain analysis of the propagation channel is based on measurement results in the frequency domain by applying a Fourier transform. For each axial distance *D*, the average delay spread is deduced from the channel impulse response (CIR) calculated for each of the 12x12, i.e., 144 channels associated to the possible positions of the antennas in the transverse plane. As shown in Table II, the delay spread remains nearly constant, whatever the distance.

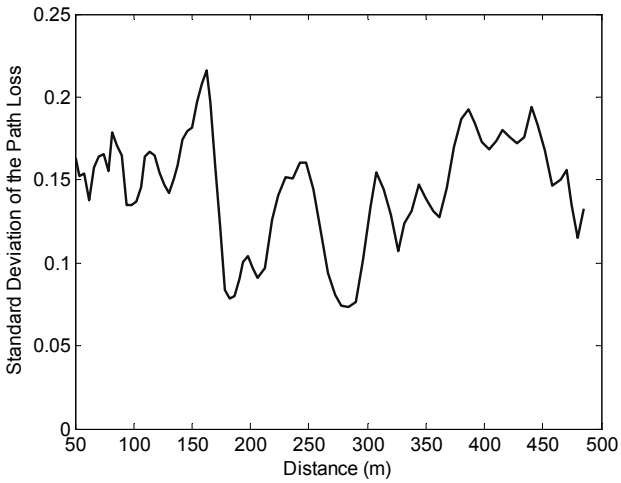

Figure 2. Standard deviation of the normalized path loss.

TABLE II. MEAN DELAY SPREAD

Distance (m)	100	200	300	400	500
Mean delay spread (ns)	2.5	1.7	2	1.8	2

This result is strongly related with the direction of the rays joining the transmitter and the receiver. In the horizontal plane, and for each value of *D*, the Angle of Arrival (AoA) and the angle of Departure (AoD) of the various rays can be deduced from measurements of the channel transfer function at various points in the transverse plane, by using high resolution estimation techniques, as the Space-alternating Generalized Expectation-maximization (SAGE) algorithm [11].

The variation of the angular spread A_s of the AoA and AoD is plotted in Figure 3. At 50 m from Tx, the angular spread is equal to about 12° and then continuously decreases with distance. The fact that the delay spread remains constant can thus be explained by this decrease of A_s with distance, which leads to rather constant time intervals between the successive rays. Consequently, the slope of the power delay profile becomes independent on the distance. It must be emphasized that measurements were done in static conditions and in an empty tunnel. In more realistic

 ISBN: 978-1-61208-123-6

situations, i.e., in presence of vehicles or obstacles, one can expect to get additional reflected signals but mainly if these obstacles are situated in the vicinity of the Rx antenna. This will lead to a slight increase of the delay spread but the previous conclusions may remain valid. One can mention that the results of narrowband and wideband propagation measurements conducted at 900 and 1800 MHz in five tunnels and described in [4] include the effects of pedestrians, vehicles, and curvature on propagation. A narrowband analysis showing the effects of vehicles is also presented in [12].

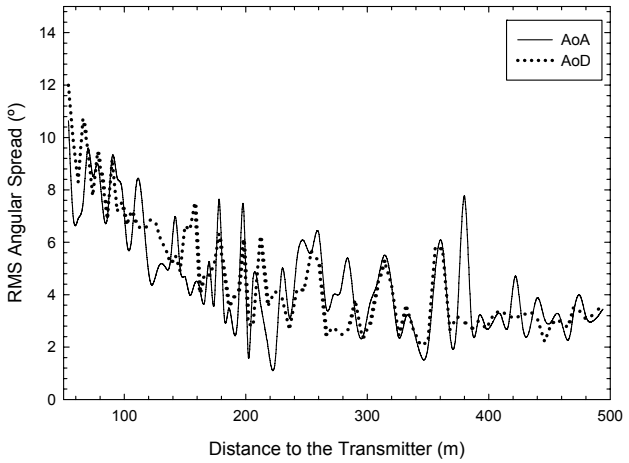

Figure 3. Angular spread of the direction of arrival and direction of departure of the rays.

IV. TIME DISPERSION AND CORRELATION

In this section, the change of the waveform of the pulse propagating in the tunnel is studied. Furthermore, the correlations between the transmitted pulse and the received pulse, on one hand, and between pulses received at different distances on the other hand, are emphasized.

A. Time dispersion

As previously outlined in Section II, the complex channel transfer function is measured in the frequency domain between 2.8 and 5 GHz. To get a real-value transmitted pulse, this transfer function is combined with its complex conjugate in the negative frequency domain before applying a Fourier transform. To avoid numerous oscillations, a Hamming window is used and the equivalent transmitted pulse is thus represented in Figure 4. Its peak amplitude is normalized to unity. The pseudo frequency corresponds to the center of the frequency band under analysis (3.9 GHz).

The pulses, which would be received at a distance of 50 m and 54 m start at 165 ns and 180 ns, respectively. However, to make an easiest comparison between these two pulses, they have been shifted in the time domain as in Figure 5 (a) and (b) to start at the same time. The origin of the time axis is quite arbitrary.

We observe a first cluster, which includes the direct path and a succession of other clusters corresponding to multipath propagation. Within this kind of clusters, the waveform may strongly vary with distance.

This means that at a distance D_1, the signal may be positive at a given time but may become negative at the same time at another distance D_2. By adding the signals measured at successive distances but shifted to start at the same time, one can thus expect to visualize the coherence between the signals received along the tunnel axis. This qualitative approach leads to curve (c) in Figure 5, this signal being obtained by averaging the waveforms at 50, 54 and 58 m. We observe, as expected, a decrease in amplitude of clusters associated with multipath propagation.

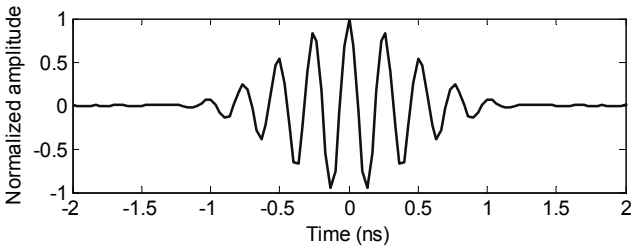

Figure 4. Equivalent transmitted pulse

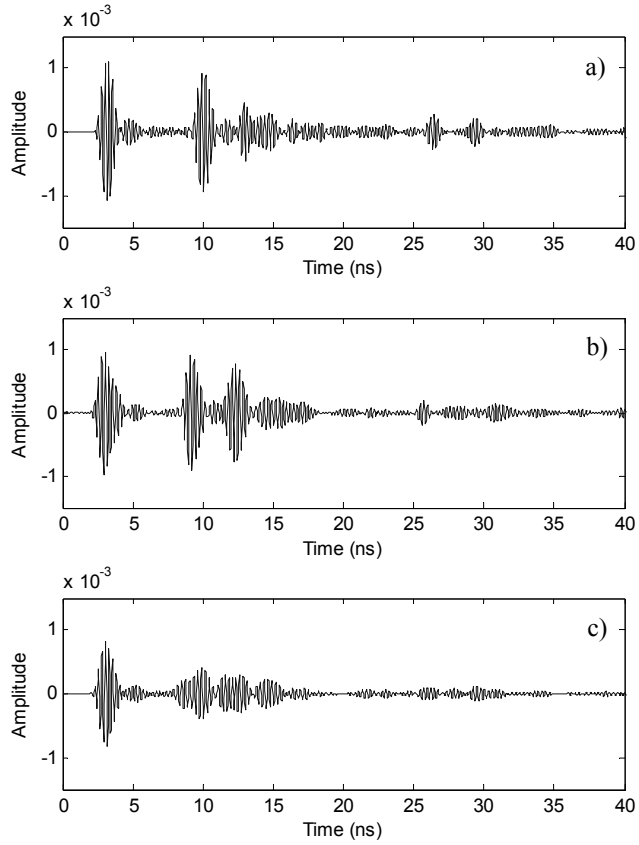

Figure 5. Waveforms of the pulse received at a distance of 50 m (curve (a), and at 54 m (curve (b). Curve (c) is the sum of the waveforms received at 50, 54 and 58 m and aligned in time domain. The origin of the time axis is thus quite arbitrary.

One can do the same approach to visualize the coherence in the transverse plane. Let us consider, for example, a distance of 50 m between Tx and Rx.

To plot the curve in Figure 6, the 144 signals obtained by combining the 12 possible positions of both Rx and Tx in the transverse plane, have been summed. We see that all clusters, except the one, which includes the direct path, have negligible amplitude.

The received power and the channel impulse response can be easily deduced from the amplitude of the received signal and from the correlation between the transmitted signal and the received signal.

A quantitative approach of the correlation is presented in the next paragraphs.

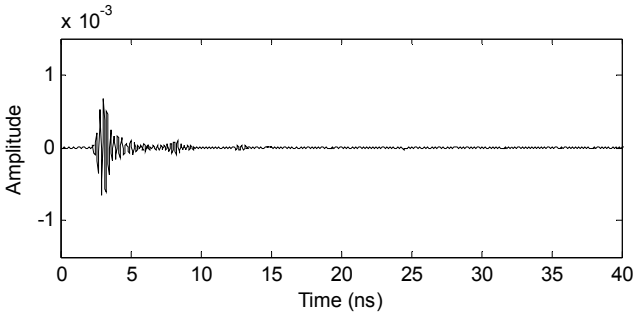

Figure 6. Average waveform by summing signals received in the transverse plane.

B. Transverse correlation

For a given axial distance D, one can compute the correlation, in the transverse plane, between the signal received by one Rx antenna and the signal received by the 11 others, the spatial step being 3 cm. This correlation is calculated for each of the 12 positions of the transmitter. This allows getting the average value of the correlation between the received signals in the transverse plane; the maximum distance between the receiving points being 33 cm. Results are presented in Figure 7 for three values of the axial distance D.

If we first consider a distance of 102 m, we see that the correlation coefficient rapidly decreases and reaches 0.5 for a distance between receiving points of 9 cm. For larger axial distance D, 314 and 498 m in this example, the slope of the decrease is less important.

This result can be explained in frequency domain by the modal approach of the propagation of electromagnetic waves in the tunnel, which acts as an oversize waveguide. At large distances, the number of modes significantly contributing to the received power decreases. This gives rise to a more coherent transverse field [7].

C. Axial correlation

Due to experimental constraints, the successive points of measurements along the tunnel axis were 4 m or 6 m apart, depending on the distance D. This distance is not small enough to clearly point out the decrease of the correlation ρ_{ax} between signals. Indeed, for the first step, i.e., at 4 m, the correlation coefficient between Rx points situated at $D = 50$ m and at $D = 54$ m is already equal to 0.4.

The only point, which could be studied is the variation of ρ_{ax} between points situated at $D = z$ and at $D = z + 4$ or at $D = z + 6$, when z varies from 50 m up to 500 m.

The calculation shows that ρ_{ax} increases from 0.4 for $z = 50$ m to 0.7 for $z = 500$ m. This can be explained, as in the case of the correlation in the transverse plane, by the decrease of the number of propagating modes at large distance from the transmitter.

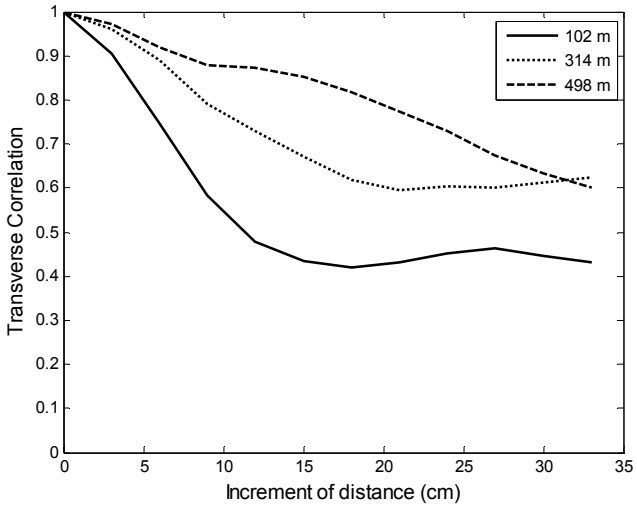

Figure 7. Correlation in the transverse plane

V. CONCLUSION

In this contribution, the time domain channel characteristics for a tunnel environment have been studied. The guiding effect of the tunnel clearly appears on the mean path loss, the small scale fading related to the energy of the UWB pulse being very small as it is the case for in-building environment.

The signals received at different locations in the transverse plane of the tunnel are rapidly uncorrelated, the correlation coefficient being equal to 0.5 if the receiving points are 9 cm apart.

However the correlation increases at large distance of the transmitter due to the attenuation of high order propagating modes, which leads to a decrease of the number of modes playing a non negligible role in the received signal.

Further work will be to develop a time domain statistical model, based on measurement results. This model will then be used to extend the physical layer approach described in this paper to simulate a communication link, taking the modulation scheme into account, in order to predict flow throughput and bit error rate.

ACKNOWLEDGMENT

This work has been supported by the Fundación Séneca de la Región de Murcia (14809/EFPI/10 and 06640/FPI/07) in the frame of PCTRM 2007-2010 with foundation of INFO

 ISBN: 978-1-61208-123-6

and FEDER funds of up to 80%; Ministerio de Industria, Turismo y Comercio (Spain), under the project CORAGE (TSI-0201100-2009-653); and by the European FEDER funds, the Region Nord Pas de Calais and the French Ministry of Research, as part of the CISIT project (France).

REFERENCES

[1] A. Chehri and P. Fortier, "Frequency Domain Analysis of UWB Channel Propagation in Underground Mines", Proc. IEEE Conf. on Vehicular Techno., 25-28 Sept. 2006, 5p.,

[2] A. Chehri, P. Fortier, and P. M. Tardif, "Characterization of the Ultra-Wideband Channel in Confined Environments with Diffracting Rough Surfaces', Wireless Personal Communications, Aug. 2010, pp. 1-19, DOI: 10.1007/s11277-010-0097-2,

[3] M. Lienard and P. Degauque, "Propagation in Wide Tunnels at 2 GHz: A Statistical Analysis", IEEE Trans. on Vehicular Techno., vol. 47, no. 4, Nov. 1998, pp. 1322 – 1328,.

[4] Y. P. Zhang and Y. Hwang, "Characterization of UHF Radio Propagation Channels in Tunnel Environments for Microcellular and Personal Communications", IEEE Trans on Vehicul. Techno., vol. 47, no. 1, Feb. 1998, pp. 283 – 296.

[5] G. S. Ching, G.S., M. Ghoraishi, M .Landmann, M., N. Lertsirisopon, J. Takada, T. Imai, I. Sameda, and H. Sakamoto, " Wideband Polarimetric Directional Propagation Channel Analysis Inside an Arched Tunnel", IEEE Trans. on Antennas and Propag., vol. 57, March 2009, pp. 760-767.

[6] J.-M. Molina-Garcia-Pardo, M. Lienard, P. Degauque, C. García-Pardo, and L. Juan-Llacer, "MIMO channel capacity with polarization diversity in arched tunnels", IEEE Antennas and Wireless Propagation Letters, vol. 8, 2009, pp. 1186-1189.

[7] J.-M. Molina-Garcia-Pardo, M. Lienard, and P. Degauque, "Propagation in Tunnels: Experimental Investigations and Channel Modeling in a Wide Frequency Band for MIMO Applications" EURASIP J. on Wireless Com. and Networking,, 2009, Article ID 560571, 9 pages, doi:10.1155/2009/560571.

[8] A. Muqaibel, A. Safaai-Jazi, A. Attiya, B. Woerner, and S. Riad, "Path loss and time dispersion parameters for indoor UWB propagation", IEEE Trans. on Wireless Comm., vol. 5, March 2006, pp. 550-559.

[9] A. F. Molisch, "Ultra-wide band propagation channels", Proc. of the IEEE, vol. 97, Feb. 2009, pp. 353-371.

[10] M. Z. Win and R. A. Scholtz, "Characterization of ultra-wideband wireless indoor channels: a communication-theoric view", IEEE J. on Selected Areas in Com., vol. 20, Dec. 2002, pp. 1613-1627.

[11] J. A. Fessler and A. O. Hero, "Space-alternating generalized expectation-maximization algorithm," *IEEE Trans. on Signal Processing*, vol. 42, no.10, Oct. 1994, pp. 2664–2677, Oct 1994.

[12] M. Liénard, S. Bétrencourt, and P. Degauque, "Propagation in Road Tunnels: a Statistical Analysis of the Field Distribution and Impact of the Traffic", Annales des Télécom., vol 55, n° 11-12, Dec. 2000, pp. 623-631.

 ISBN: 978-1-61208-123-6

Time Slot Assignment Algorithms for Reducing Upstream Latency in IEEE 802.16j Networks

Shimpei Tanaka
Graduate School of Information Science and Technology
Osaka University, Japan
sinpei-t@ist.osaka-u.ac.jp

Go Hasegawa, Yoshiaki Taniguchi and Hirotaka Nakano
Cybermedia Center, Osaka University, Japan
{*hasegawa, y-tanigu, nakano*}*@cmc.osaka-u.ac.jp*

***Abstract*—In IEEE 802.16j wireless multihop networks, transmission latency from relay nodes to a gateway node is one of the important performance metrics. The transmission latency is mainly affected by a scheduling delay at every relay node, which is determined by algorithms for assigning time slots to wireless links between relay nodes. In this paper, we propose 2 kinds of time slot assignment algorithms for upstream wireless links in IEEE 802.16j multihop networks. One of the proposed algorithms assigns time slots considering the hop count from a gateway node, and the other takes the path from the relay node to the gateway node into account. We evaluated the performance of the proposed algorithms through simulation experiments and confirmed that our algorithms can decrease the upstream latency by up to 15% compared with the existing method, without increasing the average transmission latency of the entire network.**

Keywords-IEEE 802.16j, wireless multihop network, upstream, time slot, latency.

I. Introduction

IEEE 802.16j wireless multihop networks [1] have received a significant amount of attention as a network technology providing a wide-area broadband wireless access environment at low cost. As depicted in Figure 1, in an IEEE 802.16j network, each relay node connects to other nodes with wireless links so that the overall topology becomes a tree structure, unlike the star structure in typical IEEE 802.11-based networks. In general, IEEE 802.16j consists of three kinds of nodes: gateway nodes that have wired connections to external networks, relay nodes that are interconnected with other nodes by wireless links, and user nodes that are connected to the nearest relay node [2]. Generally, the wireless channel used for communication between relay nodes and user nodes is different from that used among the relay nodes and the gateway nodes, and the wireless channel used for upstream communication is different from that used for downstream communication [3]. In this research, we ignore user nodes and focus on the communication between relay nodes.

One problem in wireless networks in general is that 2 nodes that exist in transmission range of each other cannot communicate simultaneously due to radio interference [4]. To solve this problem, IEEE 802.16j uses a time-division scheduling mechanism based on Orthogonal Frequency Division Multiplexing Access (OFDMA) at the MAC layer

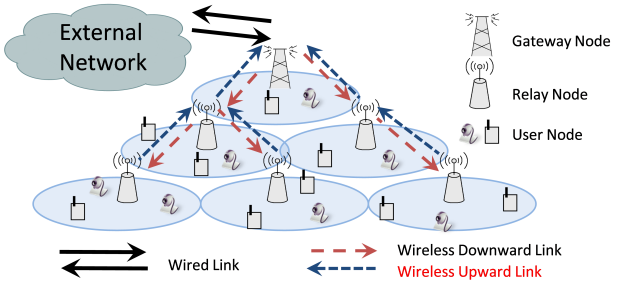

Figure 1. IEEE 802.16j wireless multihop network.

[5]. In the OFDMA-based mechanism, time is divided into constant intervals called *frame*s, each of which consists of multiple time slots of constant time duration. The time slots are assigned to links in the network as communication opportunities, and communication on the links can take place only at the assigned time slots [6]. The gateway node performs centralized control of the time slot assignment for the links, while considering interference relationships in order to avoid radio interference.

In such wireless multihop networks using the time-division scheduling mechanism, we cannot ignore a scheduling delay at each relay node during packet transmission between relay nodes. The scheduling delay is defined as the period of time between the arrival of a packet at a relay node and the departure of the packet at the assigned time slot for the relay node. The end-to-end transmission latency between a relay node and a gateway node increases due to accumulation of scheduling delays at each relay node on the path between the relay node and the gateway node. The degree of scheduling delay is mainly dependent on the time slot assignment to the wireless links in the network.

We have already proposed a time slot assignment algorithm for reducing scheduling delay and evaluated its performance in [7]. The proposed algorithm tends to assign time slots to links in order of the density of interference relationships. Therefore, the links with small hop count from the gateway node obtain earlier time slots, and the links with large hop count from the gateway node obtain later time slots, when traffic demand is concentrated at the gateway node. As a result, the method in [7] can

 ISBN: 978-1-61208-123-6

decrease the scheduling delay and the transmission latency for downstream transmissions from the gateway node to the relay nodes, compared with random method. On the other hand, it decreases a little in the scheduling delay at upstream transmissions from the relay nodes to the gateway node.

Therefore, in this paper, we focus on the upstream transmission in IEEE 802.16j wireless multihop networks and propose 2 kinds of time slot assignment algorithms to give small transmission latency from the relay nodes to the gateway node. Our proposed algorithms aim to decrease the scheduling delay at each relay node on the path between the starting relay node and the gateway node. One of the proposed algorithms assigns time slots by considering the hop count from the gateway node, and the other takes the path from the starting relay node to the gateway node into account. Performance evaluation of the proposed algorithms was conducted through packet-level simulation experiments. The evaluation results showed that the proposed algorithms can improve the average transmission latency as compared with an existing algorithm described in [7] without increasing the average transmission latency of the entire network. The rest of this paper is organized as follows. In Section II, we describe the model of IEEE 802.16j wireless multihop networks. In Section III, we propose 2 kinds of time slot assignment algorithms. In Section IV, we present simulation evaluation results. Finally, in Section V, we conclude this paper and describe future work.

II. IEEE 802.16j Wireless Multihop Network

IEEE 802.16j uses an OFDMA-based mechanism for avoiding radio interference. When assigning time slots to links between relay nodes, the connections and the interference relationships between relay nodes are very important. In this section, we describe the network model and notation of the IEEE 802.16 wireless multihop network. We also explain the radio interference model and time slot assignment mechanisms based on TDMA.

A. Network Model

Figure 2(a) depicts a *directed communication graph* $G_c = (V_c, E_c)$ that indicates the communication relationship between relay nodes and a gateway node. $V_c = \{v_0, v_1, v_2, \ldots, v_n\}$ is a set of relay/gateway nodes deployed in a plane, and v_0 is the gateway node. We assume that there is only one gateway node in the network. E_c is a set of the directed communication links $e_{i,j}$, which represents an edge directed from v_i and v_j when $\|v_i - v_j\| < t_i$. Here, t_i is the communication range of v_i, and $\|v_i - v_j\|$ is the distance between v_i and v_j. We define the hop count of a directed communication link $e_{i,j}$ as the larger hop count between 2 nodes v_i and v_j.

In this paper, we assume that the gateway node connects to an external network, and each relay node communicates with the gateway node via other relay node(s) on the path between the relay node and the gateway node. The path between the relay node and the gateway node is determined by a routing algorithm, and the *directed transmission graph* $G_t = (V_t, E_t)$ is constructed as a tree-like graph whose root is the gateway node v_0, as shown in Figure 2(b). Here, G_t is a subset of G_c, V_t is a set of nodes satisfying $V_t = V_c$, and E_t is a set of directed transmission links that is determined by the routing algorithm and satisfies $E_t \subseteq E_c$.

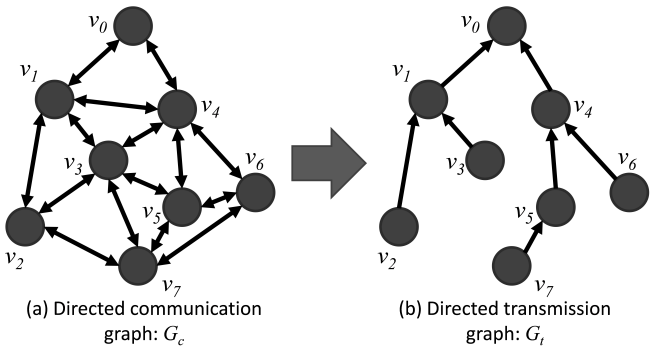

Figure 2. Directed communication graph G_c and directed transmission graph G_t.

In what follows, the directed transmission links $e_{i,j} (\in E_t)$ are called *links*, the links on the path from a relay node to the gateway node are called *upstream links*, and the links on the path from the gateway node to a relay node are called *downstream links*. We assume that G_t is given in advance by the routing algorithm, and each link $e_{i,j}$ has a link weight $w_{i,j}$ that represents the required time slots according to the traffic load. In this paper, we consider algorithms to assign time slots only to upstream links in the network.

B. Interference Model

In this paper, we use the radio interference model proposed in [8]. The model defines the interference relationship from $e_{i,j}$ to $e_{p,q}$ based on the distances among 4 vertices v_i, v_j, v_p and v_q. Each relay node v_i has the interference range r_i. The condition to determine the interference relationship is as follows: $e_{i,j}$ interferes with $e_{p,q}$ when and only when $\|v_i - v_q\| < r_i$. On the other hand, $e_{p,q}$ interferes with $e_{i,j}$ when and only when $\|v_p - v_j\| < r_p$. On the basis of these conditions, $e_{i,j}$ and $e_{p,q}$ are in the interference relationship; that is, they cannot communicate simultaneously when $\|v_i - v_q\| < r_i$ or $\|v_p - v_j\| < r_p$ is satisfied. Typically, $r_i > t_i$, and the ratio of interference range to communication range for node v_i, denoted as $\gamma_i = \frac{r_i}{t_i}$, is in the range of 2–4 in practice [8]. We define a function $I(e_{i,j}, e_{p,q})$ that indicates whether or not 2 links $e_{i,j}$ and $e_{p,q}$ are in the interference relationship. The function returns 1 if the 2 links are in the interference relationship, or returns 0 it the 2 links are not in the interference relationship.

We introduce the *conflict graph* $F_{G_t} = (F_{V_t}, F_{E_t})$ obtained by applying the interference model to a directed transmission graph G_t, as depicted in Figure 3. $F_{V_t} = \{f_{e_{i,j}} | e_{i,j} \in E_t\}$ is a set of nodes which are all elements of a link set E_t in G_t, and $F_{E_t} = \{l^{i,j}_{p,q} | f_{e_{i,j}}, f_{e_{p,q}} \in F_{V_t}\}$ is a set of links which exist when $I(e_{i,j}, e_{p,q}) = 1$, that is, F_{E_t} represents the interference relationship among links in G_t.

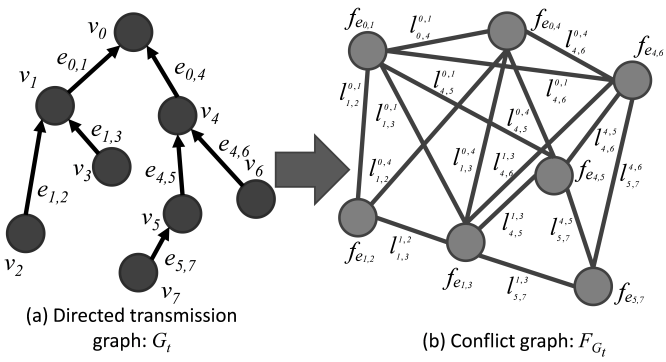

Figure 3. Directed transmission graph G_t and conflict graph F_{G_t}.

C. Time Slot Assignment based on TDMA

IEEE 802.16j controls transmission opportunities, called *time slots*, using the TDMA mechanism and assigns time slots to links in the network. Each link can communicate only in assigned time slots. IEEE 802.16j does not assign the same time slot to links that are in the interference relationship. Meanwhile, multiple links can communicate simultaneously in one time slot when the time slot is assigned to multiple links that are not in the interference relationship. This is called *spatial reuse*, which enhances the network throughput [9–13], and algorithms for assigning time slots are required to consider the interference relationship to increase the degree of spatial reuse. The algorithm in [7] increases the degree of spatial reuse; however, it is not applicable to upstream links in IEEE 802.16j because it would increase the upstream latency. Therefore, we propose algorithms in which priority is given to the time slot schedule over spatial reuse.

III. Proposed Time Slot Assignment Methods

On upstream transmissions in an IEEE 802.16j wireless multihop network, the time slot assignment to each link affects the scheduling delay and the end-to-end transmission latency. The transmission latency of the relay node that has large hop count from the gateway node is significantly affected by the time slot assignment.

In this section, we propose 2 kinds of methods for assigning time slots for reducing upstream transmission latency, based on the models described in Section II.

A. Hopcount-based Method

The hopcount-based method is based on the following idea. The order of the links for assigning time slots is determined based on the hop count of each link from the gateway node. The links with large hop count are assigned earlier time slots than those with small hop count. In detail, when a link $e_{i,j}$ is assigned a time slot(s), the hopcount-based method assigns $w_{i,j}$ time slot(s) that are not assigned to links in the interference relationship with $e_{i,j}$ and that are not assigned to links with larger hop count than $e_{i,j}$. Note that we utilize a greedy approach, meaning that we assign the earliest available time slots. Since the upstream transmissions in the network utilize the links on the path in the reverse order of hop count, we expect that the scheduling delay in upstream transmissions will be reduced by using this method.

algorithm 1 Hopcount-based algorithm

INPUT: $G_t = (V_t, E_t)$, $F_{G_t} = (F_{V_t}, F_{E_t})$, $w_{i,j}$ of $^{\forall}e_{i,j}$
OUTPUT: time slot assignment to $^{\forall}e_{i,j}$

```
for all e_{i,j} ∈ E_t do
    H_k ← {e_{i,j} | h_{i,j} = k} ∪ H_k
end for
h_max = (the largest hop count in E_t)
for H = H_{h_max}, H_{h_max−1}, ..., H_1 do
    y = z
    for all e_{i,j} ∈ H do
        for all e_{p,q} ∈ (E_t ∩ (I(e_{i,j}, e_{p,q}) = 1)) do
            X_{e_{i,j}} ← T_{e_{p,q}} ∪ X_{e_{i,j}}
        end for
        for a = 1 ~ w_{i,j} do
            m = (the earliest number of time slot satisfying
            ((m > z) ∩ (s_m ∉ X_{e_{i,j}})))
            T_{e_{i,j}} ← s_m ∪ T_{e_{i,j}}
            if y < m then
                y = m
            end if
        end for
    end for
    z = y
end for
```

Algorithm 1 represents the hopcount-based method in pseudo-code. $h_{i,j}$ is the hop count of $e_{i,j}$. H_k is a set of the links with k hop count from the gateway node, and $T_{e_{i,j}}$ is a set of the time slots assigned to $e_{i,j}$. $X_{e_{i,j}}$ is a set of the time slots assigned to the links in the interference relationship with $e_{i,j}$. s_m is the mth time slot.

B. Path-based Method

The path-based method assigns time slots to links along with the paths from relay nodes to the gateway node. For determining the order of assigning time slots to links, the method first determines the order of paths to which the time slots are assigned. In detail, it orders the relay nodes in the network by visiting them in the depth-first order. When the method assigns time slot(s) to links, it chooses a relay node from the reverse order in which it visited relay nodes and assigns *1* time slot to each link on the path from the chosen relay node to the gateway node in descending order of hop count. We use a greedy approach in which the interference relationship is considered, as in the hopcount-based method. The method is applicable when the traffic demand on a path is determined only by the sender relay node, regardless of the path's characteristics.

Algorithm 2 shows the pseudo-code of the path-based method. $T_{e_{i,j}}$ is a set of the time slots assigned to $e_{i,j}$. $X_{e_{i,j}}$ is a set of the time slots assigned to the links in the interference relationship with $e_{i,j}$. s_m is the mth time slot, and *seq* is an

algorithm 2 Path-based algorithm

INPUT: $G_t = (V_t, E_t)$, $F_{G_t} = (F_{V_t}, F_{E_t})$, $w_{i,j}$ of ${}^{\forall}e_{i,j}$
OUTPUT: time slot assignment to ${}^{\forall}e_{i,j}$

```
n = (the number of relay nodes), w = 0
while D_w ≠ φ do
    seq[n] = v_m(m|m ∈ D_w)
    n = n − 1
    D_w ← D_w \ {m}
    if D_m ≠ φ then
        w = m
    end if
    if (D_w = φ) ∩ (w ≠ 0) then
        w = u_w
    end if
end while
for a = 1 ∼ ((the number of relay nodes) do
    v_k = seq[a], l = w_{k,u_k}
    repeat
        for all e_{p,q} ∈ (E_t ∩ (I(e_{k,u_k}, e_{p,q}) = 1)) do
            X_{e_{k,u_k}} ← T_{e_{p,q}} ∪ X_{e_{k,u_k}}
        end for
        for b = 1 ∼ l do
            m = (the earliest time slot not in X_{e_{i,j}})
            T_{e_{i,j}} ← s_m ∪ T_{e_{i,j}}
        end for
        k = u_k
    until (v_k = v_0)
end for
```

array of the relay nodes in the reverse order in which the relay nodes were visited. D_i is a set of the node numbers of downstream nodes of v_i and u_i is the node number of the upstream node of v_i.

We can easily implement these 2 methods and their computing overheads are following: overhead of hopcount-based method and the existing method discussed below is $O((\alpha + \beta \times w) \times n)$ and that of path-based method is $O((\alpha + \beta) \times w \times n)$. α, β, w and n denote computing time of interference relationships, time of determining time slot to assign, average of link weight and the number of relay nodes, respectively. The path-based method is unsuitable for network that the topology or the traffic demand is frequently changed compared with the hopcount-based method and the existing method, because time slot assignment must be done when one of them is changed.

IV. Performance Evaluation

We show the evaluation results of our time slot assignment algorithms obtained by conducting packet-level simulation experiments.

A. Evaluation Environment

We randomly located 99 relay nodes uniformly in a 1×1 square area and one gateway node at the center of the area. All relay nodes had a communication range of 0.2. As described in Section II-A, after obtaining a directed communication graph based on the node location and the communication range, we constructed a directed transmission graph as a tree-like graph rooted at the gateway node and optionally minimized the hop count from the gateway node to each node. Note that the detailed implementation of the algorithm of the directed transmission graph is outside the scope of this paper, and we used the method in [14]. We determined the interference relationship among links between relay nodes using the interference model explained in Section II-B. The traffic demand of the network was uniform, and we generated one packet from a randomly chosen relay node destined to the gateway node at regular intervals, which were equal to the time slot duration. This traffic demand setting means that the weight of each link was equal to the number of paths between relay nodes and the gateway node passing through the link. For packet-level simulation experiments, we implemented a wireless multihop network simulator that can simulate the packet-level behavior of IEEE 802.16j-based networks, including topology generation from the locations of relay/gateway nodes, TDMA-based time slot assignment, and store-and-forward packet transmission based on the FIFO principle. In each experiment, we ran the simulation until 5,000 packets were generated and arrived at the gateway node. For one parameter set we conducted 3,000 simulations by changing the relay nodes' locations. When the interference ratio is 2.5, though they change according to the topology, the average of hop count is around 2.6–3.0 and the max of that is around 9–10.

We observed the frame size and the transmission latency as performance metrics. The frame size represents the total number of time slots needed for assigning time slots to all links and is desired smaller because the large one decreases network throughput. The transmission latency is defined as the time duration from when a packet is generated at the relay node to when the packet arrives at the gateway node. Note that in the packet-level simulation, some packets were queued at some relay nodes when congestion occurred, which may have increased the end-to-end transmission latency.

We evaluated the proposed methods and the existing method in [7] as the interference ratio γ was changed, taking values 1.5, 2.5 and 3.5, for all relay nodes.

B. Existing Method for Comparison

Here we describe the existing method in [7] used for comparison purposes. The method first determines the order of assigning time slots to links by using a conflict graph. The assignment order is roughly the same as the order of the degree of nodes in the conflict graph. The links are assigned time slots along this order in a greedy manner, as in the proposed methods. Since the conflict graph is likely to be dense around the gateway node and have space around the nodes far from the gateway node, the method in [7] can decrease the transmission latency for downstream

 ISBN: 978-1-61208-123-6

transmission. We evaluated the upstream transmission of the method to compare it with the proposed methods.

Note that we also consider the modified algorithm from the above method to possibly decrease the upstream transmission latency. The method utilizes the reverse order of time slot assignment given by the above existing method. Although we do not show the results due to space limitation, we have confirmed that the modified method cannot outperform the proposed method in this paper.

C. Frame Size

We first evaluated the frame size. The results are shown in Figures 4(a), 4(b), and 4(c) for γ = 1.5, 2.5 and 3.5, respectively. The x-axis of the graphs shows the topology ID ($1 \sim 3,000$), which corresponds to the simulation experiments with 3,000 patterns of node locations. The results are sorted in ascending order of the frame size of the existing method.

From Figure 4, we can see that the frame size of the existing method was the smallest, and that of the hopcount-based method was the largest for all interference ratios. In the hopcount-based method, the wireless resource efficiency was lower than that in the other methods due to spatial reuse only among links with the same hop count. On the other hand, the frame size of the path-based method was smaller than that of the hopcount-based method because of spatial reuse among all links. However, since the path-based method assigns time slots to links along the path from the relay node to the gateway node in the descending order of hop count, the ratio of spatial reuse was less than with the existing method. As a result, the frame size of the path-based method was larger than that of the existing method.

On the one hand, by comparing Figures 4(a)–4(c), we can find as the interference ratio became larger, the frame size of all methods increased, and as the interference ratio became larger, the difference in the frame sizes among the three methods decreased. This is because the large interference ratio decreased the wireless resource efficiency due to less spatial reuse.

From these results, we conclude that our proposed methods are less effective than the existing method in terms of the frame size.

D. Transmission Latency

Figures 5(a), 5(b), and 5(c) are the results of the end-to-end transmission latency for γ = 1.5, 2.5 and 3.5, respectively. The x-axis of the graphs is the hop count of the relay nodes from the gateway node at which packets are generated.

From Figure 5, we can see that the transmission latency of the path-based method was the smallest for all interference ratios. Since the path-based method sequentially assigns time slots to the links on a path from a relay node to the gateway node, the links on the path are assigned close time slots. Therefore, the transmission latency of path-based method decreased. In addition, when the interference ratio became large, the path-based method showed small latency, especially for large hop count. In particular, in Figure 5(c), when the interference ratio was 3.5, for the packets generated at the relay nodes with seven or larger hop count, the path-based method reduced the transmission latency by up to 15% as compared with the existing method. On the other hand, from Figure 5(c), we can also see that the transmission latency of the hopcount-based method was smaller than that of the existing method when the interference ratio was large. This is because the scheduling delay at each relay node decreased due to the time slot assignment of the hopcount-based method. However, when the interference ratio was small, the difference in transmission latency between the hopcount-based method and the existing method became small due to the large difference in frame size of the 2 methods, as depicted Figure 4(a).

We can also observe from Figure 5 that as the interference ratio became larger, the transmission latency of all methods increased. The reason for this is the increase of the frame size shown in Figure 4. The scheduling delay at each relay node increased because the communication opportunities per unit time for each link decreased when the frame size was large. Furthermore, the transmission latency of the packets with large hop count increased notably compared with small hop count since the number of relay nodes traversed was large.

From these results, we conclude that the hopcount-based method is more effective than the existing method when the interference ratio is large, and that the path-based method is superior to the existing method for all interference ratios in terms of the upstream end-to-end transmission latency. While both of them improve the upstream end-to-end transmission latency, they do *not* degrade average transmission latency of the entire network. Considering the increase in the frame length of the proposed algorithms in Figure 4, the proposed algorithms can make a good trade-off between the network throughput and latency.

V. Conclusion and Future Work

In this paper, we proposed 2 kinds of time slot assignment algorithms for upstream wireless links in IEEE 802.16j multihop networks to reduce the upstream end-to-end transmission latency. One of the proposed algorithms is a method based on the hop count from the gateway node. The other takes the path from relay nodes to the gateway node into account. Through simulation experiments, we confirmed that the proposed methods can reduce the upstream transmission latency by up to 15% as compared with the existing method without degrading average transmission latency of the entire network, though the methods increase the frame size.

In future work, we need to evaluate the proposed methods in other cases where parameters other than the interference ratio change, and to consider the implementation complexity and the overhead. We plan to improve the method not only to reduce the transmission latency but also to enhance the network throughput and to reduce the cost of assigning time slots, to apply the methods to other radio interference

 ISBN: 978-1-61208-123-6

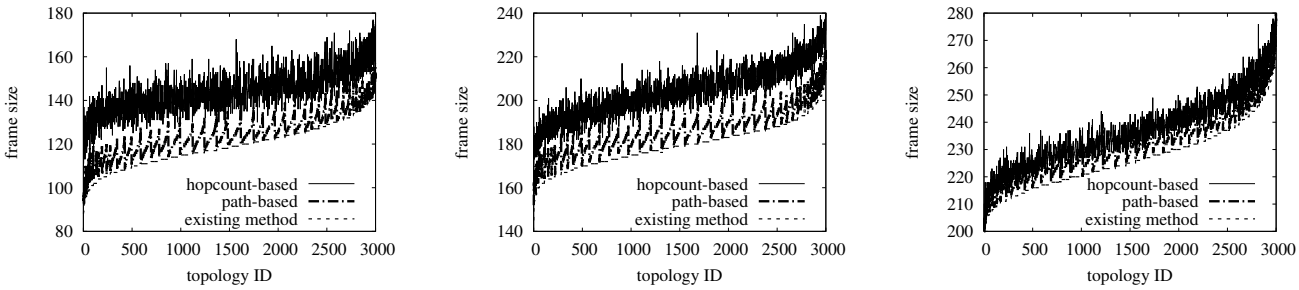

(a) Interference ratio 1.5 (b) Interference ratio 2.5 (c) Interference ratio 3.5

Figure 4. Frame size

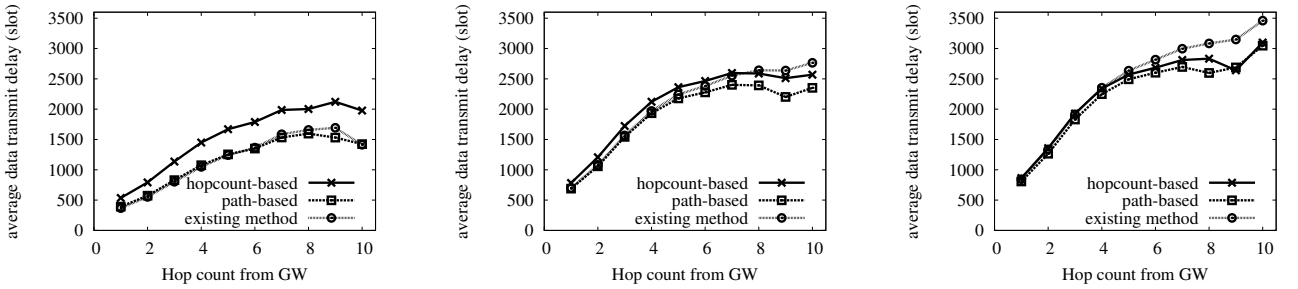

(a) Interference ratio 1.5 (b) Interference ratio 2.5 (c) Interference ratio 3.5

Figure 5. Average of transmission latency.

model using Signal to Interference and Noise Ration (SINR) that is more realistic than the radio interference model in this paper, and to develop the methods to a dynamic scheme adapting the change of topology, the change of traffic demand, condition of wireless channel and so on.

References

[1] IEEE 802.16 Working Group, "IEEE standard for local and metropolitan area networks, part 16: Air interface for broadband wireless access systems, amendment 1: Multihop relay specification," *IEEE Standard 802.16j-2009*, June 2009.

[2] D. Niyato, E. Hossain, D. I. Kim, and Z. Han, "Joint optimization of placement and bandwidth reservation for relays in IEEE 802.16j mobile multihop networks," in *Proceedings of IEEE ICC 2009*, pp. 1–5, June 2009.

[3] V. Genc, S. Murphy, Y. Yu, and J. Murphy, "IEEE 802.16j relay-based wireless access networks: An overview," *IEEE Wireless Communications*, vol. 15, no. 5, pp. 56–63, Oct 2008.

[4] P. Gupta and P. R. Kumar, "The capacity of wireless networks," *IEEE Transactoins on Information Theory*, vol. 46, no. 2, pp. 388–404, Mar 2000.

[5] T. Zhifeng, L. Anfei, T. Koon, and Z. Jinyun, "Frame structure design for IEEE 802.16j mobile multihop relay (MMR) networks," in *Proceedings of IEEE GLOBECOM 2007*, pp. 4301–4306, Nov 2007.

[6] N. Salem and J. Hubaux, "A fair scheduling for wireless mesh networks," in *Proceedings of WiMesh 2005*, Sep 2005.

[7] R. Ishii, G. Hasegawa, Y. Taniguchi, and H. Nakano, "Time slot assignment algorithms in IEEE 802.16 multi-hop relay networks," in *Proceedings of ICNS 2010*, pp. 265–270, Mar 2010.

[8] W. Weizhao, W. Yu, L. X. Yang, S. WenZhan, and F. Ophir, "Efficient interference-aware TDMA link scheduling for static wireless networks," in *Proceedings of MobiCom 2006*, pp. 262–273, Sep 2006.

[9] L. Kleinrock and J. Silvester, "Spatial reuse in multihop packet radio networks," in *Proceedings of the IEEE*, vol. 75, pp. 156–167, Jan 1987.

[10] P. Djukic and S. Valaee, "Link scheduling in polynomial time," *IEEE Transactions on Information Theory*, vol. 34, pp. 910–917, Sep 1988.

[11] H.-Y. Wei, S. Ganguly, R. Izmailov, and Z. J. Haas, "Interference-aware IEEE 802.16 WiMax mesh networks," in *Proceedings of IEEE Vehicular Technology Conference 2005*, vol. 5, pp. 3102–3106, May–June 2005.

[12] S. Liu, S. Feng, W. Ye, and H. Zhuang, "Slot allocaton algorithms in centralized scheduling scheme for IEEE 802.16 based wireless mesh networks," *Computer Communications*, vol. 32, pp. 943–953, Mar 2009.

[13] L.-W. Chen, Y.-C. Tseng, Y.-C. Wang, D.-W. Wang, and J.-J. Wu, "Exploiting spectral reuse in routing, resource allocation, and scheduling for IEEE 802.16 mesh networks," *IEEE Transactions on Vehicular Technology*, vol. 58, pp. 301–313, Jan 2009.

[14] P. A. Humblet and S. R. Soloway, "Topology broadcast algorithms," in *Proceedings of Computer Networks and ISDN Systems*, vol. 16, pp. 179–186, Jan 1989.

 ISBN: 978-1-61208-123-6

Space and Time Localization in Wireless Sensor Networks

Ustijana Rechkoska. Shikoska
University for Information Science & Technology, "Sv. Apostol Pavle"
Ohrid, Republic of Macedonia
e-mail: ustijana@t-home.mk

Ilinka Ivanoska, Danco Davcev
"Sv. Kiril i Metodij" University, Faculty of Electrical Engineering and Information Technologies"
Skopje, Republic of Macedonia
ilinkai@feit.ukim.edu.mk
etfdav@feit.ukim.edu.mk

Abstract **- Wireless sensor networks *(WSN)* are an increasingly attractive means to bridge the gap between the physical and virtual world. *WSNs* are envisioned to be used to fulfill complex monitoring tasks. Space and time play a crucial role in wireless sensor networks, since sensor nodes are used to collaboratively monitor physical phenomena and their space-time properties. A number of techniques and distributed algorithms for location estimation and time synchronization have been developed specifically for sensor networks. There are many similarities in space and time domains. This affects the location estimation and time synchronization, ranging from applications and requirements to basic approaches and concrete algorithmic techniques. An improved approach for space and time localization in *WSNs* is given in this paper. The main aspect of the algorithm is the use of a mobile beacon for both localization and synchronization. A mobile beacon is a node that moves around the sensor's field and it is aware of its time and position, equipped with a Global Positioning System (*GPS)* receiver. The synchronization component uses the packets required by the positioning component to improve its performance. The positioning component benefits from the communication, required by the synchronization component to decrease errors. A set of experiments and simulations are presented to evaluate the performance of the algorithm in order to reduce communication and processing resources and save energy and network resources.**

Keywords - space localization; time synchronization; mobile beacon; delay measurement; wireless sensor networks; global positioning system

I. INTRODUCTION

Enabled by technological advancements in wireless communications and embedded computing, wireless sensor networks were first considered for military applications, where large-scale wireless networks of autonomous sensor nodes would enable the unobtrusive observation of events in the real-world. The use of sensor networks has also been considered for various civil application domains.

The categories time and location are fundamental for many applications of sensor networks, due to the close integration of sensor networks with the real world. Interpretation of sensing results or coordination among sensor nodes are some of the implementations, time synchronization and sensor node localization are fundamental and closely related services in sensor networks.

In the synchronization problem [20, 21, 22, 23, 24, 25], the nodes' local clocks must be synchronized based on a reference node or in Coordinated Universal Time (*UTC*).

On the other hand, in the positioning problem [11, 12, 13], the concept of a reference system between sensor nodes is performed by identifying the physical location (e.g., latitude, longitude, and altitude) of these nodes. In general, traditional solutions such as the Network Time Protocol (*NTP* [26]) and Global Positioning System *(GPS*) are not suitable for sensor networks due to resource limitations. Furthermore, current solutions for the synchronization [20, 21, 22, 23, 24, 25] and positioning [11, 12, 13] problems are independent from each other and consequently, these problems are solved separately. As a result, the independent execution of these algorithms leads to lower efficiency regarding cost and accuracy. As it is demonstrated in this paper, by jointly solving these two problems, both synchronization and positioning errors can be reduced and energy can be saved.

In some previous work [4, 14, 15], algorithms for time-space localization are proposed. In this paper, an improved algorithm for solving this problem using a mobile beacon is proposed. A mobile beacon is a node that is aware of its time and position (e.g., equipped with a *GPS* receiver) and that has the ability to move around the sensor field. This beacon can be a human operator, an unmanned vehicle, an aircraft, or a robot. A mobile beacon has been successfully applied to solve the positioning problem. To the best of our knowledge, the current work is the first to address the use of a mobile beacon in synchronization and time-space localization problems. The proposed time-space localization algorithm can synchronize nodes by using the packet delay measurement [23, 24]. Synchronization can be improved by the extra packets required for location discovery. The algorithm is implemented for different network topology.

Existing solutions for time synchronization and node localization do not cover all important parts. Here, an integrated solution to jointly solve the localization and data routing problems in sensor networks is proposed, using a mobile beacon equipped with *GPS*, for grid, but also for randomly chosen network topology, reducing communication and processing resources, also saving energy and network resources.

In the next section, the related work is described. Section *3* presents an overview and definition of the positioning and synchronization problems in *WSNs*. Section *4* is presenting different types of topologies for wireless sensor networks used in our work. Section *5* describes the

 ISBN: 978-1-61208-123-6

proposed algorithm, which is evaluated in Section *6*. Section *7* presents the conclusions and future work.

II. RELATED WORK

There are different ways of classifying general *space and time localization algorithms*, they can be classified according to the measurement assumptions as four types: 1) connectivity-only 2) range-based 3) angle-based 4) hybrid. A comparison between the well - known algorithms such as *DV-Hop (Distance and Euclidean)*, Euclidean and Multi-lateralization can be obtained from [3]. The comparison is done in the context of specific constraints of sensor networks, such as error tolerance and energy efficiency, results indicate that there is no single algorithm that performs "best" and that there is possibility for further improvement.

A number of localization methods rely on connectivity information only. These types of methods are also referred to as "range-free" methods. The *Centroid method* [5] estimates the location of an unknown node as the average of its neighbors' locations. The *APIT* method *(Ad Hoc Positioning* [6] estimates the node location by isolating the area using various triangles formed by beacons. The *DV-Hop method* [7] counts the hop numbers to beacons and uses them as crude estimates for distances. Range-free methods require no additional hardware, but they generally only work well when networks are dense. Sparse networks by nature contain less connectivity information, and thus they are more difficult to localize accurately.

Range-based methods include the *Ad Hoc Positioning System (APS*) methods such as *DV-Distance and Euclidean* proposed in [7, 8]. In [9], ranging data are exchanged between the neighbors to refine the initial location guess. While those methods compute the absolute node locations, the *GPS-Free method* [10] calculates the relative node locations from the distance measurements. Compared to range-free methods, range-based methods give more accurate location estimates when ranging data is reliable. However, depending on the deployment environment, ranging techniques based on *RSSI-Received Signal Strength Indicator* tend to be error-prone and strong filtering is required. The ranging error could ultimately destroy the localization accuracy if it is allowed to propagate through the network unbounded.

Different methods generally exploit the trade-off between the estimation accuracy and the estimation coverage. For instance, given the same network scenario, the Euclidean method is capable of generating more accurate location estimates of a smaller subset of nodes, whereas the *DV-Hop* method has better coverage but worse accuracy. Regardless of the tradeoff, a common characteristic shared by distance-based *algorithm* is that they require a relatively high network density in order to achieve better results. Based on the extensive simulation of *DV-Distance, Euclidean* and *multilateration methods* performed in [16], it can be concluded that those distance-based *GAHLA*s "require an average degree of *11-12* nodes within the ranging neighborhood in order to achieve *90%* localization coverage with *5%* accuracy [16]."

Even though the future of AoA sensing devices is still unclear, some works have been published on localization using angle information. Simulation studies in [16] also show that when AoA (angle of arrival) of the signals is used in addition to the distance measurement, the localization accuracy and coverage can be drastically improved.

A combination of the above techniques can be employed to form a hybrid method. For instance, a hybrid method is proposed in [17] that uses both *APS* and Multi-dimensional Scaling *(MDS)*.

The probabilistic method and particle filters have been used in visual target tracking and computer vision location systems [18, 19] in the context of robotics. The particle filter method is also used to obtain the mobile node location based on received signal strengths from several known-location base stations in wireless cellular networks. The probability grid system in is a centralized probabilistic localization algorithm that updates the distribution based on a grid system.

Some recent researches [27, 28, 29] have proposed the use of mobile beacons to assist the nodes of a *WSN* in estimating their positions. A mobile beacon is a node that is aware of its position (e.g., equipped with a *GPS* receiver) and that has the ability to move around the sensor field. This beacon can be a human operator, an unmanned vehicle, an aircraft, or a robot. The localization algorithm proposed by Sichitiu and Ramadurai [27] uses mobile beacons to allow nodes to compute their positions by using range-based distance estimations. A similar but range-free positioning system is proposed by Ssu et al. [29]. In Pathirana et al. [28], the mobile beacon itself computes the positions, instead of the nodes. Mobile beacons have also been used to localize nodes in underwater *WSNs* [30]. In these networks, a boat equipped with a *GPS* receiver can be used as a mobile beacon or can send *GPS* position information to submerged equipment. These solutions address only the spatial localization problem, ignoring the need for time localization.

In the Flooding Time Synchronization Protocol (*FTSP*) [23], all delays in the packet transfer time are computed to synchronize precisely both sender and receiver using only one broadcast. An accuracy of about *1.5 μs* is reported. The multihop synchronization algorithm includes a leader selection (root node) and a flooding-like algorithm to propagate the timing information. Multiple floodings can be used to compute the clock drift. A similar algorithm is Delay Measurement Time Synchronization (*DMTS*) [24], which reports a single hop accuracy between *2 μs* and *32 μs.* These synchronization solutions solve only the time synchronization problem, ignoring the need for a common spatial reference system.

Global Positioning System (*GPS)* [1] is a good example of a time-space localization system that can both localize and synchronize sensor nodes; however, to equip all the sensors in a *WSN* with a *GPS* receiver is not a good

 ISBN: 978-1-61208-123-6

solution because it increases their cost, size and energy consumption. Romer [31, 32] also addressed and solved these two problems separately. Then, Romer and Mattern [33] presented both problems as related to each other, but no integrated solution was proposed. The Synapse algorithm is proposed [14], a time-space localization algorithm that computes the average multi-hop time of a packet to synchronize the nodes. Also, the Lightness algorithm [15] had been proposed, a novel and lightweight time-space localization algorithm that is able to localize and synchronize all nodes in a *WSN* with the communication cost of a single flooding.

In this paper, an improved algorithm for localization in time-space, using a mobile beacon, referring different network topologies is proposed to solve this problem.

III. WIRELESS SENSOR NETWORKS

Sensor networks consist of sensor nodes, computing devices that include a power source, a transceiver for wireless communication, a processor, memory, sensors, and potentially also actuators. Although the exact properties and capabilities of these components may vary, a common property of sensor nodes is their resource scarcity.

Multiple sensor nodes form a wireless network, whose topology and other properties do also depend on the application context. A large class of sensor networks can be characterized as multi-hop ad hoc networks, where sensor nodes do not only act as data sources, but also as routers that forward messages on behalf of other nodes, such that no additional communication infrastructure is required for operating the network.

The output of the sensor network may be used for various purposes. The output is delivered to a human user for further evaluation. It may be used to control the operation of the sensor network without human intervention by enabling/disabling sensors, or by controlling operation parameters of sensors (sampling rate, sensitivity, orientation, position). Using the output of the sensor network to control sensors or actuators can effectively create a closed-loop system that strives to achieve a particular nominal condition in the sensor network or in the real world.

The characteristics of wireless sensor networks can present a number of major challenges to the development of algorithms, protocols and systems. The main technical challenges are resource and energy constraints, network dynamics, network size and density, unattended and untethered operation.

It is important to ensure that resource usage and energy consumption are equally spread among the nodes of the network. If some nodes exhaust their battery quickly and fail early, resulting permanent network partitions may render the network in-operational. Usage of resources may lead to bottlenecks such as network congestions. Sensor nodes send sensor readings along a spanning tree to a base station for evaluation. Nodes close to the base station will run out of power since they forward messages from nodes further away.

Depleted batteries and corruptive environmental conditions (e.g., pressure, humidity, temperature, destructive chemicals) often lead to node failures. Temporary environmental obstructions may influence the communication range of nodes. Nodes may be mobile, new nodes may be added to replace failed ones. All these issues may lead to frequent topology changes in sensor networks. Temporary network partitions are likely to exist in sparse networks.

Despite intermittent connectivity, messages can be forwarded across partitions by mobile nodes as illustrated in Figure *1*.

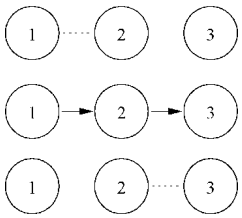

Figure *1*: Message transport across partition boundaries through node mobility.

The delay of the message flow can be arbitrarily high and is hardly predictable unless the mobility pattern of node *2* in the figure *1* is known in advance. Ensuring robust operation of a sensor network in such setups can be a very challenging task.

A. The Positioning Problem

To define the positioning problem in Wireless Sensor Networks, we take a *WSN* composed of p nodes, with a communication range of c units, and distributed in a two-dimensional squared sensor field $S = [0, q] \times [0, q]$.The network is presented by a graph $P = (L,M)$ with $L = \{l_1, l_2, \ldots, l_n\}$ like a set of sensor nodes; $h_i, j_i \in M$ *iff* l_i reaches l_j , i.e., the distance between; l_i and l_j is smaller than c; $u(e) \leq c$ is the weight of edge $e = h_i, j_i$, i.e., the distance between l_i and l_j . We also consider only two dimensions for a node's location, but the methods presented here can be extended to accommodate three dimensions. P is Euclidean graph in which every node has a coordinate $(x_i, y_i) \in R^2$ in a two-dimensional space, which represents the location of node i in S. Here there are: the unknown node, which is a node that doesn't know its position, then settled node which was initially an unknown node, but has managed to estimate its position by using a positioning system. Also, there is a beacon node or anchor, which is always aware of its physical position and helps to locate other nodes. Its position is obtained by manual placement or by external means such as a *GPS* receiver. This node forms the basis for most positioning systems in *WSN*s. The *positioning problem* is stated as finding the position of as many unknown nodes as possible, referring to a given multihop network,

represented by a graph, and a set of beacon nodes and their positions.

An example of a positioning system is localization with a mobile beacon proposed by Sichitiu and Ramadurai [27]. Once the nodes are deployed, the mobile beacon travels through the sensor field broadcasting messages that contain its current coordinates. When an unknown node receives more than three messages from the mobile beacon, it computes its position being based on the received coordinates and on the *RSSI* (Received Signal Strength Indicator) distance estimations. The communication cost for the *WSN* is null, since the nodes do not need to send any packets.

An advantage of this mobile beacon approach is that the nodes' positions are computed based on the same node -mobile beacon, keeping the mean localization error low and preventing the propagation of this error. It avoids the use of nodes equipped with *GPS*, except for the mobile beacon.

An important aspect that influences the position estimates is the trajectory of the mobile beacon. The less rectilinear the trajectory, the better the estimates will be. Rectilinear trajectories must be avoided. Two possible trajectories are evaluated in this work: sinusoidal and spiral trajectory.

B. Time synchronization

The significance of physical time for sensor networks has been reflected by the development of a number of time synchronization algorithms in the recent past. Most computer systems in use today are based on clocked circuits and hence contain so-called digital clocks. Such hardware clocks are a valuable tool for time synchronization, since they can be used to maintain synchronization over time [2].

A typical hardware clock consists of a quartz-stabilized oscillator and a counter that is incremented by one every oscillation period. If the periodic time T of the oscillator is known, the counter h can be used to obtain approximate measurements of real-time intervals in multiples of T.

The clock counter displays value $h(t)$ at real time t and is incremented by one at a frequency of f. The rate of the counter is defined as $f(t) = dh(t)/dt$. An ideal digital clock would have a rate of 1 at all times. The periodic time of the oscillator and hence the clock rate depend on various parameters such as age of the quartz, supply voltage, environmental temperature and humidity. This clock drift is formally defined as the deviation of the rate from 1 or:

$$\rho(t) = f(1) - 1 \quad (1)$$

Since sensor nodes are typically operated under a well-defined range of the above parameters, it is reasonable to assume a maximum possible drift ρ_{max}, such that:

$$|\rho(t)| \leq \rho_{max} \quad (2)$$

Obtaining temporal constraints is typically implemented by communication among sensor nodes. In practice, the relationship between synchronized time and hardware clock is often not linear. By repeating the line fitting procedure frequently, a linear approximation of that nonlinear relationship can be achieved. The hardware clock can be considered a time sensor, calibrated using the observed past behavior of synchronized time. The precision of the chosen approach should be evaluated and the imprecision of time synchronization algorithm should be decreased, depending on the age of time marks and hop-distance between nodes of the sensor network, providing accuracy ordered in milliseconds.

In this work, the actual time of the network is considered, in which the nodes must be synchronized (e.g., *UTC*), is represented simply by t. The hardware clock of node i is defined as $t_i(t)$, since it is a monotonically non-decreasing function of t. Because no hardware clock is perfect, $t_i(t)$ has two components: $t_i(t) = d_i t + o_i$, where o_i is the offset, i.e., the difference between t and t_i at that instant, and d_i is the drift, i.e., how the local clock gradually deviates from t due to conditions such as temperature or battery voltage. The unsynchronized node is a node whose clock is not synchronized with the reference; synchronized node is a node which was initially unsynchronized, but managed to synchronize its local clock by using a synchronization system; the beacon node is the node that already has a synchronized clock (e.g., by using *GPS*) and it is called a beacon node. The *synchronization problem* is stated in finding the offset and drift (o_i, d_i) of as many unsynchronized nodes $i \in N$ as possible, by a given multihop network, represented by a graph, a set of beacon nodes and their synchronized clocks. In the packet *delay measurement*, all delays in the packet transfer time are estimated to synchronize precisely both sender and receiver by using only one packet. The packet delay measurement synchronization technique has been used in a number of synchronization protocols for *WSNs* [23, 24].

C. Localization in Time and Space

In a wireless sensor network, most of the applications that require position information also require time information. Number of similarities can be identified [14, 15].

The need of both time and space information and the similarities between them, have shown the importance of combining these two problems into a single one: *localization in time and space*. Doing so, energy and network resources could be saved, also the opportunity to improve time and position estimations in contrast to the scenarios in which these problems are solved separately is given. Synchronization algorithms can take advantage of the greater number of beacon nodes required by the positioning algorithms, while positioning algorithms can take advantage of the techniques and additional communication resources used to synchronize nodes.

The *time-space localization problem* can be stated as finding the position (x_u, y_u) and time $t_u(t)$ for all

 ISBN: 978-1-61208-123-6

unsynchronized and *unknown nodes*, by a given multihop network, represented by a graph and a set of *beacon nodes*, their *positions* (x_b, y_b) and *synchronized clocks* $t_b = t$, where *u* and *b* belong to the sets of unknown nodes and beacon nodes, respectfully.

IV. WIRELESS SENSOR NETWORK TOPOLOGIES

Several wireless sensor networks topologies are considered in our work and they are presented on Figure *2*. The first network topology presented here is *C* – random network topology (Figure 2 *(a)*). Together with the presented *H* – random topology (Figure 2 *(d)*) are irregular network topologies, as well as the random topology, shown in Figure *2 (e)*.

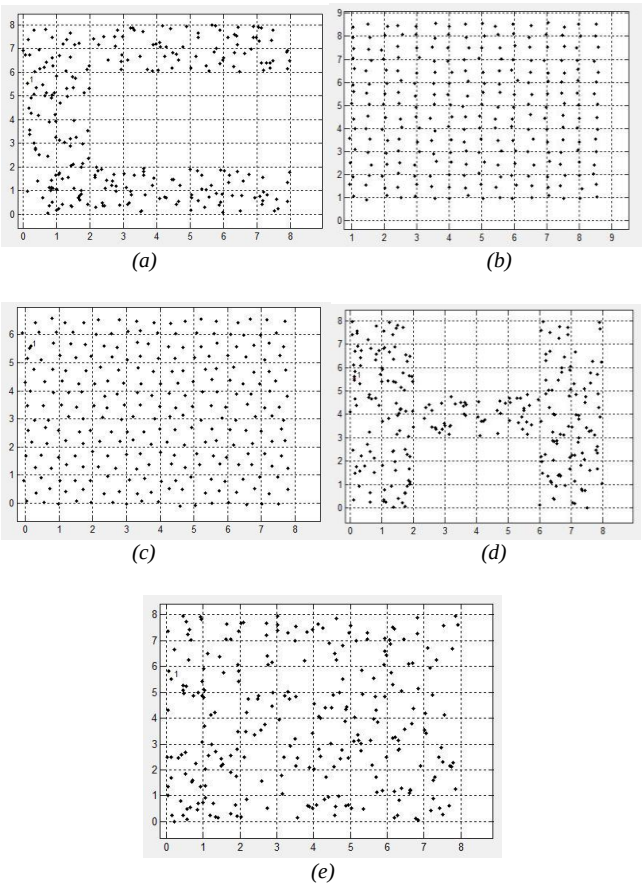

Figure *2*: Network topologies - *(a) C* – random topology *(b)* Disturbed grid topology *(c)* Disturbed hexagonal topology *(d) H* – random topology *(e)* Random topology

The C and H – random topologies are random topologies, but irregular ones, because only a part of the square of the surface is considered.

Disturbed grid topology and disturbed hexagonal topology shown on Figure *2* - *(b)*, *(c)* are more regular network topologies than previous mentioned ones.

V. A MOBILE BEACON APPROACH FOR LOCALIZATION IN TIME AND SPACE ALGORITHM

An improved approach for space and time localization, for different network topologies, is presented in this section. The positioning component is essentially the mobile beacon localization algorithm [27]. The synchronization component obeys the same principle as the positioning algorithm, but it is extended to deal with time estimations [4]. These two components are combined in the algorithm. The *delay measurement technique* is used to synchronize nodes.

Different network topologies are employed, generated by our algorithm.

Once nodes are deployed, the mobile beacon travels through the sensor field broadcasting messages that contain its current coordinates and timestamp. When an unknown node receives a packet from the mobile beacon, it can estimate the packet travel time and, based on the times tamp stored in the packet, its own offset. Also, when an unknown node receives more than three messages from the mobile beacon, it can estimate its position based on the received coordinates and on the *RSSI* distance estimates. Since the nodes will require at least three packets for positioning, synchronization can be improved by computing the average offset of all packets. An advantage of this algorithm is that the communication cost of localizing and synchronizing regular nodes is null, since these nodes do not need to send any packets.

Set of position information is given as a variable, also, set of received timestamps. Timer to send packets is put, position and time information through variables is given. After that, the nodes' *GPS* info is returned, packets' travel distance estimation is given, the nodes' position is computed. Later, packets' travel delay estimation is given and also the nodes' offset is computed. Case if this node is a beacon node is explored and number of references is tested, if there are three received messages from mobile beacon, it confirms enough references and proceeds with the algorithm.

The running application of this algorithm is presented on figure *3*. The red color point is the mobile beacon which is moving through the sensor network, marked with blue color on the figure *3*. The options for choosing five types of sensor networks is put here whether the user wants to choose grid oriented network, randomly chosen network, hexagonal network topology, or *H* and *C* random network topologies, presented in the previous section. Also, information about the parameters used and display options are given. Choice by the user, according to the parameters and network topology, is enabled.

Running the sensors, the energy, which the mobile beacon is spending on moving itself and sending messages, is overviewed. This energy is much bigger than the one which is spent on local calculations for each sensor in the *WSN*. This is very low energy consumption.

 ISBN: 978-1-61208-123-6

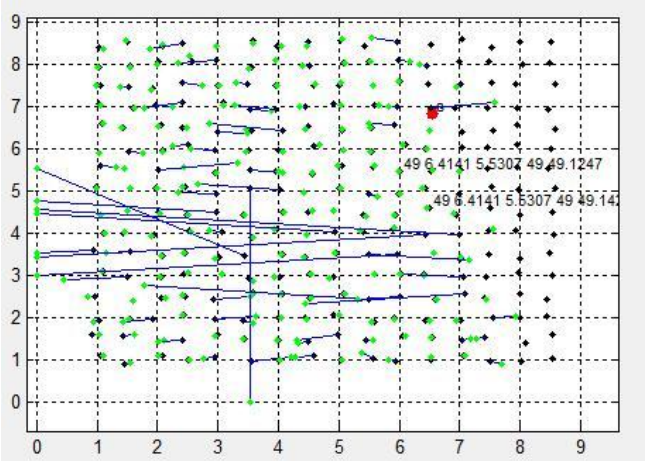

Figure 3: The running application of the algorithm

VI. EVALUATION

The evaluation of our algorithm is done, by performing simulations, parameters used and their values are given in the next table.

An experiment was done within the sensor field *92 x 92 m^2*. *256* nodes are employed, for different network topologies, we have chosen five types of network topology, explained previously, for this evaluation. The density of a sensor network is picked to be *0,03* nodes/m^2 and the communication range is *15 m*.

TABLE I. SIMULATION PARAMETERS AND THEIR VALUES

Parameter	**Value**
Sensor field	*92 × 92 m^2*
Number of nodes	*256* nodes (different network topologies)
Density	*0.03* nodes/m^2
Communication range	*15 m*
Number of beacons	*1* - mobile beacon
RSSI inaccuracy	*10 %* of communication range

The evaluation is done by taking two types of trajectories for the mobile beacon: sinusoidal and spiral trajectories, presented on figure *4*.

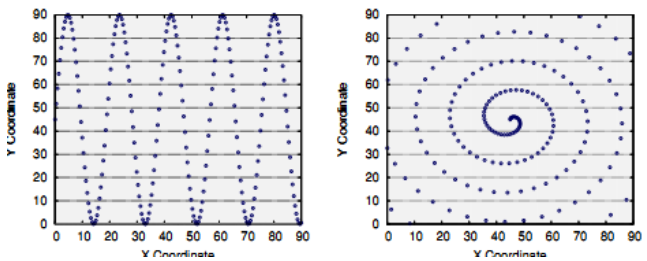

a) b)

Figure 4. Evaluated trajectories for the mobile beacon: a) sinusoidal; b) spiral trajectory.

On the next figure, localization error, synchronization error and also impact of *RSSI* inaccuracy are presented, in different color, for two evaluated trajectories of the beacon, sinusoidal an spiral ones, and for five types of network topologies: *C* – random topology, disturbed grid topology, disturbed hexagonal topology, *H* – random topology and random topology.

Localization Error - the distribution of position errors among the sensor nodes is depicted in Figure *5 (a)*. The cumulative error identifies the percentage of nodes (*y*-axis), with a positioning error, smaller than a parameterized value (*x*-axis). A sharp curve means that the majority of nodes has a small error. This graph also shows that spiral trajectories result in better positioning than sinusoidal ones, since these trajectories are less rectilinear.

Synchronization Error - the distribution of synchronization errors among the sensor nodes is depicted in Figure *5 (b)*. In this case, the cumulative error identifies the percentage of nodes (*y*-axis) with a synchronization error smaller than a parameterized value (*x*-axis). Again, a sharp curve means that the majority of nodes have a small error.

Impact of RSSI Inaccuracy – since the fact that the distance estimations using *RSSI* measurements are not accurate, depending on the environment, such an inaccuracy may lead to greater errors in the estimated positions. The evaluation of this impact is done by adding some noise to the real distances. This noise is generated by a normal distribution, with the actual distance as the mean and a percentage of this distance as the standard deviation. The comparison between the increase of the standard deviation of the normal distribution and the actual distance for the algorithms is presented on Figure *5(c)*.

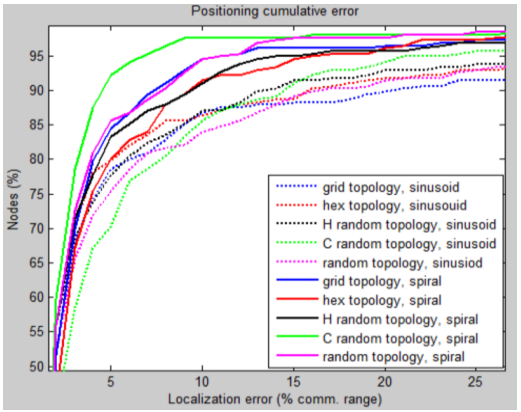

(a)

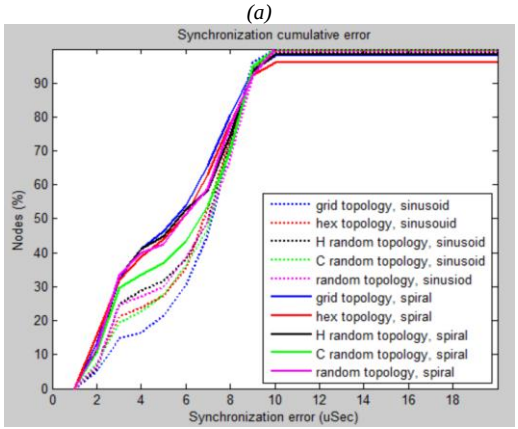

(b)

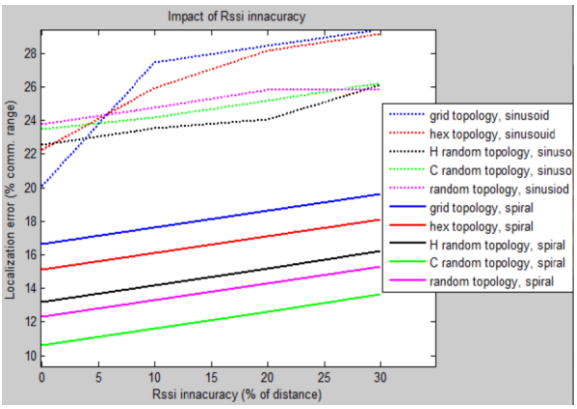

(c)

Figure 5. *(a)* Positioning cumulative error *(b)* Synchronization cumulative error *(c)* Impact of *RSSI* inaccuracy

It can be noticed that the positioning part takes advantage of the synchronization part to improve its performance, which shows the significance of solving both positioning and synchronization problems at the same time.

VII. CONCLUSION

Due to the close integration of sensor networks with the real world, the categories time and location are fundamental for many applications of sensor networks, to interpret sensing results or for coordination among sensor nodes. Time synchronization and sensor node localization are fundamental and closely related services in sensor networks.

Existing solutions for these two basic services have been based on a rather narrow notion of a sensor network as a large-scale, ad hoc, multi-hop, un-partitioned network of largely homogeneous, tiny, resource-constrained, mostly immobile sensor nodes that would be randomly deployed in the area of interest. However, recently developed prototypical applications indicate that this narrow definition does not cover a significant portion of the application domain of wireless sensor networks.

Existing solutions for time synchronization and node localization do not cover all parts of space and time in wireless sensor networks problem. Different, proposed approaches should be implemented to support these concepts adequately.

In this paper, we have proposed and evaluated an improved algorithm for the time-space localization, a mobile beacon approach, for different network topologies. By using a mobile beacon, all sensor nodes are able to localize themselves both in time and space. The beacon node sends packets and all regular nodes are able to synchronize and compute their positions with a zero communication cost algorithm. The proposed algorithm shows the importance of combining both positioning and synchronization into a single unified problem: localization in time and space. By doing so, the proposed algorithm manages to improve synchronization in the algorithm, comparing to the previous implemented approaches. In this case, communication and processing resources can be reduced, thus saving energy and network resources.

REFERENCES

[1] U. R. Shikoska and D. Davcev, “Sensitivity Analysis for GPS in land vehicle navigations”, IEEE International Conference on Wireless and Mobile Computing, Networking and Communcations, WiMob' 2008, pp. 221 – 222, Paris, France, October 2008.

[2] U. R. Shikoska and D. Davcev, “Time Synchronization in Wireless Sensor Networks,” PCO' 2010, Kucing Borneo, Sarawak, December 2010, in press.

[3] K.Langendoen and N. Reijers. "Distributed Localization in Wireless Sensor Networks: a Quantitative Comparison," Computer Networks, vol 43(4), pp. 499-518, Nov. 2003.

[4] A. Boukerche, H. Oliveira, E. F. Nakamura, and A.F. Loureiro, “Localization in Time and Space for Wireless Sensor Networks: A Mobile Beacon Approach,” IEEE ISCC 2008, 04594838, pp. 1-8, August 2008.

[5] N. Bulusu, J. Heidemann, and D. Estrin. "GPS-less Low Cost Outdoor Localization for Very Small Devices," IEEE Personal Communications Magazine, vol. 7/5, pp. 28-34, October 2000.

[6] T. He, C. Huang, B. M. Blum, J. A. Stankovic, and T. F. Abdelzaher. "Range-Free Localization Schemes in Large Scale Sensor Networks," in Proc. of ACM MOBI-COM'03,pp. 81-95, 2003.

[7] D. Niculescu and B. Nath. "Ad Hoc Positioning System (APS)," in Proc. of IEEE GLOBECOM'01, vol. 5, pp. 2926-2931, San Antonio, 2001.

[8] D. Niculescu and B. Nath. "DV Based Positioning in Adhoc Networks," Telecommunication Systems, vol. 22, no. 1-4, pp. 267-280, January-April 2003.

[9] C. Savarese, J. Rabay, and K. Langendoen. "Robust Positioning Algorithms for Distributed Ad-Hoc Wireless Sensor Networks," in Proc. of USENIX Technical Annual Conference, pp. 317-327, Monterey, CA, June 2002.

[10] S. Capkun, M. Hamdi, and J.-P. Hubaux. "GPS-Free Positioning in Mobile Ad-Hoc Networks," in Proc. of 34th Hawaii International Conference on System Sciences, vol. 9, pp. 9008, 2001.

[11] H. A. Oliveira, E. F. Nakamura, A. A. Loureiro, and A. Boukerche. “Directed position estimation: A recursive localization approach for wireless sensor networks,” In IC3N’05, pp. 557–562, San Diego, USA, October 2005.

[12] A. Boukerche, H. A. Oliveira, E. F. Nakamura, and A. A. Loureiro, “A voronoi approach for scalable and robust dv-hop localization system for sensor networks,” In IC3N’07, pp. 497 – 502, Honolulu, Hawaii, USA, Aug 2007.

[13] A. Boukerche, H. A. Oliveira, E. F. Nakamura, and A. A. Loureiro, “Towards an integrated solution for node localization and data routing in sensor networks,” In ISCC’07, pp. 449 – 454, Aveiro, Portugal, July 2007.

[14] H. A. Oliveira, E. F. Nakamura, A. A. Loureiro, and A. Boukerche, “Localization in time and space for sensor networks,” In AINA’07, pp. 539-546, Niagara Falls, Canada, May 2007.

[15] A. Boukerche, H. A. Oliveira, E. F. Nakamura, and A. A.Loureiro, “A novel lightweight algorithm for time-space localization in wireless sensor networks,” In MSWiM’07, pp. 336-343, Chania, Crete Island, Greece, October 2007.

[16] K. Chintalapudi, R. Govindan, G. Sukhatme, and A. Dhariwal. "Ad-Hoc Localization Using Ranging and Sectoring," in Proc. of IEEE INFOCOM '04, pp. 2662-2672, April 2004.

[17] A. A. Ahmed, H. Shi, and Y. Shang. "SHARP: A New Approach to Relative Localization in Wireless Sensor Networks," in Proc. of 25th IEEE International Conference on Distributed Computing Systems Workshops (ICDCS 2005), pp. 892-898, June 2005.

[18] D. Fox, W. Burgard, F. Dellaert, and S. Thrun. "Monte Carlo Localization: Efficient Position Estimation for Mobile Robots," in Proc. of National Conference on Artificial Intelligence, Orlando, FL, pp. 343-349, July 1999.

[19] S. Thrun. "Particle Filters in Robotics," in Proc. of 18th Annual Conference on Uncertainty in Artificial Intelligence (UAI-02), pp. 511, San Francisco, CA, August 2002.

[20] F. Sivrikaya and B. Yener, “Time synchronization in sensor networks: a survey,” IEEE Network, 18(4), pp. 45–50, 2004.

 ISBN: 978-1-61208-123-6

[21] K. Romer, P. Blum, and L. Meier, "Time synchronization and calibration in wireless sensor networks," In I. Stojmenovic, editor, Handbook of Sensor Networks: Algorithms and Architectures, pp. 199–237. John Wiley & Sons, Sept. 2005.
[22] J. Elson, L. Girod, and D. Estrin, "Fine-grained network time synchronization using reference broadcasts," SIGOPS Oper.Syst. Rev., 36(SI), pp. 147–163, 2002.
[23] M.Maroti, B. Kusy, G. Simon, and A. Ledeczi, "The flooding time synchronization protocol," In SenSys'04, pp. 39–49, Baltimore, MD, USA, 2004. ACM Press.
[24] S. Ping, "Delay measurement time synchronization for wireless sensor networks," Technical Report IRB-TR-03-013, Intel Research, June 2003.
[25] S. Ganeriwal, R. Kumar, and M. B. Srivastava, "Timing-sync protocol for sensor networks," In SenSys'03, pp. 138–149, New York, NY, USA, 2003. ACM Press.
[26] D. L. Mills, "Network time protocol version 4 reference and implementation guide," Technical Report 06-06-1, Department of Electrical and Computer Engineering, University of Delaware, 2006.
[27] M. L. Sichitiu and V. Ramadurai,"Localization of wireless sensor networks with a mobile beacon,", In MASS'04, pp. 174–183, Florida, USA, October 2004.
[28] P. Pathirana, N. Bulusu, S. Jha, and A. Savkin, "Node localization using mobile robots in delay-tolerant sensor networks," IEEE Trans. on Mobile Comput., 4(4), pp. 285 – 296, August 2005.
[29] K.-F. Ssu, C.-H. Ou, and H. Jiau, "Localization with mobile, anchor points in wireless sensor networks," Vehicular Technology, IEEE Transactions on, 54(3), pp. 1187–1197, 2005.
[30] V. Chandrasekhar,W., K. Seah, Y. S. Choo, and H. V. Ee, "Localization in underwater sensor networks: Survey and challenges," In WUWNet'06, pp. 33–40, New York, NY, USA 2006. ACM Press
[31] K. Romer, "Time and location in sensor networks," GI/ITG Fachgespr¨ ach Sensornetze, Berlin, pp. 57–60, July 2003.
[32] K. Romer, "Time Synchronization and Localization in Sensor Networks," PhD thesis, ETH Zurich, Zurich, Switzerland, June 2005.
[33] K. Romer and F. Mattern, "Towards a unified view on space and time in sensor networks," Computer Communications, 28(13), pp. 1484–1497, August 2005.

 ISBN: 978-1-61208-123-6

Nonlinearity Compensation for Super-Positioning Satellite System with Interference Canceller

Hiroki MATSUDA,Takehiro ISHIGURO, Takao HARA, and Minoru OKADA

Graduate School of Information Science, Nara Institute of Science and Technology
8916-5 Takayamacho,Ikoma,Nara,630-0101 Japan
Tel:+81-743-72-5348,Fax:+81-743-72-5349
Email: {hiroki-ma,takehiro-i,takao-ha,mokada}@is.naist.jp

***Abstract*—The Carrier Super-Positioning Satellite System is a promising telecommunication system because the efficiency of frequency usage is twice as much of that in existing satellite systems. Interference canceller used in the carrier super-positioning system is greatly effected by the nonlinear distortion of satellite TWTA. A scheme of the nonlinearity compensation for P-MP VSAT network has been proposed by us before. In this paper we propose and verify a new method to compensate the nonlinearity of satellite TWTA for P-P system to improve the interference canceller for the Carrier Super-Positioning System.**

***Keywords*-satellite; frequency reuse; nolinear compensation; interference canceller.**

I. INTRODUCTION

As the traffic demand for high speed data and images increases, effective utilization of frequency resources of satellite communications is more important than ever. Carrier super-positioning is a promising telecommunication system for frequency reuse since the frequency efficiency becomes double that of existing satellite systems. In this system outbound signal (outgoing from the station) and the inbound signal (incoming to the station) can use common frequency band which are conventionally used in separate bands. In this system, the signal sent from the station becomes the interference to the station itself, and the interference shall be removed by the interference canceller which is discussed in this paper.

The interference canceller is realized by generating its replica and subtracting it from the received signal [1]-[5]. In this process, some parts of the interference remaine not cancelled unless the waveform of generated replica is exactly the same as that of interference. One of the major reasons of the difference comes from the nonlinear distortion which the received signals suffer from the satellite transponder TWTA (Traveling Wave Tube). The effects of the nonlinear TWTA on to the conventional communications systems have ever been reported[6][7]. On the other hand, the effects of the nonlinearity on the canceller performance have been reported by us in the previous papers [8]. And a method has been proposed to compensate the nonlinearity by

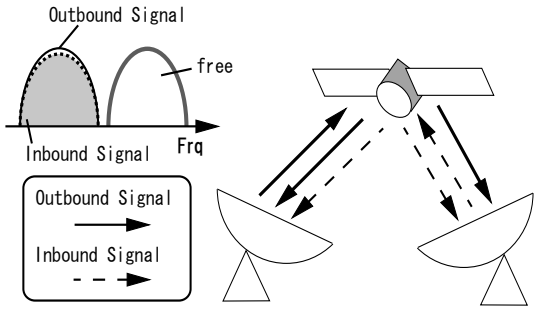

Figure 1. Typical carrier super-positioning systems for Point to Point network

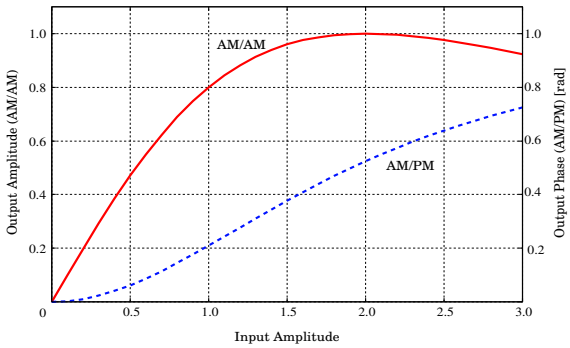

Figure 2. Nonlinear characteristics of TWTA

intentionally giving same nonlinearity to the replica as that of satellite TWTA. This method is , however, applicable only to the P-MP VSAT system in which the power of outbound signal in much large than that of inbound[9][12].

In this paper, we will show the nonlinear compensation method in the P-P system in which the power of both inbound and outbound signal in the same.

One network is composed of two large Hub stations. And a wide band outbound(OB) carrier is sent from the Hub to another wider band inbound(IB) carriers are from another, to the Hub. This is called a point-to-point network. Figure 1 shows the point-to-point network.

 ISBN: 978-1-61208-123-6

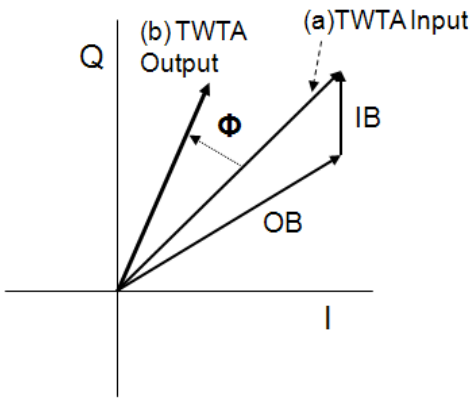

Figure 3. Signal vectors of TWTA Input and Output

II. Effects of Nonlinearity

In the satellite communications, the transponder TWTA is preferably operated in the region of saturation in order to use power effectively. Then, the signals amplified there suffer from the effects of inter-modulation and distortion due to the AM/AM and AM/PM conversion. Figure 2 shows a typical nonlinear characteristics of the TWTA used in the conventional communications satellite. In the case of a carrier superposed system, two or more carriers are commonly amplified. Figure 3 shows a vector diagram of input and output signals through the TWTA. Composite signal (a) of outbound(OB) and inbound(IB) is provided to TWTA and converted to the TWTA output signal (b). If the power of OB is large enough in comparison with IB, the conversion which the composite signal(a) is received by the nonlinearity is the same as that by which OB is received. On the other hand, it is not true in such system that the power of IB is not smaller enough than OB like point-to-point network.

As mentioned, the difference between received OB and its replica becomes interference. And if the received OB is distorted by the nonlinearity of TWTA, it causes the difference between received OB and its replica.

III. Nonlinearity Compensation

As described above, interference power is generated due to the nonlinear distortion of unwanted signal (OB). Our purpose in this study is to compensate the distortion. We take different approaches for two types of networks. First, it is for the VSAT system in which the power level of OB is much higher than those of IBs. In this system, the distortion which the composite signal suffers from the nonlinearity is almost the same as the distortion which OB signal suffers from. In this case, therefore, major part of the difference between received unwanted signal and its replica is removed by intentionally giving the same nonlinearity to the replica[9][12]. Secondly, the approach took for point-to-point network is, as shown in Figure4, to put the compensator which has inverse nonlinear characteristics of the TWTA in front of the canceller since we can not apply same approach to P-P system as in the VSAT system where we give nonlinearity to the replica. Here we call replica compensation for the P-MP system and post compensation for the P-P system. The detailed configurations and the effects of both approaches are then discussed.

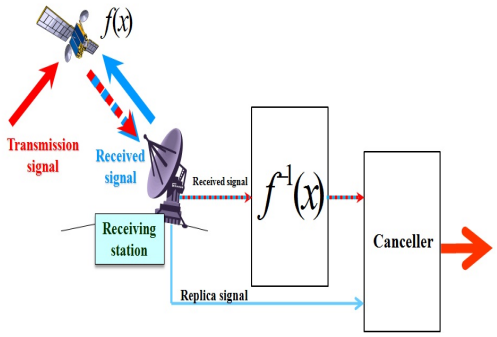

Figure 4. Interference canceller-introduced nonlinear compensations

A. Replica compensation

Here, we refer the method and the effect of replica compensation shown in the reference [9] and [12]. This approach is to compensate the distortion by intentionally giving the same distortion to the replica. Figure 4 shows the conceptual block diagram of replica compensation. The upper side of this block diagram is the path where the received signals (OB+IB) are provided to the canceller. The lower path is to generate the replica of OB by demodulating received signal. The output of the demodulator is then fed to the nonlinearity. This function is achieved not by adding actual non-linear devices such as a Sohottky diode but by a numerical approach of signal processing in a degital filter and does therefore not impact significantly on the hardware size. Here the issue is how to estimate the nonlinear characteristics of satellite TWTA in the replica generator of the canceller unit. It is not difficult to know the satellite TWTA nonlinearity itself by getting the data of the transponder from the satellite operator. Also, there are not so many variations in the nonlinear characteristics in the same class of TWTA. However, even though it is possible to know nonlinear characteristics, we still have to know the operating point (back off) of the satellite TWTA in order to give the same nonlinearity to the replica because the effects of nonlinearity on to the signals depends greatly on the operating level (back off) of the amplifier. Furthermore, the uplink power to the satellite frequently deviates due to the rain attenuation or other reasons. It is therefore mandatory for the nonlinearity compensation to have a function which automatically tracks the operating level of the transponder.

 ISBN: 978-1-61208-123-6

Namely adaptive back off function is mandatory. Figure 5 and 6 show the effects of replica compensation. The extrated carrier to interference ratio is improved by about 10 dB(Figure 5) and half of the BER degradation is improved in dB as shown in Figure 6.

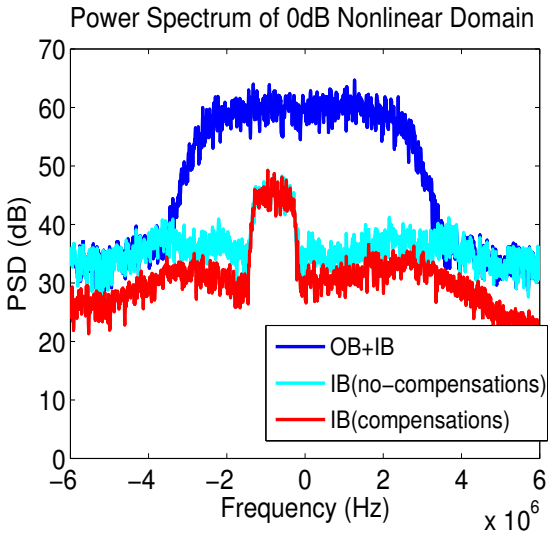

Figure 5. Power spectrum of canceller input and output,IBO=0[dB](refer to [9])

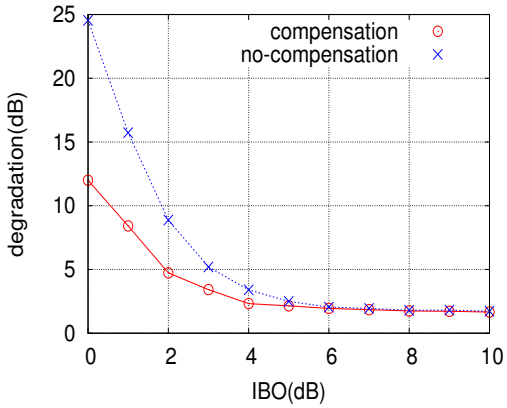

Figure 6. BER degradation at 10^{-4} and its improvement by replica compensation(refer to [9])

In this method, it is assumed that the nonlinear characteristics given to the replica is the same as that of satellite TWTA for both amplitude and phase. However, it is important to investigate the effects of the difference between two nonlinearities. We think it is not difficult to adopt same amplitude nonlinearity of the replica as that of the satellite TWTA since it is not difficult to get precise data of the amplitude nonlinearity of the TWTA Then, we have investigated the effects in case some difference exists between two phase nonlinearities. As shown in these figures,

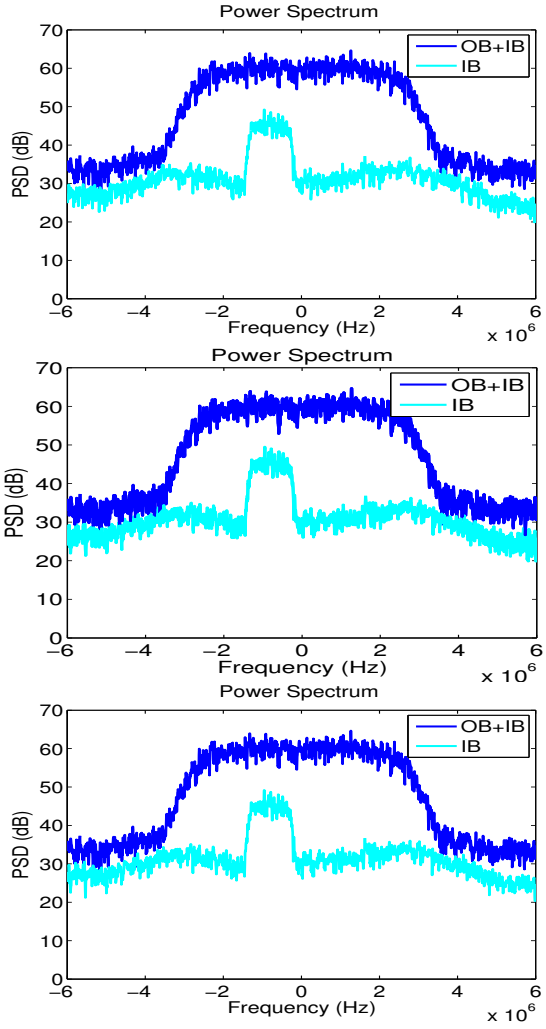

Figure 7. Power spectrum for three cases of phase nonlinearity
Upper : +20%of satellite AM/PM
Middle: ±0% of satellite AM/PM
Lower : −15%of satellite AM/PM

(refer to [12])

it can be said that the change of phase nonlinearity up to +20 and -15 % does not give significant degradation to the performance of nonlinearity compensator.

B. Post compensation

As mentioned, the replica compensation is useful only when the unwanted OB signal level is much higher than wanted IB signals. We propose here another method to compensate distortion which the received signals (composite of both OB and IBs) suffer from the satellite nonlinearity. By this approach, the distortion should be basically removed from the received signal regardless the relation between OB and IB levels.

Figure 8 shows the vector diagram distorted by the nonlinearity. Phase and amplitude of a vector is converted

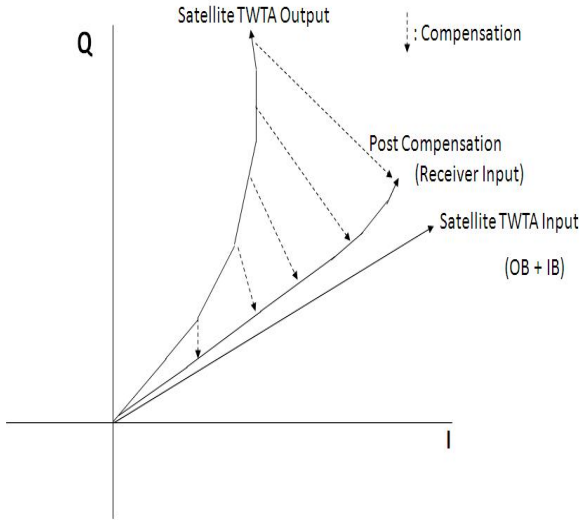

Figure 8. Vector diagram of TWTA input/output and receiver input by post compensation

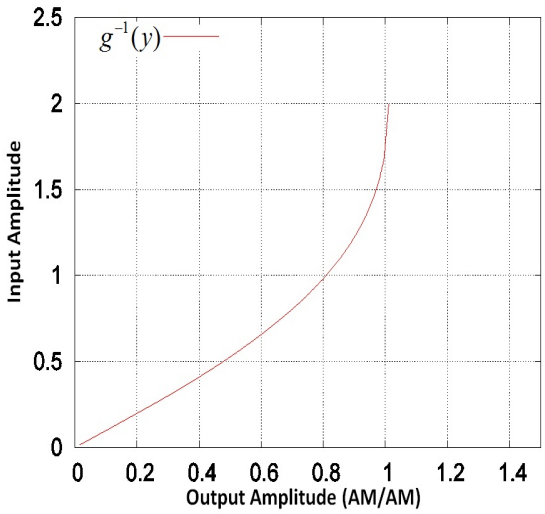

Figure 9. Inverse Nonlinear Characteristics of TWTA

(twisted) according to the AM/PM and AM/AM conversion characteristics of TWTA respectively. Our method is to put the inverse characteristics of the nonlinearity at the canceller input. It is theoretically expected that large part of the distortion can be removed from the received signal before it is provided to the canceller. By this operation, the twisted vector should be stretched as shown in Figure 8. But it shall be notified, in this case, that the inverse operation for the amplitude conversion (AM/AM) increases the noise since this operation is to expand larger portion of amplitude of the received signals which contain thermal noise.

1) Theory of post compensation: Lets assume the nonlinear characteristics of the TWTA as , where r is the input signal of TWTA, then the output of TWTA can be expressed by,

$$g(r) = \frac{\alpha_x r}{1+\beta_x r^2} \quad (1)$$

for AM/AM

$$f(r) = \frac{\alpha_\phi r^2}{1+\beta_\phi r^2} \quad (2)$$

for AM/PM

Table I
PARAMETERS OF TWTA CHARACTERISTICS

α_x	1.0
β_x	0.25
α_ϕ	$\pi/12$
β_ϕ	0.25

In the carrier superposed network, the satellite input signal is the summation of outbound signal (A) and inbound signal (B). Therefore the satellite output signal is obtained by,

$$y = g(A+B) \quad (3)$$

Our proposal is to put inverse nonlinear characteristics $g^{-1}(y)$ at the receiver input, then the original signal A+B can be principally attained by

$$A+B = g^{-1}(y) \quad (4)$$

$$g^{-1}(y) = -\sqrt{\frac{\alpha_x^2}{4\beta_x^2 y^2} - \frac{1}{\beta_x^2}} + \frac{\alpha_x}{2\beta_x y} \quad (5)$$

The input-output characteristics of the path is shown in Figure 10 which is compensated by inverse nonlinearity shown in Figure 9.

2) Simulation results: Figure 11 and 12 show the results of computer simulation. The post compensation improves BER by about 1 $\sim$ 1.5 dB as shown these figures. Figure 13 shows the effects of post compensation for two case of TWTA operation points. As shown in Figure 13, large improved can be expected for small input back off.

IV. CONCLUSION

This paper proposes a new nonlinearity compensation method for the interference canceller used in carrier superpositioning point to point(P-P) satellite system. In this system, both inbound and outbound signals are transmitted in the same frequency band and therefore the interference canceller that subtracts the unwanted signal from received signal is required. However, the amplifier used at satellite,

 ISBN: 978-1-61208-123-6

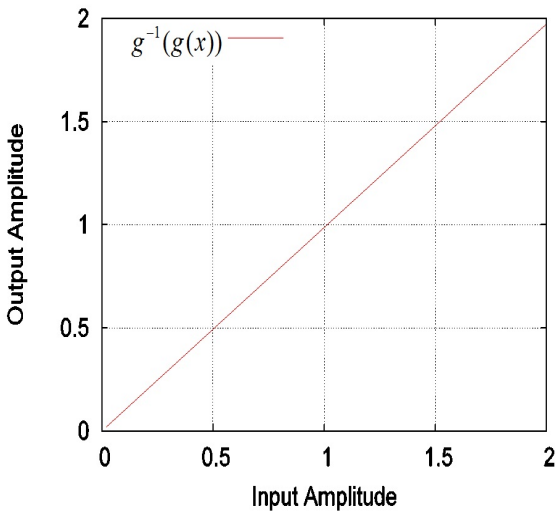

Figure 10. Path Characteristics Compensated by Inverse Nonlinearity

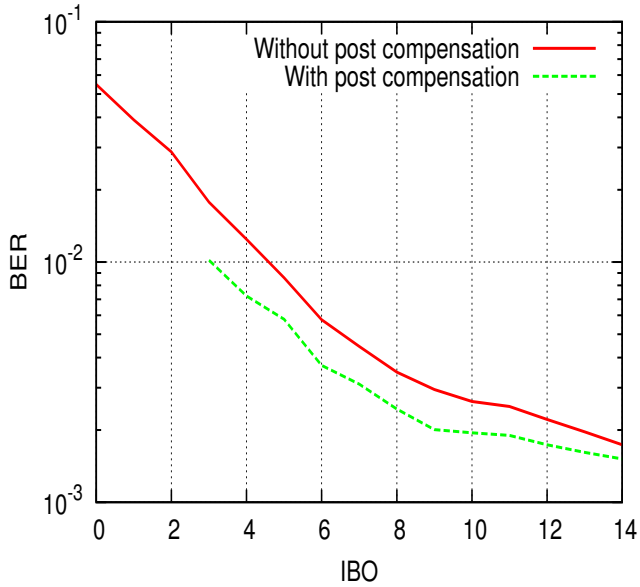

Figure 11. BER Performance vs input back off of TWTA for with and without post compensation, CN = 10[db]

TWTA, shows nonlinear characteristics when it is used at high input level. To compensate this nonlinear distortion, received signal is deformed with reverse characteristics of TWTA to achieve nondistorted signal. Also, the method which is applicable to P-MP VSAT can not be applied to this case. Therefore we proposed here post compensation method. In this paper, this method is evaluated with computer-based simulation and the result shows that it is able to decrease the effect of nonlinearity which is distorted at satellite's TWTA. For future work, we must check if this

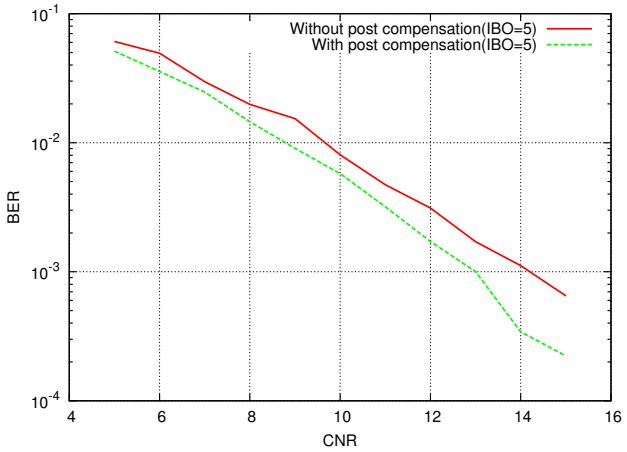

Figure 12. BER Performance vs CNR for with and without post compensation, IBO = 5[dB]

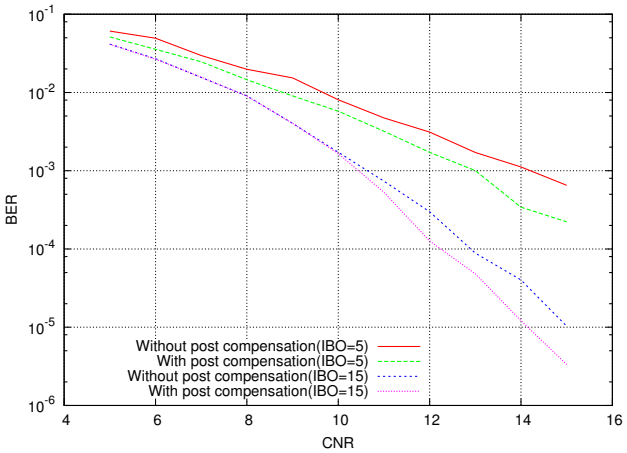

Figure 13. BER Performance for two cases of operating point of TWTA

method is useful in such conditions that the received signal is attenuated by rain. We also must check if this method does not make worse in the heavier noisy conditions due to the inverse nonlinear operation.

The BER data shown here are now under the further study since these are the case in the simplified transmission path which does not include filters in the down link. (satellite output filter and receiver input filter)

ACKNOWLEDGMENT

Authors would like to thank peoples of SKY Perfect JSAT for their support of this study specifically Mr. Takeda and Mr. Naoi. We also would like to thank all colleagues in our laboratory who gave us kind suggestions and useful discussions.

 ISBN: 978-1-61208-123-6

REFERENCES

[1] N. Ishida,"Common-band satellite communication system,"IEICE Transactions, vol. J82-B, no. 8, pp. 1531-1537, Aug.1999

[2] Hideki Toshinaga,Kiyoshi Kobayashi and H.Kazuma, "Interference cancellation for multimedia satellite communication systems employing superposed transmission,"Technical Report of IEICE, vol. SAT2000-86, Dec.2000

[3] Takao Hara,Michihiro Ichikawa, Minoru Okada and Heiichi Yamamoto,"Canceller Design for Carrier Super-Positioning for Frequency Reuse Satellite Communications,"IEICE Transactions of Communications, Vol. J88-B, No. 7, pp. 1300-1309, July.2005.

[4] M.Osato,H.kobashi,T.Hara,M.Okada,and H.Yamamoto, "Simplified canceller for multi-level modulation super-positing for frequency reuse satellite communications," ICT2006, May 2006

[5] H.Kobashi,M.Osato,T.Hara,M.Okada,and H.Yamamoto, "Signal cancellation for satellite frequency reuse by super-positioning multi-level modulation," IEEE-ISCC2006,June 2006.

[6] Victor del Razo,Taneli Riihonen,Fernando Gregorio,Stefan Werner ,and Risto Wichman, "Nonlinear amplifier distortion in cooperative amplify-and-forward OFDM Systems,"WCNC2009

[7] Marinella Aloisio,Piero Angeletti,Enrico Casini,Enrico Colzi,Salvatore D'Addio,and Roger Oliva-Balague, "Accurate characterization of TWTA distortion in Multicarrier operation by means of a correlation-based method,"IEEE Transactions, vol. 56, no. 5, May.2009

[8] T.Uratani,R.Miyamoto,T.Hara,and M.Okada,"Performance of an interference canceller for P-MP satellite networks with nonlinear TWTA," ISCCSP2008, March 2008, Malta

[9] Kenta Kubo,Shigeo Naoi,Yozo Takeda,Ryusuke Miyamoto, Takao Hara, and Minoru Okada, "Compensation of Nonlinear Effect for Signal Super-positioning satellite Communications,"PSAT2010, Feb.4-6, 2010, Rome Italy.

[10] Shoko Kuroda,Sho Tanaka,Ryusuke Miyamoto,Takao Hara and Minomu Okada, "A configuration of carrier super-positioning satellite system using extended matched filter,"IEICE Technical Report, SAT2008-57(2008-12), pp. 23-28

[11] Shoko Kuroda,Sho Tanaka,Shigeo Naoi,Yozo Takeda, Ryusuke Miyamoto,Takao Hara, and Minoru Okada, "Development of an Interference Canceller in Satellite Communications using a Muti-level Modulation with Superposed Transmission",IEICE Trans. Commun.vol. E92-B, No.11, pp. 3354-3364, Nov.2009

[12] Takao Hara,Hiroki Matsuda,Kenta Kubo and Minoru Okada, "Performance Improvement of Interference Canceller for Carrier Super-positioning by the Nonlinearity Compensation in Satellite Communications", ICWMC2010, Sep.20-25, Valencia, Spain.

 ISBN: 978-1-61208-123-6

Extending the Protocol Interference Model Considering SINR for Wireless Mesh Networks

Gyeongyeon Kang
Graduate School of Information Science and Technology
Osaka University, Japan
Email: g-kang@ist.osaka-u.ac.jp

Yoshiaki Taniguchi, Go Hasegawa, Hirotaka Nakano
Cybermedia Center
Osaka University, Japan
Email: {y-tanigu, hasegawa, nakano}@cmc.osaka-u.ac.jp

***Abstract*—Radio interference should be taken into account to assign time slots to links in time division multiple access (TDMA)-based wireless mesh networks. In many graph theory-based time slot assignment algorithms, the protocol interference model is widely used to obtain radio interference information, although this model is considered to be inaccurate when compared with actual radio interference. On the other hand, the signal-to-interference-plus-noise-ratio model (SINR model) is a well-known and accurate model of radio interference. However, the SINR model requires time slot information to obtain radio interference relationship, and thus it is difficult to apply the SINR model to graph theory-based time slot assignment algorithms. In this paper, we extend the protocol interference model to represent radio interference more accurately for wireless mesh networks. To do this, we adjust the interference ratio parameter of the protocol interference model by considering SINR. We propose three methods for adjusting this parameter. Through simulation, it is shown that higher accuracy of the protocol interference model can be achieved by adjusting the interference ratio parameter for each node.**

***Keywords*-wireless mesh networks, protocol interference model, signal-to-plus-noise-ratio model, time slot assignment.**

I. INTRODUCTION

Wireless mesh networks have attracted a great deal of attention for providing wireless broadband access because of their expandability and cost efficiency [1]. Wireless mesh networks consist of a gateway node which is connected to a wired network and mesh nodes which relay the messages between the gateway node and client terminals as shown in Fig. 1. A mesh node is connected with another node through a wireless link when they are within transmission range of each other. A mesh node provides wireless broadband access service to client terminals within its service area.

In wireless networks, when closely located links are simultaneously used, a receiver node cannot correctly receive radio signals from the corresponding sender node due to radio interference. That is why it is necessary to avoid radio interference in wireless networks. In the time division multiple access (TDMA) protocol, time is divided into frames, each of which consists of time slots of constant duration. Different time slots are then assigned to links that interfere with each other. The performance of the wireless mesh networks highly dependent on the time slot assignment algorithms, and graph theory-based time slot assignment algorithms for wireless mesh networks have been studied

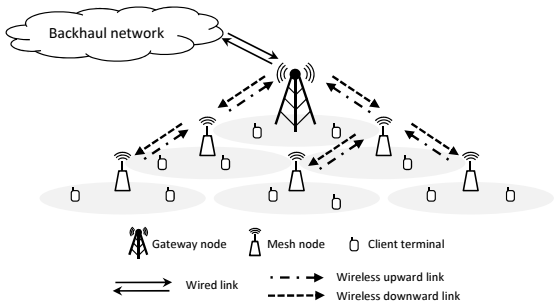

Figure 1. Wireless mesh network

[2, 3, 4] since time slot assignment algorithms can be regarded as the graph coloring in graph theory.

Graph theory-based time slot assignment algorithms require information on the interference relationships among links before assigning time slots to links. In these algorithms, the *protocol interference model* (a.k.a. unified disk graph model) [5, 6] has been widely used to obtain radio interference information. In the protocol interference model, a radio interference range is defined as a circle centered on a sender node. Since the interference relationships among links are defined according to the location of nodes, the protocol interference model can be easily used in theoretical analysis. However, the protocol interference model is not accurate in comparison with physical radio interference [6]. For example, closely located links can be used simultaneously when each receiver node can receive signals of sufficient strength from the corresponding sender node, even if the protocol interference model indicates that the links interfere with each other [7]. In addition, there is a situation in which a receiver node cannot correctly receive radio signals from the corresponding sender node when many links are simultaneously used and interfere with the receiver node, even if there are no interference relationships among the links in the protocol interference model.

On the other hand, the *signal-to-interference-plus-noise ratio (SINR) model* [6, 7] is known for accurate radio interference representation. In the SINR model, when the signal-to-interference-plus-noise ratio of a link is beyond a threshold value, the receiver node of the link can successfully receive the radio signal from the sender node of the

 ISBN: 978-1-61208-123-6

link. The SINR model can handle features of wireless radio propagation such as Rayleigh fading, shadowing effects and capture effects[8]. However, to obtain interference relationships among links, the SINR model requires information not only on the location of nodes, but also on sender nodes which simultaneously emit radio signals. Therefore, it is difficult to apply the SINR model to the graph theory-based time slot assignment algorithms.

To apply the graph theory-based time slot assignment algorithms to actual wireless mesh networks, accurate information on interference relationships is needed in order to avoid interference among links and to assign time slots to links efficiently. In other words, accurate radio interference models are needed that can be applied in graph theory-based time slot assignment algorithms. For this purpose, in this paper we extend the protocol interference model considering SINR. This is accomplished by adjusting the interference ratio parameter of the protocol interference model. The overview of our proposal is as follows. For a wireless mesh network, interference relationships are at first determined based on the protocol interference model. Then, time slots are assigned for all links based on the information on the interference relationships. These steps are repeated by adjusting the interference ratio parameter until all links satisfy certain SINR criteria. We propose three heuristic methods for adjusting the parameter. The accuracy and effect of our proposed radio interference models are evaluated through simulation experiments.

The rest of this paper is organized as follows. In Section II, we introduce some related studies. In Section III, we describe the network model and radio interference models. Then in Section IV, we propose three methods for adjusting the interference ratio parameter of the protocol interference model, considering the SINR; these methods are evaluated through simulation in Section V. Finally, we conclude this paper and discuss future work in Section VI.

II. Related Work

To assign time slots to links in TDMA-based wireless networks, information on interference relationships among links is needed. There are a variety of radio interference models for wireless networks, and these radio interference models have been compared in previous studies [6, 9, 10].

Maheshwari et al. have investigated the accuracy of radio interference models in IEEE 802.15.4-based wireless sensor networks [9]. They conducted experiments using 20 TelosB commercial sensor nodes, and evaluated the accuracy of the protocol interference model, the SINR model, the hop-based interference model, the link quality-based interference model and the range-based interference model. As a result, they found that the SINR model is the most accurate among the radio interference models when compared with actual radio interference. Furthermore, they evaluated the throughput of the wireless sensor network using a time slot assignment algorithm based on each radio interference model. For the SINR model, the authors used one-shot scheduling [11]. Through experimentation, they demonstrated that the time slot assignment based on SINR model achieves the highest throughput.

Zhu and Lu have compared the physical radio interference model and the hop-based interference model, which is used in IEEE 802.16 wireless mesh networks [10]. Through simulation evaluations using a QualNet simulator, it was shown that about 7% of links cannot be used due to radio interference when we assume that there are interference relationships among links within 3-hop links in the hop-based interference model.

Shi et al. have compared the protocol interference model and the SINR model for multi-hop multi-channel wireless networks [6]. They first show that blind use of the protocol interference model is not adequate. They then show that the link capacity of wireless networks based on the protocol interference model can be close to that based on the SINR model by using appropriate parameter settings for the protocol interference model.

In the present study, we extend the protocol interference model in order to use it in graph theory-based time slot assignment algorithms for wireless mesh networks. Taking the SINR as an accurate measure of the actual radio interference, we propose methods for adjusting the interference ratio parameter of the protocol interference model.

III. Models

In this section, we explain the wireless mesh network model and the time slot assignment algorithm which are used in this paper. We then introduce the protocol interference model and SINR model.

A. Wireless Mesh Network

In this paper, we consider the same wireless mesh network that is used in [3]. We assume that there is a set of n mesh nodes $\mathcal{V}^c = \{v_1, v_2, \ldots, v_n\}$ deployed in a plane. We consider the directed communication graph $\mathcal{G}^c = (\mathcal{V}^c, \mathcal{E}^c)$ which indicates the communication relationship in each node. $\mathcal{E}^c$ is the set of directed communication links $l_{i,j}$, representing a link directed from mesh node $v_i \in \mathcal{V}^c$ to mesh node $v_j \in \mathcal{V}^c$. The existence of directed communication link $l_{i,j}$ in the directed communication graph $\mathcal{G}^c$ is determined according to the radio interference model. We assume one of the mesh nodes is the gateway node that is connected to a wired network. Without loss of generality, let mesh node v_1 be the gateway node.

There are two types of communication, namely, upward communication and downward communication. In upward communication, data is transferred from mesh nodes toward the gateway node. Conversely, data is transferred from the gateway node toward mesh nodes in downward communication. Communication between the gateway node and mesh nodes is achieved through intermediate mesh nodes in a multi-hop fashion. The communication path is determined by a routing algorithm. In this paper, we consider a tree-based routing algorithm which constructs the transmission

graph $\mathcal{G}^t = (\mathcal{V}^t, \mathcal{E}^t)$ as a tree graph. Here, $\mathcal{G}^t \subset \mathcal{G}^c$, $\mathcal{V}^t = \mathcal{V}^c$ and $\mathcal{E}^t \subset \mathcal{E}^c$. In the transmission graph, root is the gateway node and each node is connected to the gateway node through minimum hop and minimum distance links. We call the link $l_{i,j} \in \mathcal{E}^t$ in $\mathcal{G}^t$ a transmission link. In addition, a link that is on the path directed toward the gateway node is called an upward link, and a link that is on the path directed away from the gateway node is called a downward link.

B. Time Slot Assignment

In this paper, TDMA is adopted as the MAC protocol of the wireless mesh networks. In TDMA, time is divided into time slots $\mathcal{T} = \{t_1, t_2, \ldots, t_m\}$, and different time slots are assigned to the links which have an interference relationship. In this paper, the total number of time slots m is called the frame length. The interference relationships of the links are determined by the radio interference model. For the time slot assignment algorithm at the transmission link $l_{i,j} \in \mathcal{E}^t$, we adopt the greedy algorithm that is used in [2, 3]. In this time slot assignment algorithm, the order of time slot assignment for each transmission link is first determined, and then time slots are assigned to the transmission links in a greedy manner. The frame length m becomes the number of time slots, depending on the deployment of mesh nodes and the interference relationship among transmission links.

C. Radio Interference Models

1) Protocol Interference Model: In the protocol interference model [5, 6], the existence of links and interference relationships between links are determined according to the location of node v_i, transmission range r_i and interference ratio α_i as follows. When two nodes $v_i, v_j \in \mathcal{V}^c$ are satisfied with $||v_i - v_j|| < r_i$, the communication from sender node v_i to receiver node v_j is successful, and the directed communication link $l_{i,j} \in \mathcal{E}^c$ is set. Here, $||v_i - v_j||$ stands for the distance between node v_i and node v_j. In addition, sender node v_i interferes with a link whose receiver node v_k satisfies $||v_i - v_k|| < \alpha_i r_i$. The interference ratio α_i is usually set between 2 and 4 depending on the environment [12].

2) SINR Model: Let sender node and receiver node be v_i and v_j. In addition, let $\mathcal{V}_{i,x}^{int}$ be the set of sender nodes that use the same time slot with link $l_{i,j}$ except node n_i. In the SINR model [6, 7], the existence of links and interference relationships among links are determined according to the SINR, which is defined as follows:

$$s_{i,j,x} = \frac{p_{i,j}}{p_{noise} + \sum_{v_k \in \mathcal{V}_{i,x}^{int}} p_{k,j}}. \quad (1)$$

Here, p_{noise} is the signal strength of noise, which is determined depending on the environment. $p_{i,j}$ is the received signal strength from sender node v_i at receiver node v_j, and is described as follows:

$$p_{i,j} = \frac{p_i^{tr}}{||v_i - v_j||^{\eta}}. \quad (2)$$

Here, p_i^{tr} is the transmission power of wireless signal at sender node v_i. η is the parameter for considering power decay due to distance, and is usually set between 2 and 4 depending on the environment [12].

In the SINR model, when SINR $s_{i,j,x}$ from Eq. (1) satisfies $s_{i,j,x} \geq B$, receiver node v_j can successfully receive radio signals from sender node v_i at time slot t_x. B is called the capture threshold which is determined depending on the wireless devices used. On the other hand, when SINR $s_{i,j,x}$ is less than threshold B, communication from sender node v_i to receiver node v_j fails. This means that the set of sender nodes $\mathcal{V}_{i,x}^{int}$ interferes with link $l_{i,j}$.

IV. Methods for Adjusting the Interference Ratio Parameter of the Protocol Interference Model Considering SINR

In this section, we propose SINR-based methods for adjusting the interference ratio α_i parameter of the protocol interference model. Although the SINR dynamically changes in actual environments depending on fading, varying noise, etc., we assume static situation for simplicity in this paper.

A. Overview

Figure 2 shows the flowchart of our methods for adjusting the interference ratio. In our methods, transmission graph $\mathcal{G}^t$ is at first generated based on the protocol interference model. Information on interference relationships among transmission links are then determined based on the protocol interference model, where the interference ratio of all nodes is set to the initial interference ratio α_0. Next, a set of SINR $\mathcal{S} = \{s_{i,j,x} | l_{i,j} \in \mathcal{E}^t, t_x \in \mathcal{T}\}$ for all links which are used in all time slots is calculated. When the minimum SINR $s_{min} = \min \mathcal{S}$ is less than the capture threshold B, it means that there is a link which cannot be used in the SINR model. In this case, we adjust the interference ratio α, and then again determine the relationship of interference among transmission links and assign time slots based on the protocol interference model. This process is repeated until $s_{min} \geq B$ is satisfied. In the following, we propose three methods for adjusting the interference ratio.

B. Interference Ratio Adjustment Methods

1) All Nodes Adjustment (ANA) Method: In the ANA method, the interference ratio α_i of all nodes is adjusted by adding δ. Figure 3 shows an example transmission graph for the case of eight nodes and seven transmission links. Let transmission link $l_{7,4}$ have the minimum SINR in time slot t_w. In addition, let the time slot t_w be assigned to transmission links $l_{8,1}$, $l_{7,4}$, $l_{6,5}$ and $l_{3,2}$. In the ANA method, the interference ratio of all nodes, that is, v_1–v_8, are adjusted.

However, the ANA method is simple and increases the interference ratio of all nodes even if there is no difference

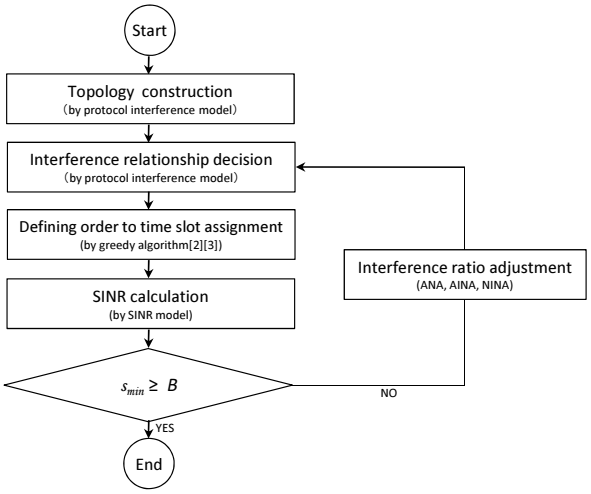

Figure 2. Flowchart for adjusting interference ratio

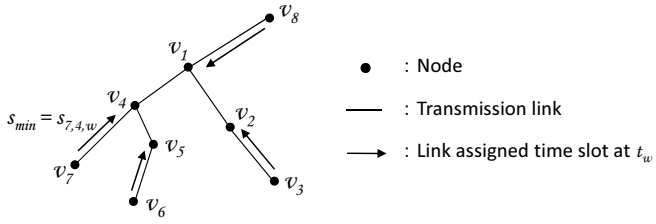

Figure 3. Example of transmission graph

in the result of the determined radio interference between the protocol interference model and the SINR model in a local region. If the interference ratio is increased more than necessary, more links are considered to have interference relationships, and the number of time slots is increased.

2) All Interference Nodes Adjustment (AINA) Method: In the AINA method, the interference ratio is adjusted locally. Let the SINR of transmission link $l_{g,h}$ in time slot t_w become the minimum SINR s_{min}, and the set of sender nodes which give interference to transmission link $l_{g,h}$ be $\mathcal{V}_{g,w}^{int}$. At transmission link $l_{g,h}$, there is the largest difference in the resulting interference relationship between the protocol interference model and SINR model. The AINA method adjusts the interference ratio of all nodes in $\mathcal{V}_{g,w}^{int}$ by adding δ. In the example of Fig. 3, the interference ratio of sender nodes v_3, v_6 and v_8, which are assigned the same time slot with transmission link $l_{7,4}$, are adjusted.

The AINA method adjusts the interference ratio of all sender nodes within $\mathcal{V}_{g,w}^{int}$. Therefore, it may increase the interference ratio of a node more than necessary when the node is far enough from a receiver node that has the minimum SINR.

3) Nearest Interference Node Adjustment (NINA) Method: In the NINA method, the interference ratio of the node that is the closest to the receiver node v_h, among the set of nodes $\mathcal{V}_{g,w}^{int}$, is adjusted by adding δ. In Fig. 3, node v_6 is the nearest from receiver node v_4, and the interference ratio of node v_6 is adjusted.

V. Simulation Experiments

In this section, we evaluate the performance of our interference ratio adjustment methods through simulation experiments. We use a self-developed IEEE 802.16j mesh network simulator which is developed by Visual C. In the simulations, one gateway node is placed at the center and $n-1$ nodes are randomly distributed in a 1×1 square area. We exclude the cases of a disconnected graph. In the protocol interference model, transmission distance r_i is set to 0.18. In the SINR model, transmission power p_i^{tr} and the parameter of power decay η are set to 1 and 3.0, respectively. Environment noise p_{noise} is set to 32, which is set when there are four nodes within a distance of 0.5 from the receiver node. Capture threshold B is set to 3 dB. In our proposed model, the initial interference ratio α_0 and the incremental ratio δ are set to 0 and 0.01, respectively.

A. Evaluation of Accuracy

We first evaluate the accuracy of the protocol interference model using our proposed methods through a comparison with the SINR model. For all combination sets of transmission link $\mathcal{E}^t$, we evaluate whether a set of links has interference relationships for each radio interference model. Here, we exclude sets of transmission links where neighboring links are simultaneously selected. When both the SINR model and the proposed protocol interference model agree on whether or not a set of transmission links can be successfully used simultaneously, the proposed model's result is classified as a true positive or a true negative. When the SINR model produces the result that a set of transmission links can be used simultaneously and the proposed model produces the result that the set of transmission links cannot be used simultaneously, the proposed model's result is classified as a false negative. In the opposite case, its result is classified as a false positive. We adopt the *false positive rate* and *false negative rate* as measures of the accuracy of the radio interference model. False positive rate is defined as the number of false positives divided by the number of true negatives and false positives. False negative rate is defined as the number of false negatives divided by the number of true positives and false negatives. For comparison purposes, we also show the results for the protocol interference model where α is set to 2, 3 and 4. We refer to this as the *conventional method*.

Figure 4 shows the average of false positive rate and false negative rate with 99% confidence intervals from results for 100 topologies when $n = 50$. As shown in Fig. 4(a), the false positive rate for our proposed methods are larger than that for the conventional method. However, all of the false positive rate are quite low and are less than 0.22%. On the other hand, the false negative rate for the proposed methods decreases between 5% and 15% compared to that for conventional method as shown in Fig. 4(b). Among our proposed methods, the NINA method achieves the lowest false negative rate, while the ANA method has the highest

 ISBN: 978-1-61208-123-6

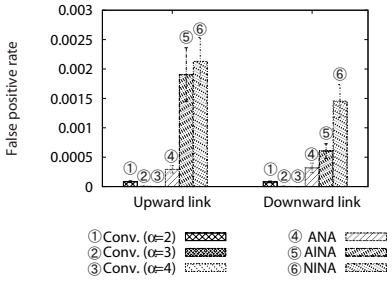

(a) False positive rate

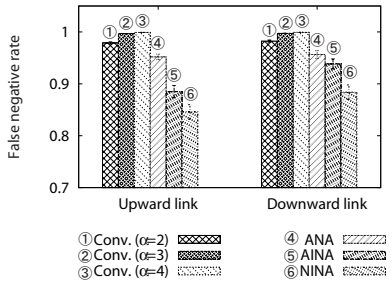

(b) False negative rate

Figure 4. Accuracy for all combinations of transmission link sets

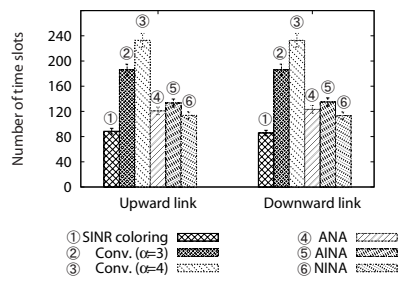

(a) Number of time slots

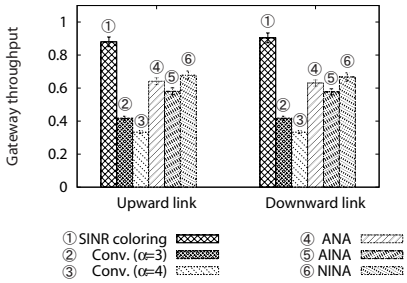

(b) Gateway throughput

Figure 5. Performance of a wireless mesh network

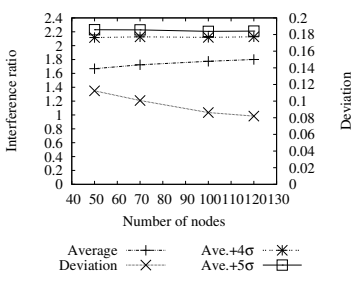

(a) Interference ratio

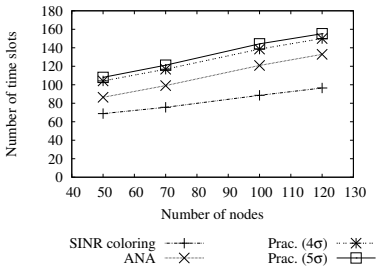

(b) Number of time slots

Figure 6. Practical interference ratio and its performance

false negative rate. Since the NINA method is designed not to increase the interference ratio more than necessary, the number of false negatives decreases and the number of true positives increases. As a result, the false negative rate for the NINA method becomes lower. However, the false negative rate for the NINA methods is still high, and is about 84% for upward links. This is due to the limitation of the protocol interference model which employs a binary decision of existence of radio interference based on a circular region.

When we compare the false positive rate and the false negative rate between upward links and downward links, the values are slightly different. In this paper, since we assume a tree topology whose root is the gateway node of the wireless mesh network, the number of sender nodes in upward communication is larger than that in downward communication. For example, leaf nodes become sender nodes in the case of upward communication. Therefore, the interference relationships among links become more complex in upward communication, and the results between upward links and downward links become slightly different.

B. Evaluation of the Network Performance

We next evaluate the performance of wireless mesh networks when the protocol interference model with our proposed methods is used. As evaluation metrics of performance, we use the *number of time slots* and *gateway throughput*. The former metric is the number of time slots required by the greedy algorithm [2, 3], and indicates the efficiency of spatial reuse. The gateway throughput is the number of assigned time slots to the gateway node in a frame, and it represents communication efficiency between the wireless mesh network and the external wired network. For comparison, we also conduct simulations where a SINR-based time slot assignment algorithm is used (hereinafter, SINR coloring). SINR coloring checks to assign a time slot to a transmission link in an order that is determined by the greedy algorithm. If the SINR of all transmission links are over the capture threshold by assigning the time slot to the transmission link, the time slot is assigned to the transmission link. Otherwise, a new time slot is assigned to the transmission link. Although SINR coloring is a time slot assignment algorithm, we use it as a method to achieve an upper bound of performance.

Figure 5 shows the average number of time slots and the average gateway throughput with 99% confidence intervals from results for 100 topologies when $n = 100$. Since there are links that cannot be used simultaneously under the SINR model but can be assigned based on the conventional method with $\alpha = 2$, we only show results for the conventional method where α is set to 3 and 4. As shown in Fig. 5, both the number of time slots and the gateway throughput of our proposed methods are closer to the results for SINR coloring than of the results for the conventional method. Among our proposed methods, the results for the NINA method are the closest to the results for SINR coloring. Because the accuracy of the interference model of the NINA method is the highest as described in the previous subsection, time slots are efficiently assigned to the links and communication efficiency becomes higher. When we compare the number of time slots and the gateway throughput between upward links and downward links, the results are almost same.

C. Discussion of Practical Interference Ratio

When we consider the usefulness of radio interference models, the models should be used without the calculation

of SINR and time slot assignment. In particular, the interference ratio of the protocol model should be determined in advance. We call such previously decidable interference ratio the *practical interference ratio*. In this subsection, we investigate the practical interference ratio when all nodes use the same interference ratio, and evaluate the performance of wireless mesh networks with the practical interference ratio. Because the results for upward and downward links are similar, we only show the results for upward links.

We first conduct simulations of the ANA method and investigate the distribution of the adjusted interference ratio from 1000 topologies. The number of nodes n is set to 50, 70, 100, and 120. Although figures are not shown because of space limitations, the distribution of interference ratio becomes a normal distribution. The average and the standard deviation σ of the normal distributions are shown in Fig. 6(a). The maximum interference ratio is considered to be the average interference ratio plus $k\sigma$. The maximum interference ratio where $k = 4$ and $k = 5$ are also shown in Fig. 6(a). As shown in Fig. 6(a), the maximum interference ratio has a similar value for any number of nodes. Therefore, we use the average of the maximum interference ratios as the practical interference ratio in the following. In particular, we use 2.1 and 2.2 as the practical interference ratio in the case of $k = 4$ and $k = 5$, respectively.

Figure 6(b) shows the average number of time slots from the results for 100 topologies when the protocol interference model with the practical interference ratio is used. For comparison, we also show the results for the ANA method and SINR coloring. As shown in Fig. 6(b), the number of time slots using the practical interference ratio is greater than that of SINR coloring and the ANA method. In addition, the number of time slots using the practical interference ratio is 16% and 20% higher than that of ANA method when $k = 4$ and $k = 5$, respectively. This means that the accuracy of the protocol interference model using the practical interference ratio is less than that of the ANA method. However, by using the practical interference ratio, it is not necessary to calculate SINR or time slot assignment.

VI. Conclusions

To devise an accurate radio interference model, we proposed three methods, namely, ANA, AINA and NINA, for adjusting the interference ratio parameter of the protocol interference model, taking into consideration SINR. Through simulations, we showed that the NINA method achieves the highest accuracy. In addition, we found that the performance was highest in the case of a wireless mesh network based on the NINA method, among the proposed methods and the conventional method. Furthermore, we discussed the practical value of the interference ratio, which can be set without calculation of SINR and time slot assignment.

In future work, we plan to consider heterogeneous and dynamic cases where the transmission power of nodes is different and SINR is affected by Rayleigh fading and shadowing effect. In addition, we should take into account hop-based interference models, which are widely used in practical wireless networks, such as IEEE 802.16j networks. We plan to compare and investigate the relationships among the protocol interference model, the SINR model and the hop-based interference model.

Acknowledgments

This work was partly supported by KAKENHI (21700075) of MEXT, Japan.

References

[1] I. F. Akyildiz, X. Wang, and W. Wang, "Wireless mesh networks: a survey," *Computer Networks*, vol. 47, pp. 445–487, Mar. 2005.

[2] W. Wang, Y. Wang, X.-Y. Li, W.-Z. Song, and O. Frieder, "Efficient interference-aware TDMA link scheduling for static wireless networks," in *Proceedings of ACM MobiCom 2006*, pp. 262–273, Sep. 2006.

[3] R. Ishii, G. Hasegawa, Y. Taniguchi, and H. Nakano, "Time slot assignment algorithms in IEEE 802.16 multi-hop relay networks," in *Proceedings of ICNS 2010*, pp. 265–270, Mar. 2010.

[4] Z. Tao, A. Li, K. H. Teo, and J. Zhang, "Frame structure design for IEEE 802.16j mobile multihop relay (MMR) networks," in *Proceedings of IEEE GLOBECOM 2007*, pp. 4301–4306, Nov. 2007.

[5] P. Gupta and P. R. Kumar, "The capacity of wireless networks," *IEEE Transactions on Information Theory*, vol. 46, pp. 388–404, Mar. 2000.

[6] Y. Shi, Y. Hou, J. Liu, and S. Kompella, "How to correctly use the protocol interference model for multi-hop wireless networks," in *Proceedings of ACM MobiHoc 2009*, pp. 239–248, May 2009.

[7] D. Son, B. Krishnamachari, and J. Heidemann, "Experimental study of concurrent transmission in wireless sensor networks," in *Proceedings of ACM SenSys 2006*, pp. 237–250, Nov. 2006.

[8] A. Chockalingam, M. Zorzi, L. B. Milstein, and P. Venkataram, "Performance of a wireless access protocol on correlated Rayeigh fading channels with capture," *IEEE Transactions on Communications*, vol. 46, pp. 644–655, May 1998.

[9] R. Maheshwari, S. Jain, and S. R. Das, "A measurement study of interference modeling and scheduling in low-power wireless networks," in *Proceedings of ACM SenSys 2008*, pp. 141–154, Nov. 2008.

[10] H. Zhu and K. Lu, "On the interference modeling issues for coordinated distributed scheduling in IEEE 802.16 mesh networks," in *Proceedings of BROADNETS 2006*, Oct. 2006.

[11] O. Goussevskaia, Y. A. Oswald, and R. Wattenhofer, "Complexity in geometric SINR," in *Proceedings of ACM MobiHoc 2007*, pp. 100–109, Sep. 2007.

[12] M. Zorzi and R. R. Rao, "Capture and retransmission control in mobile radio," *IEEE JSAC*, vol. 12, pp. 1289–1298, Oct. 1994.

 ISBN: 978-1-61208-123-6

Impact of Scheduling and Buffer Sizing on TCP Performance over IMT-Advanced

Kunimasa Kakuda
Graduate School of Computer Science
and Systems Engineering
Kyushu Institute of Technology, Fukuoka, Japan
Email: kakuda@infonet.cse.kyutech.ac.jp

Masato Tsuru
Network Design Research Center,
Kyushu Institute of Technology, Fukuoka, Japan
Email: tsuru@ndrc.kyutech.ac.jp

***Abstract*—IMT-Advanced is gaining much attention as the next-generation mobile communication technology. In this study, we evaluate the TCP throughput performance of mobile users competing on an IMT-Advanced shared downlink via a network simulation by using realistic environmental parameters. Our focus is on evaluating the impact of two basic types of time-frequency scheduling in which not only a time-varying wireless condition is used but also a frequency-block-dependent wireless condition of each user is exploited using various buffer sizes at radio base stations and various user moving speeds. We investigated the subtle tension between the scheduling, buffer sizing, and user moving speed for the TCP throughput. Our results imply that more TCP awareness is necessary for sharing the large bandwidth of IMT-Advanced downlinks more efficiently.**

***Keywords*-IMT-Advanced, TCP throughput, MaxCIR scheduler, Proportional Fair scheduler**

I. INTRODUCTION

Recently, mobile communications have expanded rapidly worldwide. Third-generation mobile communication systems (3G), including wideband code division multiple Access (W-CDMA) and high-speed packet access (HSPA) are now being used. Moreover, cellular-phone-oriented mass contents and individual user-data traffic are increasing in conjunction with each other every year. Therefore, the demand for high-speed mobile communications is currently increasing. Subsequently, the international mobile telecommunication-Advanced (IMT-Advanced) known as 4G, which attains improvement in communication speed, is also gaining much attention [1]. To achieve high-speed wireless access, IMT-Advanced would need a wireless bandwidth wider than the 5 MHz of the wireless bandwidth of W-CDMA.

Generally, because the wireless condition of each user, i.e., mobile station (MS), varies in time because of the interference, fading, or the movement of the MS, the shared wireless channel for downlink access is divided into fixed-length time slots at every transmission time interval (TTI). A scheduler at the radio base station (BS) allocates individual time slots to MSs that depend on the wireless condition of each MS and by using feedback information from each MS to each BS. Furthermore, in order to utilize the wider bandwidth efficiently, the entire bandwidth is divided into smaller bandwidths (i.e., frequency blocks or *subchannels*); and *time-frequency scheduling* assigns each subchannel to one MS at each time slot, whereas traditional *time scheduling* assigns the entire bandwidth to one MS for every time slot. A subchannel assignment in a wireless link with time-frequency scheduling is illustrated in Fig. 1, where different colors/patterns denote different users (MSs).

The transmission control protocol (TCP) is a dominant transport-layer protocol for end-to-end reliable data transfer, and most of the Internet applications rely on TCP. However, because TCP adaptively controls its sending rate of IP datagrams in response to datagram losses and delay-time variations, its throughput characteristic is highly sensitive to diverse factors, and is difficult to estimate its throughput characteristic analytically when the network condition varies dynamically (e.g, [2]) . On IMT-Advanced environments, the performance of TCP-based applications such as file transfer is expected to be greatly affected by both configurable conditions, such as the type of scheduling mechanism and the buffer sizing of the BS; and environmental conditions, such as the delay time of a core network and the moving speeds of MSs. Therefore, it is indispensable to conduct the evaluation and investigation of the TCP throughput performance of competing mobile users quantitatively.

Performance evaluation of IMT-Advanced communications using network simulators have begun to get more attention (e.g., [3]). However, for TCP flow-level performance of competing mobile users in IMT-Advanced via realistic network simulations, little is found in the literature. In our previous work [4], the TCP performance in the Evolved UTRA and UTRAN environments by using time scheduling and time-frequency scheduling was evaluated using a network simulation by employing realistic packet-error patterns. Building upon that work, here we examine the TCP performance in the new IMT-Advanced environments by using typical time-frequency schedulers (i.e., MaxCIR and Proportional Fair schedulers). Our focus is on evaluating the subtle tension between the scheduling, buffer sizing, and user moving speed for the TCP throughput.

The rest of this paper is organized as follows. In Section II, we introduce two typical scheduling algorithms. Section III explains our network simulation settings for large (continuous) file downloads, and the simulation results are investigated in terms of the impact on the base-station buffer size in Section

 ISBN: 978-1-61208-123-6

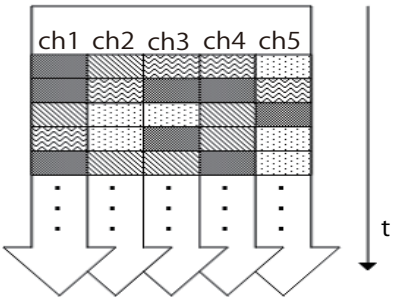

Fig. 1. Subchannel assignment in time-frequency scheduling

IV and the user moving speed in Section V. Concluding remarks are presented in Section VI.

II. Time-Frequency Scheduling in IMT-Advanced

We briefly explain time-frequency scheduling on downlinks in IMT-Advanced involving the BS, the MS, and their interactions. When the BS receives an IP datagram as a service data unit (SDU) from the upper link (i.e., the Internet), it divides the IP datagram into fixed-size small radio link control (RLC) protocol data units (PDUs).

Before being sent to the MS, each PDU is queued to an individual buffer dedicated to each destination user (i.e., MS) before being sent to the MS. Each individual user buffer consists of a transmission buffer and a retransmission buffer. The number of PDUs transmitted at TTI in a subchannel depends on the achievable transmission rate that is determined using the modulation and coding scheme (MCS). The MCSs used in our simulation are shown in Table I, where the right-most column *Transmission Rate* indicates the achievable transmission rate in the entire bandwidth and not in each divided subchannel. If a PDU is damaged during transmission and cannot be fully decoded by the destination user, the original PDU is moved to the retransmission buffer, which is preferentially sent compared with the normal PDUs in the transmission buffer. In our simulation (Section III), to reduce multiple retransmissions, we use a hybrid automatic repeat request (ARQ) with packet combining [5] as a retransmission scheme, which can combine the retransmission PDU with the previously received erroneous PDUs for effective decoding.

At each TTI and for each subchannel, the BS selects one preferable user and one MCS is adopted for sending PDUs to the selected user. This selection is based on the instantaneous wireless conditions, i.e., the single-to-interference plus back ground noise ratio (SINR), of individual users, which are reported by the channel-state information (CSI) feedback from each user to the BS with some delay (e.g., $3\times$TTI). In our simulation, a mapping from every pair of an SINR value and a sending rate (MCS) to the block error rate, which is the error probability of transmitting PDUs within current TTI, is prepared beforehand. Note that this delay of the SINR value feedback may cause an inaccurate estimation of the current wireless condition, and thus, may result in the improper selection of both, the user to whom data has to be sent and the MCS to be used.

TABLE I
MCS Table

MCS	Modulation Scheme	Encoding Ratio	Transmission Rate [Mb/s]
1	QPSK	1/8	15.128
2	QPSK	1/4	30.344
3	QPSK	1/2	60.8
4	QPSK	2/3	81.04
5	16QAM	1/2	121.76
6	16QAM	2/3	162.32
7	64QAM	1/2	182.64
8	64QAM	2/3	243.6
9	64QAM	3/4	274

Hereinafter, we briefly introduce two typical schedulers that were used in this study. Although those schedulers are simple and some modified or compound versions may be used in commercial services, these fundamental schedulers are of practical importance for designing more complex schedulers. To describe the scheduling, we use a user-selection metric $M_{m,c}(n)$ at time-slot n in subchannel c for user m; this means that the user m who has the highest $M_{m,c}(n)$ is selected in c at n. If more than one user has the same highest value of $M_{m,c}(n)$, a user is randomly selected from these users.

The maximum carrier-to-interference power ratio (MaxCIR) scheduler maximizes the system throughput by selecting a user who has the best wireless condition in the subchannel for that particular time slot. In this study, the usage of the achievable transmission rate $R_{m,c}(n)$ as the wireless condition leads to the following user-selection metric:

$$M_{m,c}(n) = R_{m,c}(n). \tag{1}$$

The Proportional Fair (PF) scheduler (e.g., [6]) provides a good trade-off between maximizing the system throughput and satisfying fairness among users. The PF scheduler in time scheduling can be easily implemented so as to preferentially select a user who has not been served sufficiently in the past (i.e., with a low time-averaged throughput), who has a good wireless condition at that particular time (i.e., with a high achievable transmission rate), and who is proven to approximately fulfill the proportional fairness. However, optimal time-frequency (multi-carrier) PF scheduling is computationally complex, and a number of low-complexity algorithms have been proposed (e.g., [7], [8]) to achieve near-optimal performance. In this study, among these time-frequency PF schedulers, we adopt the conventional multi-carrier proportional fairness scheduling (MC-PFS) algorithm [7], which is a simple extension of the time PF scheduler and is easy to deploy. The user selection metric is formulated as follows:

$$M_{m,c}(n) = \frac{R_{m,c}(n)}{T_m(n)}, \tag{2}$$

where the time-averaged throughput of a user m before a time-slot n is denoted by $T_m(n)$, and is updated according to the following equation in which $\delta_{m,c}$ equals 1 if user m is the selected user at the time slot n in subchannel c, and equals 0

 ISBN: 978-1-61208-123-6

otherwise:

$$T_m(n+1) = (1-\frac{1}{L})T_m(n) + \frac{1}{L}\sum_c R_{m,c}(n)\delta_{m,c}(n), \quad (3)$$

$$L = \min(n, t_a),$$

where t_a is a time-scale parameter that represents the number of time slots used for averaging the past throughput.

III. Simulation Model

The simulation model is illustrated in Fig. 2, which is implemented using the network simulator NS-2 (ver. 2.27) with an extended link layer module of the shared wireless downlink we developed. The transmission rate of the wired access links (Source–R) is 1 Gb/s, and propagation delays are set from 1 ms to 5 ms at random to prevent TCP synchronization. The transmission rate of the core link (R–BS) is 1 Gb/s, and propagation delay is set to 10 ms. The shared wireless link from the BS to the MSs of the 80 MHz bandwidth is divided into 400 subchannels in the frequency domain, and is also divided into many time slots with a TTI of 1 ms in the time domain. According to the MCS, the total transmission rate of all subchannels ranges from 15.128 Mb/s to 274 Mb/s (Table I). The actual transmission rate per subchannel can be obtained by dividing it by 400. The data-propagation delay between the BS and each MS, including the processing delay, is 1.75 ms, and the CSI feedback delay from each MS to the BS is 3 TTI (3 ms). We assume that the uplink is error free. Thus, neither data (TCP ACKs) nor signaling (CSI feedbacks) are ever lost or degraded.

The time series of the wireless condition, i.e., SINR, on the link from the BS to each MS in each subchannel at each TTI is given in advance; the time series data is created on the basis of the position (distance from the BS) and the moving speed of the MSs under the 6-path GSM typical urban multi-path model when considering realistic environments. We use data for 30 users distributed around a BS in a signal cell; according to the distance from the BS (from near to far), the users are divided into 10 groups of three users each, implying that the users are roughly sorted by the order of the time-averaged wireless condition (from good to bad) and grouped. User (group) ID-1 is assigned to the nearest group, and ID-10 is assigned to the farthest group. In each simulation trial, we choose one user from each group randomly and conduct the simulation with these 10 selected users.

As shown in Fig. 2, ten TCP flows from Sources (servers on the Internet) to Destinations (MSs) are established in parallel, and each Source sends a large file in 60 s. The starting time of each flow is randomly selected and ranges from 0 to 2 s. Other simulation parameters are listed in Table II.

We use the "user throughput" U_m as a performance index for user m; it is a time-averaged throughput that is formulated as follows:

$$U_m[b/s] = \frac{b_m[bit]}{t_m[s]}, \quad (4)$$

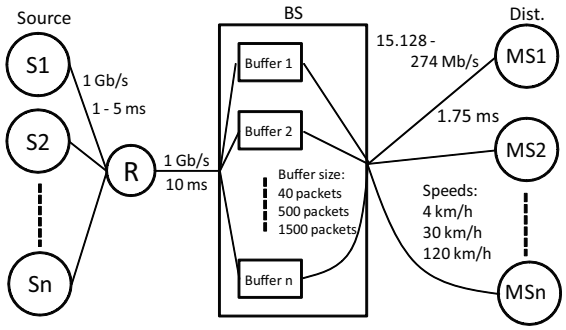

Fig. 2. Simulation topology

TABLE II
Simulation Parameters

Parameter	Value
TCP algorithm	New Reno + Sack
TCP packet size	1500 bytes (including IP header)
RLC PDU size (payload + header)	40 bytes + 2 bytes
Max. num of retransmissions	10
Individual buffer size	40,500,1500 packets
TTI	1.0 ms
subchannel bandwidth	200 kHz
Num of subchannels	400

where b_m is the number of received bits of the file of user m at the destination, and t_m is the file-transfer time (from the starting time to 60 s).

Then, "active time ratio" is defined as:

$$active\ \ time\ \ ratio = \frac{a_m[s]}{t_m[s]} \quad (5)$$

where a_m is the sum of the time period during which user m has at least one PDU in the individual buffer on BS.

In addition, the "selection ratio" and "retransmission ratio" are defined as follows:

$$selection\ \ ratio = \frac{s_m}{\sum_{m=1}^{M}(s_m)}, \quad (6)$$

$$retransmission\ \ ratio = \frac{r_m}{u_m}, \quad (7)$$

where s_m is the number of selections of user m, r_m is the number of retransmission PDUs for user m, and u_m is the number of PDUs sent to user m.

IV. TCP Throughput with Varying Buffer Size

We investigate the TCP performance for large file downloads at various buffer sizes (40, 500 and 1500 packets) of individual buffers on the BS.

A. Performance of MaxCIR Scheduler

The user throughputs of 10 individual users (and their average) and the selection ratio are illustrated in Figs. 3 and 4, respectively, by using MaxCIR at each buffer size of all BSs. To maximize the system throughput, the MaxCIR scheduler selects User 1 frequently because it is likely that User1 is the best wireless-condition user among 10 users. In fact, in the case of the buffer size of 500 packets shown in Fig. 4, the selection ratio of User 1 is extremely high; moreover,

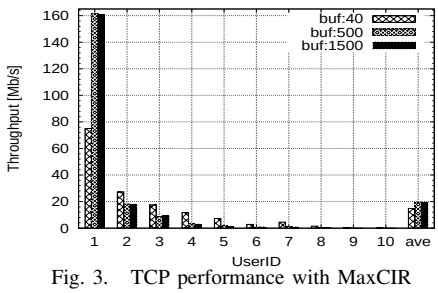

Fig. 3. TCP performance with MaxCIR

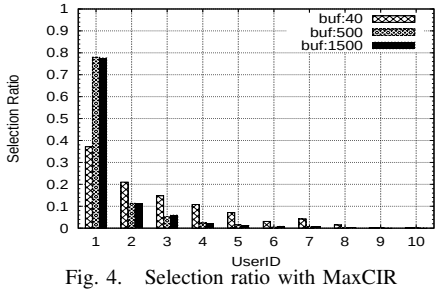

Fig. 4. Selection ratio with MaxCIR

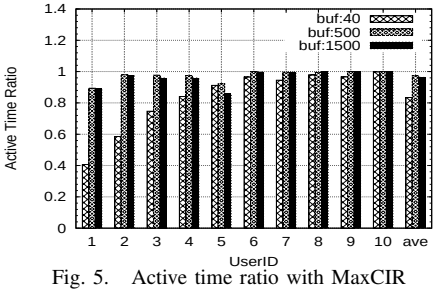

Fig. 5. Active time ratio with MaxCIR

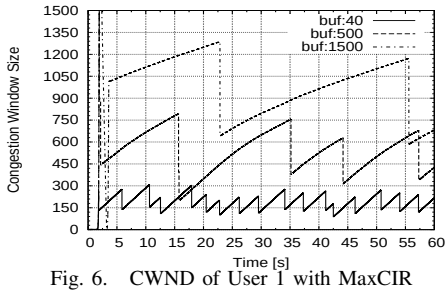

Fig. 6. CWND of User 1 with MaxCIR

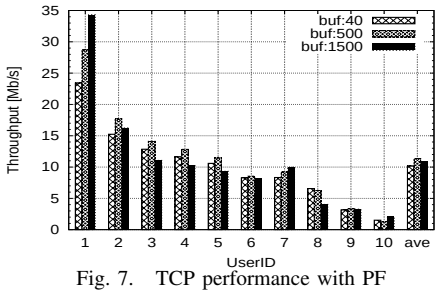

Fig. 7. TCP performance with PF

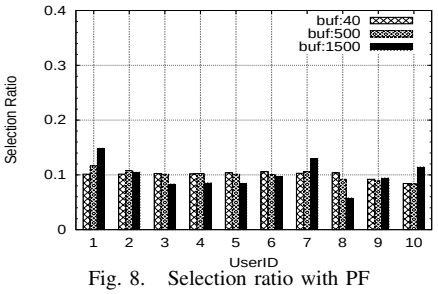

Fig. 8. Selection ratio with PF

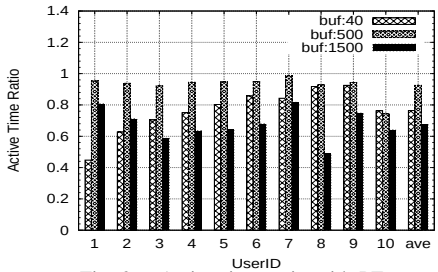

Fig. 9. Active time ratio with PF

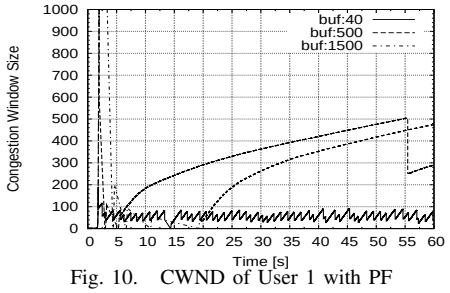

Fig. 10. CWND of User 1 with PF

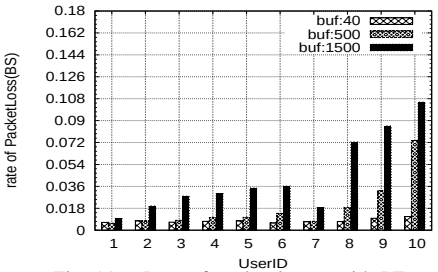

Fig. 11. Rate of packet losses with PF

TABLE III
AVERAGED RTT AND TCP-BANDWIDTH OF USER 1 FOR EACH BUFFER SIZE

buffer size	40 packets	500 packets	1500 packets
RTT	28 [ms]	37 [ms]	65 [ms]
TCP-bandwidth	86 [Mb/s]	175 [Mb/s]	183 [Mb/s]

as the User ID increases, the selection ratio decreases. The high achievable transmission rate and the high selection ratio directly lead to the superior throughput of User 1, as shown in Fig. 3.

However, on comparing the different buffer sizes, this tendency considerably weakens in the case of a shorter buffer size of 40 packets while the tendency remains in the case of a larger buffer size of 1500 packets. The average throughput over all users is also decreased in the case of 40 packets and unchanged in the case of 1500 packets. In order to clarify this tendency, the active time ratio is examined, as shown in Fig. 5. In the case of 40 packets, the active time ratio of User 1 is approximately 40% while in the cases of 500 and 1500 packets, the active time ratios are maintained at approximately 90%. In other words, by using a short buffer size of 40 packets, in approximately 60% of the total time slots, User 1 has no PDU at the BS to be transmitted. Therefore, another user could be selected even if the wireless condition of User 1 is considerably better than that of the selected user, resulting in an increase in throughputs of Users 2-8 in the case of a 40 packet buffer. From Fig. 5, a buffer size of 500 packets is so efficient that it can keep the active time ratio ≈ 1 for all users.

To investigate the reason why the active time ratio of User 1 in the case of 500 packets is much higher than that of 40 packets while it is equivalent to that of 1500 packets, a sample of the time variation of the TCP congestion window size (CWND) of User 1 is shown in Fig. 6. Note that the TCP CWND is a variable and is used to adaptively control the number of allowable in-flight packets at Sender. This figure indicates that the TCP CWND in the case of 500 packets is much higher than that in the case of 40 packets because of a reduction in the IP datagram losses at the buffer on the BS. In other words, a buffer size of 40 packets is so small (for a possible TCP throughput of User 1) that it often causes packet losses at User 1's buffer, limits the TCP CWND, and often makes the buffer empty. Conversely, a buffer size of 500 packets is sufficient to increase the TCP CWND for maintaining a non-empty buffer.

Similarly, the TCP CWND in the case of 1500 packets is much higher than that in the case of 500 packets. However, between the cases with buffer sizes of 500 and 1500 packets, the active time ratio, and thus, the user throughput remain unchanged. In fact, the average round-trip time (RTT) and TCP-bandwidth of User 1 for each buffer size are summarized in Table III, where the "TCP bandwidth" denotes the size of the time-averaged CWND in bytes divided by the time-averaged RTT, implying the time-averaged TCP sending rate.

 ISBN: 978-1-61208-123-6

A larger buffer size of 1500 packets only causes a longer RTT rather than a higher TCP bandwidth. This implies that User 1's TCP bandwidth approaches the wireless bandwidth available to User 1.

B. Performance of PF Scheduler

Throughputs of individual users and their average, and selection ratio are illustrated in Figs. 7 and 8, respectively, with the PF scheduler at each buffer size on the BS. Because the PF scheduler selects users in a fair fashion, in contrast to the MaxCIR case, the selection ratio does not differ much among the users and tends to be 0.1 (implying to be shared evenly), as shown in Fig. 8. The user-throughput balance is expected to approximate the proportional fairness if each user buffer is not empty for all of the time. At least the throughput balance tends to be milder compared with the MaxCIR case at the expense of a lower (approximately halved) user average throughput (i.e., a lower system throughput).

On comparing the different buffer sizes, the impact on the user throughputs is more complicated than the MaxCIR case discussed in the previous subsection. As the buffer size increases from $40, 500, to 1500$ packets, the throughput of User 1 monotonically increases. In contrast, for most users such as Users 2–6, the throughput with a buffer size of 500 packets is the highest among the examined buffer sizes. The average of all user throughputs is also maximized in the case with a 500-packet buffer size. In terms of the active time ratio shown in Fig. 9, for all users, a buffer size of 500 packets is the best case (i.e., closest to one) compared with the other buffer sizes, i.e., 40 and 1500 packets. This implies that the case of the 500-packet buffer size exhibits mostly expected behavior in terms of the proportional fair scheduling.

In further investigation, the subtle impacts of buffer sizing can be observed. For example, in terms of the selection ratio shown in Fig. 8, the selection ratio of User 1 with a 500-packet buffer size is higher than that with a 40-packet buffer size. Accordingly, the throughput of User 1 is improved. A sample of the time-variation in the TCP CWND of User 1, as shown in Fig. 10 indicates that the TCP CWND with a buffer size of 500 packets is much higher than that with a buffer size of 40 packets. In contrast, despite the fact that the selection ratios of Users 3–6 with a 500-packet buffer size were unchanged (or slightly reduced) from those with a 40-packet buffer size, the throughputs with a 500-packet buffer size are higher. Figure 9 implies a possible reason. The active time ratios of Users 3–6 in the case of a 40-packet buffer size are clearly lower than those in the case of a 500-packet buffer. In the case of a 40-packet buffer, because PF scheduler tends to maintain the selection ratio evenly, Users 3–6 are likely to be selected even if their wireless condition is unsuitable. This results in a lower transmission rate and a higher retransmission rate. In contrast, by using a buffer size of 500 packets, because of higher active time ratios, users could be selected at a better wireless condition.

On the other hand, comparing the cases of a 500-packet buffer and a 1500-packet buffer, the selection ratios of Users 1, 7, and 10 in the case of a 1500-packet buffer are considerably higher than those in the case of a 500-packet buffer. Accordingly, those users' throughputs are higher in the case of a 1500-packet buffer while those of the other users are lower in that case. In particular, Users 3–5 and 8 suffer from a considerable reduction. Figure 9 implies a possible reason. For all users, the active time ratios in the case of a 1500-packet buffer are lower than those in the case of a 500-packet buffer. However, the reduction in User 1 is smaller than the reductions in Users 3–5 and 8. Those active-time-ratio reductions might result from packet losses at the buffers on the BS because of a mismatched buffer sizing. A sample of the time variation of the TCP CWND of User 1 (Fig. 10) indicates that the CWND with a 1500-packet buffer size is decreased from that with a 500-packet buffer size because of the increasing IP-datagram losses. In fact, as shown in Fig. 11, the packet loss rate at the individual buffer on the BS increases for every user when the buffer size is changed from 500 packets to 1500 packets. In addition, while User 1's degradation is small, those of Users 3–5 and 8 are significant. Those unnecessary packet losses in the case of a 1500-packet buffer cause imbalance and inefficient behavior of the PF scheduler.

V. TCP Throughput with Varying Moving Speed

We investigate the TCP performance for large file downloads at various moving speeds (3, 30, and 120 km/h) of users, i.e., MSs, in which all 10 users move at the same speed. Note that, in our settings, each MS does not really move to experience a different average wireless condition (i.e., a different distance from the BS) in the cell. Instead, a different moving speed means to choose a different variation in the SINR because of a different Doppler frequency. In other words, each MS is assumed to move along a circle around the BS. The buffer size is set to 500 packets.

On comparing the different moving speeds, it is noted that most users' throughputs and the average decrease as the moving speed increases. More precisely, with the MaxCIR scheduler, as shown in Fig. 12, the throughput of User 1 is strongly reduced at a higher moving speed while the throughput of another user may have the potential to be improved if its selection ratio increases because of the reduction of User 1's active time. On the other hand, by using the PF scheduler, as shown in Fig. 13, the degradation equally appears in each user's throughput because the scheduler tends to maintain the selection ratio evenly.

In order to investigate the reason for this throughput reduction, a sample of the time series of the SINR value averaged over all 400 subchannels for User 1 is examined in Fig. 14, which simply indicates that the SINR is worse (lower) and more rapidly variable at a higher moving speed. The distribution of the selected MCS number for User 1 is illustrated in Fig. 15, where a higher MCS number indicates a better wireless condition. This figure indicates that the number of PDUs transmitted in a higher MCS number decreases and in a lower MCS number increases, as the moving speed increases. This is the first reason for the decrease in user throughputs.

 ISBN: 978-1-61208-123-6

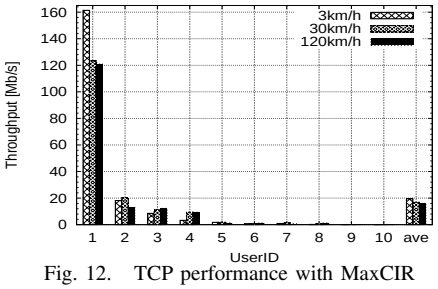

Fig. 12. TCP performance with MaxCIR

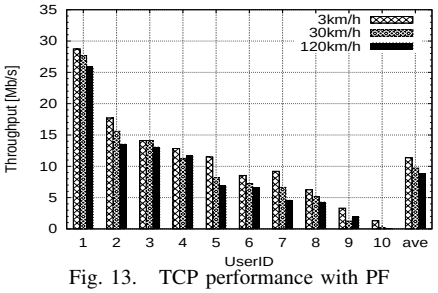

Fig. 13. TCP performance with PF

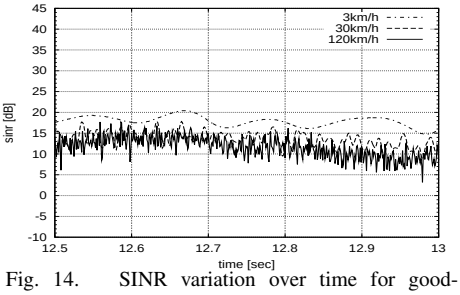

Fig. 14. SINR variation over time for good-condition user (User 1)

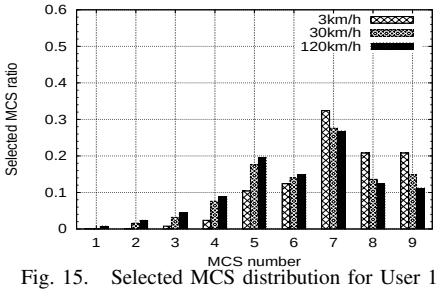

Fig. 15. Selected MCS distribution for User 1

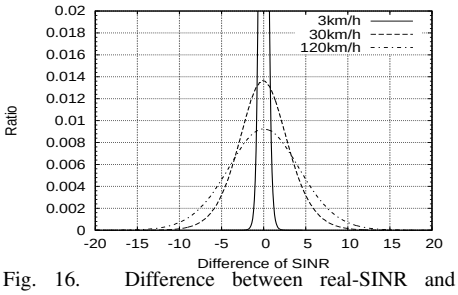

Fig. 16. Difference between real-SINR and advertised-SINR

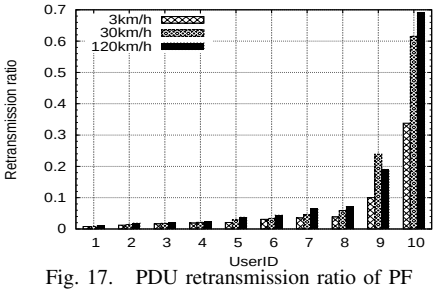

Fig. 17. PDU retransmission ratio of PF

Furthermore, the difference between the real SINR, which directly affects the error rate of the transmitted PDUs, and the advertised SINR, which is reported by CSI feedback and used to select an optimal transmission rate, i.e., an MCS number, is examined, as shown in Fig. 16. This figure indicates that as the moving speed increases, the difference between the real SINR and the advertised SINR increases because of the rapid variation of the SINR; that is, the MCS number selection at the BS based on the advertised SINR is frequently misestimated. In fact, we found that the retransmission ratio increases as the moving speed increases, as shown in Fig. 17. This is another reason for the decrease in user throughputs.

VI. Concluding Remarks

The contribution of this work is two-fold. First, we have evaluated the quantitative TCP throughput performance of individual users on IMT-Advanced by using two typical schedulers with various user moving speeds via realistic network simulations, regarding which little is found in the literature. When 10 users with diverse distances from the BS are competing for the IMT-Advanced shared downlink, the MaxCIR scheduler doubles the total TCP throughput over 10 users compared with PF scheduler, while it allows an extreme imbalance among the users.

Second, we have investigated a subtle tension between the scheduling and buffer sizing for the TCP throughput. We found that the large bandwidth of the IMT-Advanced downlink is not fully utilized by TCP flows. This inefficiency mainly results from the fact that the active time ratio (namely, the probability that at least one PDU is held in the user's individual buffer on the BS and is ready to consume the shared link bandwidth) of each user is lower than one and sometimes even lower, which strongly depends on the user's wireless condition, scheduling, and buffer sizing.

To make the process more efficient, there may be two directions to take. One is to improve the TCP rate-control mechanisms with an awareness of mobile wireless networks, and the other is to improve scheduling with an awareness of TCP flows. For the first direction, because a number of TCP variants have already been proposed for high-speed large-delay and/or wireless networks, we are preparing to investigate the performance of them over IMT-Advanced. Conversely, for the second direction, one simple idea is to change the individual buffer sizes on the BS adaptively and automatically. We will investigate this idea in future work.

The present work was supported in part by the JSPS KAKEN-HI (S) (18100001) and NTT DoCoMo Inc.

References

[1] Press Release: ITU-R IMT-Advanced 4G standards to usher new era of mobile broadband communications. http://www.itu.int/net/pressoffice/press_releases/2010/40.aspx, October 2010.

[2] M. Choon and R. Ramjee: TCP/IP performance over 3G wireless links with rate and delay variation. Proc. Intl. Conf. on Mobile Computing and Networking (Mobicom'02), pp. 71– 82, September 2002.

[3] S. Max, D. Bueltmann, R. Jennen, and M. Schinnenburg: Evaluation of IMT-Advanced scenarios using the open Wireless Network Simulator. Proc. ICST SIMUTools'10, 10 pages, March 2010.

[4] M. Hirose, M. Uchida, M. Tsuru, and Y. Oie: TCP Performance over Evolved UTRA and UTRAN with Time-Frequency Scheduling. Proc. Intl. Conf. on the Latest Advances in Networks (ICLAN 2008), 6 pages, December 2008.

[5] N. Miki, H. Atarashi, S. Abeta, and M. Sawahashi: Comparison of throughput employing Hybrid ARQ packet combining in forward link OFCDM broadband packet wireless access, IEICE Trans. Commun., E88-B(2):594-603, February 2005.

[6] A. Jalali, R. Padovani, and R. Pankaj: Data Throughput of CDMA-HDR a High Efficiency-High Data Rate Personal Communication Wireless System, Proc. IEEE VTC 2000 Spring, pp. 1854-1858, May 2000.

[7] S. Yoon, Y. Cho, C.B. Chae, and H. Lee: System Level Performance of OFDMA Forward Link with Proportional Fair Scheduling, Proc. IEEE PIMRC 2004, pp. 1384-1388, September 2004.

[8] A. Dominguez, J. Luo, R. Halfmann, and E. Schulz: Parameter Controlled Fairness Enhancement in an OFDMA System, Proc. 8th World Wireless Congress, May 2007.

 ISBN: 978-1-61208-123-6

Performance Study for End-point Links of Networks

Eleftherios Stergiou, Spyridoula V. Margariti
Department of Informatics and Telecommunications Technology
ATEI of Epirus, Arta, Greece
ster@art.forthnet.gr , smargar@teiep.gr

Gerasimos C. Meletiou, George E. Rizos and Dimitrios C. Vasiliadis
Network Operations Center
ATEI of Epirus,
Arta, Greece
gmelet@teiep.gr, georizos@teiep.gr, dvas@teiep.gr

***Abstract*—The rapid deployment of networks in various environments demands accurate, efficient measurement in order to estimate path links. In this work, we considered the challenges posed by broadband networks for available bandwidth capacity evaluation. We focused on rate, using token bucket in cable modem end link with non-FIFO scheduling, and on burstiness type of traffic applied by multi-rate end-links in wireless network that follows the IEEE 802.11 protocol. We used a software tool for estimating the path rate capacity and we found that raw links and the corresponding token bucket rates were calculated in a quick and accurate manner. The accurate prediction of the available bandwidth in an end-point network link can help to avoid traffic bottlenecks, server choice, and overlay networks.**

Keywords - end-point links; cable links; wireless links; throughput; performance evaluation.

I. INTRODUCTION

As the Internet grows in size and connection complexity, new application and services requirements necessitate the performance analysis of network paths using either some estimation techniques or developing appropriate software tools for monitoring and measuring the properties of end-to-end paths. In the context of performance evaluation the *available bandwidth* of a point-to-point path is a metric of crucial interest in packet switched networks and is therefore the key in studying network management, server selection, routing, and other network issues.

At previous works in literature, some performance metrics which referred to end-to-end paths have already been estimated. Some papers assume simple models of network links [1]. For example, Strauss et al. [1] admits that the narrow links -the links with the minimum capacity among all links- and the tight links –the links with the minimum available bandwidth among all links- along a specific path have a well-defined raw bandwidth that shows the rate at which bits can be traversed via the link. However, some of these assumptions used by the traditional model do not work with access networks like cable modem and wireless 802.11 [15], [16]. This discrepancy may be happen due to any of the following reasons:

(a) A network end link is likely to appear as variable values of row bandwidth because of the token-bucket rate regulation (like cable modem links). A similar behaviour can be noticed in wireless 802.11 end links, which appear as various multi-rates schemas.

(b) The packets may not be delivered via first input first output (FIFO) policy.

(c) Wireless 802.11 links may experience interference from high cross-traffic.

By this work, the challenges posed by broadband networks to existing capacity estimation techniques were identified. Many experiments for *available bandwidth* estimation of end-point links were done. The experiments demonstrated the impact of packet size on the maximum *achievable throughput* in wireless links. Finally, quantitative results revealed the effect of the multirate environment on the *available bandwidth*.

The paper has the following structure. In Section II, the basic performance definitions are presented and some related work is overviewed. In Section III, different types of network access and their characteristics of end-points are explained, while in Section IV the methodology of our experiments is outlined. Subsequently, in Section V the results of our experimental testbeds are reported, while Section VI provides the concluding remarks and outlines the future work.

II. BASIC DEFINITIONS- PREVIOUS WORK

A. Basic Definitions

Network path can be defined as any sequence of links, where a store-and-forward routing mechanism is used in order to transfer packets from one point (sender) to the other point (receiver). In our case study, each path is considered to be fixed and unique that implies no routing changes are applied in this path.

Link capacity (C_i in bps) at a specific link (i) is considered the maximum constant rate of bits that can be applied on this link when it is empty.

End-to-end link capacity (C in bps) of a path p is defined as the maximum rate of bits that can be applied at the path p when no other traffic is concurrently applied on this path C is therefore assumed the maximum rate that path p

 ISBN: 978-1-61208-123-6

can provide to a flow. Consequently, the e*nd-to-end link capacity* of a path *p* can be estimated as:

$$C = \min_{i=1...v} C_i \quad (1)$$

where *v* is the total number of links at the sequence of store-and-forward links of path *p*.

Available link bandwidth [$A_i^{\Delta t}(t_0)$ in bps] of a link (*i*) at the time interval $(t_0, t_0 + \Delta t)$ is defined as a fraction of the *link capacity* that has not been utilized during this time interval. Denoting the average utilization of a link (i) during the time interval $(t_0, t_0 + \Delta t)$ as $u_i^{(\Delta t)}(t_0)$ the corresponding available bandwidth of link can be expressed as:

$$A_i^{(\Delta t)}(t_0) = C_i[1 - u_i^{(\Delta t)}(t_0)] \quad (2)$$

In the same manner, the *end-to-end available bandwidth* $A^{(\Delta t)}(t_0)$ of a path *p* can be considered as the minimum available rate among all links in this path. Thus, the *end-to-end available bandwidth* of a path *p* expresses the maximum rate that can be provided to a flow, without shortening the bandwidth of the rest of the traffic in this path. Formally, it can be estimated as:

$$A^{(\Delta t)}(t_0) = \min_{i=1..v}\{C_i[1 - u_i^{(\Delta t)}(t_0)]\} \quad (3)$$

Finally, another two significant metrics in performance analysis are the following:

Narrow link is the link with the minimum capacity among all links in a path, expressing thus the capacity of the whole path.

Tight link denotes the minimum available bandwidth among all links of path, which is therefore an indicator of the path's available capacity.

B. Previous Work

In the last two decades many efforts have been devoted by researches for estimating the network capacity of access links. The performance calculations in [2],[3] were based on the packet pair principle. Thus, various techniques have been designed to avoid interference; e.g., in [4] in order to transmit a packet subsequence with variable packet sizes like trains' wagons have been proposed. Efforts like [5], [6] and [7] based on packet/train approach have also been addressed; all these efforts investigated the relationship among packet sizes and packet delays, as well.

Nowadays, the *available bandwidth* estimations are distinguished into two main approach classes. The first bandwidth estimation class addresses the packet rate methods, while the other class concerns the packet gap methodology. Regarding the related work the first estimation class methodologies were applied by [8][9][10][11], while studies as [1], [12] conducted the second one class.

A time based and per nodes approach for *available bandwidth* is presented by Sarr *et al.* in [14]. The analytical approach is based on some controversial assumptions. Moreover another new effort for *available bandwidth* estimation in IEEE 802.11 networks is presented in [19].

The first class of estimations (based on packet rate) watches the sequence packets' probes. When the packet transmitted rate exceeds the *available bandwidth* then the receiver rate became lower (in comparison with sender rate) and the probe packets tend to queue up, causing an increment in one way delay.

On the other side the second method of estimation's class (based on packet gap) transmit probes with equal-sized packets which are spaced apart depending the transmission time of the probes on the specific link. The increment of the packets' spacing is used for make approaching the volume of cross-traffic. In this case the spacing say the cross-traffic is subtracted from the capacity obtained by the yielded *available bandwidth*.

III. TYPES AND BASIC CHARACTERISTICS OF UNDER STUDY NETWORK ACCESS

We chose two typical cases of network access for study. One was the case of cable modems; the other was the wireless 802.11 case. Both extensively use typical access links. In the following paragraphs, we present four basic characteristics that are observed in broadband network access.

(1) *Link's Bandwidth.* Reversers consider that the link's bandwidth is the parameter that shows the bit rates that can be transmitted down to the link. Nevertheless, that is not true when a traffic regulation schema is used. The Internet service provider (ISP) can distribute a physical access link into smaller separate parts corresponding to the customers. So, the bandwidth divisions reveal that the traffic regulation schema is applied by ISP. With a cable modem, the token bucket technique is used; thus, the mean packet rate and maximum burst size in bytes is determined. It is noteworthy to distinguish the raw link bandwidth from maximum achievable packet rate.

(2*) Service order.* In classic performance studies, all packets have FIFO order for service distribution. As a result, the packets suffer from queuing, which increases delay. Nevertheless, in 802.11 accesses link, the stations access to broadband in a distributed fashion. Also, in cable modem case, the Cable Modem Termination System (the cable head) periodically distributes control messages assigned to various stations, inviting them to earn in unused slots. Hence, in both cases, the packet waiting among various stations would not be serviced in FIFO order.

(3) *Links with variable values of rates.* The wireless 802.11b employee radio links can operate at 1, 2, 5.5 end 11Mbps relative to the environmental conditions. Similarly, the 802.11a network operates between 6 and 54 Mbps. Different stations belonging to the same network can operate at different rates, although all stations share the same spectrum. This situation may cause cross-traffic to each station.

 ISBN: 978-1-61208-123-6

For the IEEE 802.11 [15], [16] distributed medium access protocol used in ad hoc networks the distributed functions are based on Carrier Sense Multiple Access with Collision Avoidance (CSMA/CA) principles. When an emitter gains access to the medium, the whole frame is transmitted. Collision detection by the sender is impossible in radio networks. Emitters are notified of good frame reception by the corresponding acknowledgment packet.

Network behavior may have an impact on the *available bandwidth* estimation technique. The estimation model works well when the cross-traffic matches the fluid model, which happens when the traffic is interspersed uniformly with the probe packets.

The address hidden nodes situation, an optional RTS/CTS mechanism, can be triggered. RTS/CTS exchange prior to transmission provokes a mechanism reservation in a one hop neighborhood of both peers. When receiving such a packet, a node considers the medium busy for the duration of the subsequent transmission. This technique is named *virtual carrier sense*.

A. Available Bandwidth Estimation

The *available bandwidth* depicts the rates at which a packet flow can be climbed without disturbing the existing traffic. Thus, the quantity of interest remains the *available bandwidth*. In the next Section we describe the methodology and the experimental testbeds.

IV. Methodology Of Experiments

A. Networks' Cases of Study

For our experiments, we chose two special networks. The first was the cable modem testbed and the other was the 802.11 a/b/g wireless access network.

- In the case of the cable modem as head-point, we used a CISCO universal broadband router 7200 series; as 'cable modem' on the other side, a ZyXEL Prestige 971M – external Cable modem was used [17]. On the head-point side we were able to obtain the link's values of traffic.
- The second testbed equipment had seven 802.11a/b/g stations working ad hoc in the same building area. The wireless configuration consisted of 6 PCs (2.8GHz Pentium 4 with 1024 MB RAM). All PCs were equipped wtth a Linksys WPC55AG 802.11a/g/b Wireless Adapter [18]. PC1 and PC6 ran the Pathrate tool in order to estimate the bandwidth metrics, while the other four nodes were used for generating cross-traffic.

  All the nodes were arranged to work in 802.11a and the link was set at 6 and 54 Mbps. We chose two of them for obtaining our measurements, as the other two produced cross-traffic.

B. Estimation Tools

We downloaded the source code from the Pathrate's site [13], along with the relevant documentation.

Pathrate is a measurement tool used for estimating the capacity of Internet paths. An important feature of Pathrate is that it is robust to cross traffic effects, meaning that it can measure the path capacity even when the path is significantly loaded. This is crucial, since the hardest paths to measure the heavily loaded ones. By this software tool the two most significant bandwidth metrics associated with end-to-end paths namely capacity and available bandwidth can be quickly estimated. Pathrate is publicly available with source code, documentation, and installation instructions.

We studied the available source code after making some small changes for better adaptation. We used this software for our experiments.

V. Experimental Results

Here we demonstrate the results. The first figure shows the results of data transmitted over the cable modem, while the second and the third depict the results concerning the 802.11 wireless access networks.

A. Results of Cable Link Access

In Fig. 1, the *available bandwidth* versus various levels of cross-traffic, which was estimated for cable modem downlink, is illustrated. We ran the Pathrate software, trying various values of cross traffic. For each value of cross traffic, the software returned two values of capacity, low and high.

By performing various experiments, we obtained values of *available bandwidth* (Fig. 1).

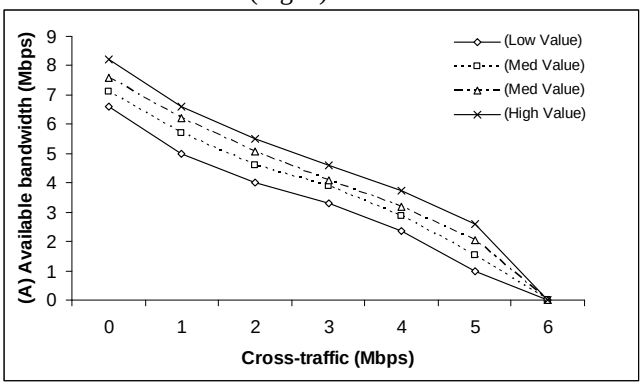

Figure 1. *Available bandwidth* versus *cross-traffic* in cable modem downlink in Mbps

According to Fig. 1, when the cross-traffic was absent, the bandwidth oscillated among the 6.6 and 8.2 Mbps. As the cross-traffic increased, the values of *available bandwidth* gradually decreased. In the limiting case of 6Mbps cross-traffic, the available traffic decreased to zero values.

B. Results of IEEE 802.11 Wireless Network

Like the packet transmission in 802.11, networks suffer when operations are significantly affected by the overhead of the packets. The minimum spacing among successive packets is considered overhead.

Experiments revealed that the packet size affected the maximum achievable *throughput*. Thus, the cumulative *throughput* was a little different when the payload used 300-bytes probe packets as opposed to 1000-bytes probe packets. As packets became bigger, we obtained higher values of cumulative bandwidth. We then created a series of

 ISBN: 978-1-61208-123-6

experiments with small-value sized packets (small probes) and another one with high value packets.

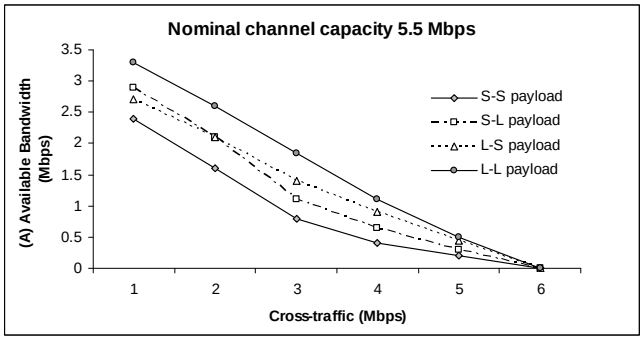

Figure 2. *Available bandwidth* versus *cross-traffic* in 802.11 access link with nominal channel capacity 5.5 Mbps

In Fig. 2, the *available bandwidth* versus various levels of cross-traffic, estimated for IEEE 802.11b wireless network access link runs at 5.5 Mbps, is illustrated.

The 'S-S payload' ('Small-Small payload') curve depicts the *available bandwidth* when the two nodes with determined *available bandwidth* used packages with 300-bytes probe size, while the cross-traffic was created (by the remaining nodes) by packages with 300-bytes probe size.

The 'S-L payload' ('Small-Large payload') curve depicts the *available bandwidth* when the two communicating nodes used packages of 300-bytes probe size, while the cross-traffic was created by a larger size probe package (here 1000-bytes probe size).

Similarly, the 'L-S payload' ('Large-Small payload') curve depicts the *available bandwidth* when the two measured nodes communicated using packages with a large size probe, while the cross traffic was created by a load consisting of packages with small size probes (for our experiment, 300-bytes probe).

Finally, the 'L-L payload' ('Large-Large payload') curve shows results when both loads of a pair of communicating nodes and their environmental traffic were created by packages with large size probes.

Fig. 2 shows how two communicating nodes were affected by the size of packets. As the packet size increased, the *available bandwidth* also increases. The cross-traffic of 2 Mbps was a focal point for our experiments. When the cross traffic created by packages with small probes exceeded this point of 2 Mbps and the communicating nodes used packages with large size probes, then the *available bandwidth* was higher compared to the corresponding case created by a smaller package size.

In all cases, when the cross-traffic increased, the *available bandwidth* was gradually reduced. Hence, in the limiting case of 5.5 Mbps cross-traffic, the available traffic decreased to zero values.

In Fig. 3, the quantitative results reveal the effect of the multirate environment in two nodes communicating at 54 Mbps.

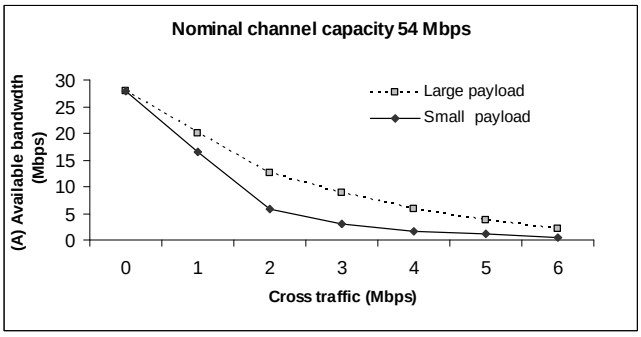

Figure 3. *Available bandwidth* versus *cross-traffic* in 802.11 access link with nominal channel capacity 54 Mbps

More specifically, in Fig. 3, the *available bandwidth* versus various levels of cross-traffic is appeared. The available bandwidth was estimated for IEEE 802.11 wireless network access link which was working at 54 Mbps.

The solid curve ('Small payload') depicts results obtained when the packages with 300-bytes probe were used; the two measured nodes ran at 54 Mbps, while cross traffic was generated by a pair of nodes running at 6 Mbps.

On the other hand, the dotted curve ('Large payload') depicts results obtained when the packages used 1000-byte probes and the node system worked in the same pattern of running.

In both cases, the available bandwidth gradually decreased as the cross traffic increased.

VI. CONCLUSION

The effective evaluation and measurements of capacities along end paths are of realistic interest, especially to activities such as capacity planning, protocol design, performance analysis, and system deployment.

We investigated broadband access networks. Focus was placed on the case of cable modem and the wireless 802.11 networks. The under study links could employ mechanisms such as token bucket rate regulation. The packets were scheduled in a non-FIFO manner, and the networks were available to support multiple distinct rates. All experiments were based on actual 802.11a and cable modems links. Our experiments quantitatively demonstrated how the *available bandwidth* was reduced when the cross-traffic increased.

Our future work will focus on several points. One idea is to study in detail the backoff periods in the estimation technique; another idea involves making cross traffic appear bursty for faster links, forcing the problem to be more complex.

 ISBN: 978-1-61208-123-6

REFERENCES

[1] J. Strauss, D. Katabi, and F. Kaashoek, "A Measurement Study of Available Bandwidth Estimation Tools," In Proc. of of ACM Internet Measurement Conference (IMC), pp. 27-35, 2003.

[2] V. Jacobson and M. J. Karels, "Congestion Avoidance and Control". In Proc. of ACM SIGCOMM, pp. 314, 1988.

[3] S. Keshav, "A Control-Theoretic Approach to Flow Control," In Proc. of ACM SIGCOMM, pp. 191-201, 1991

[4] R. L. Carter and M. E. Crovella, "Measuring Bottleneck Link Speed in Packet Swicthed Networks," Performance Evaluation, Volumes 27-28, pp. 297-318, October 1996.

[5] A. Downey, "Clink: a Tool for Estimating Internet Link Characteristics," 1999. http://allendowney.com/research/clink/ (2010)

[6] A. B. Downey, "Using pathchar to Estimate Link Characteristics," In Proc. of ACM SIGCOMM, pp. 241-250, 1999.

[7] B. Mah. "pchar: A Tool for Measuring Internet Path Charateristics", 1999. http://www.employees.org/˜bmah/software/pchar (2011)

[8] M. Jain and C. Dovrolis, "End-to-End Available Bandwidth: Measurement Methodology, Dynamics, and Relation with TCP Throughput," In Proc. of ACM SIGCOMM, pp. 295-308, 2002.

[9] Vinay J. Ribeiro, Rudolf H. Riedi, Richard G. Baraniuk, Jiri Navratil and Les Cottrell, "pathChirp: Efficient Available Bandwidth Estimation for Network Paths," In Proc. of PAM Workshop, pp. 14–25, 2003.

[10] N. Hu and P. Steenkiste, "Evaluation and Characterization of Available Bandwidth probing Techniques," IEEE J.Selected Areas in Communications, Special Issue in Interet and WWW Measurement, Mapping and Modeling, Volume: 21 Issue:6, pp. 879-894 , 2003.

[11] B. Malander, M. Bjorkman and P. Gunningberg, "A New End-to-End Probing and Analysis Method for Estimating Bandwidth Bottlenecks," In Proc. of Global Telecommunications Conference, vol.1, pp. 415-420, 2000.

[12] V. Ribeiro, M. Coates, R. Riedi, S. Sarvotham, B. Hendricks, and R. Baraniuk "Multifractal Cross-traffic Estimation," In ITC, pp. 481–492, 2000.

[13] http://www.pathrate.org (2011)

[14] Chaikh Sarr, Claude Chaudet, Guillaume Chelius and Isabelle Guerin Lassous, "A node-based available bandwidth evaluation in IEEE 802.11 ad hoc networks," International Journal of Parallel Emergent and Distributed Systems Volume 21, Number 6; pp. 423-440, December 2006.

[15] Jian Ni and R. Srikant, "Distributed CSMA/CA algorithms for achieving maximum throughput in wireless networks," Conf. Proc. of Information Theory and Applications Workshop, 8-13 Feb 2009, ISBN: 978-1-4244-3990-4 , pp. 250 – 250, San Diego, CA .

[16] M.Durvy, O.Dousse and P. Thiran, "Self-Organization Properties of CSMA/CA Systems and Their Consequences on Fairness," IEEE Transactions On Information Theory, Issue Date: March 2009 , Volume: 55 Issue:3 pp. 931 – 943, ISSN: 0018-9448.

[17] http://us.zyxel.com/upload/download_library/P971M_v1_QuickStart Guide.pdf (2010)

[18] http://www.linksysbycisco.com/UK/en/support/WPC55AG/download (2011)

[19] Haitao Zhao, Emiliano Garcia-Palacios, Jibo Wei and Yong Xi., "Accurate available bandwidth estimation in IEEE 802.11-based ad hoc networks," Elsevier Computer Communications, Volume 32, Issue 6, pp. 1050-1057, 27 April 2009..

 ISBN: 978-1-61208-123-6

Bit Error Rate Performance of ESPAR antenna-based Single-RF Diversity for IEEE802.15.4

Tomoya Kozu, Satoshi Tsukamoto, Minoru Okada
Nara Institute of Science and Technology, Ikoma 630-0192 Nara Japan
E-mail: tomoya-ko@is.naist.jp, satoshi-t@is.naist.jp, mokada@is.naist.jp

***Abstract*—This paper presents a single-RF diversity scheme for spread spectrum receiver based on IEEE 802.15.4 standard. The proposed scheme employs an Electronically Steerable Passive Array Radiator (ESPAR) antenna with periodically changing directivity at the symbol rate. IEEE 802.15.4 focuses on a low power consumption short range communication systems. However, the bit error rate performance is not good enough in a severe multipath fading environment. Diversity is a well-known technique to compensate the performance degradation due to multipath fading. However, the complexity for diversity reception is a major problem. In this paper, we propose a new single-RF diversity scheme using ESPAR antenna with periodically changing directivity. The proposed scheme is capable of obtaining the diversity gain in a frequency selective fading environment and it solves the slow convergence rate problem in the conventional ESPAR antenna based diversity scheme. Computer simulation result and theoretical analysis show that the proposed scheme gives diversity gain.**

***Index Terms*—IEEE802.15.4, Zig-Bee, diversity, ESPAR**

I. INTROCUTION

Diversity is a efficient technique capable of mitigating the performance degradation due to fading and is used in wide range of wireless communication systems such as mobile communication, Wireless LAN (Local Area Network), and PAN (Personal Area Network) systems.

In case of space diversity, signals are received by two or more antennas, and the received signals are combined in order to reduce the attenuation. The received signal occasionally attenuated and its strength falls below the thermal noise level due to fading. Since the amount of attenuation due to fading is different from each other when the antennas are spatially separated, the probability of deep fade after combining can be reduced and drastically improves the transmission performance.

There are a lot of combining technique for diversity reception such as selection combining, equal gain combining, and maximum ratio combining. Among them, the maximum ratio combining diversity is known to be the optimum in terms of maximizing the signal to noise power ratio (SNR) after combining.

However, the maximum ratio combining has a major drawback in terms of required hardware complexity. The maximum ratio combining receiver requires RF (Radio Frequency) front-end, ADC (Analog to Digital Converter), and baseband demodulation circuitry for each antenna branches, that is, it rises the power consumption of the receiver. In case of handheld terminals where the power consumption is strictly limited, it is difficult to apply the maximum ratio combining diversity.

In order to solve this problem, switch diversity scheme was used. It first chooses either one of the elements, and change the element when the received signal strength falls below the predetermined threshold. Although the switch diversity scheme is efficient in terms of reducing the hardware complexity, the diversity gain is small compared to the maximum ratio combining. Furthermore, it is not capable of tracking the fast variation of the channel because of the nature of feedback control.

Recently, the passive array antenna called ESPAR (Electronically Steerable Passive Array Radiator) antenna has been proposed [1]. ESPAR antenna is composed of a director and the parastic elements which are placed in the vicinity of the director. The parastic elements are terminated by the varactor diode. The beam pattern can be controlled by changing the reactance values of the varactor diode.

A diversity receiver using ESPAR antenna has been proposed. The principle operation of the diversity is the same as that of the switch diversity. That is, it inherits the diversity gain and tracking problems in the switch diversity.

In order to solve this problem, we propose a diversity using fast directivity controlled ESPAR antenna. A part of authors has already proposed a fast directivity contolled ESPAR antenna based diversity receiver for OFDM (Orthogonal Frequency Division Multiplex) [2]. This scheme makes efficient use of ICI (Inter-Channel Interference) caused by the fast motion of directivity. This ICI can be eliminated because the motion of directivity is known at the receiver. By using the MMSE (Minimum Mean Square Error) frequency domain equalizer after FFT (Fast Fourier Transform), we can get an implicit diversity gain. Since this scheme does not require feedback control and switching, we can solve the problems in switch diversity. Furthremore, the proposed scheme is efficient in a severe frequency selective fading channel.

This paper proposes a diversity receiver based on fast directivity controlled ESPAR antenna for IEEE 802.15.4 which employs direct sequence spread spectrum. In IEEE 802.15.4, 250kbit/s of binary data are divided into 4-bit blocks and mapped onto the 16-level symbol. Then the transmitter

 ISBN: 978-1-61208-123-6

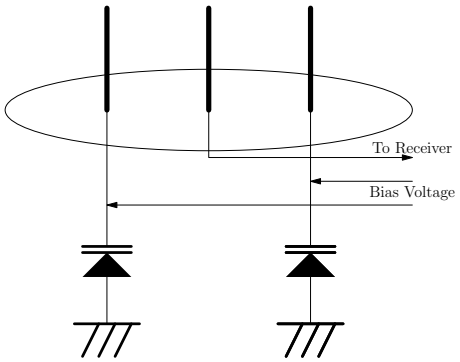

Fig. 1. A typical ESPAR antenna structure

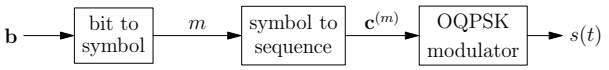

Fig. 2. Block diagram of the transmitter based on IEEE 802.15.4 PHY standard

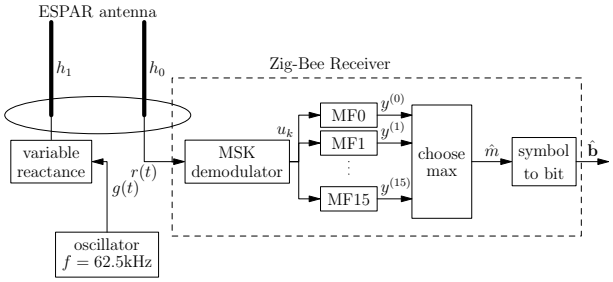

Fig. 3. Block diagram of the proposed receiver

chooses one of the 16 spreading sequences depending on the symbol. The proposed scheme changes the steering pattern of the ESPAR antenna at 62.5kHz which is the same as the symbol rate of the IEEE 802.15.4 standard. Despite OFDM systems, IEEE 802.15.4 is robust to the distortion due to fast variation of the channel, the proposed scheme gives the diversity gain without equalizations. Other elements in the vicinity of the director are terminated by the variable capasitors. These elements are referred to as the parastic elements. Therefore, the steering beam pattern varies depending on the bias voltages applied to the variable capasitors.

The rest of paper is organized as follows. Section 2 illustrates the principle of ESPAR antenna followed by the physical layer signaling of the IEEE 802.15.4 standard in Section 3. Section 4 proposes an ESPAR-antenna based diversity scheme for IEEE 802.15.4. Section 5 shows the bit error rate performance of the proposed scheme by computer simulation.

II. Principle of ESPAR Antenna

Fig. 1 shows a typical configuration of ESPAR antenna. ESPAR antenna is composed of three quarter-wavelength monopole antennas. Although ESPAR antenna has one RF port, it is capable of steering the beam pattern similar to the well-known adaptive array antennas having multiple RF ports. The ESPAR antenna in Fig. 1 is composed of three monopole antennas, each of which is quarter-wavelength antenna. The director at the middle of the array is connected to the RF input of the receiver. Two other elements in the vicinity of the director are terminated by the variable capasitors. These elements are referred to as the parastic elements. The phase of the induced currents flows at the parastic elements can be controlled by the reactance value according to the bias voltages. Therefore, the steering beam pattern varies depending on the bias voltages applied to the variable capasitors connected to the parastic elements.Since the variable capacitors, which terminate to parastic elements,are passive devices, and their reactance value are controlled by the bias voltages.ESPAR antenna does not consume the power in principle.

As applications of ESPAR antennas, estimation of the arrival direction of the signal using MUSIC (multiple signal classification) method or ESPRIT (estimation of signal paramters via rotational invariance technique) method have been proposed [3,4]. Hasuike et al. [5] proposed on use of ESPAR antenna for wireless ad-hoc network in order to reduce radio interference. However, this method require modifications in MAC layer protocol.

The diversity receiver based on ESPAR antenna has also been proposed as mentioned in introduction. However, the conventional ESPAR antenna-based diversity receiver is not efficient in terms of diversity gain and tracking capability.

III. IEEE 802.15.4 PHY standard

Fig. 2 illustrates the block diagram of the transmitter based on IEEE 802.15.4 physical layer standard. Four-bit block $\mathbf{b} = (b_0, b_1, b_2, b_3)$ is mapped onto the 16-level symbol according to the conversion formula, $m = 2^3 b_3 + 2^2 b_2 + 2b_1 + b_0$ at the bits-to-symbol converter. One of 16 spreading sequences is chosen according to the symbol at the symbol-to-sequence converter. The output sequence is given by $\mathbf{c}^{(m)} = (c_0^{(m)}, c_1^{(m)}, \ldots, c_{31}^{(m)})$. This spreading sequence is applied to OQPSK (Offset Quadrature Phase Shift Keying) modulator to generate the transmit signal. The output of the OQPSK modulator in the equivalent low pass expression is given by

$$s(t) = \sum_k c_{2k} f(t-2kT_b) + j \sum_k c_{2k+1} f(t-(2k+1)T_b), \quad (1)$$

where a sinusoidal waveform is chosen as a spreading chip pulse waveform. The pulse waveform is given by

$$f(t) = \begin{cases} \cos\left(\dfrac{\pi t}{2T_b}\right); & (|t| \le T_b) \\ 0; & (|t| > T_b) \end{cases} \quad (2)$$

where $T_b = 1/(2 \times 10^6) = 5 \times 10^{-7}$ is the chip duration.

IV. Proposed ESPAR Antenna-based Diversity Receiver

Fig. 3 shows the block diagram of the proposed ESPAR-antenna-based diversity receiver for IEEE 802.15.4. The steering beam pattern varies at a frequency of $T_s = 1/(32T_b) = 62.5$kHz, which is the same as the symbol rate.

 ISBN: 978-1-61208-123-6

In the following, we assume a slow Rayleigh fading channel. The received signal at the output of the ESPAR antenna is then given by

$$r(t) = (h_0 + h_1 g(t))\, s(t) + z(t), \tag{3}$$

where h_i $(i = 0, 1)$ represents the attenuation and phase rotation due to fading. In Rayleigh fading channel, h_i is a zero-mean complex Gaussian random variable. $g(t)$ is the channel variation due to the change in the steering beam pattern of the ESPAR antenna. Furthermore, $z(t)$ is an additive white Gaussian noise (AWGN) component. By substituting Eq. (1), we can rewrite the received signal as

$$r_k = (h_0 + h_1 g_k)\, d_k + z_k, \tag{4}$$

where

$$d_k = \begin{cases} c_k & (\text{even } k) \\ jc_k & (\text{odd } k) \end{cases}, \tag{5}$$

where $r_k = r(kT_b)$, $g_k = g(kT_b)$, and z_k AWGN component after sampling.

The received signal is then applied to the non-coherent MSK (Minimum Shift Keying) demodulator. The output of the MSK demodulator is given by

$$u_k = \Im \left[r_k r_{k-1}^* \right]. \tag{6}$$

The output, u_k is applied to the bank of 16 matched filters (MFs). The impulse response of the m-th MF is given by

$$q_{2k}^{(m)} = \begin{cases} -1 & (c_{2k-1}^{(m)} = c_{2k}^{(m)}) \\ +1 & (c_{2k-1}^{(m)} \neq c_{2k}^{(m)}) \end{cases} \tag{7}$$

$$q_{2k+1}^{(m)} = \begin{cases} +1 & (c_{2k}^{(m)} = c_{2k+1}^{(m)}) \\ -1 & (c_{2k}^{(m)} \neq c_{2k+1}^{(m)}) \end{cases}. \tag{8}$$

The output of the m-th MF is then given by

$$y^{(m)} = \sum_{k=0}^{N-1} q_k^{(m)} u_k. \tag{9}$$

The output of the m-th MF, $y^{(m)}$, is fed to the maximum value selector. The symbol which maximizes the MF output $m = \hat{m}$ is supposed to be transmitted at the maximum value selector. The estimated symbol is applied to the symbol-to-bit converter to convert the bit stream, $\hat{\mathbf{b}}$.

V. Error Rate Analysis

Now, let us define the received signal after sampling as $w_k = (h_0 + h_1 g_k) + z'_k$. The received signal is represented in vector-form as:

$$\mathbf{w} = [w_0, w_1, \ldots, w_{N-1}]^T, \tag{10}$$

Then, the m-th MF output can be expressed in quadratic form as:

$$y^{(m)} = \mathbf{w}^H \mathbf{F} \mathbf{w}, \tag{11}$$

where

$$\mathbf{F} = \begin{bmatrix} 0 & 1 & 0 & \cdots & & 0 \\ 1 & 0 & 1 & 0 & \cdots & 0 \\ 0 & 1 & 0 & 1 & 0 & \vdots \\ \vdots & \ddots & \ddots & \ddots & \ddots & \vdots \\ 0 & \cdots & 0 & 1 & 0 & 1 \\ 0 & & \cdots & 0 & 1 & 0 \end{bmatrix}, \tag{12}$$

is a matrix representing the demodulator and MF.

The covariance matrix of $\mathbf{w}$ is given by

$$\begin{aligned} \mathbf{R} &= \frac{1}{2} E\left[\mathbf{w}^* \mathbf{w}^T\right] \\ &= [\rho_{ik}]_{i,k=0,1,\ldots,N-1}, \end{aligned} \tag{13}$$

where the i-th row, the k-th column element is given by

$$\rho_{ik} = \begin{cases} b + \sigma_z^2 & (i = k) \\ \dfrac{b}{2}\left(1 + g_i^* g_k\right) & (i \neq k) \end{cases}, \tag{14}$$

where b is the average received signal power, and σ_z^2 is the variance of the AWGN component.

Now we can derive the pairwise error probability that the m' is transmitted when m was transmitted. Suppose that the probability density function of $X = y^{(m)}$ is defined as $p(X)$. The pairwise error probability is given by

$$\begin{aligned} P\{m \to m'\} &= \int_{-\infty}^{0} p(X) dX \\ &= \int_{-\infty}^{0} \int_{-\infty}^{\infty} G(\xi) \exp(-j\xi X)\, d\xi dX \\ &= \int_{-\infty}^{\infty} \frac{G(\xi)}{\xi} d\xi \end{aligned} \tag{15}$$

where $G(\xi)$ is the characteristic function of $X = y^{(m)}$, and given by

$$G(\xi) = \frac{1}{\det\left(\mathbf{I} - 2j\xi \mathbf{R}^* \mathbf{F}\right)} \tag{16}$$

Let $C = \{\lambda | \det(\mathbf{A} - \lambda \mathbf{I}) = 0\}$ be a set of all the eigen-values of $\mathbf{A} = 2\mathbf{R}^* \mathbf{F}$. The characteristic function is further rewritten as

$$G(\xi) = \left[\prod_{\lambda \in C} (1 - j\lambda\xi) \right]^{-1} \tag{17}$$

From the above analysis, the pairwise error probability is given by

$$P\{m \to m'\} = \sum_{\lambda \in C_m} \left[\prod_{\substack{\lambda' \in C \\ \lambda' \neq \lambda}} \left(1 - \frac{\lambda'}{\lambda}\right) \right]^{-1} \tag{18}$$

where $C_m = \{\lambda | \lambda \in C, \Re[\lambda] < 0\}$ of $\mathbf{A}$ is a set of eigenvalues whose real components are negative.

 ISBN: 978-1-61208-123-6

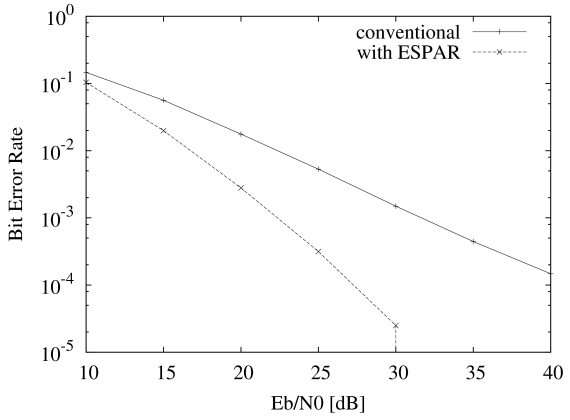

Fig. 4. Bit Error Rate Performance of the Proposed Diversity Receiver

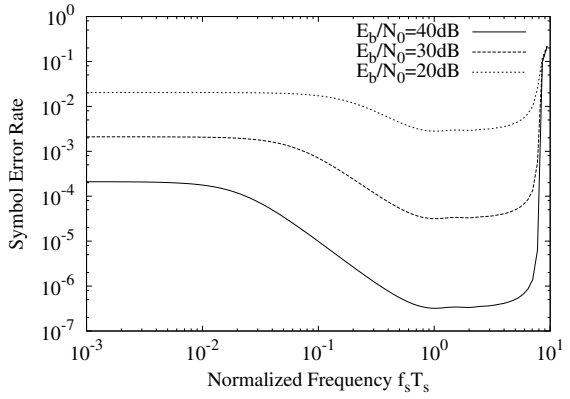

Fig. 5. Error Rate Performance against the normalized frequency for directivity change

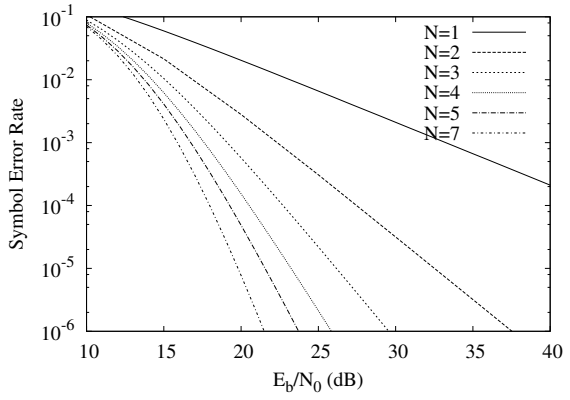

Fig. 6. Error Rate Performance against the number of elements

VI. Numerical Ayalysis

In this section, we analyze the bit error rate performance of the proposed diversity receiver by computer simulation. In the following, we assume that the function corresponding to the fast time variation of steering beam pattern is given by

$$g_k = \exp\left(\frac{j2\pi\alpha t}{T_s}\right) \tag{19}$$

where α is the beam pattern variation frequency normalized by the symbol rate ($1/T_s = 62.5$kbit/s).

Fig. 4 shows the bit error rate performance of the proposed scheme. In this figure, we assume $\alpha = 1$. We can confirm that proposed scheme gives diversity gain.

Now, the bit error rate against the steering beam pattern variation frequency is shown by making use of Eq. (18). Fig. 5 shows the symbol error rate performance against the normalized variation frequency. We can not get the diversity gain when the normalized frequency of beam pattern variation is less than 0.5. This is because the received signal strength variation is reduced. On the other hand, the symbol error rate drastically degrades when the normalized frequency exceeds 5 since the distortion due to beam pattern variation affects the detection. From this result, we have to set the normalized frequency for $0.5 < \alpha < 5$. It also shows that it is no need to synchronize the frequency to symbol rate.

In the discussions above, we assume the two-element ESPAR antenna. However, further improvement in error rate performance could be possible if we use two or more parastic elements. Now, let us assume that the control frequency for l-th parastic element is $k\alpha$. Fig. 6 shows the impact of the number of ESPAR antenna elements to the symbol error rate performance. From this figure, we can further improve the error rate performance.

VII. Conclusion

This paper proposed the single-RF diversity receiver using fast steering beam pattern controlled ESPAR antenna for IEEE 802.15.4. The proposed scheme is capable of obtaining diversity gain by changing the steering beam pattern at the frequency of symbol rate. Computer simulation result showed that the proposed scheme efficiently get the diversity gain in a Rayleigh fading environment. Further improvement is possible by increase in the number of parastic elements.

Acknowledgments

The authors would like to thank Dr. Ueba, President of ATR Wave Technology Laboratory for supporting this project. This study was supported by Industrial Technology Research Grant Program in 2010 from New Energy and Industrial Technology Department Organization (NEDO) of Japan.

References

[1] K. Gyoda and T. Ohira,“ Design of electronically steerable passive array radiator (ESPAR) antennas, ”Proc. Antennas and Propagation Society International Symposium, Salt Lake City, UT, USA, vol. 2, pp. 922-925, July 2000.

 ISBN: 978-1-61208-123-6

[2] S. Tsukamoto and M. Okada, " Single-RF maximal ratio combining diversity for OFDM system using an ESPAR antenna whose direction is oscillated in the symbol time, " Proc. of Thailand-Japan Microwave forum 2009, Bangkok, Thai, FR7-2, August 2009.

[3] C. Plapous, Jun Cheng, E. Taillefer, A. Hirata and T. Ohira, " Reactance domain MUSIC algorithm for electronically steerable parasitic array radiator, " IEEE Trans. Antennas and Propagation, vol. 52, issue 12, pp. 3257-3264, Dec. 2004.

[4] E. Taillefer, A. Hirata and T. Ohira, " Reactance-domain ESPRIT algorithm for a hexagonally shaped seven-element ESPAR antenna, " IEEE Trans. Antennas and Propagation, vol. 53, issue 11, pp. 3486-3495, Nov. 2005.

[5] K. Hasuike, S. Horisawa and S. Tawara," An Adaptive MAC and Directional Routing Protocol for Ad Hoc Wireless Networks Using ESPAR Antenna, " in Proceedings of ACM MobiHoc, pp. 243-246, 2001.

[6] J. G. Proakis, "Digital Communications - Fourth Edition, " McGraw-Hill, Singapore, 2001.

[7] IEEE Standard for Information technology — Telecommunications and information exchange between systems — Local and metropolitan area networks — Specific requirements, Part 15.4: Wireless Medium Access Control (MAC) and Physical Layer (PHY) Specifications for Low-Rate Wireless Personal Area Networks (WPANs), IEEE Std 802.15.4-2006, 2006.

 ISBN: 978-1-61208-123-6

Theoretical Performance of Transform Domain Communication Systems

Guillaume Fumat, Pascal Chargé, Danièle Fournier-Prunaret
LATTIS, INSA
University of Toulouse, France
gfumat@insa-toulouse.fr, pascal.charge@univ-nantes.fr

Ahmed Zoubir, Irène Mahafeno
Axess Europe
Toulouse, France
ahmed.zoubir@axesseurope.com

***Abstract*—Transform Domain Communication System (TDCS) is a cognitive-radio technology that avoids frequency underutilization by doing spectrum-scavenging. Although TDCSs' is well-known when dealing with interferers, theoretical limits of TDCS in terms of spectrum efficiency remain unknown. Based on the TDCS' multidimensional property, we detail them in terms of spectrum efficiency and Bit Error Rate (BER). It is shown that most of previous TDCSs had suboptimal performances. Guidelines are given to improve these metrics without much increase in system's complexity.**

***Index Terms*—TDCS, spectral efficiency, CSK, cognitive radio, multidimensional modulation**

I. Introduction

Introduced by Mitola in [1], Cognitive-Radio was presented to overcome the problem of spectrum under-utilization [2], [3]. Technologies were proposed to counter this waste, such as Transform Domain Communication Systems (TDCSs) that generate interference-free waveforms.

TDCS's major contributions are recent, and a significant part was achieved by the Airforce Institute of Technology [4]–[7]. However these studies mainly focused on the BER performance when bypassing jammers. More recently Han et al. proposed a phase scrambling to improve the BER of TDCS signals based on contiguous spectrum [8]. TDCS is therein described as a low bit-rate communication system, while in another article, Budiarjo et al. [9] mention they can significantly improve the BER performance and the spectrum utilization of TDCS by using simultaneously two modulations.

Thus, if we know well TDCSs' benefits in terms of cognitive radio and interference-avoidance property, its BER and spectral efficiency performance remain unknown, though these are essential performance metrics.

By means of the dimensionality property [10, pp 227-229] that applies to TDCS, we propose to fill this missing piece of literature in order to give insights on the effective speed and reliability that TDCS can achieve. We demonstrate that the granularity of the spectrum mask does impact the spectral efficiency and show that taking benefit of the whole dimensionality leads to great BER improvements while increasing the spectral efficiency. Via this approach we stress that previous TDCS implementations were suboptimum with regard to these metrics.

In this article, we first recall the definition of the dimensionality and its impacts on the BER and spectrum efficiency. Then, our TDCS system is introduced and key properties related to its dimensionality are given. In the last section, a particular care is taken on spectrum efficiency of previously studied TDCS systems, we enhance them by using system's whole dimensionality to ensure maximum spectral efficiency and minimum BER. Finally, a specific focus is done on the modulation proposed in [9] and a new result is presented by means of the dimensionality and the orthogonality point of view. We explain in which extent the spectrum efficiency and the BER of their system is improved and why.

II. Signal Dimensionality and its Impacts on System Performance

In this section, one recalls the notion of dimensionality before studying its impact on the system in terms of BER.

A. General principles, and relations with spectrum efficiency

The dimensionality N of a signal $x(t)$, which lasts T seconds and occupies a bandwidth W_u, defines the number of orthogonal signals such that $x(t)$ can be expressed by a linear combination of these orthogonal signals. In [10, pp. 227-229], it is stated that the number of dimensions N of the space of a signal $x(t)$ is well approximated by Eq. (1):

$$N \approx 2W_u T \tag{1}$$

Although this formula looks very simple, the information it contains is of the greatest importance since it has direct consequences on the spectral efficiency η_{eff} of a multidimensional system. Indeed, it is shown that [10, pp. 227-229] :

$$\begin{aligned}\eta_{\text{eff}} = \frac{R_{bit}}{W_u} &= \frac{\log_2(M_{mod})R_{symb}}{\frac{N}{2T}} \\ &= \frac{2\log_2(M_{mod})}{N}\end{aligned} \tag{2}$$

where M_{mod} is the constellation size, R_{bit} is the bit-rate, and $R_{symb} = \frac{R_{bit}}{\log_2(M_{mod})} = \frac{1}{T}$ is the symbol rate.

As a consequence, the higher the signal dimensionality is, the lower the spectrum efficiency gets. Thus, to improve the latter, M_{mod} must be increased.

Let us now briefly summarize the effects of high dimensionality systems on the achievable BER. To do so, we will take the example of the widely studied M-Ary Orthogonal

 ISBN: 978-1-61208-123-6

Signaling [10](MOS), where one symbol fills one dimension ($M_{mod} = N$), before seeing how it applies to TDCS.

B. Bit Error Probability for MOS and TDCS

While in PSK, the bigger the constellation size M_{PSK} is, worse gets the BER (following the well known "waterfall curves"), in MOS, where each symbol is represented by a waveform orthogonal to every other one, the waterfall curves' order is reversed : the higher the dimensionality, the better the BER gets, as developed in [10, pp. 203-206]. It comes from the fact that the more dimensions a signal has, the more bits are sent with the same amount of energy, while keeping a constant symbol error probability, since the distance between two orthogonal signals does not change. One can transmit information with high reliability at very low SNR, but with a low spectrum efficiency. MOS systems are in a word "power-efficient".

In the case of a given TDCS system, N is set by the spectrum mask definition as further stated in Section III-D. Thus, it does not come into question to increase or to decrease the system's dimensionality. However the chosen modulation defines the number of used dimensions. And similarly as the phenomenon described above, the more dimensions are used, the better gets the BER. Note that meanwhile, because more dimensions are used, the constellation size of the modulation increases, and thus, spectrum efficiency also increases. This phenomenon is fully described in [10], [11].

In a word, when a telecommunication system's dimensionality is $N \gg 1$, it is of paramount importance to use every possible dimensions. Otherwise it could lead to BER and spectrum efficiency leakages.

III. TDCS System Model

Hereafter, the receiver and transmitter's model are described. The waveform modulation is also detailed.

A. Transmitter's Side

The typical TDCS transceiver model presented in [7] is simple and cited in many publications, but does not well describe how the modulation stage can be implemented. We decide thus to present in Fig. 1 a model that takes into account the two main modulations used in TDCS.

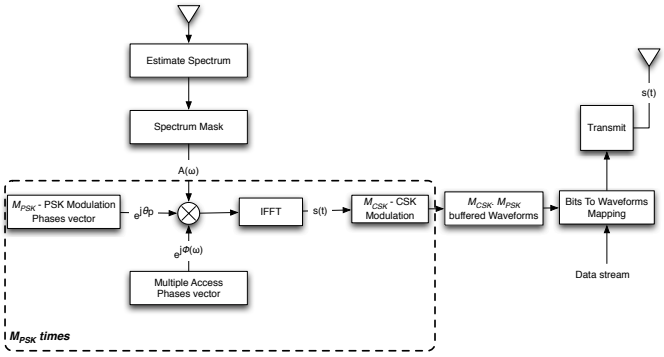

Figure 1. TDCS Transmitter

The system described in Fig. 1 starts first with sensing the available spectrum to ensure an interference-free transmission. This topic has been widely investigated through the use of different techniques to better detect the interferences [6]. From this estimate, a spectrum mask of bandwidth W_u is chosen, which the transmitted signal will have to respect. An Inverse Fourier Transform of this spectrum is then done, and the generated waveforms are stored in a buffer. These waveforms are then modulated before being sent.

B. Possible waveform modulations

As stated, two modulation processes are mainly used in TDCS: a Cyclic Shift of the waveform and a Phase Shift Keying modulation that occur in two different stages of the transmitter [4], [7]. The first one is the M_{PSK}-Ary PSK modulation and consists of generating several waveforms respecting the same spectrum mask, having the same random phase vector, but with a $\theta_{m_{\text{PSK}}} = 2\pi \frac{m_{\text{PSK}}}{M_{\text{PSK}}}$ phase offset on every component, with $m_{\text{PSK}} \in \{1, \cdots, M_{\text{PSK}}\}$ the PSK symbol index, and M_{PSK} the number of possible PSK symbols. The signal's spectrum can thus be written as in Eq. (3):

$$S^{(v)}_{m_{\text{PSK}}}(f) = \sum_{k=1}^{K} A^{(v)}_k \delta\left(f - k\Delta_f\right) e^{+j\left(\phi^{(v)}_k + \theta^{(v)}_{m_{\text{PSK}}}\right)} + A^{(v)}_k \delta\left(f + k\Delta_f\right) e^{-j\left(\phi^{(v)}_k + \theta^{(v)}_{m_{\text{PSK}}}\right)} \quad (3)$$

with $A_k \in \{0, 1\}$ the amplitude of the frequency components (determined by the spectrum sensing), K the number of frequency components, Δ_f the spectrum sample spacing, $\theta^{(v)}_{m_{\text{PSK}}}$ the data phase modulation. $\phi^{(v)}_k$ is the multiple-access phase for the k-th frequency component of the v-th user and is usually described in the literature as a random phase. This causes the signal to be noise-like and also enables multiple-access capability, as exploited in [4]. In the time domain, a PSK symbol can be written as in Eq. (4):

$$\begin{aligned} s^{(v)}_{\text{PSK}_{m_{\text{PSK}}}}(t) &= \mathcal{F}^{-1}\left(S^{(v)}_{m_{\text{PSK}}}(f)\right) \\ s^{(v)}_{\text{PSK}_{m_{\text{PSK}}}}(t) &= 2\sum_{k=1}^{K} A_k \cos(2\pi k\Delta_f t + \phi^{(v)}_k + \theta^{(v)}_{m_{\text{PSK}}}) \end{aligned} \quad (4)$$

To alleviate the notation we decide not to specify the multiple-access index (v).

Since the Eq. (4) is computed from the Fourier transform of a sampled spectrum, $s_{\text{PSK}_{m_{\text{PSK}}}}(t)$ is T-periodic with $T = 1/\Delta_f$. But in the rest of this document we consider $s_{\text{PSK}_{m_{\text{PSK}}}}(t)$ as a symbol whose duration is T.

Although the M_{CSK}-Ary CSK modulation can be applied over the PSK one, in a matter of clarity we decide to focus on CSK and omit thus the subscript $_{\text{PSK}_{m_{\text{PSK}}}}$. When present, it means the symbol also carries PSK-modulated information.

First, a waveform s_{CSK_0} is generated following the Eq. (4). Then s_{CSK_0} is shifted in time to produce different symbols, as written in Eq. (5).

 ISBN: 978-1-61208-123-6

$$s_{\mathrm{CSK}_{m_{\mathrm{CSK}}}}(t) = s_{\mathrm{CSK}_0}\left(t - \frac{m_{\mathrm{CSK}}T}{M_{\mathrm{CSK}}}\right)_T \quad (5)$$

with T the waveform duration, and $s\left(t - \frac{T}{m_{\mathrm{CSK}}}\right)_T$ the notation introduced in [4] for a $\frac{T}{m_{\mathrm{CSK}}}$ circular shift. $m_{\mathrm{CSK}} \in \{0 \cdots M_{\mathrm{CSK}} - 1\}$ is the CSK symbol index.

Depending on the narrowness of the autocorrelation function of s_{CSK_0}, it can be shown that the set of shifted waveforms $s_{\mathrm{CSK}_0} \cdots s_{\mathrm{CSK}_{(M_{\mathrm{CSK}}-1)}}$ is pseudo-orthogonal [12].

C. Receiver's side

A Maximum Likelihood (ML) receiver, known to be optimum in an AWGN channel, is used and showed in Fig.2.

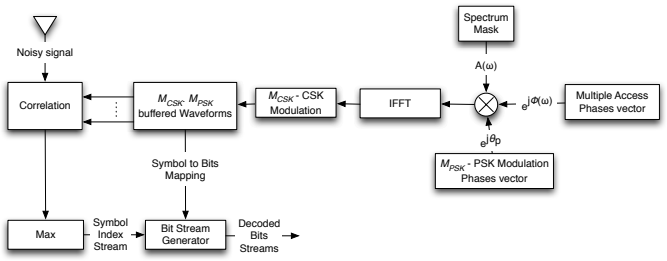

Figure 2. TDCS Optimum Receiver

We assume that the receiver and the emitter have the same waveforms buffered in their memory and also that they have the same mapping between a waveform and a bits word. To demodulate data, the receiver makes a correlation of the incoming waveform with every buffered waveform and the decision is taken by considering the maximum correlation value. Although this demodulation requires a huge amount of computations, this way of demodulating was chosen to ensure a fair comparison between all the modulation schemes. However, it is worth noting that a computation-efficient implementation is possible to demodulate CSK signals by using DFT and IDFT as stated in [12]. Now that the TDCS System is introduced, let us clarify the role that plays the dimensionality parameter $N = 2W_uT$ on the system's performance.

D. Impacts of the dimensionality N on TDCS performance

Since the symbol period is $T = \frac{1}{\Delta_f}$, and since the useful spectrum is described by $K_{\mathrm{used}} = \frac{W_u}{\Delta_f}$ frequency components, the signal dimensionality is equal to $N = 2K_{\mathrm{used}}$. Thus, it is possible to write the spectrum efficiency of the system in a simple manner in Eq. 6.

$$\eta_{\mathrm{eff}} = \frac{\log_2(M_{mod})}{K_{\mathrm{used}}} \quad (6)$$

A first tradeoff follows up: when defining the spectrum mask avoiding jammers, care should be taken not to choose a high granularity that would imply a leakage in spectrum efficiency.

As previously stated, dimensionality of a TDCS signal is set by the spectrum mask properties (the used bandwidth W_u and the frequency sampling space Δ_f). In the following, we assume these parameters are already set. However the number of used dimensions remains designer's choice and depends on the modulation stage. As explained in II-B, choosing a good modulation is of paramount importance: the system has to use as many symbols as possible to maximize the spectrum efficiency, but meanwhile it also has to occupy as many dimensions as possible to minimize the BER. In the following subsection, we study how well the standard modulations performs in TDCS.

IV. Performance of TDCS Modulation

In the studied TDCS system, the signal bandwidth is defined from 1kHz to 7MHz and avoids interferences that are present on the range from 2 to 3MHz. As a consequence, its total available bandwidth is $W_a = 6.999$ Mhz, but its used bandwidth is $W_u = 5.999$ MHz. $K_{\mathrm{used}} = 256$ frequency components describe the used bandwidth, and thus the dimensionality of our system is $N = 512$. These figures are summarized in the spectrum mask of Fig. 3.

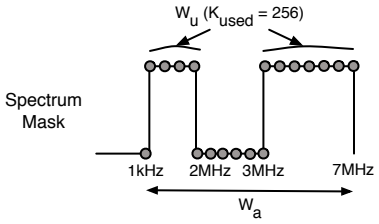

Figure 3. Spectrum description of the signal

A. Phase Shift Keying

Described in III-B, this modulation makes the symbol occupy only two dimensions as the usual PSK signals. As a consequence, the standard PSK waterfalls curves, fit perfectly PSK-TDCS BER results, as shown on Fig. 4.

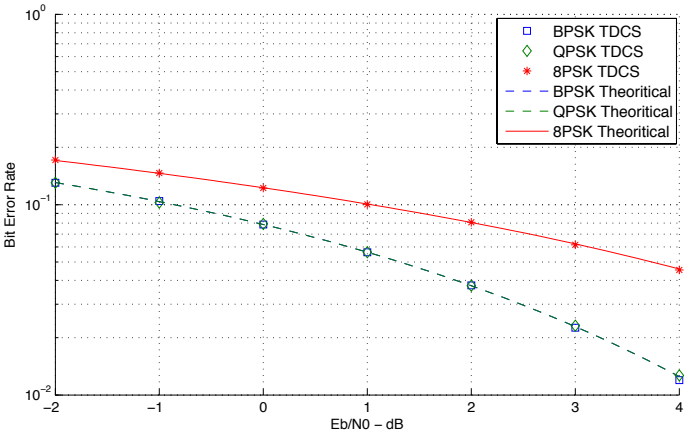

Figure 4. BER performance TDCS using M_{PSK}-Ary PSK Modulation

The modulation and demodulation processes can be easily implemented [7] and the spectrum efficiency is :

$$\eta_{\text{eff}} = \frac{\log_2(M_{\text{PSK}})}{K_{\text{used}}} \quad (7)$$

The problem is that the system is sub-optimal with regards to the attainable BER because only 2 dimensions over $2K_{\text{used}}$ are used. The BER leakage is obvious when looking at Fig. 5b.

B. Cyclic Shift Keying

As stated in [12], CSK can be seen as equivalent to M_{CSK}-Ary Orthogonal Signaling (MOS). This is effectively the case, as we can see on Fig. 5a : the theoretical BER performance of a MOS system match the simulated CSK-TDCS results.

Of course, since the cyclic shifted versions of the waveforms are inherently correlated, CSK is theoretically sub-optimal in terms of BER in comparison with MOS, but this is not detectable when the dimensionality and the E_b/N_0 are high enough.

In Fig. 5b, we observe that BER of TDCS-CSK is much lower than any PSK systems and keeps decreasing when the CSK constellation grows. The spectral efficiency follows Eq. (8) and is also higher than TDCS-PSK systems. Moreover the demodulation process of CSK has the advantage of being easily implementable as described in [12] and done in [8].

$$\eta_{\text{eff}} = \frac{\log_2(M_{\text{CSK}})}{K_{\text{used}}} \quad (8)$$

The main difference between Eq.(7) and Eq.(8) is that increasing M_{CSK} can lead to BER and spectrum efficiency improvements whereas increasing M_{PSK} leads to a BER degradation.

It is worth noting that in the literature, system configurations have always been $M_{\text{CSK}} \leq K_{\text{used}}$ without further explanation. It is possible that people fear that using CSK TDCS with $M_{\text{CSK}} > K_{\text{used}}$ would not provide enough orthogonality between CSK symbols. Yet, experimental results show that it can actually provide enough orthogonality to enhance the BER according to Fig. 5b and as thoroughly investigated in the next subsection.

We can note that using M_{CSK}-Ary CSK Modulation with $M_{\text{CSK}} = 512$, improves the spectral efficiency while achieving the same $3e^{-4}$ BER with 0.3dB $\frac{E_b}{N_0}$ less than the system using $M_{\text{CSK}} = 256$.

Moreover, it has never been tried to combine Antipodal Signaling and CSK with TDCS Systems. This results in bi-orthogonal signaling. MOS and M-Ary Bi-Orthogonal Signaling have almost identical BER functions when M is large, but Bi-Orthogonal Signaling occupies two times less dimensions (and thus bandwidth). As a consequence, it is possible to use $2K_{\text{used}}$-Ary CSK with antipodal signaling to further enhance the spectrum efficiency and the BER performance. Indeed, in Fig. 5c, we can observe a 0.5 dB $\frac{E_b}{N_0}$ gain over $M_{\text{CSK}} = 256$-Ary CSK TDCS when using $M_{\text{CSK}} = 512$ with antipodal signaling at the same $1e^{-3}$ BER. Note that the constellation size is then four times higher.

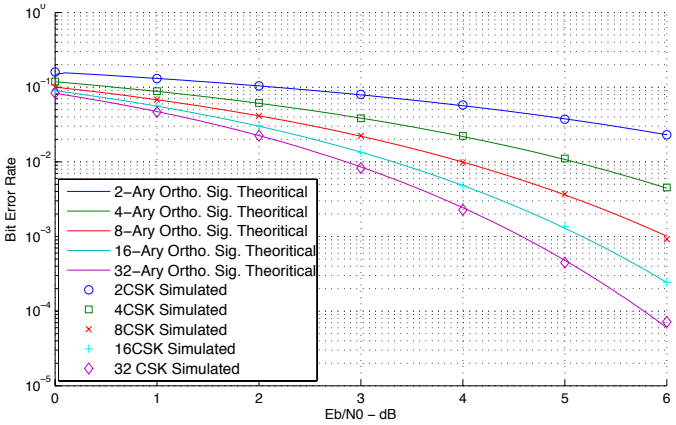

(a) BER performance of TDCS System using M_{CSK}-Ary CSK Modulation

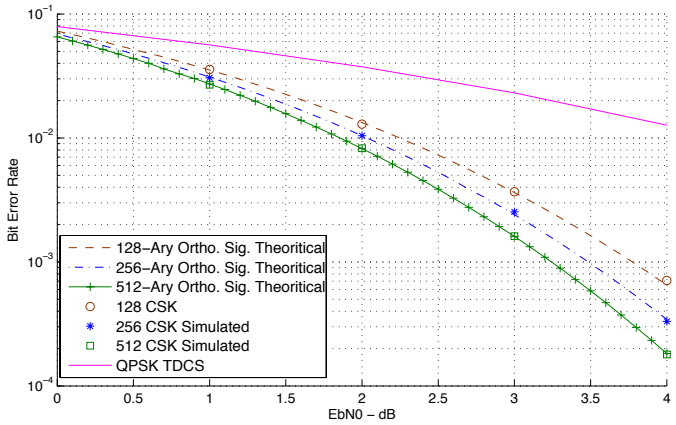

(b) BER performance of TDCS System using M_{CSK}-Ary CSK Modulation with $M_{\text{CSK}} \geq K_{\text{used}}$

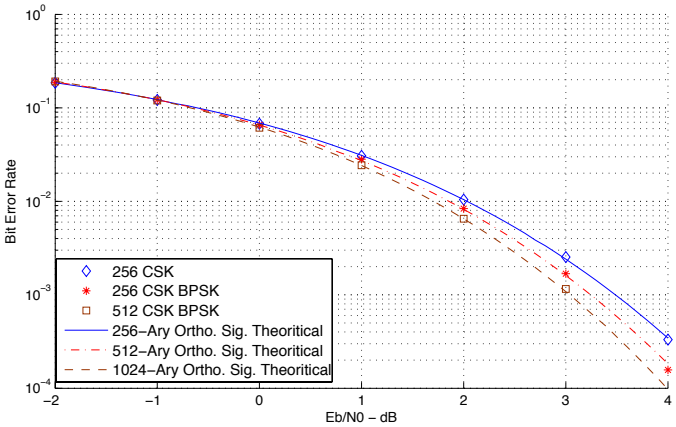

(c) BER performance of TDCS system using an Antipodal M_{CSK}-Ary CSK Modulation

Figure 5. BER performance of several CSK configurations

C. Combination of PSK and CSK

In [9], a system is presented where CSK and PSK modulations are combined. In this article, the information streams mapped by PSK or CSK are distinguished, and the BER for both streams are computed. Let first consider the spectral efficiency of such a combined M_{PSK}-Ary PSK / M_{CSK}-Ary

CSK TDCS system, we have:

$$\eta_{\text{eff}} = \frac{\log_2(M_{\text{PSK}} M_{\text{CSK}})}{K_{\text{used}}} \quad (9)$$

Budiarjo et al. were thus right when stating that this modulation leads to a better spectrum utilization but when considering the total BER of the whole system (both streams taken into account) rises up another advantage, not studied in [9]. This is what we computed for different system configurations in order to highlight the effect of dimensionality. Results are plotted in Fig. 6. Note that we use the X-axis scale E_b/N_0 with E_b computed as $E_b = \frac{E_s}{M_{mod}}$ with $M_{mod} = M_{\text{PSK}} M_{\text{CSK}}$ the total constellation size.

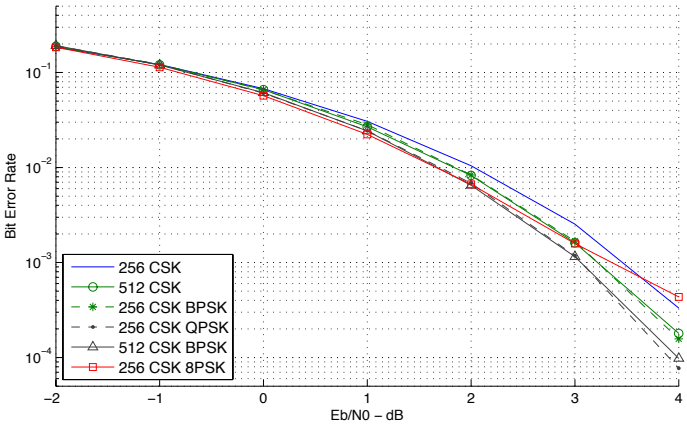

Figure 6. BER performance of PSK-CSK TDCS

As observed in Fig. 6, 512-Ary CSK and 256-Ary CSK-BPSK (equivalent to CSK with antipodal signaling) curves are overlapping. It is noteworthy to highlight that 256-CSK-QPSK has almost the same BER performance than 512-CSK-BPSK. As explained in the previous sections, it comes from the fact that in both cases, all dimensions $2K_{\text{used}}$ are used.

To provide a more accurate comparison of these modulations, Table I sums up intercorrelation statistics of the waveforms for each modulation technique:

Intercorr. Statistics	32 CSK	256 CSK	256 CSK QPSK	512 CSK BPSK	256 CSK 8PSK
mean	8.7e-5	6.9e-4	6.6e-4	6.8e-4	1.6e-3
min	1.1e-8	1.3e-9	8e-38	9.1e-10	8e-38
max	1.6e-3	8.5e-2	8.5e-2	8.5e-2	.5
var	1.6e-7	6.6e-5	4.8e-5	4.5e-5	7.6e-4

TABLE I. Intercorrelation Coefficient Statistics of WF generated by different techniques

First of all, the maximum intercorrelation coefficient increases as the constellation size does. This comes from the fact that the constellation size approaches or even exceeds the dimensionality limit. It is thus not further possible to generate more orthogonal waveforms. Concerning the minimum value, the QPSK-CSK modulation shows much better performance since QPSK generates 2 purely orthogonal waveforms for each CSK-generated one. There is no obvious rules for the other cases, since it highly depends on the autocorrelation function of the waveform : if the time shift occurs on one of its lobe or not. However, we can note that 256-CSK-QPSK average intercorrelation coefficient is slightly lower than 512-CSK-BPSK. As a matter of fact, it should results in better BER performance noticeable at higher E_b/N_0.

To end section IV, let us summarize in Table II the different rules to follow to take the most of TDCS' spectral efficiency. These guidelines are independant from the chosen spectrum mask.

Rule #	Guideline
1	Use every dimension the system offers to decrease the BER and enhance the spectral efficiency.
2	Use a spectrum granularity high enough to avoid jammers, but as low as possible to enable good spectrum efficiency.
3	Between two modulations having the same number of symbols, choose the one offering the largest intersymbol distance.

TABLE II. Guidelines to follow to improve TDCS' spectral efficiency

V. Conclusion

In this paper, using the often forgotten fact that TDCS is a multidimensional communication system enabled us to show the maximum attainable BER and spectral efficiency we can expect from any TDCS system. We show that TDCS is inherently a "power-efficient" communication system as previously suggested in [8]. However, Han et al. did not take benefit of every available dimension. We were thus able to improve their performance by using 512-Ary CSK modulation instead of 256-Ary CSK. We also further investigated the implementation proposed in [9] and show the global BER benefit of this implementation. This asset relies on the major fact we proved: the same BER can be obtained at lower $\frac{E_b}{N_0}$ when using every single dimension while enhancing the spectrum efficiency of a standard CSK Modulation. By using every dimension, the minimum BER and the maximum throughput are simultaneously gathered. This article provided guidelines to avoid further under-utilization of TDCS systems

If it is now obvious that TDCS systems fit well to low throughput transmissions in a context of poor SNR or long-haul communications, the next step is to extend the use of TDCS to high throughput communications, while ensuring a good reliability. This can be done by ensuring a better orthogonality between the dimensions and by using several dimensions at one time to transmit more bits simultaneously.

References

[1] J. Mitola, "Cognitive radio: An integrated agent architecture for software defined radio," Doctor of Technology, Royal Inst. Technol. (KTH), Stockholm, Sweden, 2000

[2] FCC, "Spectrum Policy Task Force", Rep. ET Docket no. 02-135, November 2002

[3] G. Staple and K. Werbach, "The end of spectrum scarcity," *IEEE Spectrum*, vol. 41, no. 3, pp. 48–52, Mar. 2004

[4] P.J. Swackhammer, "Performance Simulation of a Transform Domain Communication System for Multiple Access Applications", *MILCOM'99* pp. 1055-1059 Vol.2, October 1999

 ISBN: 978-1-61208-123-6

[5] A.S. Nunez, M.A. Temple, R.F. Mills, and R.A. Raines, "Interference Avoidance in Spectrally Encoded Multiple Access Communications Using MPSK Modulation", *WCNC 2005* pp. 730-734 Vol.2, March 2005
[6] M.J. Lee, M.A. Temple, R.L. Claypoole, and R.A. Raines, "Interference avoidance communications using wavelet domain transformation techniques", *WCNC2002* pp. 255-259 , March 2002
[7] A.S. Nunez, "Interference Suppression in Multiple Access Communications Using M-Ary Phase Shift Keying Generated via Spectral Encoding", Air Force Institute of Technology, Master Thesis AFIT/GE/ENG/04-20, 2004
[8] C. Han, J. Wang, S. Gong, and S. Li, "Adressing the control channel design problem : OFDM-based transform domain communication system in cognitive radio", *Computer Networks 2008* vol. 52, n.4, pp. 795-815, June 2008
[9] I. Budiarjo, H. Nikookar, and L.P. Lighthart, "On the Utilization of Embedded Symbol for CCSK BER Improvement in TDCS Dynamic Spectrum Access", *EuWiT 2008* pp. 123-126, October 2008
[10] J. G. Proakis and Masoud Salehi *Digital Communications, Fifth Edition* McGraw-Hill, 2008
[11] G. Fumat, P. Chargé , A. Zoubir, D. Fournier-Prunaret, "Transform Domain Communication Systems from a multidimensional perspective", *IET Communications*, to be published, 2011
[12] G. M. Dillard, M. Reuter, J. Zeidler and B. Zeidler, "Cyclic code shift keying: a low probability of intercept communication technique", *IEEE Transactions on Aerospace and Electronic Systems* Vol. 39, Issue 3, pp. 786-798, July 2003

 ISBN: 978-1-61208-123-6

A Scalable Decentralized MAC Scheduling for Cognitive Wireless Mesh Network

Mehdi Msakni, Luong Dinh Dung, Mohamad Haidar and Zbigniew Dziong
Electrical Engineering Department
Ecole de Technologie Supérieure (ETS)
Montréal, Quebec, Canada
e-mail : {mehdi.msakni.1, luong.dinhdung.1, mohamad.haidar.1, zbigniew.dziong}@ens.etsmtl.ca

Abstract— **Cognitive Wireless Mesh Networks (CWMN) is a promising technology that combines the advantages of Wireless Mesh Networks (WMN) with the capacity enhancement feature due to the use of available channels discovered with cognitive radio technology. In CWMN, Medium Access Control (MAC) layer has to schedule data communications in a dynamic environment in which available channels change in space and time. Therefore, scheduling in a CWMN is more difficult than scheduling in multi-channel IEEE 802.11 since each node in a CWMN can support different set of channels for data transmission where as in IEEE 802.11 all nodes share same set of channels. In this paper, we propose an efficient link scheduling algorithm in a distributed architecture in CWMN. The solution utilizes 2-distance vertex coloring scheme at the node level which increases the processing speed of the scheduling algorithm and lessens the overhead control data. Simulation results show that the proposed algorithm improves the scalability, the speed, and the amount of control data exchange when compared with existing algorithms.**

Keywords-Wireless Mesh Networks; Cognitive Radio; Medium Access Control layer scheduling; link scheduling; vertex colouring

I. INTRODUCTION

Wireless Mesh Networks (WMNs) have a growing popularity due to its simple architecture, ease of installation, and low costs of maintenance [1]. Because WMNs utilize the air medium, this makes it susceptible to radio frequency interference that limits the network capacity. In fact, the radio frequency interference limits the number of simultaneous transmissions in a single channel causing the network capacity to drop [2].

One approach to enhance the network capacity is to utilize the multiple available channels that are discovered by means of Cognitive Radio (CR) [3]. CR is a promising technology that allows communication on channels without acquiring a license. The nodes, in reference to the WMN nodes in a CR system, also referred to as secondary users (SUs), sense the spectrum periodically to find unutilized channels. Then, the SUs communicate among themselves using the discovered unutilized channels with the condition that they do not interfere with channels' owners, also known as the primary users (PUs). Therefore, a Cognitive Wireless Mesh Networks (CWMN) requires a new MAC layer enhancement that can meet the challenges of this new environment. Unlike multi-channel networks, such as IEEE 802.11, where the set of channels is shared among all nodes, this type of network faces continuous changes in availability of channels in space and time. In fact, each node in the network can have different set of channels. Consequently, any pair of nodes that wish to communicate has to establish a common communication channel and time to exchange packets without causing interference with other existing transmissions. Therefore, CWMN requires an efficient scheduling algorithm that can tackle the above challenges.

In this paper, we consider Time Division Multiple Access (TDMA) as our channel access protocol. Since it avoids collision and provides efficient channel utilization. The goal of TDMA MAC scheduling in a CWMN is to minimize the number of timeslots needed for data transmission by assigning a channel and a timeslot to each link without interfering with already scheduled links. Each TDMA slot is assigned to at least one link which represents the transmitter-receiver pair that has data to exchange. To achieve this objective, we propose an algorithm to schedule the links in a distributed manner.

The rest of the paper is organized as follows. Section II defines the problem at hand in a set of equations. Section III describes the related works to the domain. Section IV reveals our approach to the link scheduling algorithm. Section V presented the numerical results of our approach. Finally, Section VI concludes the paper.

II. PROBLEM FORMULATION

Our motivation is to improve the scalability of the network, reduce the amount of control overhead, and minimize the overall scheduling time. We consider a CWMN in which the nodes are equipped with an omni-directional radio antenna and use one common control channel. We assume that all the radios have a channel switching delay equal to zero and their interference range is equal to their communication range. Each node may have different set of data channels available.

A link *l* is defined by:

- A transmitter *t(l)* and a receiver *r(l)* which are in the communication range of each others and have a packet to exchange.

 ISBN: 978-1-61208-123-6

- $LinkChSet_l$ is the set of common available channels between nodes *t(l)* and *r(l)* and is not empty.
- $InterferenceSet_l$ is the set of links that can interfere with link *l*. Link *n* belongs to $InterferenceSet_l$ if *r(l)* is in the communication range of *t(n)* or if *r(n)* is in the communication range of *t(l)*.
- $ExclusionSet_l$ is the set of links that have at least a node in common with link *l*. Link *n* belong to $ExclusionSet_l$ if the transmitter *t(n)* or the receiver *r(n)* is also the transmitter *t(l)* or the receiver *r(l)*.
- X_{lcs} is a variable where

$$X_{lcs} = \begin{cases} 1 \text{ if link } l \text{ is active on channel } c \text{ and timeslot } s. \\ 0 \text{ otherwise.} \end{cases}$$

In CWMN, which have a set of links *LinkSet* and a set of channels *ChSet*, the scheduling algorithm should satisfy:

$$\forall l \in LinkSet, \sum_{c \in LinkChSet_l} \sum_{s=1}^{k} X_{lcs} = 1 \quad (1)$$

$$\forall l \in LinkSet, \forall c \in LinkChSet_l, \forall s 1 \le s \le k, \quad X_{lcs} + \sum_{n \in InterfercenceSet_l} X_{ncs} \le 1 \quad (2)$$

$$\forall l \in LinkSet, \forall s 1 \le s \le k, \quad \sum_{c \in ChSet} X_{lcs} + \sum_{c \in ChSet} \sum_{n \in ExclusionSet_l} X_{ncs} \le 1 \quad (3)$$

$$\forall l \in LinkSet, \forall c \notin LinkChSet_l, \forall s 1 \le s \le k, X_{lcs} = 0 \quad (4)$$

Equation (1) states that each link is assigned to one and only one channel and one timeslot. Equation (2) verifies that the interfering links are not assigned to the same channel and timeslot. Equation (3) ensures that a node does not perform two operations simultaneously (i.e. transmit two packets or receive two packets or transmit one packet and receive one packet). Equation (4) guarantees that link *l* can only be scheduled on a channel that is common to *t(l)* and *r(l)*. Our objective is to propose a scalable and fast scheduling algorithm that satisfies the four equations while minimizing the number of timeslots, *k*, used to schedule all the links in the network.

III. RELATED WORK

In multi-channel single-radio 802.11 networks, different approaches to scheduling at the MAC layer have been proposed. In [4], [5] and [6] a MAC layer scheduling based on reservation of channel by RTS/CTS mechanism on the control channel has been presented. In [7], the proposed approach is divided into two steps: The first step is a control one during which the nodes use the control channel to select the channels to be used, and, in the second step the nodes send their data on the selected channel using the RTS/CTS mechanism. In [8] and [9], nodes synchronously execute a common sequence of hops across all channels. A pair of nodes stops performing the channel hopping sequence in order to make data transmission in which they reserve the channel by RTS/CTS mechanism. Once data transmission ends, they rejoin the common hopping sequence. In [10] and [11], each node carries out a different sequence of hops generated from a random number. A pair of nodes wishing to communicate must meet on a particular channel, stops the sequence of hops to carry out the data transmission, and rejoins their respective sequence of hops at the end of the transmission.

For a single-radio Cognitive network, different MAC layer scheduling algorithms have been proposed. A MAC layer scheduling based on reservation of channel by RTS/CTS mechanism on the control channel was presented in [12], [13], and [14]. The objective of [15] is to achieve efficient channel and timeslot assignments to the links in a distributed way which is compared to the optimal scheduling solution found by an Integer-Linear Programming (ILP) formulation. In the considered cognitive radio network, the nodes are equipped with a radio and a control channel. The CSMA/CA scheme is used to access the control channel and the TDMA scheme is used to access the data channels. Each node has a rank which depends on the number of active links and the number of channels. The node with the highest rank in its two-hop neighborhood processes the algorithm of assignment of timeslots. This algorithm assigns the first available timeslot to the link. Nodes that finish the execution of the algorithm are marked as covered. Then, the uncovered nodes with the highest rank in its two-hop neighborhood execute the algorithm. As soon as all the nodes are covered, each node with the lowest rank in its two-hop neighborhood starts to examine if it has the highest schedule length (the number of timeslots needed to schedule all the links) in the network. Finally, the node that has the highest schedule length broadcasts a message to all the nodes to indicate the highest schedule length and the start time of communication phase. In case of tie among two or more nodes, the highest ID node broadcasts its message to all of the remaining nodes.

From the results shown in [15], we can see that this approach, referred to as ranking approach, demonstrates a schedule length near to the optimal. However, the ranking approach presents a problem of scalability, high overhead, and a long execution time. The channel and timeslot assignment algorithm in [15] is carried out according to an order established by the ranks of the nodes and has a low simultaneous execution number. In a chained wireless network topology whose nodes have ranks which increase gradually starting from the beginning of the chain, only one node execute the algorithm at a time. Therefore, the total time of scheduling will increase exponentially with the number of nodes in the network. Moreover, the use of CSMA/CA scheme forces to send a copy of the control packet to each of the neighbors. Each sent control packet requires RTS, CTS and an ACK packet which causes a significant increase in the amount of control data exchanged. Finally, the use of the backoff

 ISBN: 978-1-61208-123-6

mechanism also adds an additional delay to access the control channel.

IV. SCHEDULING ALGORITHM

In this section, we present our link scheduling solution in the network. To achieve a scalable solution, each node is assigned a color which is unique in its two-hop neighborhood (vertex coloring) [16] and [17]. The order of execution of the channel and data timeslot assignment algorithm is determined by the color of the node. So the nodes which have the same color carry out the algorithm at the same time. Therefore, the total time of scheduling is defined by the number of colors which depends on the network's node density.

To avoid any inconvenience due to the use of CSMA/CA, the nodes utilize the TDMA scheme to send control packets on the control channel. Therefore, there will be two sub-frames in the TDMA frame as shown in Figure 1. The control sub-frame is divided into mini-timeslots to send control packets and the data sub-frame is divided into timeslots to send data packets. By avoiding contention to access the control channel, a node can broadcast a control packet in the control mini-timeslots to its neighbors which leads to reduce the amount of data control packets. In a control sub-frame, each control mini-timeslot corresponds to a color in which the nodes with this color can transmit. It is of importance to note that TDMA synchronization in the network is achieved by using a GPS device and that the nodes sense the spectrum and exchange control information about available channels between each frame.

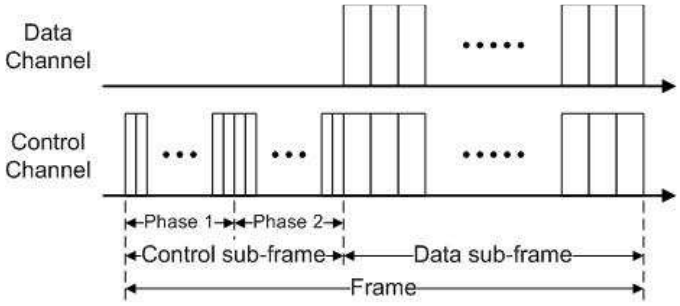

Figure 1. Structure of frame which is composed of a control phase and a data communication phase in the CWMN

In our coloring approach, the execution of the channel and data timeslot assignment algorithm needs two phases. In the first phase, referred to as the scheduling link phase, nodes schedule their outgoing links where as in the second phase, referred to as the establishing data sub-frame size, nodes determine the maximum data sub-frame size in the network. Here are more details about each phase:

A. Phase 1- Scheduling Link Phase

In the first phase, the execution order of the channel and data timeslot assignment algorithm is done according to node colors. Nodes who have the lowest color index execute the algorithm first. In a network with *M* colors, the first phase will need *M* step as described in the Figure 2. Each step has *M* control mini-timeslots. At the beginning of a step *i*, all nodes of color *i* assign channels and data timeslots to their outgoing links and broadcast the scheduling information in the message *Schedule_Information* to their neighbors in the first control mini-timeslot (which have the color *i*). In particular, a node selects the outgoing links with the lowest number of available channel. In case of a tie, the source node selects the outgoing links based on the lowest ID of the destination node and so forth. Then, this node assigns to each outgoing link a data timeslot without causing interference with the already scheduled links by starting with the first available data timeslot of each channel. Step *i* have *M* control mini-timeslots to allow the neighbors of different colors to forward the information in the two-hop neighborhood. Control mini-timeslots are colored from *i* to *M* then from 1 to *i*-1. At the end of step *i*, all nodes of color *i* are marked covered. Thus, the total number of control mini-timeslots needed to schedule all the links in the network is M^2.

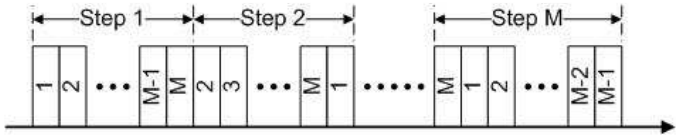

Figure 2. Timeslot colouring in the first phase of the scheduling algorithm

B. Phase 2 – Establishing the Data Sub-Frame Size

In the second phase, nodes determine the maximum data sub-frame size in the network. The control mini-timeslots are colored cyclically from *M* to 1 as presented in Figure 3. Nodes that have the highest color in its two-hop neighborhood are termed as root nodes and start to establish the maximum data sub-frame size in a breadth-first fashion. The breadth-first fashion is described as follows. A root node sends an *Attempt_size* message which includes the following information: its actual maximum data sub-frame size, identity of the root node, and identity of parent node which is equal to its identity. The neighbors of a root node become its children in the logical tree.

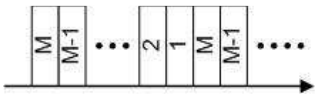

Figure 3. Timeslot colouring in the second phase of the scheduling algorithm

When a node *x* receives an *Attempt_size* message of the root node *z* from node *y* does one of the following:

- If the maximum data sub-frame size contained in the message is bigger than the actual maximum data sub-frame size of node *x*, then node *x* becomes a child of node *y* in the logical tree of root node *z* and updates its maximum data sub-frame size. In case of a tie, for the

 ISBN: 978-1-61208-123-6

maximum data sub-frame size, node *x* does one of the following: (i) if node *x* is not part of any logical tree, then, node *x* becomes a child in the logical tree of root node *z*, (ii) else node *x* is already a part of a logical tree of root node *v*. Therefore, node *x* becomes a child in the logical tree of root node *z* if the ID of node *z* is higher than the ID of node *v*. After becoming a child in the logical tree of root node *z*, node *x* writes in the *Time_Recv_Attempt* message the reception time of the message *Attempt_size*. It broadcasts the information about the maximum data sub-frame size to all of its neighbors in the message *Attempt_size* which includes the maximum data sub-frame size, the identity of the root node, and the identity of the parent node. All of the neighbors except its parent become a potential child of node *x*. By receiving the message *Attempt_size*, node *y* has a confirmation that node *x* is its child in the logical tree.

- If the maximum data sub-frame size contained in the message is lower than the actual maximum data sub-frame size of node *x*, then node *x* discards the message.
- If the message indicates that node *x* is the parent of node *y*, then node *x* changes the status of node *y* from a potential child to child.
- If node *x* is already part of the logical tree of the root node *z* and the message indicates that node *w* is the parent of node *y*, then node *x* removes node *y* from its list of potential children. When a node has empty list of potential children and has no children, it sends an *Acknowledgement* message which contains *Time_Recv_Attempt* to its parent. When a node has *Acknowledgement* messages from all of its children and has an empty list of potential children, it sends an *Acknowledgement* message to its parent. The *Acknowledgement* message contains the highest value of *Time_Recv_Attempt* message received in the *Acknowledgement* messages of its children.

The root node who has received an *Acknowledgement* message from all of its children deduce that its data sub-frame size is the highest and that all nodes in the network are part of its logical tree. So, it has spread successfully the maximum data sub-frame size to all the nodes in the network. Then, it computes the delay to reach the furthest node from the highest value of *Time_Recv_Attempt* and the time of transmission of the message *Attempt_size*. With this delay known, the node knows the time it will take for its message to reach all the nodes in the network and, then, can establish the start time of the communication phase. Then, the node sends a *Communication_Phase_Information* message which contains the start time and the number of timeslots of the data communication phase and indicates the end of the second phase. The *Communication_Phase_Information* message travel through the logical tree.

V. PERFORMANCE ANALYSIS

In this section, we compare the ranking approach and the coloring approach in two sets of simulations to determine scalability improvement and the reduction of the execution time of the channels and data timeslots assignments. To achieve this objective, we analyze the time spent for transmitting control packets and data packets, the data sub-frame size, and the goodput of a link. The results shown in the figures below present the mean value of 50 simulations of 60 seconds each. The simulation platform used in our simulations for the two approaches is NS-2 [18]. Nodes have a communication range of 250m and always have a packet of 1500 bytes to send to each neighbor. The number of channels available at each node is randomly chosen between 1 and 25. The channel identities are chosen between 1 and 50. The data timeslot is 0,6675ms which is the time necessary to transmit a packet of 1500 bytes. In the first set of simulation scenarios, nodes are placed to form a grid topology and separated by a distance of 176m. The number of nodes in the grid is 16, 25, 36, 49, 64, 81, 100, 121, and 144. In the second set of simulation scenarios, nodes are placed randomly in a square area. In this set, the area of the network is 467m x 467m, 738m x 738m, 1044m x 1044m, 1279m x 1279m, 1477m x 1477m, 1651m x 1651m, and 1809m x 1809m for 10, 25, 50, 75, 100, 125, and 150 nodes, respectively, ensuring the same density.

Figure 4 and Figure 5 show the time spent for transmitting control data for the first set of simulations and the second set of simulations. We observe an important difference between the two approaches. The time spent for transmitting control data for the ranking approach vary from 1,074s to 3,046s for the first set of simulation scenarios and from 0,416s to 2,533s for the second set of simulation scenarios. The time spent for transmitting control data for the coloring approach ranges from 4,288ms to 10,075ms for the first set of simulation scenarios and from 2,846ms to 11,211ms for the second set of simulation scenarios. The difference can be justified due to the fact that the coloring approach is using 2-distance vertex coloring to allow simultaneous execution of the scheduling algorithm where as the coloring approach is using TDMA to avoid contention to access the control channel. We notice that the curve of the time spent for the first phase of the coloring approach have similar behavior to that of the number of colors needed for the network (Figure 8 and Figure 9) because the duration of the first phase depends on the number of colors.

Figure 6 and Figure 7 show the schedule length for the first set of simulation scenarios and for the second set of simulation scenarios. We observe that the ranking approach achieve a better schedule length than the coloring approach. In the scenario of 144 nodes (12 x 12 grid) for the first set of simulations, we notice a difference of 5,58 timeslots between the two approaches which represents 3,724ms. While in the scenario of 150 nodes for the second set of simulations, we observe a difference of 4,46 timeslots between the two approaches which represents 2,977ms. The ranking approach presents a better schedule length because it gave priority to nodes that have a low ratio between the number of channels and the number of links to schedule their links. However, this difference is relatively small compared to time spent to send control data for the ranking approach. We see a difference in the schedule length between the first and the second set of simulations since in the first set the nodes are placed deterministically in the network to cover the network area and

 ISBN: 978-1-61208-123-6

to maximize the number of neighbors for each node. Therefore, this difference can be explained by the fact that in the grid topology the mean number of neighbors and outgoing links to be scheduled is higher than in the mesh topology.

Figure 8 and Figure 9 show the mean number of colors needed in the network for the coloring approach in the first set of simulation scenarios and in the second set of simulation scenarios. In the first set, we observe that the number of colors become constant for more than 100 nodes in the network. In the second set, we notice that the mean number of colors converge to 11,93 for more than 125 nodes in the network. The difference in the behavior of the curve of the number of colors between the first and the second set of simulations is because in the first set of simulations the nodes are placed deterministically in the network while in the second set of simulations the nodes are placed randomly in the network.

Figure 10 and Figure 11 show the mean goodput of a link for the first set of simulation scenarios and for the second set of simulation scenarios. As expected, the coloring approach achieves a better goodput than the ranking approach. In fact, the coloring approach accomplishes a goodput for a link of 375,048 to 672,694 Kbits/s for the grid topology and 394,102 to 987,515 Kbits/s for the mesh topology and a goodput for a node of 2,635 to 3,531 Mbits/s for the grid topology and 2,488 to 3,717 Mbits/s for the mesh topology. On the other hand, the ranking approach accomplishes a goodput for a link of 3,915 to 11,037 Kbits/s for the grid topology and 4,705 to 28,2 Kbits/s for the mesh topology and a goodput for a node of 27,519 to 57,945 Kbits/s for the grid topology and 29,713 to 106,146 Kbits/s for the mesh topology. The major difference in goodput between the two approaches can be explained by the fact that the ranking approach spends more time to exchange control information.

It is also noticed that the coloring approach uses the channels more efficiently than the ranking approach. In the coloring approach, the time spent for data transmission represents %68,51 to %75,96 for the grid topology and %63,17 to %76,57 for the mesh topology. On the other hand, in the ranking approach, the time spent for data transmission represents %0,59 to %1,13 for the grid topology and %0,63 to %2,05 for the mesh topology. Therefore, the coloring approach provides a better efficient use of the channels than the ranking approach.

The results at hand show that the coloring approach improves the scalability of the scheduling in the networks. Indeed, the 2-distance vertex coloring of the node allows achieving a scalable solution because the execution of the scheduling algorithm depends on the number of colors in the network. This permits the nodes which have the same color to schedule their outgoing links at the same time. Also, it utilizes the TDMA scheme to send control packets on the control channel which reduces the amount of data control packets sent and the time of execution of the scheduling algorithm. Nonetheless, in the coloring approach, the links need less delay to transmit a packet than in the ranking approach. As a result, the coloring approach presents an advantage for real-time application.

The ranking approach presents a better scheduling because the scheduling algorithm gives priority to nodes that present a low ratio between the number of channels and the number of links to be scheduled while the ranking approach needs a large amount of control packets exchanged leading to poor efficiency utilization of the channels.

VI. CONCLUSIONS

In this paper, we investigated the MAC-scheduling in a CWMN. We proposed an approach to improve the scalability, decrease the amount of control data sent, and diminish the time of execution of the scheduling while decreasing the schedule length. The approach utilizes 2-distance vertex coloring approach of the node to increase the simultaneous activity in the execution of scheduling algorithm in the network. It also uses the TDMA scheme to avoid contention to access the control channel. We compared our approach to another approach from the existing literature which is referred as the ranking approach. The results show a significant improvement in term of scalability, goodput, efficient utilization of channels, amount of control data sent, and the time of execution of scheduling. The ranking approach achieves a better schedule length but the gap is smaller compared to the advantages shown by the coloring approach. In future works, we plan to extend the proposed work to take the quality of service into consideration.

REFERENCES

[1] I. F. Akyildiz, X. Wang, and W. Wang, "Wireless mesh networks: a survey," *Computer Networks*, Elsevier, Netherlands, vol. 47, pp. 445-487, Mar. 2005.

[2] P. Gupta and P. R. Kumar, "The capacity of wireless networks," *IEEE Transactions on Information Theory*, IEEE, United States of America, vol. 46, pp. 388-404, Mar. 2000.

[3] J. Mitola Iii and G. Q. Maguire Jr, "Cognitive radio: making software radios more personal," *IEEE Personal Communications*, IEEE, United States of America, vol. 6, pp. 13-18, Aug. 1999.

[4] S.-L. Wu, C.-Y. Lin, Y.-C. Tseng, and J.-P. Sheu. "A New Multi-Channel MAC protocol with on demand channel assignment for mobile ad-hoc networks," In *Proc. International Symposium on Parallel Architectures, Algorithms and Networks*, Dallas/Richardson, Texas, United States of America, Dec. 2000, pp. 232-237.

[5] S.-L. Wu, C.-Y. Lin, Y.-C. Tseng, C.-Y. Lin, and J.-P. Sheu. "A Multi-Channel MAC protocol with Power Control for Multihop Mobile Ad-hoc Networks," *The Computer Journal*, Oxford University Press, United Kingdom, Vol. 45, pp. 101-110, 2002.

[6] W.-C. Hung, K. L. Eddie Law, and A. Leon-Garcia, "A Dynamic Multi-Channel MAC for Ad-Hoc LAN," In *Proc. Biennial Symposium on Communications*, Kingston, Canada, Jun. 2002, pp. 31-35.

[7] J. Chen, S. Sheu, and C. Yang, "A new multichannel access protocol for IEEE 802.11 ad hoc wireless LANs," In *Proc. International Symposium on Personal, Indoor and Mobile Radio Communications*, Vol. 3, Beijing, China, Sep. 2003, pp. 2291-2296.

[8] A. Tzamaloukas and J.J. Garcia-Luna-Aceves, "Channel-Hopping Multiple Access," In *Proc. IEEE International Conference on Communications*, New Orleans, Louisiana, United States of America Jun. 2000, pp. 415-419.

[9] A. Tzamaloukas and J.J. Garcia-Luna-Aceves, "Channel-hopping multiple access with packet trains for ad hoc networks," In *Proc. IEEE Mobile Multimedia Communications*, Tokyo, Oct. 2000.

[10] P. Bahl R. Chandra, and J. Dunagan, "SSCH: Slotted Seeded Channel Hopping for Capacity Improvement in IEEE 802.11 Ad-Hoc Wireless Networks," In *Proc. Annual International Conference on Mobile*

 ISBN: 978-1-61208-123-6

Computing and Networking, Philadelphia, Pennsylvania, United States of America, Sep. 2004, pp. 216-230.

[11] H. S. So, W. Walrand, and J. J. Mo, "McMAC: A Parallel Rendezvous Multi-Channel MAC Protocol," In *Proc. IEEE Wireless Communications and Networking Conference*, Hongkong, China, Mar. 2007, pp. 334-339.

[12] A. Chia-Chun Hsu, D.S.L. Weit, and C.-C.J. Kuo, "A cognitive MAC protocol using statistical channel allocation for wireless ad-hoc networks," In *Proc. IEEE Wireless Communications and Networking Conference*, Hongkong, China, Mar. 2007, pp. 105-110.

[13] J. Jia, Q. Zhang, and X. Shen, "HC-MAC: A hardware-constrained cognitive MAC for efficient spectrum management," *IEEE Journal on Selected Areas in Communications*, Vol. 26, pp 106-117, Jan. 2008.

[14] L.-C. Wang, A. Chen, and D. S. L. Wei, "A cognitive MAC protocol for QoS provisioning in overlaying ad hoc networks," In *Proc. Annual IEEE Consumer Communications and Networking Conference*, Las Vegas, Nevada, United States, Jan. 2007, pp. 1139-1143.

[15] M. Thoppian, S. Venkatesan, R. Prakash, and R. Chandrasekaran, "MAC-layer scheduling in cognitive radio based multi-hop wireless networks," In *Proc. IEEE International Symposium on a World of Wireless, Mobile and Multimedia Networks*, Buffalo-Niagara Falls, New York, United states, Jun. 2006, pp. 191-200.

[16] Z. Xizheng, "Efficient broadcast scheduling using a fuzzy-hopfield-network based mixed algorithm for ad hoc network," In *Proc. International Conference on Advanced Language Processing and Web Information Technology*, Luoyang, Henan, China, Aug. 2007, pp. 405-408.

[17] S. Haixiang and W. Lipo, "Broadcast scheduling in wireless multihop networks using a neural-network based hybrid algorithm," *Neural Networks*, Elsevier, United Kingdom, vol. 18, pp. 765-71, Aug. 2005.

[18] Network Simulator NS-2, http://www.isi.edu/nsnam/ns/, [15 Jun. 2010].

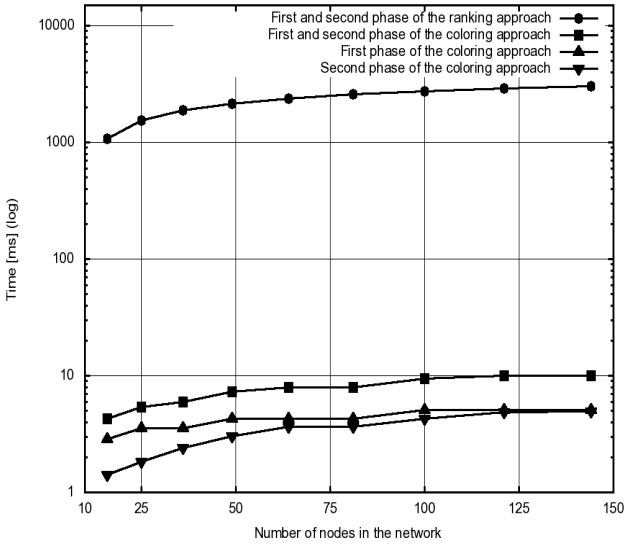

Figure 4. Time spent in a frame for scheduling links (first phase) and establishing the data sub-frame size (second phase) for the coloring and the ranking approach in the grid network

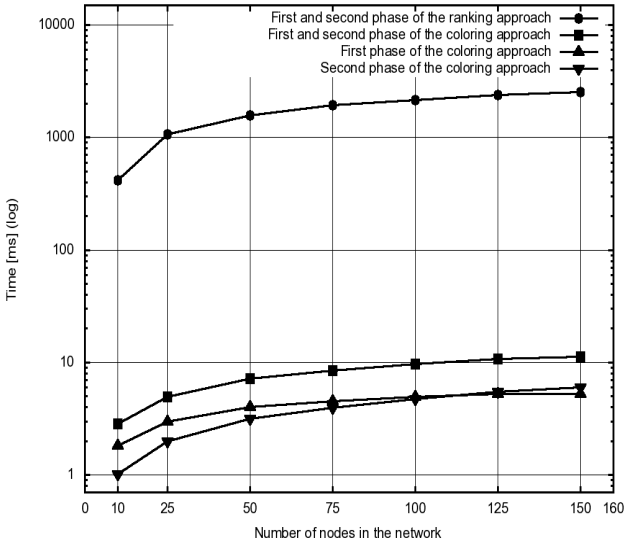

Figure 5. Time spent in a frame for scheduling links (first phase) and establishing the data sub-frame size (second phase) for the coloring and the ranking approach in the mesh network

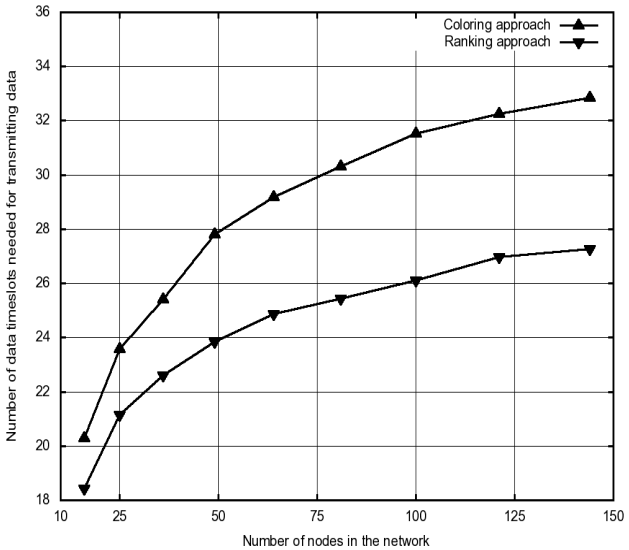

Figure 6. Schedule length of the coloring and the ranking approach in the grid network

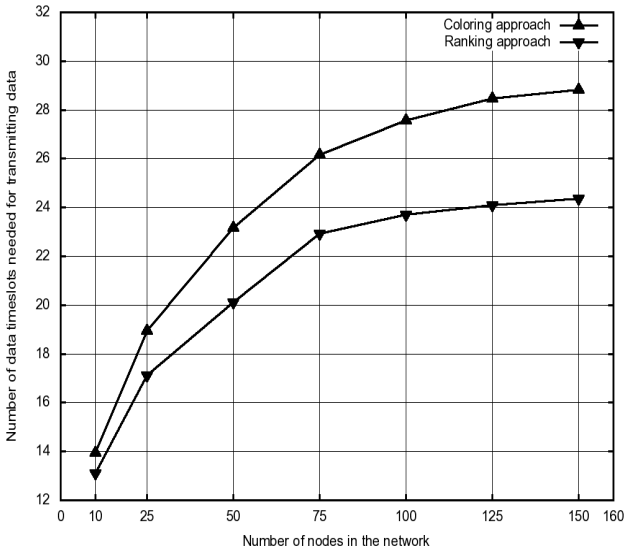

Figure 7. Schedule length of the coloring and the ranking approach in the mesh network

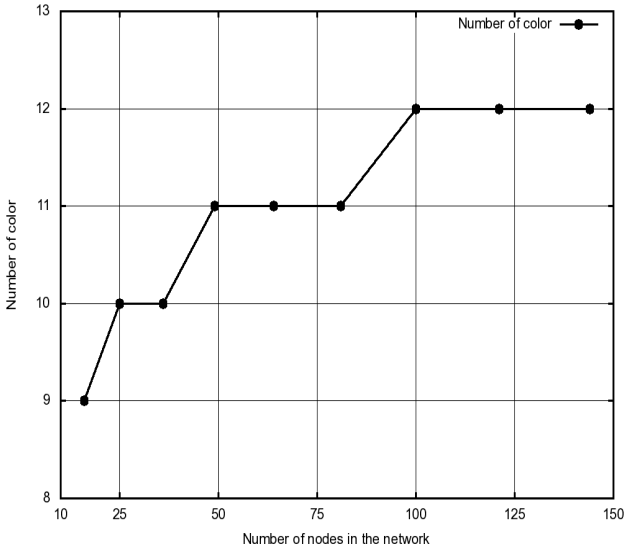

Figure 8. Number of colors needed in the coloring approach in the grid network

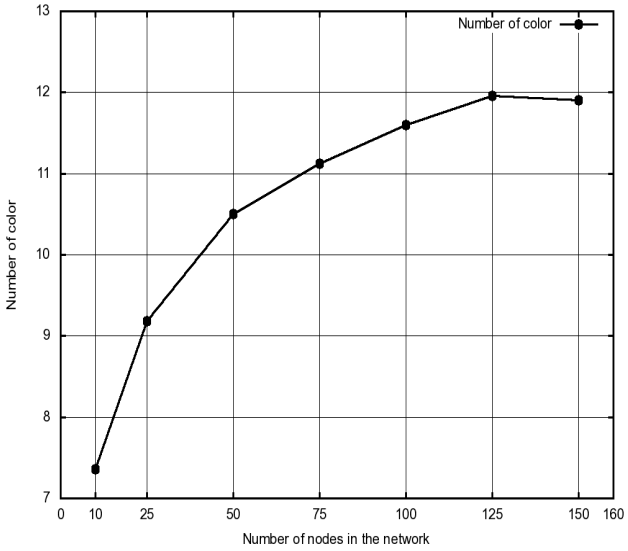

Figure 9. Number of colors needed in the coloring approach in the mesh network

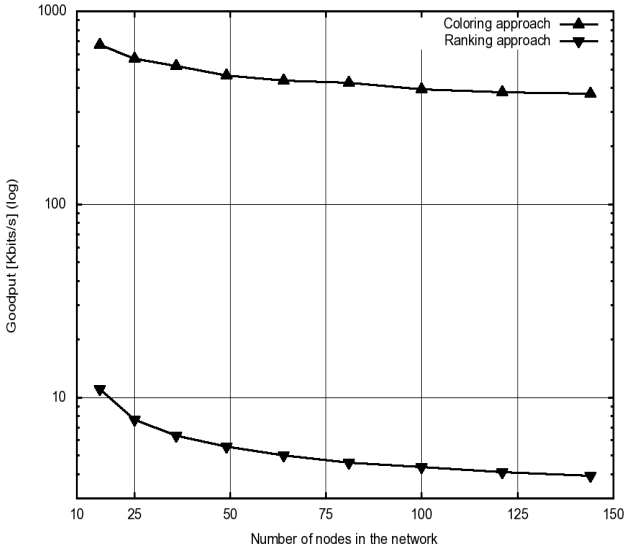

Figure 10. Mean goodput of a link for the coloring and the ranking approach in the grid network

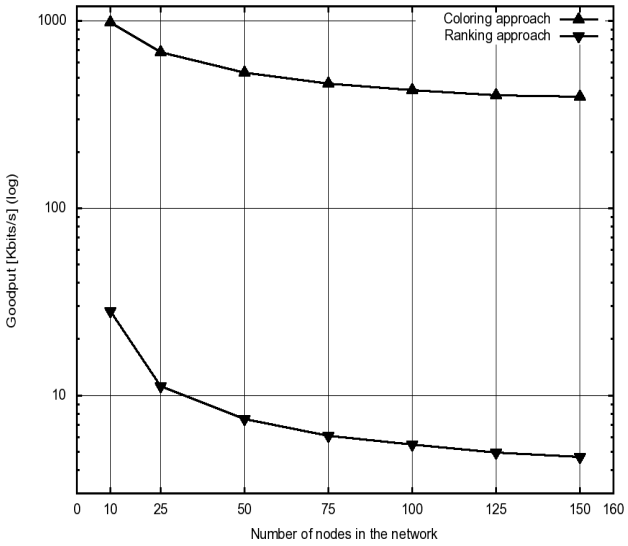

Figure 11. Mean goodput of a link for the coloring and the ranking approach in the mesh network

 ISBN: 978-1-61208-123-6

Efficient Distribution of Location Information and Locating Radio Devices for Dynamic Spectrum Allocation Systems

Toan Hoang*, Josef Noll† and Torleiv Maseng*
Email: toan@unik.no, josef@unik.no and torleiv.maseng@ffi.no

*Norwegian Defense Research Establishment (FFI)
†UNIK - University Graduate Center

***Abstract*—In the recent years, we have seen a clear trend in consumer devices being equipped with multiple radio interfaces such as GSM, UMTS, WiFi. These types of devices will soon be ubiquitous. Since radio frequency is a limited resource, the need for sharing and re-using a radio spectrum will be even more noticeable than before. Studies show that collaboration when allocating a radio spectrum will result in better network performance. This paper proposes a solution that identifies radio devices in a specific area. Starting from the identification of the location of possible interfering devices, better decisions can be made, prior and under spectrum allocation through cooperation. Our solution provides the location information in an overlay network without need for additional exchange of information messages. By storing the geographic location directly in the node-id, all members of the overlay network can extract the exact location of all known nodes. Using geocast, we show that the information provided can be used to optimize existing geocast mechanisms to identify devices. The result is an overlay-based enhanced spectrum allocation system, ObeSA.**

***Index Terms*—Dynamic Spectrum Access, geo-cast, Distance Flooding Protocol, overlay network, ObeSA**

I. INTRODUCTION

Cognitive Radio (CR) was first introduced by Mitola in 2000 [1]. Since then, the CR research field has shown great advancements. Evidence of such progression and acceptance was when the FCC approved unlicensed CR devices to access the free frequencies in the TV bands [2]. These frequencies are known as the 'TV white spaces' spectrum. The most important requirement for these radio devices is that they do not cause harmful interference to the primary users (TV receivers).

Studies [3] show that collaboration between radio units result in better network performance. In the field of CR, there have been many studies in physical spectrum sensing. This function is essential for CRs to be able to operate autonomously. Even though physical sensing has seen many advances lately, without coordination and cooperation between CRs, old issues like the "hidden-node" problems are still present. The FFC's report [2] concluded that with the technology available at the time the report was written, it is not possible to have reliable sensing.

We believe that the opening of the 'TV white spaces' is only one step towards a new future where all spectrum are allocated dynamically. In the future, there will be no such thing as primary or secondary users. All radio devices are equal users of the radio frequencies. Radio frequency will become a product that the end-users only lease when needed. Compared to how CR network is defined, for easier understanding, we can imagine that the owners of the frequencies are the primary users and all other radio devices are secondary users. Our vision of the future of spectrum allocation is presented in [4]. This paper is targeted at this type of network.

The focus of this paper is to enhance spectrum allocating by creating a solution for identifying possible interfering devices. In a heterogeneous network, we see a need of a common, dynamic and efficient way to locate devices of interest. By focusing on a solution between the network and application layer, we believe that it will be easier to implement in the different radio devices. With radio devices that have different specifications, such as battery or calculation capacities, we have focused on a solution that has low impact on the devices. By creating an overlay network where geographic position of the radio devices is provided and using a tailored geocast mechanism, we have created a platform which enables radio devices to allocate other devices of interest, which will result in better spectrum allocation through cooperation. The work in this paper has been based on achieving three goals:

- Efficiently provide the location information in a overlay network
- Add mechanisms to efficient locate radio devices based on location
- Create a lightweight solution to fit all types of radio devices

The rest of the paper is organized as follows. Section II discusses work related to the solution presented in this paper. Section III explains our solution - ObeSA, and how we provide and exploit the location information. As a part of ObeSA, we introduce our own geocast mechanism, distance flooding and compare it to existing well-known geocast flooding mechanisms. In Section IV, we explain our implementation, the simulation settings, and performance metrics. At the end of the

 ISBN: 978-1-61208-123-6

section, we look at the results. Finally, Section V concludes our work and provides suggestions for the direction of future research.

II. Related Work

Considerable work has been done to provide the physical location of a node into an overlay network. Wang and Ji have identified the need of a better way to give a node an identification based on its location [5]. In this paper, entering nodes are given a node-id which is logically selected in-between two other nodes based on their locations. The idea of setting the node-id based on the location, and not randomly, or hashed, by the overlay network, is an interesting approach. Unfortunately, their solution only gives us the relative distance between the nodes. In order to calculate e.g. possible interferences prior to a spectrum allocation, we need to know about the absolute location of the physical neighbours. Without this information, we do not know if they are in the area where we (or they) can create harmful interference to each other. For our purpose, this solution will not give us enough information about the location of the node. Compared to other overlay network implementations already presented [6], this paper does not give us added information.

Chiang et al. show the use of the *Location Estimation Technique* (LET) in [7]. They calculate a hash based on prefix of a nodes' location information. The first node which has the LET hash generated identification will represent the area and is defined as a super-peer. Other nodes with same generated identification will connect to their super-peer as normal-peers. The approach of taking the node's location and use it as a lookup key to find other nodes in a specific area is close to what we are seeking. Unfortunately, by hashing the result, there is no easy way to extract this information. The result is a hierarchy-based solution containing two levels. In a large network, we see a need to build additional levels of super-peers to be able to scale with the number of nodes and/or the size of area a super-seed should represent. The most interesting part of this paper, for us, is the idea of injecting the location information into the node-id.

Ahulló et al. have proposed a distributed hash table (DHT)-generic way to make geographical range queries in [8] by using a hierarchy and clustering approach. They support data and traffic load balancing while making it possible to search and retrieve data by storing the data key close to its physical position. The authors suggest having cluster-layers based on world/continent/country down to the granularity level that is required. The proposed solution has shown a useful way to support geographically ranged searches in DHT, while maintaining data and traffic loads. To our knowledge, this work is the closest to what we are solving in our paper: combining overlay network and a mechanism to locate nodes that are of interest in a specific area. However, the authors have yet to address how to implement the location information into the overlay network in an autonomous way. In their example, the nodes have 4 bits of addressing, 2 for prefix and 2 for suffix.

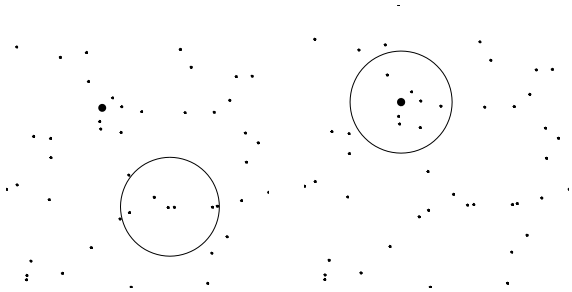

(a) Away from the node (b) Around the node

Fig. 1. Search scenarios

It is unclear how they map a node's real location with this type of addressing.

For a solution to our second goal, we have chosen to look at geocast [9]. Geocast is a mechanism to deliver a message to all nodes in a specified area. Geocast can be divided into two main categories: flooding and non-flooding protocols. Flooding generally generates more messages in the network. By introducing smarter and more controlled flooding techniques, we can exploit the provided location information in the overlay network, get better results than non-flooding and avoid the negative network performance hit introduced by full flooding. Although the non-flooding protocols show great scalability, they require additional network infrastructure. This is often achieved by creating and maintaining a hierarchy. In a fixed network with few nodes entering and exiting, the cost of maintenance is low. However, in a network based on radio devices, even if we do not take mobility into account, radio devices will come and go, thus resulting in a maintenance cost we would like to avoid.

III. ObeSA - Overlay-based enhanced Spectrum Allocation

This work is based on using radio devices that are capable of dynamically allocating radio spectrum. All radio devices have a control channel available for data communication. This channel is used for connecting to the overlay network. Additionally, radio devices must also have knowledge of their location. Location information may be gathered from a GPS (Global Positioning System) device, a network location identifying system or from other methods. For scenarios where the radio devices are indoor, solutions based on RFID may be used [10]. In this section, we first present the scenarios, then the algorithm for creating the node-id based on the location information. Last, we introduce our own version of a controlled flooding mechanism, distance flooding, which exploits the location information provided in the node-ids. It is important to keep in mind that we have focused on a solution that will work on all kinds of radio devices. This is achieved by creating a solution which has low impact on the devices involved, this is to meet the third goal of supporting all kind of radio devices stated in Section I. This implies requirements of less computational power and lower bandwidth in control channels than in alternative solutions.

 ISBN: 978-1-61208-123-6

A. Scenario

To be able to carry out cooperated spectrum allocation successfully, one must coordinate with nodes in the surroundings. Depending on the available frequency and transmitting power, it is easy to compute your own radio working area. All nodes in this area should be identified and coordinated for best results. As shown in Fig. 1, we have identified two scenarios: finding nodes in a area away from the node's location (a) and finding nodes around itself (b). Scenario (a) may be a scenario where the a device is claiming a frequency band in a given geographic location away from itself. Even though this may not be a scenario that first comes to mind, there is still a need to support it. Radio devices that are pre-allocating frequencies in another location will need the support from finding other radio devices away from themselves. Such types of users are described in [4]. Scenario (b) is a more typical scenario for a DSA network. Once the radio device is in need of allocating a frequency, the radio device connects to the overlay network to find all its geographical neighbours. Upon successfully identifying its neighbours, the radio device can coordinate and cooperate to make a better decision about its own spectrum allocation.

B. Providing the location information

As described in Section II, considerable work has been done in terms of providing the location information in an overlay-based network. We have focused on a solution which provides this essential information as efficiently and early as possible. We have chosen to implement the node's location information into the node-id as is done in [7]. However, unlike Chiang et al., we chose to store the location information directly into the node-id without hashing the information. As hashing is a one-way function, there is no way to extract the hashed information. By re-using the node-id as information carrier, no additional overhead is introduced to the distribution of the location information of the nodes. Storing the information in the node-id is also done to keep the overlay implementation as generic as possible. Node-ids from other nodes in the overlay network are available in most of the overlay implementations. With this solution, we are not tied to any specific overlay implementations which in turn may make it possible to use different, compatible, overlay implementations within same network. By storing the location information almost unaltered, keeps the processing requirement when creating and extracting the node-id at a low level.

In our algorithm, Alg. 1, each latitude or longitude results in a string containing 9 characters, combined 18 characters. If we assume that we have 24 characters available for the node-id, we have 6 characters left to fill with other information. As node-ids have to be unique for each node in the network, two nodes at the exact same position cannot have the same node-id. This can be solved by various means such as adding random characters to fill up the remaining free space.

In this paper, we assume that the nodes are equipped with a GPS device. GPS devices use the WGS84 datum [11]. For easier calculations, we use GPS decimal formatted coordinates (latitude, longitude) with 5 decimals. GPS coordinates with 5 decimals have an accuracy of approximately 1 metre. A GPS decimal formatted coordinate varies in two areas: A) The latitude and/or longitude can be a negative decimal. B) The integer part of each decimal can contain 1 to 3 integers. As shown in Alg. 1, variance A in handled by using the first character to identify whether the decimal is negative or not. A different number of integers, variance B, in a decimal is handled by filling the "missing" integers with 0's.

Algorithm 1 Creating a node-id based on location information (latitude and longitude).

Incoming coordinate must contain 5 decimals
Result node-id length is 24 characters

1: **for all** i = latitude, longitude **do**
2: Initiate $result$
3: Delete '.' from i
4: **if** i is a negative number **then**
5: Set the first character in $result$ = 2
6: **else**
7: Set the first character in $result$ = 1
8: **end if**
9: Calculate K numbers of 0 to add in the $result$
10: $K = (18/2) - i.length$
11: Concatenate $result$ with K 0's and i.
12: **end for**
13: Concatenate $result_{latitude}$ and $result_{longitude}$
14: Fill the empty free space with random characters

In order to explain how we calculate the node-id based on the location information using Alg. 1, let us take a node located at Kjeller Airport as an example. Kjeller Airport's GPS decimal formatted coordinate is 59.96944, 11.03888. Since the latitude is not a negative number (59.96944) and the integer part contains only 2 characters (59), we concatenate the latitude with 10. The first character identifies that the latitude is not a negative number. The second character is 0 filling the "missing" integer. The result is 105996944. Likewise, for the longitude, we get 101103888. The result is: 105996944101103888 plus 6 random characters.

By concatenating the latitude and longitude, and adding different paddings, there is very little computation required in this algorithm. As with the generation of node-id, the extraction of location to any given node-id is straightforward. We would like to stress that we have deliberately created a solution with as low requirements as possible, which resulted in this algorithm to store and extract location information in the node-id.

C. Geocast

Flooding, as a general opinion, scales poorly in large networks. Because radio devices have a certain transmission capability, frequencies have different capabilities, the radio coverage of a device is known and limited to the surrounding of its operation area. Based on this fact, and the location information now provided in the node-id, we believe that using a controlled geocast flooding protocol is suitable for our solution.

To study and find a geocast mechanism for our ObeSA

 ISBN: 978-1-61208-123-6

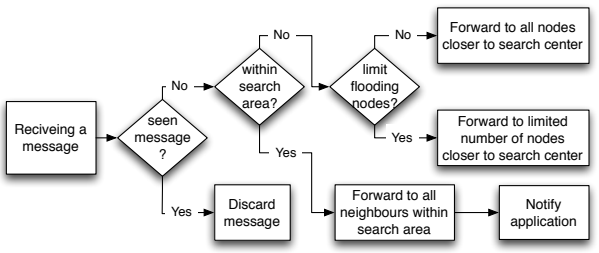

Fig. 2. Distance flooding protocol. Floods to all nodes closer to search centre, floods within search centre.

solution, we have identified 3 different types of geocast flooding protocols:

- ***Simple flooding*** - This is the simplest implementation of flooding. Each node sends the message to all known neighbours. If the message is already seen, the node will discard the message. Each node has to check whether it is within search area or not. This type of flooding does not require or is able to exploit location information if available.
- ***Unicast Routing with Area Delivery (URAD)***- This protocol has been named and simulated in [9]. Based on location information available, URAD uses regular unicast towards its search area. Once the message has entered the search area, the message will be flooded to all nodes in the area. We implemented URAD to unicast (forward) the search message to the node closest to the search *centre* before flooding in search area. This is done to create a direct path as possible towards the search area.
- ***Distance flooding*** - This is our own optimization (Fig. 2. As URAD uses unicast towards an area, we argue that forwarding to multiple nodes closer to the search centre than itself yields a better result. Further optimization of our proposal is to limit number of nodes a message should be forwarded to. We will present the results from these simulations later in this paper, but a deep analysis from these simulations are outside the scope of this paper.

IV. Simulation and results

This section explains how we implemented and which settings we used for our simulation. Then we will look at the performance metrics of the simulations. Finally, we look at and discuss the results.

A. Implementation and settings

We have used the PlanetSim simulator [12] to implement a small geocast mechanism on top of Chord[13]. We are using Chord as the overlay network, because we wanted a simple and well proven overlay network as a base for our solution. As stated before, there should be no problem to use any other overlay network implementations instead of Chord.

The simulated scenarios are flat earth models with an area of 1000 x 1000 metres, with one metre as lowest resolution. All scenarios are pre-generated and re-used for each geocast protocol. For each scenario, the node initiating the search and the search areas are set. Simulations have been run for both scenarios: the search area around the search node and search area away from the searching node. The search area is implemented as a circle, defined by position (latitude, longitude) and a search radius. The search radius is set to 100 metres. The network consists of 100 to 1000 nodes. All nodes are static and are connected to the same overlay network. The displayed results are the average of 100 simulation runs for each protocol in each scenario.

We used an Intel Core 2 Quad Q9400 CPU equipped with 3 GB RAM. The operating system is Fedora Core 12. The simulations takes approx. 7.5 hours to finish.

B. Performance metrics

The performance metrics are based on three parameters: percentage of identified nodes, network load, and number of hops before reaching the last node in a search area:

- ***Percentage of identified nodes*** - is used to measure how good the protocol is to identify all the nodes in the search area. For geocast, this is a very important metric due to the lack of delivery acknowledgement. We need to get as accurate list of nodes as possible of interest in the search area. The higher percentage, the better.
- ***Network load*** - is used to measure how many messages are sent in the overlay network. The lower the number, the better.
- ***Number of hops before reaching last node in the search area*** - is used to measure how fast a search can be finished. Given that all nodes have the same quality in terms of control channel, a lower number means less time (hop) it takes to reach all the nodes within a certain search area.

C. Results

The results shown in Fig. 3, Fig. 4 and Fig. 5 of the distance flooding protocol are with no limit. This means that a node will forward to *all* nodes it knows about that are closer to the search centre than itself. In these figures, the dotted graph lines represent the result of simulations in scenario a (search away from the node). The results from both scenarios in all three algorithms are quite similar, however, the scenario when the search area is around the node (scenario b) has a weaker performance. The reason for this is how Chord selects which neighbours to keep in its finger (routing) table by storing neighbours spread over the whole network.

Fig. 3 shows the simulation results of the percentage of identified nodes in a search area. We see that for both scenarios, simple flooding is performing as expected. It identifies all the nodes, which is not surprising for flooding in a stable network where all nodes are known. Studying the URAD protocol, we see that the more nodes there are in the network, the weaker it performs. This result was expected, and is similar to what has been presented in [9]. Our own protocol, the distance flooding performs very well. When the search area is away from the node, distance flooding has similar results to simple flooding.

 ISBN: 978-1-61208-123-6

In the other scenario, it has a weaker performance. Even though it does not have a perfect performance, it performs much better than the URAD protocol.

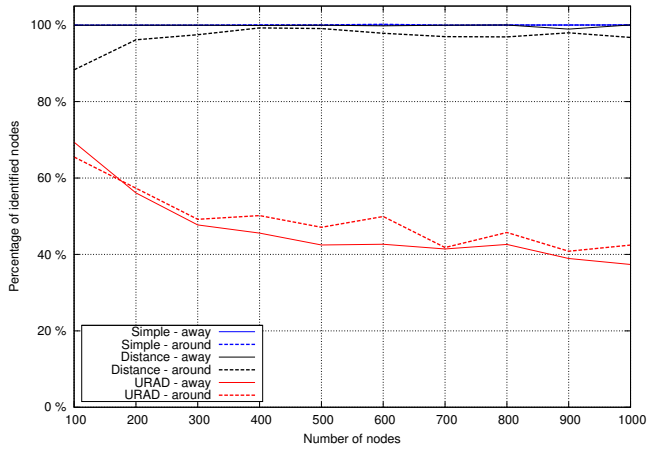

Fig. 3. Percentage of successfully identified nodes in search area.

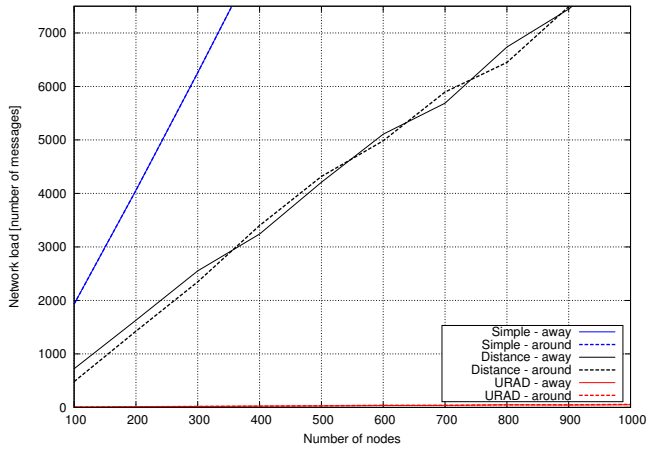

Fig. 4. Total number of messages sent in the network when flooding a message.

The results in Fig. 4 are quite clear. Simple flooding has the highest load on the network. Distance flooding has approx. 60% less network load than simple flooding and the URAD protocol has the best performance. Because URAD uses unicast towards a search area before flooding in the area, there is very little overhead when routing the message towards the search area. Combined with a routing table containing neighbours over the whole network, which is available in Chord, it does not take many hops before the message arrives at a node in the search area away from the searching node.

Fig. 5 shows the results of how many times a message has been forwarded before arriving at the last node (which is in a search area). Again, simple flooding is the worse performer and the URAD protocol is the best. The distance flooding is in the middle, approx 25-30% better than simple flooding.

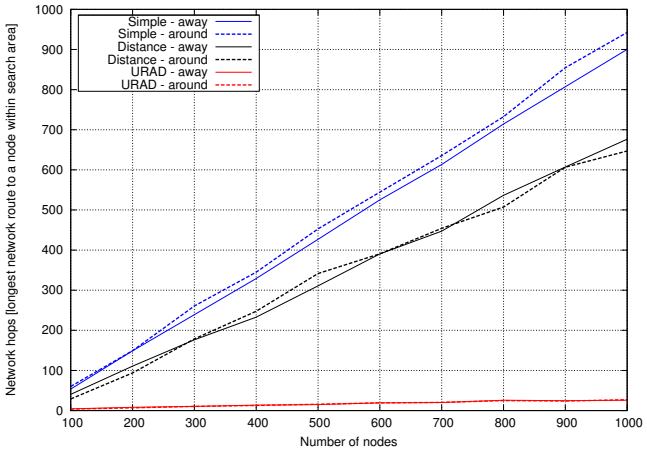

Fig. 5. The longest path a message takes to arriving the last node in search area.

The non-linear and similar results in how simple and distance flooding perform, are the result of the already mentioned Chord's way of selecting nodes in its finger table.

Except for the results in Fig. 3, the result graphs are quite linear. The more nodes there are in the network, the more messages and longer time it takes to identify all the nodes. Even though the URAD flooding protocol is performing extremely well in terms of network load and number of hops before arriving at the last node, the percentage of successfully identifying all nodes within a search area is too low.

Even though our distance protocol has a higher load on the network and takes longer time (as in number of hops) before arriving at the last node than the URAD protocol, the performance of identifying all the nodes in a search area outperforms the URAD protocol. Based on the results, we advocate that the distance protocol is the best mechanism for our solution, ObeSA.

As mentioned earlier, the distance flooding protocol can be further optimized by limiting number of nodes a message should be forwarded towards a search area. The original idea of the distance flooding is to forward to *all* nodes that are closer to the search centre than itself. The term *limit* used in the distance protocol context means that a limit number is set to control how many nodes the distance protocol should forward to. E.g. if the limit is 2, each node should only forward the message to maximum 2 nodes that are closer to the search center than itself. We have simulated the protocol using the same scenarios used earlier, with different number of limits ranging from 2 to 5. If the limit is set to 1, distance flooding will perform exactly like the URAD protocol, which is unicast towards the search area before flooding.

The results in Fig. 6 and 7 indicate that by limiting the number of neighbours a node should forward a message, the network load can be greatly lowered and the percentage rate of successfully identified nodes is still at a much better level than the URAD protocol. The results show that if the limit is set to 2, we see a great improvement in the percentage of

 ISBN: 978-1-61208-123-6

identified nodes in a search area. URADs lowest result is at 38% while the distance protocol has the lowest result at 73%. Looking at the network load, we see that URAD in scenario with 1000 nodes uses 26 messages to identify all nodes in the search area, while the distance protocol with limit = 2 uses 72 message. The number of messages is still quite low compared to simple flooding and no limit distance flooding and still maintaining a good percentage of identified nodes.

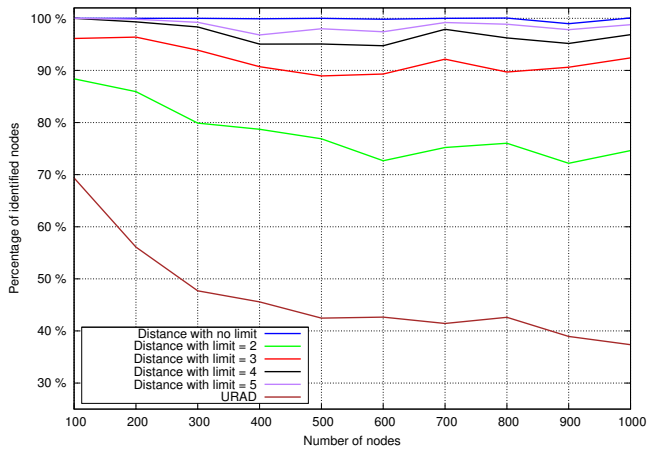

Fig. 6. Percentage of successfully identified nodes in the search area.

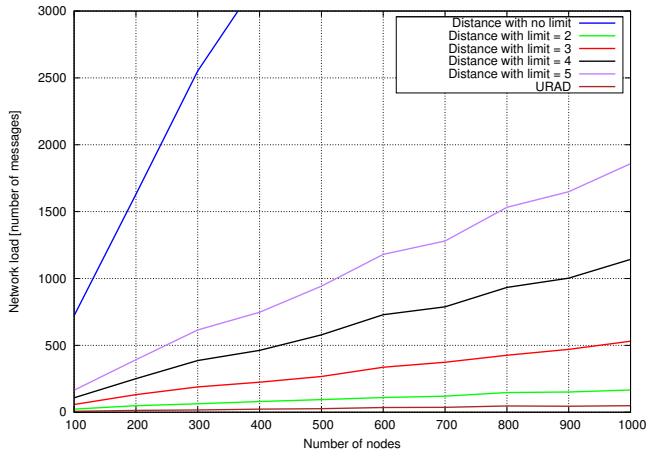

Fig. 7. Total number of messages sent in the network when flooding a message.

V. Conclusion and Future Work

The solution presented in this paper is to our knowledge one of the first examples of combining an overlay-based network and geocast providing a system for cooperation of dynamic spectrum allocation. Our main contributions are: A) creating an algorithm that takes location information and creates a valid node-id. By using the node-id as the information carrier, we have introduced an efficient way of exchanging this information. B) showing how the provided information can be exploited. Here we have created a new geocast flooding protocol called distance flooding. The result of the simulations show that by exploiting the provided location information, network performance can be greatly reduced while still keeping the accuracy of identifying nodes in the search area. Combining the distance flooding protocol and the location information stored in the node-id in the overlay network, ObeSA goes beyond the state of the art in DSA in terms of providing a cooperation platform for spectrum allocation.

As mentioned in Section IV-A, we have used a flat earth model in our simulations. In other scenarios, e.g. urban areas with high buildings, we will see situations where multiple nodes are located at the same position, but at different elevations. To distinguish between these nodes, we can use some of the 6 available characters randomly filled when creating the node-id in Alg. 1. Other information that might be interesting to store in the node-id could be the operation frequencies of the radio device.

The main limitation of this study is the lack of mobility. Even though it is not a requirement that radio devices must be mobile, radio towers or TVs, mobility support should be studied and added to ObeSA. Further study and optimization of the distance flooding protocol is also considered.

References

[1] J. M. III, "Cognitive radio an integrated agent architecture for software defined radio," *PhD dissertation, Royal Institute of Technology (KTH), Sweden*, pp. 1–313, May 2000.

[2] FCC, "Report fcc-10-174," pp. 1–88, Sep 2010.

[3] T. Ulversoy, T. Maseng, T. Hoang, and K. J., "A comparison of centralized, peer-to-peer and autonomous dynamic spectrum access in a tactical scenario," *Military Communications Conference, 2009*, pp. 1–8, 2009.

[4] T. Hoang, M. Skjegstad, T. Maseng, and T. Ulversøy, "Frp: The frequency resource protocol," *12th IEEE International Conference on Communication Systems 2010*, pp. 1–5, 2010.

[5] S. Wang and H. Ji;, "A topology-aware peer-to-peer protocol applicable to wireless network," *Network Infrastructure and Digital Content, 2009. IC-NIDC 2009.*, pp. 1004 – 1009, 2009.

[6] M. Castro, P. Druschel, Y. Hu, and A. Rowstron, "Exploiting network proximity in distributed hash tables," *International Workshop on Future Directions in Distributed Computing (FuDiCo)*, pp. 52–55, 2002.

[7] H.-K. Chiang, H.-W. Chen, and F.-L. Kuo, "Locality support for mobile p2p network," *IWCMC '07: Proceedings of the 2007 international conference on Wireless communications and mobile computing*, Aug 2007.

[8] J. Ahullo, P. Lopez, M. Artigas, and A. G. Skarmeta, "Supporting geographical queries onto dhts," *Local Computer Networks, 2008. LCN 2008.*, pp. 435–442, 2008.

[9] C. Maihofer, "A survey of geocast routing protocols," *Communications Surveys & Tutorials, IEEE*, vol. 6, no. 2, pp. 32 – 42, 2004.

[10] S. Saab and S. Nakad, "A standalone rfid indoor positioning system using passive tags," *Industrial Electronics, IEEE Transactions on*, vol. PP, no. 99, p. 1, 2010.

[11] N. Imagery and M. Agency, "Department of defense world geodetic system 1984, its definition and relationships with local geodetic systems," *Department of Defense World Geodetic System 1984, Its Definition and Relationships With Local Geodetic Systems*, vol. NIMA Technical Report TR8350.2, pp. 1–175, Jan 2000.

[12] P. Garcia, C. Pairot, R. Mondéjar, and J. Pujol, "Planetsim: A new overlay network simulation framework," *in Software Engineering and Middleware*, Jan 2005.

[13] I. Stoica, R. Morris, D. Karger, and M. Kaashoek, "Chord: A scalable peer-to-peer lookup service for internet applications," *in Proceedings of ACM SIGCOMM*, Jan 2001.

 ISBN: 978-1-61208-123-6

A Testbed Concept for Cognitive Radio Prototyping

Alexander Viessmann, Christian Kocks, Andrey Skrebtsov, Guido H. Bruck, Peter Jung
University of Duisburg-Essen
Department of Communication Technologies
Duisburg, Germany
Email: info@kommunikationstechnik.org

***Abstract*—Future wireless systems are evolving towards a broadband and open architecture for efficient multi-service operation. This has a great impact on the terminal and infrastructure component design methodology for supporting multiple radio schemes. Cooperation in wireless networks, requiring cognitive radio implementations, will facilitate a new dimension in the evolution of multimedia communications. The growing price pressure requires ever increasing levels of integration efficiency, flexibility and future proofness at the same time, setting out in the digital baseband domain. In this manuscript, the authors will illustrate a platform based prototyping process, which combines the advantages of the flexibility of a digital signal processor with the efficient parallelization capabilities of a field-programmable gate array. The primary purpose of this platform is to allow a real-time capable implementation of cognitive radio systems. It allows the integration of the entire communication chain from the antenna to the decoded bit stream. Since the increasing computational complexity complicates the dimensioning of such platforms, scalability is a crucial design constraint for the presented concept.**

***Index Terms*—Cognitive Radio, Digital Signal Processor (DSP), Field-Programmable Gate Array (FPGA), Prototyping Platform, Testbed**

I. INTRODUCTION

Reconfigurability of transceivers for wireless access networks such as IEEE 802.11, IEEE 802.16, 3GPP LTE (Long Term Evolution) and various digital video broadcasting standards will become increasingly important in the forthcoming decade. An appropriately flexible and reliable software architecture allowing the concurrent processing of different controlling tasks for wireless terminals will hence be an important asset.

The hardware manufacturers are required to accelerate the development of new products to keep up with the decreasing product life cycles. Research activities in the last two decades showed that software-defined radio helps to overcome this problem [1], [2]. A transceiver can be considered as a software radio (SR) if its communication functions are realized as programs running on a suitable processor [1]. An ideal SR directly samples the antenna output which does not seem feasible with respect to e.g. power consumption and linearity as well as resolution requirements for ADCs (Analog-to-Digital Converters). A software-defined radio (SDR), however, is a practical and realizable version of an SR [1]: The received signals are sampled after a suitable band selection filter, usually in the baseband or a low intermediate frequency (IF) band. With the availability of software-defined radio based transceivers, the architecture can be used to implement multiple communication systems running on a common hardware platform by a simple reconfiguration process. Reconfigurability is not a new technique [1]. Already during the 1980s, reconfigurable receivers were developed for radio intelligence in the short wave range. However, reconfigurability became familiar to many radio developers with the publication of e.g. the special issues on software radios of the IEEE Communication Magazine [3]. Core part of such reconfigurable software-defined radio transceivers is a digital processor running the software. This software can be divided into a signal processing part and a scheduling part [4]. One major advantage of such a solution is the ease of implementation combined with very efficient debugging methods. Nevertheless, the computational capacity is insufficient for modern communication systems. Since the utmost goal for the design of new communication systems is a higher spectral efficiency, in particular the complexity of the channel decoding algorithms increases significantly. As a result, the requirements on the signal processing performance grow steadily. Hence, even the availability of multi-core digital signal processors does not allow real-time implementations of modern communication systems. To circumvent this limitation, hardware-based implementations of the digital signal processing blocks are favorable. Therefore, field-programmable gate arrays (FPGA) are suitable devices which allow the integration of highly parallelized algorithms on the one hand and reconfigurability on the other hand. However, one considerable disadvantage of the deployment of FPGAs is the effort for debugging the implemented signal processing algorithms.

A cognitive radio (CR) is an SDR that additionally senses its environment, tracks changes, and reacts upon its findings [5]. A CR is an autonomous unit in a communications environment that frequently exchanges information with the networks it is able to access as well as with other CRs. From the authors´ point of view, a CR is a refined SDR. SDR and CR transceivers differ from conventional transceivers by the fact that they can be reconfigured via control units. Such control units need information about the type and standard of the radio communications link and software modules for the signal processing path in order to reconfigure the receiver properly.

The platform presented in this document takes advantage of both concepts. Its core components are a powerful triple-core digital signal processor (DSP) in combination with an FPGA. This platform can be used as a prototyping platform for Cognitive Radio implementation as well as during standardization

 ISBN: 978-1-61208-123-6

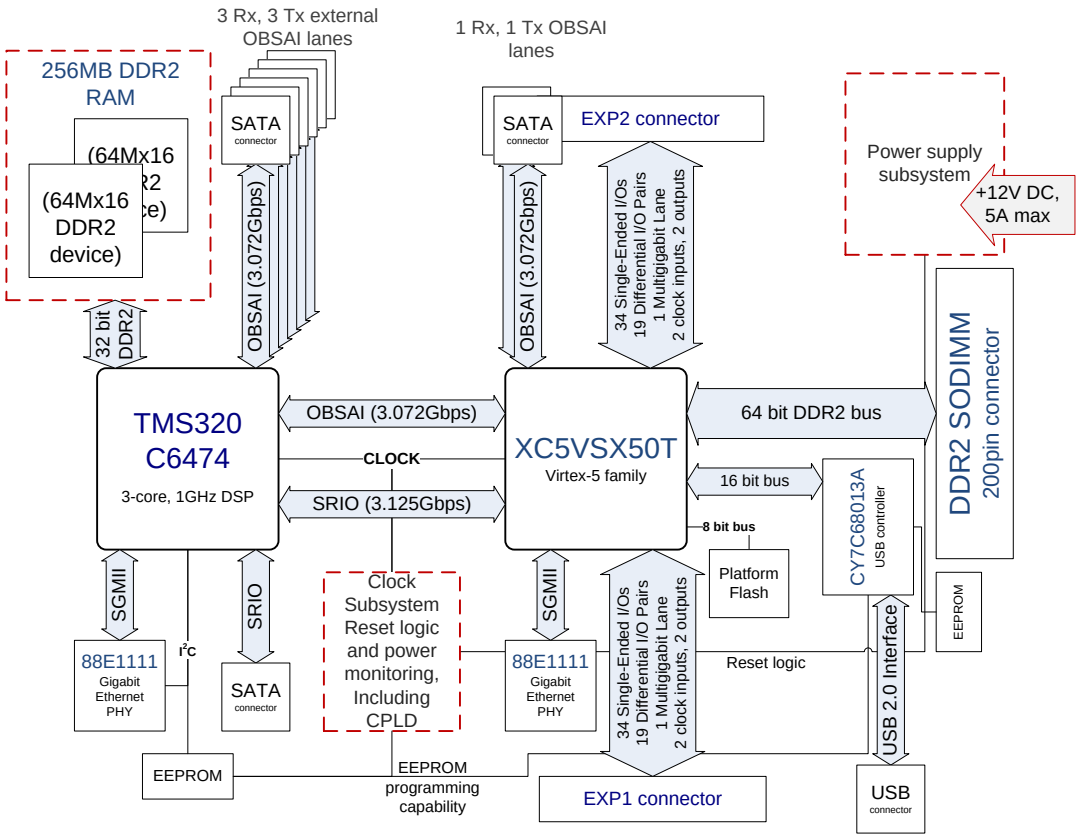

Fig. 1. *eFalcon* block diagram

processes and can be considered to fill the gap between the theoretical considerations for the algorithm design and the final system implementation. Due to its scalability this platform can be used even for next generation communication systems with multi-antenna features. In what follows, the prototyping platform developed by the authors is referred to as *eFalcon*.

The present document is organized as follows. After this brief introduction, Sect. II gives an overview of *eFalcon*. Since clock generation and distribution is a critical factor in platform design, Sect. III primarily addresses this aspect. In order to increase the computational performance of *eFalcon*, it exhibits interfaces for the interconnection of multiple platforms. This scalability aspect is discussed in Sect. IV. Sect. V presents a testbed concept for a Cognitive Radio. Finally, a conclusion is given in Sect. VI.

II. Platform Overview

As discussed in Sect. I, a prototyping platform consisting of a combination of a DSP and an FPGA is desirable. A block diagram of *eFalcon* is shown in Figure 1. Core part of this platform is the Texas Instruments triple-core DSP TMS320C6474 running at 1 GHz system clock. The DSP has 256 MB of DDR2 Random Access Memory (RAM) attached which enables the implementation of memory intensive applications. The interfaces to external components consist of a Gigabit Ethernet link, three full duplex OBSAI (Open Base Station Architecture Initiative) or CPRI (Common Public Radio Interface) lanes, commonly referred to as antenna interface, and a Serial RapidIO (SRIO) link. The clock generation and distribution network described in Sect. III provides a reference clock which is used to generate the system clock by a processor-internal phase-locked loop (PLL). The DSP supports several boot modes using either I^2C, Ethernet or SRIO.

Besides the top-level scheduling functionality, the DSP is the central signal processing unit. Depending on the hardware/software split carried out between DSP and FPGA, the DSP firstly carries out the synchronization on the incoming data signal received from the antenna interface. After a successful synchronization, a channel estimation is performed. In what follows, the incoming signal is equalized and demodulated. In general, the output of the demodulator is a likelihood information, which is fed into the channel decoder. The DSP contains very flexible hardware accelerators for Viterbi and Turbo decoding since convolutional and turbo codes can be found in a large number of communication standards. In case of channel codes like LDPC (Low-Density Parity-Check) codes employed e.g. in various modern video broadcasting standards [6], the DSP's signal processing capability is not sufficient to decode the incoming signal stream in real-time. In that case, the FPGA which is directly attached to the DSP can be used to design a DSP co-processor dedicated to a specific signal processing task. Besides the potential DSP co-processing capability, the FPGA, namely a Xilinx

 ISBN: 978-1-61208-123-6

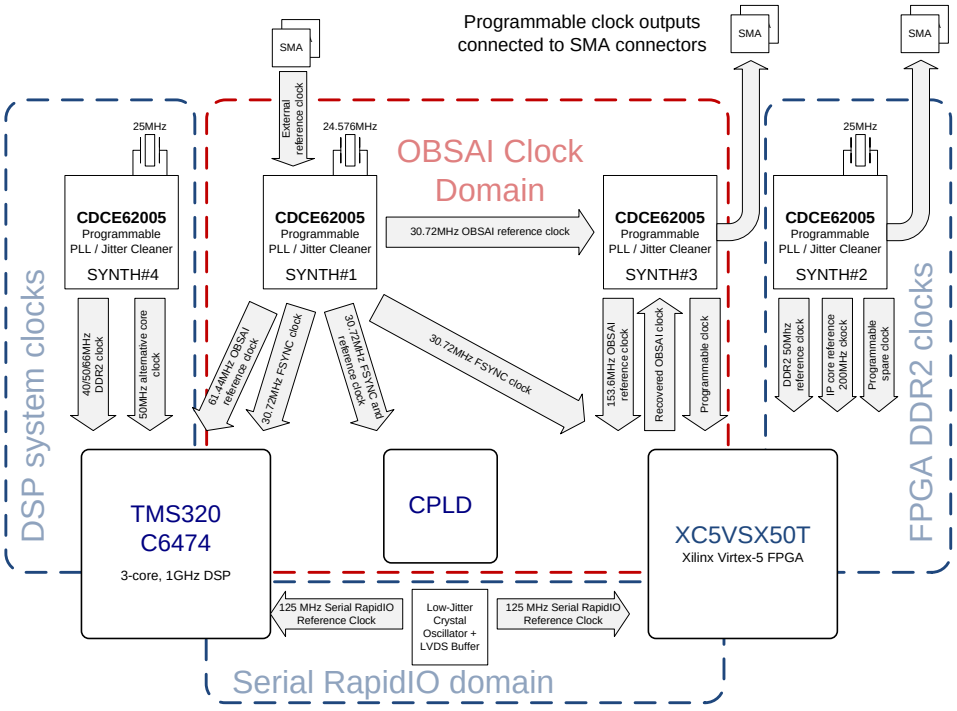

Fig. 2. *eFalcon* clock subsystem

XC5VSX50T, implements additional interfaces to external peripheral devices. Besides Gigabit Ethernet, a USB 2.0 interface is attached to the FPGA which can be used to communicate with conventional PC hardware. The connection to the DSP is realized using OBSAI, CPRI or SRIO. The FPGA offers the capability of attaching a DDR2 SODIMM which can be used to extend the memory capability of the platform significantly. Spare high-speed serial ports are routed to proprietary connectors which can be used with a variety of protocols.

One major task of the FPGA is to act as a bridge between the high-speed serial interfaces of the DSP and the parallel interfaces of analog-to-digital (A/D) or digital-to-analog (D/A) converters. Therefore, the FPGA offers a full implementation of the Avnet EXP Expansion Connector Specification [7] consisting of two connectors with 34 single-ended and 19 differential I/O pairs each. In addition, this interface consists of lines for clock inputs and outputs as well as high-speed serial connectivity. The FPGA can be used to post-process baseband data calculated by the DSP and submit it to the D/A conversion process. Digital up-conversion, up-sampling and filtering algorithms are applied in this step. In the A/D conversion process, the FPGA pre-processes the incoming data before transmitting it to the DSP. Signal statistics, which act as an input for an automatic gain control (AGC), are calculated. These statistics consist of long-term averages as well as fast detect features to enable over-range indication and can also be used to remove DC offsets. Further processing consists of digital down-conversion in case of intermediate frequency (IF) sampling, sampling rate adaptation and filtering. The FPGA is also ideally suited for the application of synchronization blocks which usually consist of autocorrelation or cross-correlation based algorithms.

In case the signal processing capability of one platform is not sufficient to operate a communication standard in real-time, additional platforms can be easily attached to increase the performance, cf. Sect. IV.

Due to the large number of different devices, a complex power supply design is mandatory. *eFalcon* works with an input voltage of 12 V. Switching regulators are used to generate voltages less than this input voltage at a high efficiency and directly supply the multitude of digital devices. Voltages which are used to supply analog parts of devices, especially the PLLs, are generated using linear low-dropout regulators. All voltages are monitored and reported to a central glue logic, which is implemented in a CPLD (Complex Programmable Logic Device). This device is the first device which is properly configured after applying power and, hence, coordinates the start-up procedure.

III. Clock Generation and Distribution

Modern digital systems have strict requirements on the clock references. Both the DSP and the FPGA contain on-chip PLLs which need to be supplied with a suitable reference frequency. These signals are required to derive the core clocks as well as the reference clocks for the high-speed serial links. Figure 2 shows a general block diagram of the platform clock subsystem. Most of the reference clocks in the system are generated by a Texas Instruments CDCE62005 device which is a fully integrated PLL including a voltage controlled oscillator

 ISBN: 978-1-61208-123-6

(VCO). A programmable loop filter is also integrated on the chip. All platform clocks generated by the CDCE62005 devices can be split into two general classes. The first class contains the 30.72 MHz derivatives which are used in the OBSAI and CPRI clock domain. The second clock class includes all other clocks which are derivatives of 25 MHz. The reference clock of 125 MHz which is necessary for SRIO is generated by a dedicated crystal oscillator. Both Ethernet PHY chips contain an internal PLL and a 25 MHz crystal resonator as frequency reference. The USB controller uses a 24 MHz external crystal resonator to generate the necessary clock for the FPGA-to-USB data transfer. Besides an internal generation of the PLL reference frequency, all devices have the capability to be fed by an external reference. These external references are routed to coaxial connectors which can be used by an external clock distribution network to synchronize an arbitrary number of platforms. This is an important feature for the case that multiple platforms are connected to work on a single signal processing task.

IV. Scalability

eFalcon is based on a flexible architecture which paves the way towards a rapid implementation of algorithms deployed in modern communication systems. It offers the opportunity to directly attach two daughter cards following the Avnet EXP Expansion Connector Specification. One possible scenario is the implementation of a full transceiver chain so that one EXP interface is used for attaching an A/D converter board and the second one is used for attaching a D/A converter board. Furthermore, it is possible to establish a multi-antenna system with two receive or two transmit antennas.

One crucial aspect during the concept phase of *eFalcon* was scalability in order to be prepared not only for current communication systems but also for next generation systems with increased complexity requirements. On the one hand, *eFalcon* consists of multiple serial high-speed interfaces such as OBSAI, CPRI and SRIO to allow intra-board communication but also board-to-board communication with data rates beyond 1 GBit/s. On the other hand, the elaborate clock distribution concept of this platform allows an accurate synchronization of multiple platforms. Thus, the interconnection of two or more prototyping platforms by a combination of serial high-speed interfaces and a clock synchronization enables the implementation of multi-antenna systems with even more than two antennas. In that case, one platform acts as a master device which is responsible for the clock generation and distribution to the attached platforms acting as slaves as well as for the main scheduling parts of the signal processing chain.

V. Cognitive Radio Implementation Aspects

Figure 3 shows the Cognitive Radio demonstrator concept implemented using the *eFalcon* platform.

The concept consists of a transmitter branch which is intended for the real-time generation of arbitrary signal waveforms. The baseband signal in either complex inphase and quadrature (I/Q) or real valued intermediate frequency (IF) representation is generated using the *eFalcon* platform and is fed into a D/A converter. After a suitable reconstruction filter, the resulting analog signal is upconverted to a carrier frequency using an I/Q modulator. The local oscillator (LO) signal which is used in the up-conversion process is generated by an LO synthesizer and ranges from 300-4800 MHz. The synthesizer accepts external reference signals which can be used to synchronize the LO phase in case of multi-antenna applications. In addition, the LO signal can be externally fed in or distributed to other platforms. The I/Q up-converter is followed by an optional power amplifier branch which can be used to obtain signal levels up to +30 dBm. Optionally, the up-converter can also be driven by an IF signal.

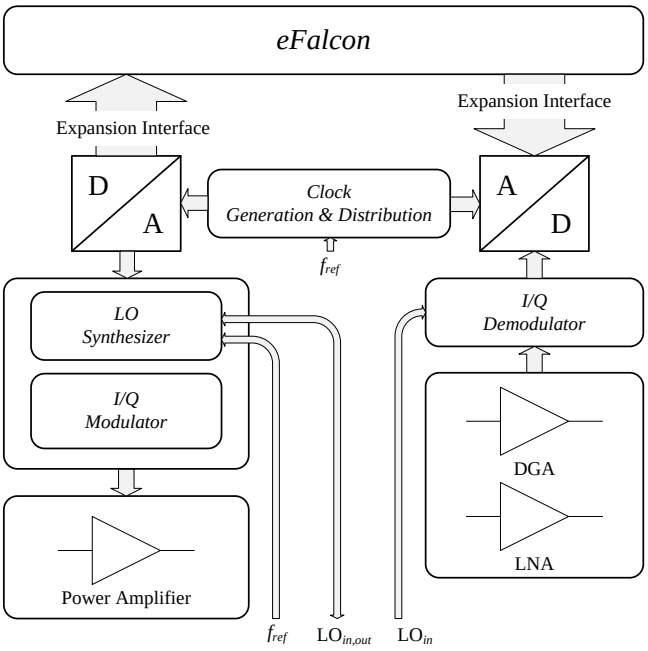

Fig. 3. *eFalcon* Cognitive Radio demonstrator concept

The receiver branch consists of a gain stage implemented by a combination of a low noise amplifier (LNA) and multiple digitally controlled amplifiers (DGA) which allow the amplification of signals at very low input levels. The gain vectors which lead to an optimal behaviour in terms of noise figure and linearity are calculated in the *eFalcon* platform according to the signal level detectors implemented at several positions within the amplifier chain. The resulting signal is fed into an I/Q demodulator which converts the signal to complex baseband using an external LO signal. The down-converter can also be configured for IF applications where the I/Q branches can be used for the implementation of a Hartley image reject receiver [8]. The baseband signal is sampled and the resulting signal samples are transferred to the *eFalcon* platform using the expansion interface. The *eFalcon* platform performs the desired cognitive operation and reports the results to a data sink.

 ISBN: 978-1-61208-123-6

VI. Conclusion

Within this document, the authors presented a Cognitive Radio demonstrator concept. Besides powerful digital baseband processing capabilities, the demonstrator concept consists of analog transmitter and receiver branches which allow signal sensing applications in the range of 300-4800 MHz. The architecture based on a combination of a triple-core digital signal processor and a field-programmable gate array paves the way towards rapid implementation of arbitrary communication systems and Cognitive Radio concepts accompanying the standardization process. Thereby, the advantage of both digital processors running software and programmable logic allowing massive parallelization to guarantee real-time operation has been merged to one single platform. The basic ideas during the concept phase were a high flexibility, modularity and scalability to even allow the integration of multi-antenna systems.

Acknowledgment

The authors would like to thank Texas Instruments for their continuous support throughout the recent years.

References

[1] F. K. Jondral, "Software-Defined Radio: Basics and Evolution to Cognitive Radio," *EURASIP Journal on Wireless Communications and Networking*, vol. 2005, no. 3, pp. 275–283, 2005.

[2] FP6 - Integrated Project, "E2R - End-to-End Reconfigurability."

[3] J. Mitola, "The Software Radio Architecture," *IEEE Communications Magazine*, vol. 33, no. 5, pp. 26–38, 1995.

[4] A. Viessmann, A. Burnic, C. Spiegel, G. H. Bruck, and P. Jung, "Petri Net Based Controller Concept for Cognitive Radios in Wireless Access Networks," *Journal of Communications*, vol. 2, no. 2, 2007.

[5] J. Mitola, "Cognitive radio - an integrated agent architecture for software defined radio," Ph.D. dissertation, Royal Institute of Technology, Kista, Sweden, 2000.

[6] *Digital Video Broadcasting (DVB): Frame Structure Channel Coding and Modulation for a Second Generation Digital Terrestrial Television Broadcasting System (DVB-T2)*, ETSI Std. DVB Document A122 Draft, June 2008.

[7] Avnet, "EXP Expansion Connector Specification Revision 1.4," September 2007.

[8] B. Razavi, *RF Microelectronics*. Upper Saddle River, NJ, USA: Prentice-Hall, Inc., 1998.

 ISBN: 978-1-61208-123-6

ICT-Based Software as a Supervision Tool in Nursing Students' Clinical Training

Sari Mettiäinen, Anna-Liisa Karjalainen
Tampere University of Applied Sciences
Tampere, Finland
sari.mettiainen@tamk.fi,
anna-liisa.karjalainen@tamk.fi

***Abstract*—The paper describes nursing students' opinions on how a mobile application and a web-based reporting tool could act as a supervision method during their clinical training. In a Finnish university of applied sciences we selected software called eTaitava to our piloting project. The aim of the project was to find out about the possibility to establish a new supervising method to teaching by using information and communication technology. Lecturers can use this software in supervising and supporting nursing students' learning process. The empirical study was made by a survey in May 2010. All in all 430 students have used this method and been sent a web-based questionnaire. 112 of them answered the survey, which consisted of 33 questions. According to the findings, two thirds of the students thought that answering almost daily to the questions sent by eTaitava was useful for their learning process, including setting of objectives, daily activities, self-assessment and cognitive reflection. They felt it easy and fast to use by computer, only 9 % used it by mobile phone. The first feedback showed that the information and communication technology-based method is a useful and effective way to supervise learning in nursing education. It is worth developing this idea further.**

Keywords-eLearning; mobile application; nursing; clinical training; supervision

I. INTRODUCTION

In this paper, we describe the results of our pilot project which started with the support of EU-funding and where we tested the possibility to use ICT, or indeed mobile technology in nursing students' clinical training. The software we used was called eTaitava [1].

The ICT-based computer and mobile program could provide an active supervision method for lecturers to supervise many students at the same time. Via such a helpful tool it could be possible for the lecturer to be aware of many students' clinical learning process during the whole training period.

Clinical training is an important part of nursing education in all EU countries. In Finland there are long distances to the clinics and lecturers have lack of time for supervision. Travelling to the hospitals to meet students, which is the traditional method to supervise students, takes quite a lot of time. Therefore, new methods are needed.

The purpose of the empirical study was to find out nursing students' opinions on how ICT-based software like eTaitava could act as a supervision tool. The studied questions were how the students experienced its use as a tool for reporting their learning process, their feelings and experiences as learners and what kind of significance eTaitava had for their learning process during the clinical training.

We describe first clinical training supervision in nursing education, related use of eTaitava program and its features. Then we present a case study on student views and its findings. The Conclusion part presents a short summary on implementation of our development project, the case study, the most significant findings and further development challenges.

II. SUPERVISION OF CLINICAL TRAINING

Nursing education in Finland comprises 210 ECTS (European Credit Transfer System) Credits. Of these, 75 credits (50 weeks) are performed in clinical sites in hospitals or other health care organizations. In universities of applied sciences training is always supervised by a senior lecturer and a training supervisor. Students have to plan individual objectives for the clinical training period based on theory and the curriculum. The objectives are approved by the senior lecturer at the university of applied sciences and the named supervisor at the clinic. At the end of the clinical training, the student, the lecturer and the training supervisor evaluate together how the student achieved his or her objectives.

The aim of the supervision is to support the students' learning process towards professional growth. Due to the underlying cognitive approach, the aim is to help students to analyse the learnt contents. Supervision is most successful when the relationship between the supervisor and the student is active [2]. The relationship between the nursing student and the supervisor has been the topic of many studies [3], but innovative ICT-based methods have been overlooked.

 ISBN: 978-1-61208-123-6

III. ICT-BASED SOFTWARE ETAITAVA

We utilized software called eTaitava in students' training supervision. It has been developed in Finland for vocational school students' training periods. eTaitava is a multimedia reflection and feedback tool on mobile phones and personal computers. It connects learners, teachers and workplace mentors in on-the-job training environments. Its strength lies in its capability to provide all parties involved with continuous and immediate feedback on the learning progress of trainees [4, 5].

The teacher constructs questions through the eTaitava web-based user interface to map the student's learning experiences and learning progress. The questions are saved and set to be sent on certain days. The daily questions can be either open ended questions or statements formulated e.g. as follows: "I have the basic knowledge of medical diseases" and the student can answer the questions e.g. on a scale of 1-5 (fully disagree – fully agree) or "I have practised giving medical injections" and the answering scale could be 1-5 (not at all - very much). The teacher can formulate diverse series of questions for different clinical training periods.

Students can answer the questions using either a computer or a mobile phone. In order to use a mobile phone for answering, eTaitava client has to be downloaded to the phone. The use of mobile phone requires a colour screen and a data connection [4]. To use the software by computer only requires an Internet connection. The software is hosted by Wellworks Oy.

The teacher constructs similar series of questions for the supervisors as for the students. The supervisors respond to the questions once a week by computer and thus participate in evaluating the students' learning progress.

The answers are saved to the database of the eTaitava program, where the teacher can easily see the individual answers and group-specific summaries by means of graphs. The teacher can in real time follow students' learning during the clinical training [4].

Pirttiaho *et al*. [5] have described in more detail the technical features of the program in their paper. Paalanen [6] has studied the first pilot-group who used eTaitava. Those 46 vocational school students were studying forestry, travel services, catering etc. According to the survey eTaitava was considered clear and simple. 71% of the respondents reckoned that answering by mobile phone was pleasing. The attitude towards eTaitava and its use was found positive and only 4% of the respondents did not want to use eTaitava in the future. eTaitava has since been introduced in approximately 30 educational institutions in Finland.

IV. CASE STUDY

eTaitava software has been in use with Finnish nursing students at Tampere University of Applied Sciences since autumn 2009 by suggestion of the authors. It has been in use during surgical, medical, preoperative, public health nursing and basic nursing training periods. The training periods consist of 3–7 weeks depending on the substance area (Table 1).

TABLE 1. CLINICAL TRAINING PERIODS DURING WHICH THE STUDENT RESPONDENTS USED ETAITAVA

Clinical Training Period	*Weeks*	*Number of Students*	*Number of Teachers*	*Number of Supervisors*
Basics of Nursing	4	27	2	-
Medical Nursing	4	17	4	6
Surgical Nursing	4	6	2	-
Perioperative Nursing	7	22	2	4
Public Health Nursing	3	51	4	-
Home Care	3	53	4	-

Before a training period, students usually have an orientation hour during which they are told about the clinical training objectives and taught to use eTaitava by the authors of this paper, who have taken care of the whole implementation process of eTaitava. The students are invited to answer the questions every day after their shift on the ward.

In all 430 students, 15 lecturers and 10 training supervisors had used eTaitava until spring 2010 when this data was collected. Use of the program has been expanded gradually and supervisors from two special fields only participated in the project when the questionnaire was carried out (Table 1).

All the students were sent a link to the survey by email. They were told that the aim of the survey was to evaluate a new way of supervising training periods by utilizing ICT technology. The students were told that answering the survey was voluntary and they were able to answer anonymously. The survey consisted of 26 structural quizzes, 6 of them concerned background information and 7 were open ended questions.

Qualitative data of the open ended questions was analysed by using thematic analysis and categorization. The analysis was conducted according to a three-step inductive process based on the data [7]. The data was reduced by identification. After that, similar data was categorised. Quantitative data of the structural quizzes was analysed

 ISBN: 978-1-61208-123-6

using frequency distributions, and the results were described using percentage distributions.

V. FINDINGS

A. Information on respondents

112 students answered the survey; the response rate was 26 %. Most of the students who have answered the questionnaires, have used eTaitava in three-weeks training period of public health nursing or in clinical training in home care (Table 1).

83 % of the respondents were 20–25 years old and 95 % of them were female. 94 % of the students who answered the survey had positive attitude towards using information and communication technologies in education.

B. Answering and using eTaitava software

79 % of the students answered the questions almost every day during their training period. 15 % of them answered 3–4 times a week and rest of them once or twice a week. The most important reason for not answering every day was that students did not remember to do it. For 5 % of the students the reason was that they did not consider eTaitava as a sensible method.

9 % of the participants answered the questions via mobile phone, and thus most of the students answered via computer. Students were asked why they did not use mobile phone to answer the questions. The most important reasons were data communication costs and the fact that they felt it was easy to answer by computer. All the answers are described in Table 2.

TABLE 2. REASONS GIVEN BY STUDENTS FOR WHY THEY DID NOT USE MOBILE PHONE TO ANSWER THE QUESTIONS

Reason	*Number of Mentions*
Costs which I should pay	21
It is so easy with the computer which I use daily	20
It was not possible with my phone	19
I did not consider it necessary	15
I do not use internet by mobile phone	8
Loading of the program would have been too difficult	6
I do not want to use my phone for school assignments	5
It is too difficult and slow to use it by phone	5

If the student answered that it was not possible with his/her phone, the reasons were: small screen, too little memory, the phone is iPhone, into which it cannot be loaded, or the phone does not support the software.

The students were asked whether they preferred to use eTaitava via mobile phone if it was cheaper. More than half of them disagreed (Table 3).

TABLE 3. STUDENTS' (N=112) VIEWS ON USING MOBILE PHONE FOR ANSWERING THE QUESTIONS IF USE WAS CHEAPER

Answer	*%*
Yes	13
Maybe	23
No	46
I cannot say	18

68 % of the respondents reported that it took 5 minutes to answer the questions. Rest of the students estimated they used 10–15 minutes to answer the questions. 83 % of the respondents thought it was easy and rest of them answered it was quite easy to use eTaitava.

C. Opinions on questions and their significance for learning process

The questions used on eTaitava were similar in different weeks. The students were asked what they thought about that. Half of them (46 %) reported they understand that it offers a useful way to follow their development process but 13 % of them did not understand the idea of repeated questions (Table 4.)

TABLE 4. STUDENTS' (N=112) OPINIONS ON THE QUESTIONS BEING SIMILAR IN DIFFERENT WEEKS

Answer	*%*
I understand it offers a useful way to follow my development process	46
I do not mind even if similar questions repeat week after week	9
I think it is boring to answer same questions repeatedly	32
I do not understand why same questions are asked every day	13

Students were asked what they thought about the content of the questions. Half of them (49 %) estimated them well designed, 12 % estimated them too difficult, 24 % too easy and 15 % thought they were boring.

Students were asked whether the questions supervised their activities on the ward. 8 % of them estimated "quite a lot", 56 % "somehow" and 36 % "not at all". The open ended questions asked the students how eTaitava supervised their activities on the ward and what was the significance of eTaitava for their learning process. This question was answered by 53 students.

According to the answers, eTaitava helped the students to construct their learning objectives and update them. They become more aware of what they should learn.

> *"Helped to understand what should be practised and what should be paid more attention to during the clinical training."*

 ISBN: 978-1-61208-123-6

On the basis of the answers, eTaitava supervised students' work and helped them to pay their attention to the things asked. Answering also reminded of the objectives during the whole clinical training.

"I maybe did some things more frequently as eTaitava reminded of them weekly."
"encouraged to patient contact etc."

eTaitava was also an encouraging factor. It encouraged students to practise even things that were not in their own objectives.

"It gave a buzz to my clinical training as it brought out the development needs"
"I noticed that there was something I had not done at all, and I had not even thought that it could be done"

Answering eTaitava questions also helped students to evaluate their learning experiences and their competence development. It also showed what the student had to practise more.

"It mainly helped to analyse my own learning and clinical training as a whole."
"Guided thinking and evaluation of clinical training…usefulness"

Answering eTaitava questions helped students to think about matters both more independently and with their supervisor.

"And answering the questions and giving vent to my feelings probably helped as I only met the teacher for a couple of times and did not much talk about the clinical training matters to others."
"answering the questions made me think what had happened during the day"

eTaitava questions also helped students to become aware of some matters.

"I more considered the meaning of the work community"
"'have you given feedback to your supervisor' made me understand that it can also be done."

According to these themes we can say that the significance of the continuous ICT-based supervision tool for learning during clinical training is that it can

1. supervise students to create better learning objectives
2. supervise students' daily training activities
3. help students in self-assessment
4. inspire students' cognitive learning process.

69 % of the students who answered the questionnaire, saw some benefit of it. 55 % of them reported that eTaitava was somehow useful and 14 % clearly useful for their learning process (Table 5). 74 % of the students thought eTaitava would be useful if the lecturer only met them in the final evaluation meeting on the ward.

TABLE 5. STUDENTS' PERSPECTIVES ON USEFULNESS OF ETAITAVA

Answer	*%*
It was clearly useful, I knew what I should learn	14
It was somehow useful	55
It was not useful for me	32

30 % answered "yes" to the question "Are you willing to use eTaitava in future?", 45 % "maybe" and 25 % "no".

The students gave many useful ideas and feedback on how to develop the questions which are sent by eTaitava in such a way that they could support students' learning process even better.

VI. CONCLUSION

With the traditional method, lecturers met students maybe once or twice during a clinical training period. Via the ICT-based program the lecturers were able to follow and supervise students' learning process step by step. The challenge for the lecturers is to create right and appropriate questions for different training periods.

eTaitava was introduced in Tampere University of Applied Sciences in autumn 2009. During the first academic year, it was used by a total of 430 students, who were sent a questionnaire in May 2010 in order to map their experiences on the program. 26 % of them answered the questionnaire. The low response rate may have been influenced by the fact that more than six months had gone since some students had used the eTaitava program and some students had already started their summer holiday. Due to the low response rate, the findings cannot be generalised, but they however provide valuable information for further development and research on training supervision.

Two thirds of the students who have answered the questionnaires thought eTaitava was useful for their learning process. It supervised students in creating better learning objectives and in their daily training activities. It helped students in self-assessment and inspired students' cognitive learning process.

75 % of the respondents were willing to use eTaitava in future. It was surprising that so few students were willing to use mobile phone to answer the questions. 91 % of the students used eTaitava by computer and only 36 % thought it could be sensible to use it by phone in future. Answering the questions via computer was experienced easy and it took about 5 minutes a day. These findings differ from the findings of Paalanen [6], where 71 % of the respondents felt the mobile phone was a good way to report their experiences. If students use computer daily, they maybe think they do not need other methods to answer. On the other hand, when students do not have experiences of mobile use of eTaitava, they have not found the benefit

 ISBN: 978-1-61208-123-6

which it maybe could offer. We believe that in a few years web-based use of mobile devices increases considerably and thus enables increase in using mobile devices also in studies. That is the topic which should be studied in future.

Most teachers who participated in the pilot project experienced the program useful, which was manifested in discussions with them. The responses showed which of the students needed personal supervision. The teachers also considered it was easy to use the program but it took time to follow it weekly. Efficient utilization of reports thus also calls for learning.

As project coordinators we consider it important to integrate the program to a learning environment used in the educational institution, such as Moodle. In this case, separate user identifications would not be needed for the program. Otherwise, usability of the program is good.

We have also used web-based discussion in clinical training supervision with some groups. Activation of students to discuss is sometimes difficult, but if it succeeds, web-based discussion is a workable method. It was easier to activate students to use eTaitava, almost all students used it several times every week.

The purpose of this study was not to investigate features of the eTaitava software but its benefits for learning. This pilot study yielded results that were particularly encouraging, indicating that the project is worth further development**.** Anyway, attention should be paid to the software features, such as user-friendliness, in program introduction. We believe this can be a useful supervision method in all fields of education.

REFERENCES

[1] Quality and transparency for on-the-job learning. Wellworks Oy. http://mobiilioppiminen.files.wordpress.com/2011/01/etaitava.pdf 20.01.2011

[2] R. Vuorinen, R. Meretoja, and E. Eriksson. ”Contents, prerequisites and effects of supervised clinical training in nursing. A systematic review.”, Hoitotiede, Vol 17, No. 5, pp. 270-281. 2005.

[3] B. Lindgren, C. Brulin, K. Holmlund, and E. Athlin. “Nursing students’ perception of group supervision during clinical training”, Journal of Clinical Nursing, Vol 7, No. 4, pp 822-829, 2005.

[4] eTaitava. Ao Jyväskylä Vocational Institute. http://www.peda.net/img/portal/664066/eTaitava_en.swf?cs=1164287053 15.01.2011.

[5] P. Pirttiaho, J.-M. Holm, H. Paalanen, and T. Thorström. eTaitava – Mobile Tool for On-the-Job-Learning. 2007. http://www.iadis.net/dl/final_uploads/200706C036.pdf.

[6] H. Paalanen. User acceptance in eTaitava mobile service. Pro gradu -työ (Master's thesis), in preparation. Department of Computer Science and Information Systems, Faculty of Information Technology, University of Jyväskylä, Finland. 2007.

[7] M.B. Miles and A.M. Huberman. Qualitative data analysis (2nd edition), Sage, California. 1994.

 ISBN: 978-1-61208-123-6

Didactic Embedded Platform and Software Tools for Developing Real Time Operating System

Adam Kaliszan
Poznan University of Technology
Chair of Communication and Computer Networks
Email: adam.kaliszan@gmail.com
http://www.adam.kaliszan.yum.pl

Mariusz Głąbowski
Poznan University of Technology
Chair of Communication and Computer Networks
Email: mariusz.glabowski@et.put.poznan.pl

***Abstract*—This paper presents a new didactic platform that is capable of running an embedded Real Rime Operating System. The proposed platform consists of hardware, firmware and software tools. The project of the hardware part is distributed according to GPLv2 license. The firmware of the platform is based on FreeRtos distributed according to the modified GPL license, ported by the authors on the microcontrollers not originally supported, i.e., Atmega128 and Atmega168. All the software tools work on the Linux operating system and are free of charge; most of them have open source code. The main aim of the proposed platform is to familiarize students with the basics of embedded RTOS.**

***Keywords*-Embedded systems, Real Time Operating System, Multitasking, Interprocess communication**

I. INTRODUCTION

An important addendum of an embedded and operating systems theory course is practice. The practical part of the course is often conducted with the help of one of the existing operating systems, usually Linux or Windows. Linux has advantages, such as its versatility ranging from small embedded devices to powerful supercomputers. Owing to the Linux open source code, there are many written kernel modules [1] supporting new devices, what ensures such a great versatility of the system and it is applicable in many embedded systems. Microsoft offers different versions of its own operating system, ranging from Windows CE or Windows Mobile that are working on mobile phones, PDA devices and car navigation, to Windows Server. On account of Microsoft .NET framework, it is possible to write software in a very easy way. It should be noted that the software produced by Microsoft is not free. The fact that its code is closed complicates porting the operating system to new, not particularly common, hardware devices. Its application is limited to few basic CPU architectures.

Irrespective of a chosen operating system, the practical part is often limited to learning the basis of operating systems, i.e., learning Linux fundamental commands such as creating and removing files or directories, changing file attributes and launching programs. Such laboratory classes do not introduce the subject of embedded systems, as well as they have no connection to the operating system theory, since the laboratories do not cover topics like multitasking, interprocess communication and its synchronization or operations on file system. The mentioned difficulties are caused by the absence of a proper platform with a simplified programming interface that is capable of building (compiling) in a short amount of time. In the Linux case, the complication results mostly from a required compatibility with various standards, e.g., Linux is compatible with posix and sysV standards [2]. In order to provide the compatibility with each of these standards, separate interfaces have been introduced. Consequently, it takes a lot of time to get familiar with the whole programming interface and, finally, students getting prepared to their laboratories are generally focused on studying the documentation instead of understanding the sense of presented mechanisms of the operating systems. Additionally, the build time of the embedded Linux requires about one hour, while laboratory classes last usually 90 minutes. In view of the above-mentioned difficulties the authors felt encouraged to elaborate a new didactic platform, including hardware, firmware and software tools. In the presented system the handling of mechanisms such as files, multi-tasking, interprocess communication and process synchronization, have been simplified. The software code, worked out to meet the demand of the new platform, is open, distributed according to GPLv2 [3] license and it allows students to get familiar with particular mechanisms of the operating systems.

The remaining part of the paper is organized as follows. Section II presents the hardware of the proposed platform. In Section III the software architecture is described. In Section IV an exemplary exercise conducted with the help of the proposed platform is presented. Section V concludes the paper.

II. HARDWARE

The hardware part was designed with the help of a freeware version of Eagle [4] CAD software. The dimension of PCB board was limited to 10 by 8 centimeters (i.e., the maximum dimensions of PCB board allowed by freeware version of Eagle CAD software). The complete

 ISBN: 978-1-61208-123-6

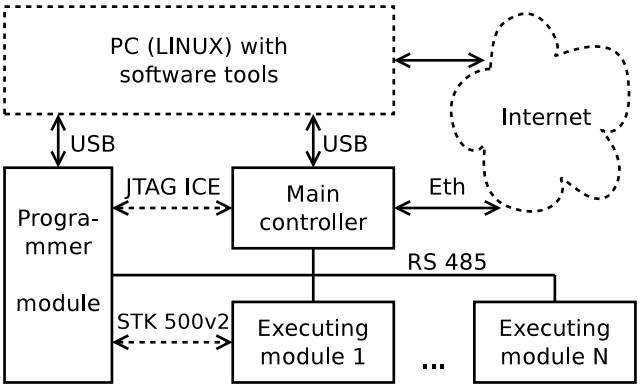

Figure 1. Modular schematic of the platform's hardware

project of the hardware is available at svn repository http: //akme.yum.pl/eagle/ssw, where the login and the password is "student". In order to download the project, the following command must be executed in the shell prompt: *svn co http://akme.yum.pl/eagle/ssw*. The limited dimension of the board allows students to modify the project using freeware version of Eagle CAD. The hardware was designed in a user friendly manner: it uses a common interface and does not need any external power supply. The platform is connected to a PC by via USB, since RS 232 is not very common in modern personal computers. There is a place on the main controller for power converter. It allows the platform to work as a standalone device that does not require power supply from USB. The hardware project bases on AVR microcontrollers [5], [6]. This reduces instruction set computing CPU architecture is preferred by students because of its simplicity, freeware C compiler (avrgcc) and high performance in comparison with other 8-bit microcontroller architectures.

Figure 1 shows a schematic diagram of the platform. The system is distributed and consists of the main controller and executing modules. Both modules are being programmed, using universal programmer designed for the platform purposes. The solid line rectangles belong to the platform's hardware. The solid lines indicate communication interfaces or buses and the dotted lines indicate the programmer interfaces. The main controller is connected with the executing modules by RS 485 bus. The programmer module has also RS 485 interface in order to facilitate debugging or controlling the executing module if the main controller is disabled.

A. Main controller

The main controller is responsible for controlling the executing modules connected to the RS 485 bus, storing logs in its memory and communication with users by USB or Ethernet interface. The modular schematic of the main controller is presented in Fig. 2. The functional modules are presented as solid line rectangles and connectors or

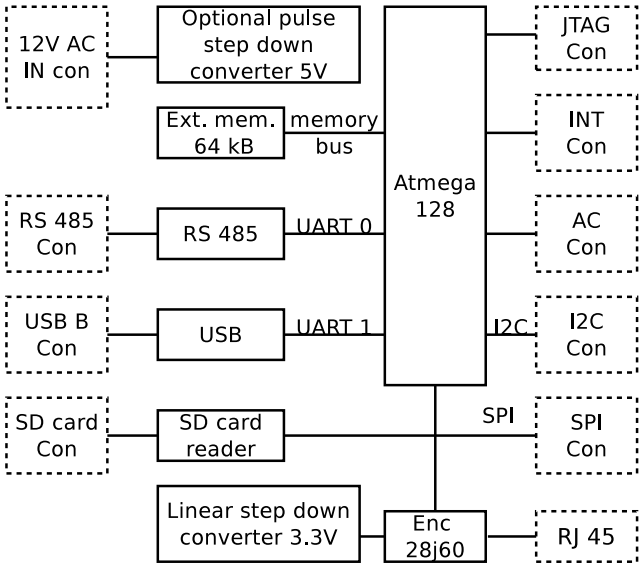

Figure 2. Ideological schematic of the main controller

jacks are presented as dotted line rectangles. The main controller consists of: microcontroller Atmega128, 64 kB of data external memory, USB interface (Ft232Rl chip), RS 485 interface (Max481 chip), Ethernet interface (Enc28j60 chip) and Secure Digital card reader. The microcontroller uses SPI bus to communicate with Ethernet driver and SD card reader. It is also possible to connect 8 additional devices to this bus through a SPI connector placed on the main controller. The controller also has the optional pulse step down converter, which can be useful if we want to use external power supply. This converter provides power supply to executing modules. In order to communicate with external devices, sensors and modules, the controller uses the following buses: SPI, I2C and RS 485. All buses have their own connectors. In order to reduce costs, a user communicates with the controller by console (VTY100 protocol) connected to USB port. The main controller has neither display nor keyboard. The CPU is programmed using JTAG interface that allows the user to debug the software. Additionally, there is connector (AC Con) with analogue inputs and connector (Int Con) with inputs generating interruptions.

B. Executing module

The executing module is responsible for switching on/off various devices, for example lights or roller shutters in an intelligent home. The executing module consists of: microcontroller Atmega168, RS 485 interface, 4 relays, 2 outputs for LED, two connectors with two inputs each, 5 jumpers for setting device address. The relays have independent power supply in order to avoid brownouts. The executing module can be programmed using SPI bus (STK 500v2 programmer) or RS 485 bus (bootloader with xModem protocol).

 ISBN: 978-1-61208-123-6

C. Programmer module

The Programmer module was designed to provide various functionality and reduce the costs. The programmer module uses USB interface and therefore it does not require additional power supply. Its main function is flashing firmware to the main controller or executing modules. Both devices have different programming interfaces (JTAG and SPI). The constructed programmer provides additional RS 485 and RS 232 TTL interfaces. The JTAG programmer bases on Atmega16 microcontroller and Atmel JTAG ICE firmware, therefore is compatible with AVR Studio. The archetype of SPI programmer is an open source project [7]. The hardware was slightly modified but the firmware remained unchanged. The SPI programmer uses STK 500v2 protocol and is compatible with AVR Studio.

III. Firmware

The firmware was written in C language. The complete source code is available at svn repository http://akme.yum.pl/FreeRtos/FreeRtos, where the login and the password is "student". The firmware part of the presented didactic platform consists of two basic parts: the firmware for the main controller and the firmware for the executing modules. Each device has a different microcontroller and has other functions, therefore it needs specialized firmware. There is embedded RTOS on both modules. The authors chose FreeRtos as RTOS because it is distributed under modified GPLv2 license [8]. FreeRtos uses two methods of providing multitasking: tasks and coroutines. Its kernel needs 4 kB of program memory, hence it is possible to use FreeRtos on microcontrollers with 8kB of program memory. Originally, FreeRtos was ported to the Atmega32. In the case of the proposed platform, it was necessary to make a port for Atmega168 and Atmega128 microcontrollers.

A. Main controller

Main controller is responsible for controlling the executing modules and communication with users. It stores logs and allows to schedule some operation, e.g., moving up the roller shutters. The main modules of the main controller firmware are the following: kernel, Command Line Interpreter, file system, Communication protocol, TCP/IP stack and xModem protocol.

1) Kernel: Multitasking in the main controller is provided with the help of tasks without preemption. Such an approach has numerous and significant advantages. Tasks are simple, have no restrictions on use and support full preemption (not used in our case). Moreover, they are fully prioritized [9]. The firmware was written without preemption, so re-entry to the task does not need to be carefully considered. The main disadvantage is that each task has its own stack. The Atmega128 has 128 kB of program memory and 4 kB of internal data memory extended by external chip to 64 kB and allows us to use FreeRtos with tasks. It is recommended to

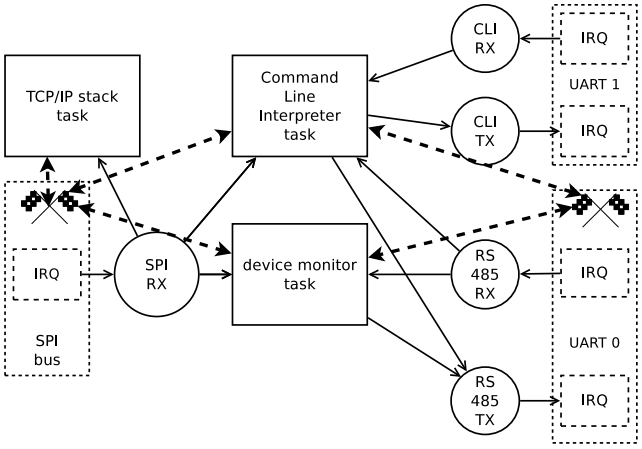

Figure 3. Architecture of main controller firmware

place stacks of the tasks in internal memory, hence there is 4 kB for stacks available. There are three tasks: Command Line Interpreter task, device monitor task and TCP/IP stack task. 4 kB is enough for three stacks. In order to save internal memory, buffers and other structures were moved to two times slower external memory. Constant strings and constant structs are stored in flash memory. In Figure 3 the firmware architecture of the main controller is presented. It bases on the mentioned three tasks.

The Command Interpreter task is responsible for communication with users through a console attached to USB port. This task uses serial port UART 1 for its exclusive use. This simplifies the implementation because it is not necessary to add the semaphore, which is responsible for blocking simultaneous access of many tasks to serial port UART 1. This task uses additionally the SPI bus and serial port UART 0. Other tasks are also using these resources, therefore they required semaphores to synchronize tasks. The semaphore blocks simultaneous access to one of the resources by more than one task. In Figure 3 the semaphores are marked by a racing checkered flag symbol. When the task is attempting to enter the critical section (e.g., read or write to serial port UART 0), it has to pass through the semaphore. If the semaphore is locked, the task is suspended as long as the semaphore is locked. Once the semaphore is unlocked, the task is released automatically and the semaphore is locked again by this task. The task unlocks the semaphore again after leaving the critical section. FreeRtos provides special API for handling semaphores. The task is suspended as long as the semaphore is locked, or until its optionally specified timeout.

FreeRTOS supports API for buffer handling in order to simplify the implementation of the main controller firmware.

 ISBN: 978-1-61208-123-6

There is a special function for writing to the buffer. If the buffer is full, the task is suspended as long as the buffer is full and optional specified timeout is not exceeded. The function informs (returns the result) if the operation was successful or not. Similarly there is a function for reading the buffer. If the buffer is empty, the task is suspended. The task is released when data is available in the buffer or timeout is exceeded. All the mentioned FreeRTOS API functions are not blocking. If the task is suspended, the microcontroller is executing other, not suspended, tasks. The developer has to care about avoiding deadlocks. Programming tasks is thus complementary to the operating systems theory within the range of topics related to deadlocks.

The task of the device monitor is to check the state of modules connected to RS 485 bus or SPI bus. This includes polling all devices connected to the RS 485 bus, reading analogue inputs values and communicating with devices connected to SPI bus (e.g., RTC clock). The task uses the resources such as SPI BUS or serial port UART 0. The task is synchronized with other tasks by semaphores.

The TCP/IP stack task is responsible for listening and establishing new TCP connections and handling them. The task uses SPI bus and is also synchronized. This tasks has a lower priority than two other tasks.

2) Command Line Interpreter: The main controller provides interactive communication with a user thanks to Command Line Interpreter. Initially, the CLI was taken from the AVRlib project [10]. Original CLI was not designed for multi task environment: only one instance of CLI was possible and, furthermore, it was working on global variables. The original CLI was not ready to cooperate with *stdio* C library. As a result, for the purpose of the proposed platform, most of the codes of the original CLI has been rewritten. Now, it is possible to use many independent instances of CLI. Each CLI has the history of 4 last commands and works on a new engine. The proposed CLI is compatible with *stdio* library and it is possible to use *fprintf* functions in order to make a print.

The new CLI API is friendly (it allows users to add new commands easily) and communication with the main controller is simple. The command *help* displays all available commands and its description.

3) File system: An important part of operating system theory is devoted to file systems. For the purpose of the didactic platform, a simple file system, the so-called Fat8, has been written. It can address up to 256 clusters. Each cluster, contrary to CP/M operating system, has 256 bytes instead of 128, what simplified the file system implementation. The whole implementation takes about 500 lines of code and is compatible with avr-libc [11] API. The file is visible as a stream. Writing to a file is possible using *fprintf* function.

4) Communication protocol: The main controller and the executing modules are connected to a common medium – RS 485 bus. The communication model looks as follows. The main controller (master) starts the transmission on the bus. Each frame sent by the master main controller has an address of a slave device (an executing module) – the receiver of the message. The slave device can answer to the message. The frame format is Type Length Value. The frame fields are the following: synchronization sequence, address, type of message, message length and message data. Two bytes with CRC sum end the frame.

5) TCP/IP stack: The TCP/IP stack implemented in the presented didactic platform is based on the stack proposed within *HTTP/TCP with the Atmega88 microcontroller (AVR web server)* [12] project. For the purpose of our project, the TCP/IP working on Atmega88 with 8 kB of program memory was adopted for multitasking system. The TCP/IP stack is supported in the presented didactic platform only partially. At the current stage, only the ICMP protocol and a simple WWW server is working. The next releases of the didactic platform will also include an implementation of servicing several TCP connections.

6) Xmodem protocol: This protocol allows to send or receive files. It cooperates with *stdio* library and input/output stream. This protocol is useful for bootloader handling. It allows to flash executing module by new firmware image. Implementation of TFTP protocol is much more complicated.

B. Executing module

The executing module controls 4 relays and reads four inputs. It is suitable for controlling two roller shutters or four light sources. Some controlling functions can be fulfilled automatically, e.g., after pressing the button the relay is switched on. The relay state may be changed after receiving special command from main controller.

1) Kernel: The executing module is not well equipped. Its microcontroller has 16 kB of program memory and 1 kB of data memory. In order to save data memory, the FreeRtos is using coroutines. The coroutines share common stack. The coroutines in FreeRTOS are automatically restored by the scheduler and a developer does not need to focus on them. Moreover, they are very portable across other architectures [9]. The disadvantage of the coroutines is a requirement of a special consideration. The lack of stack causes that data stored in local variables are destroyed after restoration of coroutine, what complicates the use of coroutines. The coroutine API functions can be called only inside the main coroutine function. In FreeRTOS, the cooperative operation is only allowed among coroutines, not between coroutines and tasks. For this reason there are only coroutines and no tasks in firmware of the executing module.

In Figure 4 the architecture of the executing module that controls two roller shutters is presented. For driving single roller shutter two relays are required; since one executing module can coordinate two roller shutters. The firmware consists of 4 coroutines, presented in Fig. 4 as solid line

 ISBN: 978-1-61208-123-6

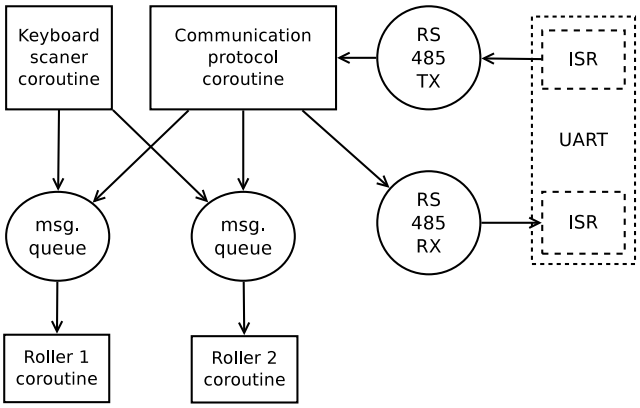

Figure 4. Architecture of executing module firmware

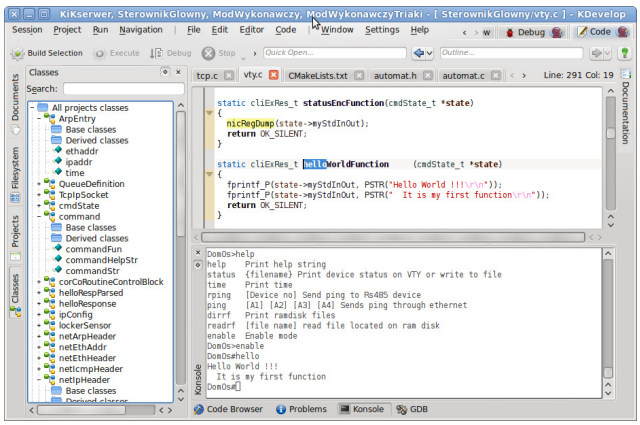

Figure 5. IDE and Hello world function

rectangles. Two coroutines drive the rollers, additionally there is a coroutine that scans the keyboard connected to the executing module and another one responsible for communication within RS 485 bus. The coroutines communicate with each other by 2 buffers presented in Fig. 4 as circles. The coroutine responsible for communication with RS 485 bus can send appropriate commands to driving roller shutter coroutine with the help of the buffer. The same buffer can be used by the scanning keyboard coroutine to send a message. The messages sent by the buffer includes information about relay (its number), which should be switched on or off at a specified time.

2) Communication protocol: Executing modules work as slave devices. The communication is always started by a master device by sending a message with a slave device's address (destination address). All slave devices check destination address of the received messages. If the address is matching, the slave device answers and executes the command issued by the main controller. In most cases, messages with not matching address are ignored. There is only one exception to this rule, which is presented in the next section.

3) Bootloader: The bootloader is mainly used when STK 500v2 programmer is not available or when it is not connected. The main controller can flash firmware to the executing module. With the help of the xModem protocol the firmware image is first uploaded to the main controller and stored in a file. Next, the main controller sends restart command to the executing module and if the address is matched, the device restarts. Otherwise, the device disconnects from RS 485 bus for 60 seconds – this is enough to write firmware to the executing module. After restart of the executing module the bootloader code is executed. The bootloader waits 30 seconds for flash command. After receiving it, the executing module is trying to download firmware using the xModem protocol. The main controller sends firmware according to the xModem protocol.

4) Keyboard scanner: There is a coroutine described in Section III responsible for keyboard scanning. It can distinguish a key press from stick bumping on keyboard.

C. Software tools

The prepared toolset for the platform purposes works on Linux and consists of editor (Integrated Development Environment – IDE), compiler, repository and programmer software. In the Ubuntu distribution all of required programs are available in its repositories and can be installed using apt-get install command. Thanks to this advantage it is very easy to write the instruction for students, explaining how to prepare the system for work.

IV. Laboratory Exercises

The presented platform allows users to prepare many exercises. For example, students can add new commands to main controller's CLI as it is shown in Fig. 5, as well as modify the interface of the application programming system File System API. It is also possible to add a new task to the main controller that is periodically sending messages to executing modules, for example to move roller shutters up or down.

An exemplary exercise for students can be focused on modification of executing module firmware. It is possible to use the execution module for controlling 4 light sources. The code is very similar to the code of executing module that is controlling roller shutters. The architecture of the firmware is presented in Fig. 6. Each light source, analogically to roller shutter firmware, is controlled by a separate coroutine. Therefore, it was necessary to add two more coroutines. Each coroutine that controls light shares the same code and has its own buffer with messages. The message format is one byte long. There is information in the message for how long the light has to be switched on. If the value is equal to zero, the light has to be switched off. The algorithm of the coroutine is shown in Fig. 7. Initially – during the initialization phase – the light is switched off, therefore

 ISBN: 978-1-61208-123-6

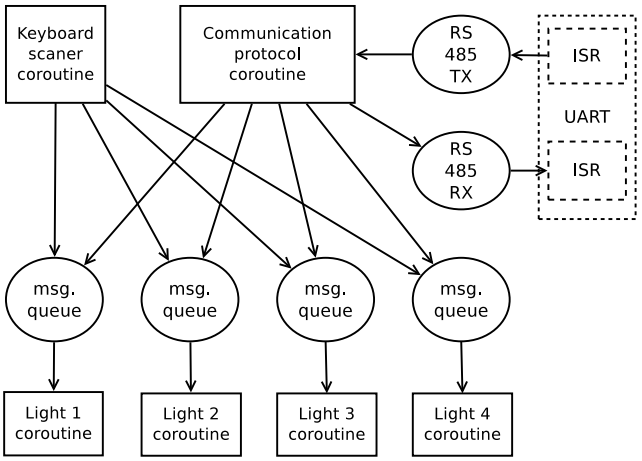

Figure 6. Architecture of executing module firmware controlling 4 light sources

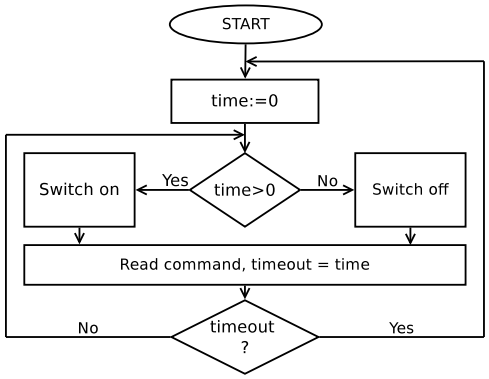

Figure 7. Algorithm for coroutine handling single light source

the variable *time* is equal to zero (analogically to message format). In the next step, the coroutine checks the value of *time* variable. If it is grater than zero, the light is switched on. Otherwise, the light is switched off. Next, the coroutine is waiting for a new message in the buffer, not longer than the time of switching on the light. If the timeout is exceeded and there is no message, the algorithm goes back to the initialization phase and the light will be switched off in the next step. If there is a new message, the light is switched on for a time specified in the message.

The solution based on using multitasking is easier and more readable. Each coroutine in this case is responsible for a different job.

V. Conclusion

The presented didactic system is a valuable addition to the theory of operating and embedded systems. It enables students to get familiarized with the aspects like multitasking, interprocess communication, and process synchronization. The platform has been designed in such a way as to facilitate its quick and easy implementation. For this effect AVR microcontrollers, which are increasingly popular among students taking interest in electronics, have been used. The presented solution is inexpensive and most of students can afford to build the presented platform and use it for didactic or practical purposes limited only by their imagination.

The paper focuses on technical details to assists other users in building a similar didactic platform that would support teaching of the theory of operating systems. Because of the limited size of the present article, only a selection of possible didactic exercises supported by the platform is presented, while further possibilities are only indicated.

Further refinement of the platform, with active participation of students, will include an implementation of the TCP/IP stack, telnet server (enabling CLI communication) and the operation of the FAT32 file system and SD cards.

The aptitude tests carried out among students indicate that the introduction of the presented didactic platform to the process of teaching the theory of operating systems have resulted in a considerable improvement in the exam performance (by 25%).

Acknowledgement

The authors would like to thank all the developers taking part in open source projects cited in the article.

References

[1] R. Love, *Linux Kernel Development*, 2nd ed. Novell Press, 2005.

[2] W. R. Stevens and S. A. Rago, *Advanced Programming in the UNIX Environment*. Addison-Wesley, 2005.

[3] F. S. Foundation, “Gnu general public licence v2,” http://www.gnu.org/licenses/gpl-2.0.html, 1991.

[4] Cadsoft, “Eagle,” http://www.cadsoft.de, 2010.

[5] Atmel, “Atmega128 datasheet,” http://www.atmel.com/dyn/resources/prod_documents/doc2467.pdf, Aug. 2010.

[6] ——, “Atmega168 datasheet,” http://www.atmel.com/dyn/resources/prod_documents/doc2545.pdf, Jul. 2010.

[7] G. Socher, “Avrusb500v2 – an open source atmel avr programmer, stk500 v2 compatible, with usb interface,” http://tuxgraphics.org/electronics/200705/article07052.shtml.

[8] FreeRTOS, “Copyright notice,” http://www.freertos.org/copyright.html.

[9] ——, “Freertos api reference,” http://www.freertos.org.

[10] P. Stang, “Procyon avrlib api,” http://www.mil.ufl.edu/~chrisarnold/components/microcontrollerBoard/AVR/avrlib, 2006.

[11] “Avr-libc api,” http://avr-libc.nongnu.org/, 2010.

[12] G. Socher, “Http/tcp with an atmega88 microcontroller (avr web server),” http://www.tuxgraphics.org/electronics/200611/embedded-webserver.shtml, 2006.

 ISBN: 978-1-61208-123-6

Snap or Point and Click?

Realizing the Potential of a Teacher Education Self-Study

Lorayne Robertson, Dianne Thomson, Lori May & Jim Greenlaw
Faculty of Education, UOIT
University of Ontario Institute of Technology
Oshawa, Canada
Lorayne.robertson@uoit.ca

***Abstract*—This research work-in-progress centers on the views of participants in a higher education self-study as they compare the web-centric self-study environment with the opportunities and challenges of the traditional written self-study format. Participants include approximately 100 faculty; preservice teachers; district school board personnel; and the reviewers. Through this process, we seek to identify their perceptions of most productive use of professionals' time in a self-study process. The research methodology is mixed and involves the use of a survey mechanism within the web-enabled self-study environment. Several key questions focus participants' attention on the levels of their awareness of the mission, vision and higher education program outcomes. Participants also compare the helpfulness of the written self-study and the web-enabled self-study for purposes of continuous improvement of the overall student learning experience, and engagement. This study is underway and anticipates initial findings by March, 2011 to be presented at the conference.**

Keywords - education, digital technologies, self-study, preservice education, technology affordances, new literacies.

I. I. INTRODUCTION

The context for this study is the self-study of a teacher education program at a designated University of Technology, with a laptop-enabled program. All teacher candidates in the one-year post baccalaureate program are assigned a laptop imaged with educational curriculum policy documents and educational software. Technology is almost ubiquitous in the program: WebCT is the learning management system (LMS), Adobe Connect is used for teaching some of the live, synchronous classes, and teacher candidates learn a wide range of technology-supported teaching and learning methodologies. Some of these include: the construction and deconstruction of digital media; the application, construction and critical analysis of web-based learning objects (WBLO's); and the educational applications and potential of graphic design programs, blogs, wikis, and other similar learning platforms.

A self-study of the teacher education program is required every 5 years by the government regulatory board for teacher certification, and the university's regulatory board for planned quality assurance review. Both boards require the teacher education program to provide evidence to demonstrate compliance with established standards by providing written analytical self-study documents. Although the teacher education program is technology-centric, this descriptor does not necessarily apply to the accrediting agencies. The licensing board, the Ontario College of Teachers (OCT) requires a somewhat traditional lengthy narrative (in the area of five or more heavy binders) while the higher education board requires a somewhat more concise 100 page analytical written report. This, for us represents the "snap" aspect of the review. Once the binders snap shut, the self-study is sent to the reviewers.

Both accrediting agencies require the submission of the self-study document to the external reviewers several months before the site visits of the external review teams; site visits include both interviews with stakeholders the reviewers identify and the establishment of an evidence room. For the self-study that is the focus of this research, the faculty of education is experiencing both external reviews in one semester. A lengthy narrative for the self-study has been provided to both agencies but both have

 ISBN: 978-1-61208-123-6

allowed the use of a virtual evidence room for the site visits.

While it is generally acknowledged that the purpose of a self-study is for improvement, research on self-studies identifies that improvement and faculty engagement are not necessarily generated through the traditional form of an externally-mandated self-study mechanism within an external review (Van Kemenade & Hardjono, 2010). To date, little research has been undertaken on a potential further source of association or disassociation for a faculty - that of requiring the accreditation self-study reporting through a written narrative script that is no longer the central communication norm in a technology-centric university. This study focuses on the participant perceptions of gains or affordances from the traditional self-study narrative (the *snap* of the binder) compared to participant perceptions of the gains from a *point and click* web-enabled self-study environment.

II. REVIEW OF THE LITERATURE

Self-evaluation or a self-study in the context of an external review is a mechanism that is intended to engage a faculty in the examination of itself in order to demonstrate that the faculty merits recertification. Whether or not improvement is an outcome of the self-study depends on many factors such as whether or not the study actually reflects the demonstrated outcomes of the faculty's efforts (veracity); whether or not the evidence is valid (trustworthiness of the data); if the external reviewers have the requisite expertise and context to suggest relevant improvements (helpfulness); or whether or not the faculty actually engage in the self-improvement aspect of the self-study (engagement).

There is a field of research on self-study in education. There are, for example, findings regarding the most effective mechanisms for sufficient faculty engagement for an effective self-study (Kollenberg, 2003). Other research identifies tensions in the self-study research field such as disagreement as to what constitutes valid research in a self-study (e.g, Craig, 2009). Another tension surrounds whether or not the most productive self-studies have an external focus and control, or an internal focus and control (Van Kemenade & Hardjono, 2010). In addition to the tensions identified, we sought studies that address the potential of "new literacies" (Lankshear & Knobel, 2006) to improve the self-study experience and we find little evidence of work in this field. In the section that follows, we will briefly touch upon identified self-study tensions and then introduce "new literacies" as a potentially promising theoretical framework to investigate the efficacy of the self-study as a mechanism for improvement.

The field for self-study research concerns itself with several distinct fields of interest. One is the practical side of self-study - mechanisms for gathering self-study data and faculty engagement, meeting timelines, organizing for the site visit, reporting mechanisms to survive the ordeal, and inviting faculty engagement (e.g., Van Kollenburg, 2003). A second aspect of self-study research concerns itself with identification - wrestling with distinctions between self-study and action research (e.g., Samaras & Freese, 2009) or self-study and teacher-as-researcher (e.g., Turner, 2010). Another tension is around the definition of what constitutes robustness or acceptable evidence in self-studies. Craig (2009) reminds us that "signs of struggle abound" in the field of self-study, which she identifies as a struggle to accept the trustworthiness of reports from the field of practice and reflection, noting that "the hegemony of the dominant research paradigm" brings into question the validity of "self-study research contributions" (p.21) as a relatively new field of study.

A further tension in the research appears to focus around the helpfulness of the study. For example, is an externally-regulated self-study more likely to engage a faculty in self-improvement than a study that is internally-generated? Are self-studies a legitimate means of assuring quality in tertiary education? Van Kemenade and Hardjono (2010) remind us that it is critically important for a self-study to involve and engage the participants or it may result in

 ISBN: 978-1-61208-123-6

something that resembles a window-dressing exercise or one that could potentially decrease the motivation of the participants in their work efforts. Their extensive two-year study identifies that, in most European countries, self-study in accreditation is compulsory and designed for accountability – in Norway, Finland, Denmark and Sweden, self-study is also compulsory but is designed for self-improvement. The methods are somewhat similar in both processes: a self-evaluation followed by a peer review. Their findings indicate that while accreditation is not a key focus of faculty in general, there are factors that can influence their support of the process. They are more willing to contribute to a process if they see that it has an added value for their organization (i.e., out of loyalty) or if the process has value for their key interests (their students and their disciplines). They are also more likely to contribute if the focus is not control and if the processes are simple and supported by the management. They are also more likely to contribute if an internal quality assurance mechanism already exists. Van Kemenade and Hardjono conclude that professionals will be careful in writing down the truth and showing their vulnerability in an accreditation system that is compulsory and has serious consequences. There appear to be benefits to a system that is not compulsory, invites participation, is less formal, and occurs frequently (e.g., annually).

There is some interest in the literature in how digital technologies can support the self-study process. Askins (2003) identifies some of the advantages of the use of a learning management system (LMS), in this case, Blackboard, for a self-study. These include: the fluid nature of documents; ease of holding synchronous online meetings despite distance between participants and weather conditions; ease of collecting files through a digital drop box system; virtual access to faculty policies and procedures; and ease of managing requests for information to faculty through email. Challenges with an LMS-enabled self-study process include; a need for technical support person; faculty resistance to technology; and faculty comfort with the LMS (Askins, 2003). She sees the potential that a web-enabled environment holds for supporting a self-study, but finds that a web-enabled environment may not be needed in smaller self-studies.

There appears to be a gap in teacher education self-study research to address issues that are of central importance to us in our study, that is, *matching the needs of a review system that was designed for an earlier era with the skill set and communication practices of a faculty that works with web-enabled technologies*. Our study explores the potential and affordances of "new literacies" (Lankshear & Knobel, 2006) to address previously-identified challenges with the self-study process: logistics; faculty engagement; trustworthiness of data; and the potential of a self-study to lead toward improving the program under review.

III. THEORETICAL FRAMEWORK

Lankshear and Knobel identify new literacies as "practices that are mediated by post-typographical forms of text" and identify these practices as the "technical stuff" and the "ethos stuff" (2006, p. 25). Extrapolating from the dichotomy they present, some of the *technical* practices for the purposes of a self-study might include: using and constructing hyperlinks between documents; pointing and clicking to access text; providing evidence with movie files; using sound with images for digital stories; and building a website environment for the self-study. Some of the *ethos* practices might include: more participation, collaboration and shared authoring; less presentation of text in a final form and single-authored; more immediate distribution of information to constituents; and a format that reflects contemporary literacies.

IV. RESEARCH STUDY

The research in progress involves the systematic examination of participant perceptions between the traditional written self-study binder submissions and opportunities and challenges

 ISBN: 978-1-61208-123-6

presented by the web-centric self-study. Participants include approximately 100 faculty, key stakeholders and reviewers. We seek to find the most respectful use of participants' time toward a process that is both engaging and produces results. The research methodology is mixed but essentially qualitative and involves the use of a survey mechanism within a web-enabled self-study environment. Within a password-protected web-based environment, participants identify themselves as faculty, members of the internal review team, stakeholders, or members of the external review team. They are invited but not required to participate in an online survey.

The survey asks them to consider past experiences with self-studies – to identify the types of self-studies in which they have participated in the past; the most important things learned from past processes; and challenges encountered (Atnip, Vasquez and Kahn, 2003). The survey then asks them to identify aspects of the web-enabled self-study that have helped them to learn or have created challenges for them. Several key questions focus participants' self-assessment of their awareness of the mission, vision and program outcomes during both the written self-study submission process and the web-enabled self-study process. Other questions ask the participants to compare the helpfulness of the written self-study and the web-enabled self-study for purposes of continuous improvement of the overall student learning experience, as well as perceptions regarding the factors identified by research that affect the strength of faculty engagement in the self-study process.

This study is presently underway and anticipates some early findings by March, 2011 to be presented at the conference.

REFERENCES

[1] G. Atnip, M. Vasquez, and S. Kahn. "Deciding how to approach the self-study: Three campuses, three choices." A Collection of Papers on Self-Study and Institutional Improvement, Chicago: North Central Association of Colleges and schools, 2003.

[2] C. Beck and C. Kosnik, Innovations in Teacher Education: A Social Constructivist Approach. Albany, NY: State Univ of New York Pr. 2006.

[3] S.Dixon and R. Moorse, Self-assessment for improvement [and] preparing for accreditation: Colleges and self-assessment.London,UK:Further Education Development Agency, 2000.

[4] T. Friedman. The world is flat: The globalized world in the twenty-first century . London, Penguin, 2006.

[5] P.L.B. Kohl and V. Gomez. Reaccreditation self-study: A tool for curricula improvement. Paper presented at the annual meeting for the association of teacher educators. St. Louis, MO, 1996.

[6] C. Lankshear and M. Knobel. New literacies: Everyday practices and classroom learning. Berkshire, UK:Open Univ Pr, 2006

[7] A. Samaras and A. Freese. "Looking back and looking forward: An historical overview of the self-study school," In *Self-study research methodologies for teacher educators* , C. A. Lassonde, S. C. Galman & C. M. Kosnik, Eds.,Rotterdam, The Netherlands:Sense Publishers, 2009

[8] I. Silver, C. Campbell, B. Marlow, and J. Sargeant. "Self-assessment and continuing professional development: The canadian perspective." *Journal of Continuing Education in the Health Professions*, vol. 28(1), pp. 25-31, 2008.

[9] B. Trilling and C. Fadel. 21st century skills: Learning for life in our times, San Francisco, CA:Jossey-Bass, 2009.

[10] E. Van Kemenade and T.W. Hardjono. "A critique of the use of self-evaluation in a compulsory accreditation system." *Quality in Higher Education*, vol. 16(3), 2010, pp. 257-268.

[11] S.E. Van Kollenburg. A collection of papers on self-study and institutional improvement. Volume 4. The self-study process for commission evaluation. Chicago: North Central Association of Colleges and schools, 2003.

[12] B.M. Whitehead, D. Jensen, and F. Boschee. Planning for technology: A guide for school administrators, technology coordinators, and curriculum leaders. Thousand Oaks, CA:Corwin Press, 2003.

 ISBN: 978-1-61208-123-6

Multi-Stage Threshold Decoding of High Rate Convolutional Codes for Optical Communications

Muhammad Ahsan Ullah, Ryousuke Omura, Takuma Sato, and Haruo Ogiwara
Department of Electrical Engineering
Nagaoka University of Technology
Kamitomioka-cho, 1603–1
Nagaoka-shi, Niigata-ken, 940–2188, Japan
Email: {ahsan,omura,t-sato}@comm.nagaokaut.ac.jp and ogiwara@vos.nagaokaut.ac.jp

***Abstract*— For 100 Gb/s optical transport network, researchers are searching a suitable error correction coding scheme that can provide coding gain more than 10 dB at the bit error rate less than 10^{-12}, provided that the redundancy does not exceed 20 percent. This paper presents a least complex error correction coding scheme based on iterative threshold decoding called multi-stage threshold decoding with difference register (MTD) for the 100 Gb/s optical transport network. High rate (code rate 0.8) self-orthogonal convolutional codes are considered. The MTD achieves lower bound error performance of maximum likelihood decoding at higher bit energy to noise density ratio. The codes with orthogonal checking 10 and larger satisfy the requirements of 100 Gb/s optical transport network. The bit error rate of MTD with parity check decoding becomes less than 1/100 times in the error floor region compared to ordinary MTD. The MTD based decoding with parity check decoding for the code with orthogonal checking 12 produces 10.60 dB coding gain at the bit error rate 10^{-15}. The coding gain further improves 0.25 dB in the waterfall region by using 2-step decoding.**

***Keywords*- threshold decoding, convolutional codes, self-orthogonal codes, optical transport network.**

I. Introduction

Forward error correction codes (FECs) play an important role in the newly considered optical transport network (OTN) with network capacity 100 Gb/s. International telecommunications union (ITU–T) primarily consider the Reed–Solomon (RS) codes as FEC [1] in the G.975 recommendation. It considers RS(255,239) code with 7% redundancy. The expected coding gain is 4 to 5 dB per fibre span, but it is not sufficient for 100 Gb/s OTN operation.

There have been a number of proposals for higher gain FECs; one is iterated code based on (1023,992,8) BCH code claimed as the best choice as FEC for 100 Gb/s OTN system that produced the coding gain around 9.3 dB at the output bit error rate 10^{-15} [2]. However, more than 10 dB coding gain is required for the 100 Gb/s OTN system at the output bit error rate less than 10^{-12} with the maximum allowable redundancy 20% [3].

Most of the codes proposed as FECs for the 100 Gb/s OTN system are block codes and their hard decoding technique is considered. The low density parity check (LDPC) codes with soft decoding have been adopted for the 10 Gb/s Ethernet (IEEE 803.3an), WiFi (IEEE 802.11n), WiMAX (IEEE 802.16e) wireless LAN standards and are being considered for a range of application areas, from optical transport network to digital storage [3][4]. An LDPC code concatenated with RS code may be the main candidate as FEC for the 100 Gb/s.

However, the convolutional codes for optical communications are rarely shown as FEC due to their latency and error floor [3]. This paper presents a least complex decoding method for self-orthogonal convolutional codes that can reduce the decoding latency by parallel processing and improves the error floor performance with concatenation of parity check (PC) decoding that fulfills the requirements of 100 Gb/s optical transport network. Moreover, implementation of convolutional encoding is simpler than the encoding of block codes. In addition, the proposed decoding is mainly based on the several shift registers and high speed decoding is expected.

The proposed decoding method is an iterative bit flipping decoding based on the threshold decoding [5] called multi-stage threshold decoding with difference register (MTD) which, is treated as MTD-DR in [6]. Similar decoding idea, called multi threshold decoding, is shown in [7][8]. They did not show why and how the threshold value changes in each iterations. Moreover, necessary information to rebuild the system is absent.

The iterative decoding based on min-sum decoding, instead of bit flipping, for the self-doubly orthogonal codes is shown in [9]. The decoding decision depends on the log likelihood ratio (LLR) of a posteriori probability and updates it after decoding each information bit. Moreover, the LLR increases the decoding complexity. Instead of LLR value, MTD uses a set of magnitude of the received signals for decoding an information bit and updates the binary value of the related signals by the flipping decision. The decoding latency, however, depends on the span of information shift register in the encoder and the average number of iterations.

The lower bound of maximum likelihood (ML) decoding has been presented in [10] and it is seen that, MTD achieves lower bound of ML decoding performance at higher bit energy to noise density ratio, E_b/N_0. That means, MTD gives optimum decoding performance of a given code and the error floor experiences due to the number of orthogonal checking of the code. Moreover, if we allow maximum 1.5% more redundancy by concatenating parity check code, the bit error performance in the error floor becomes less than 1/100 times

 ISBN: 978-1-61208-123-6

compared to conventional MTD.

Lower the orthogonal checking of a code gives better error performance in the waterfall region. In this context, the 2-step decoding, 1st decoding step uses a part of parity bit sequences (lower number of orthogonal checking) and 2nd decoding step uses all the parity sequences (all the orthogonal checking of the code), has been presented for rate 1/2 codes and the decoding scheme produces more coding gain in the waterfall region [10].

Rest of the paper is arranged as follows. Section II gives the concepts of iterative threshold decoding with difference register. In this section, we give soft decoding algorithms. Section III gives high rate self orthogonal convolutional codes. Section IV discusses about 2-step decoding that produces additional coding gain in the waterfall region. Section V gives an idea for high speed decoding that reduces total decoding latency. Section VI gives the bit error performance of decoding schemes. Section VII gives the decoding complexity in terms of basic operations (e.g., modulo 2 summation, real number summation, minimum value searching etc.) and compared with the complexity of min-sum based decoding scheme and Section VIII concludes this paper.

II. Decoding Concept

This section provides decoding algorithms of self-orthogonal convolutional codes (SOCCs) on the basis of threshold decoding. Soft decoding algorithms are also given.

A. Multi-Stage Threshold Decoding

A systematic SOCC with the rate R=1/2, shift register length M and the number of orthogonal checking J is considered. The orthogonal checking is denoted by the tap connection in the shift register of the encoder and the code is determined by its connection positions. Let g_a, a=1, 2, ..., J, be a tap connection position in the shift register involving to generate a parity bit sequence. The minimum Hamming distance (d_{min}=J + 1) depends on the orthogonal checking of the codes [11]. The dotted section in Figure 1 shows an encoder of the SOCC with R=1/2, M=8, J=3, d_{min}=J+1=4. The information bit sequence $\mathbf{u}$=$\{u_0, u_1, \ldots\}$ is fed to the encoder and generates a parity bit sequence $\mathbf{v}$=$\{v_0, v_1, \ldots\}$. The i-th parity bit is determined by

$$v_i = \sum_{a=1}^{J} \oplus\, u_{i-g_a}, \;\; i = 0, 1, \ldots \tag{1}$$

where $\oplus$ is the modulo-2 addition operator in this paper. The information and the parity bit sequences make a systematic codeword and is transmitted through the additive white Gaussian noise (AWGN) channel as BPSK signals. The tail biting termination is used.

Let $\mathbf{y}_u \triangleq \{y_0^u, y_1^u, \ldots\}$ be received information signals, $\mathbf{y}_v \triangleq \{y_0^v, y_1^v, \ldots\}$ be received parity signals, $\tilde{\mathbf{u}} \triangleq \{\tilde{u}_0, \tilde{u}_1, \ldots\}$ be hard decision information bits and $\tilde{\mathbf{v}} \triangleq \{\tilde{v}_0, \tilde{v}_1, \ldots\}$ be hard decision parity bits. The threshold decoding generates a syndrome bit sequence by the help of received information and parity bit sequences. The i-th syndrome bit is given by

$$s_i = \tilde{v}_i \oplus \sum_{a=1}^{J} \oplus\, \tilde{u}_{i-g_a} \tag{2}$$

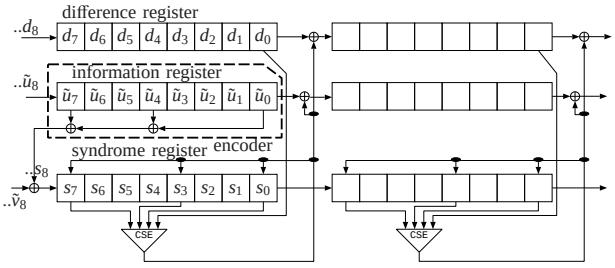

Fig. 1. Multi-stage threshold decoder for the Self-orthogonal convolutional code with m=n=1, J=3, M=8 and R=1/2. CSE means checksum-threshold element.

Figure 1 shows a hard decision multi-stage threshold decoding scheme. The decoder contains an extra shift register against an information shift register called difference register (DR). The DR holds pairwise difference between the received and decoded information bits. At the initial stage, DR contains all zero bits.

The soft decoding MTD (SMTD) calculates the checksum value from a set of the magnitude of parity signals related to the information signal under decoding and the magnitude of the information signal itself [6]. In this case, the checksum value L_j is calculates by

$$L_j = \sum_{a=1}^{J} w_{j+g_a} \tilde{x}_{j+g_a}^v + w_{d_j} \tilde{x}_j^u \tag{3}$$

where w_k represents the magnitude of the signal y_k^v and w_{d_k} represents the magnitude of the signal y_k^u and the value $\tilde{x}_k^u \triangleq (1\text{-}2d_k)$ and the value $\tilde{x}_k^v \triangleq (1\text{-}2s_k)$. If the checksum value becomes negative, i.e., $L_j < 0$, the decoding is done by flipping the information bit. At the same time, related DR and syndrome bits are inverted. After flipping each information bit, the Euclidean distance between the received signals and the decoded codeword, where bits are represented by +1 or -1, becomes shorter [6].

B. Weighted Bit Flipping Multi-Stage Threshold Decoding

The weighted bit flipping (WBF) algorithm is proposed for decoding low density parity check (LDPC) codes [12]. By the similar way, the weighted bit flipping MTD (WMTD) explores the value w_k as the minimum magnitude among the received signals related to the syndrome bit s_k. Then, the checksum value is calculated by using (3) and the decoding decision is made accordingly.

C. Combined Soft Decoding Multi-Stage Threshold Decoding with Feedback

The individual error performance of SMTD and WMTD is not attractive. The concatenation of WMTD and SMTD called combined soft decoding MTD with feedback (CMTDF) produces attractive error performance. Figure 2 shows the schematic diagram of CMTDF where weighted bit flipping MTD works first and terminates its decoding when no information bit is flipped or by the maximum number of iterations. Then SMTD works by the same manner and feedback again.

 ISBN: 978-1-61208-123-6

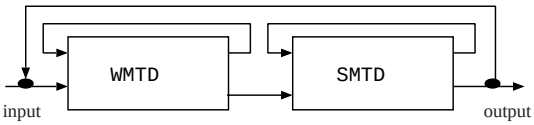

Fig. 2. Schematic diagram of combined soft decoding multi-stage threshold decoding.

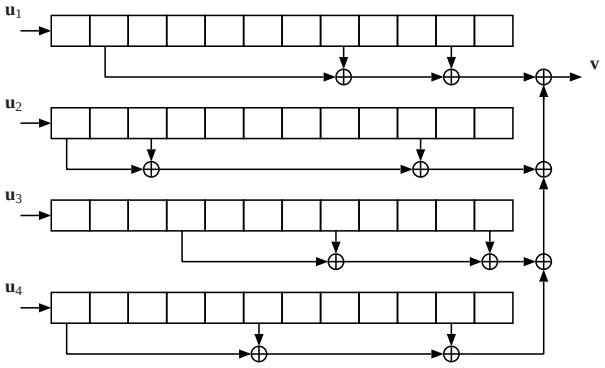

Fig. 3. Self-orthogonal convolutional code type 1 with m=4, J=3, M=12 and code rate R=4/5=80%.

If no information bit is flipped in both component decoders or completed maximum number of iterations, final output is made.

D. Combined Soft Decoding Multi-Stage Threshold Decoding with Parity Check Decoding

A parity check decoding is serially concatenated with CMTDF. The CMTDF with parity check (PC) decoding achieves attractive bit error performance in the error floor region [6]. The PC encoder adds a parity check bit in the information bit stream after each n_1 bits. When parity check is not satisfied, the PC decoder searches the minimum absolute checksum value, provided by the CMTDF after the final iteration, related to each n_1 information bits. The decoding is done by flipping the information bit related to the minimum absolute checksum value. In this paper n_1 is set to 50 bits.

III. High Rate Self-Orthogonal Convolutional codes

This section gives high rate (code rate 80%) SOCCs that can produce redundancy around 20%. The SOCC is categorized into two types: 1) the self-orthogonal convolutional codes type 1 and 2) the self-orthogonal convolutional codes type 2 [6].

A. Self-Orthogonal Convolutional Code Type 1

The self-orthogonal convolutional code type 1 (SOCC:TP1) generates only one parity bit sequence by using $m \geq 1$ information bit sequences. That means, the encoder of SOCC:TP1 has m information shift registers and each shift register contains one set of tap connection with J_k $(k = 1, 2, ..., m)$ elements and the m tap connection sets make a SOCC. The orthogonal checking distribution of this code is defined by $\{J_1; J_2; \ldots; J_m\}$. Figure 3 shows an encoder of such code with m=4, $J = J_1 = J_2 = J_3 = J_4 = 3$ and the shift register length M=12. The code rate of this code is R=$m/(m+1)$ and the code length becomes N=$K(m+1)$, where K is the number of information bits in each sequence. The orthogonal checking distribution of this code is $\{3; 3; 3; 3\}$. Unfortunately, MTD makes an unavoidable error grouping in the decoded information bit sequences for this type of code and degrades the error performance [6].

B. Self-Orthogonal Convolutional Code Type 2

The self-orthogonal convolutional code type 2 (SOCC:TP2) generates $n \geq 2$ parity bit sequences by using $m \geq 1$ information bit sequences. i.e., an encoder of SOCC:TP2 has m information shift registers and each shift register contains n tap connection sets with $J_p^{(k)}$ $(k = 1, 2, ..., m,\ p = 1, 2, ..., n)$ elements and the $m \times n$ tap connection sets make the SOCC. The orthogonal checking distribution of the code is defined by $\{J_1^{(1)}, J_2^{(1)}, ..., J_n^{(1)}; J_1^{(2)}, J_2^{(2)}, ..., J_n^{(2)}; ...; J_1^{(m)}, J_2^{(m)}, ..., J_n^{(m)}\}$. Figure 4 shows an encoder of SOCC:TP2 with m=12, $n = 3$, $J = \sum_{p=1}^{3} J_p^{(k)} = 2 + 2 + 2 = 6$ and the shift register length M=12. The code rate of this code is R=$m/(m+n)$= 12/15. The orthogonal checking distribution of this code is $\{2, 2, 2; 2, 2, 2; 2, 2, 2; 2, 2, 2; 2, 2, 2; 2, 2, 2; 2, 2, 2; 2, 2, 2; 2, 2, 2;$-$2, 2, 2; 2, 2, 2; 2, 2, 2\}$. The SOCC:TP2 successfully breaks down the error groping and produces better error performance by the MTD compared to the SOCC:TP1 [6]. Therefore, this paper only consider the SOCC:TP2 for the encoding schemes.

IV. 2-Step Decoding

As is described in Section VI, MTD based decoding achieves lower bound of ML decoding performance at higher E_b/N_0. That means, error floor is realized due to the minimum Hamming distance $(J + 1)$ of the code. On the other hand, larger the J of a code shifts the waterfall error performance to higher E_b/N_0 and opposite situation is occurred due to smaller J value [6]. In this context, a 2-step decoding (2SD) has been proposed [10]. At the 1st decoding step, MTD uses a part of parity check bits so that decoding is done by approximately 50% of J of the code and the 2nd decoding step works just like an MTD. The code is constructed such a way that, one parity sequence is to be generated by approximately $J_s \approx J/2$ orthogonal checking. Other $J - J_s$ orthogonal checking are distributed evenly for generating rest of the parity sequences. The 1st decoding does not use a parity sequence which, is generated by the J_s orthogonal checking. MTD works with the orthogonal checking $J - J_s$ in the 1st decoding step and produces additional coding gain in the waterfall region. The 2nd decoding step then works by the all parity sequences. In this case, decoding is done by the J orthogonal checking. By this way of decoding, 0.55 dB additional coding gain is observed for the code with rate 1/2 [10]. In this paper we apply this idea for the codes with rate around 80%.

V. High Speed Decoding

This section gives an idea of parallel processing that speeds up the decoding process. Since, tail biting termination is used, the decoding can start from any position of the received

 ISBN: 978-1-61208-123-6

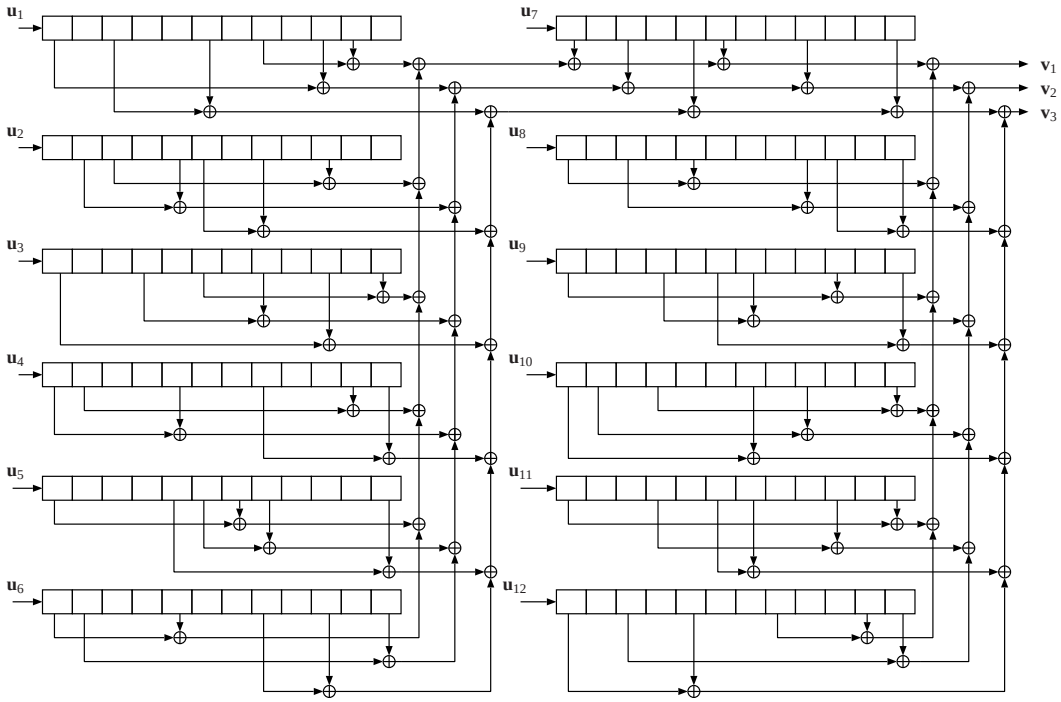

Fig. 4. Self-orthogonal convolutional code type 2 with m=12, n=3, J=6, M=12 and code rate R=12/15=80%.

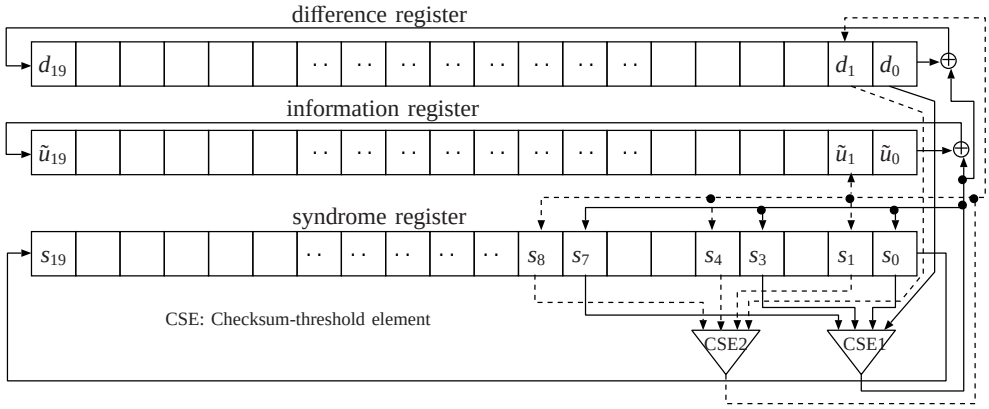

Fig. 5. Parallel processing of MTD with two checksum-threshold elements. The code with m=n=1, J=3, M=8, R=1/2 and code length N=40.

information sequence. If any syndrome is not commonly shared to decode other information bit, decoding can take place in parallel. Among the M positions in the shift register, only J points are involved to decode an information bit. When the minimum tap spacing (tap position difference in the syndrome register) is more than one, MTD can add more than one checksum-threshold elements (CSEs) where different CSE decodes different information bit at the same time. Figure 5 shows a simple example of such decoding scheme for a code with the minimum spacing 3 and two CSEs are shown. For this code, total 3 bits are decoded by the single period of shift register clock. In addition, to reduce the error propagation effect, it is necessary to use information bit length around twice of shift register length [13]. The length of the information bit stream is more than two times (20 bits in this example) of M = 8 value. Therefore, we have possibility to use another set of CSE with 3 elements in the decoding circuit and the decoding is done 6 times faster compared to the single CSE decoding scheme.

VI. Performance of Combined Soft Decoding Multi-Stage Threshold Decoding and 2-Step Decoding

Simulation results and ML decoding performance of the codes are presented in this section. In this case, channel is considered as AWGN and the data modulation is considered as BPSK. Before going to show the error performance, CMTDF with parity check (PC) decoding performance is estimated by using the lower bound of ML decoding of SOCCs and the simulation results of them with PC decoding.

 ISBN: 978-1-61208-123-6

TABLE I
SELF-ORTHOGONAL CONVOLUTIONAL CODES TYPE 2 WITH CODE RATE R=1/2.

Code parameter	# of shift register		orthogonal checking distribution
	m	n	
J=10 $M = 10^4$	2	2	{5, 5; 5, 5}
J=10 M = 1000	5	5	{2, 1, 1, 1, 5; 1, 2, 1, 1, 5; 1, 1, 2, 1, 5; 1, 1, 1, 2, 5; 2, 1, 1, 1, 5}
J=12 M = 1000	6	6	{1, 1, 1, 1, 2, 6; 1, 1, 1, 2, 1, 6; 1, 1, 1, 2, 1, 1, 6; 1, 2, 1, 1, 1, 6; 2, 1, 1, 1, 1, 6; 1, 1, 1, 1, 2, 6}

TABLE II
SELF-ORTHOGONAL CONVOLUTIONAL CODES TYPE 2 WITH CODE RATE R=4/5.

Code parameter	# of shift register		orthogonal checking distribution
	m	n	
J=8 M = 5000	8	2	{4, 4; 4, 4; 4, 4; 4, 4; 4, 4; 4, 4; 4, 4; 4, 4}
J=10 M = 5000	8	2	{5, 5; 5, 5; 5, 5; 5, 5; 5, 5; 5, 5; 5, 5; 5, 5; 5, 5; 5, 5}
J=12 M = 5000	8	2	{6, 6; 6, 6; 6, 6; 6, 6; 6, 6; 6, 6; 6, 6; 6, 6; 6, 6; 6, 6}
J=10 M=4000	12	3	{2, 2, 6; 2, 2, 6; 2, 2, 6; 2, 2, 6; 2, 2, 6; 2, 2, 6; 2, 2, 6; 2, 2, 6; 2, 2, 6; 2, 2, 6}

The lower bound of bit error rate of ML decoding is calculated for the self-orthogonal convolutional code with the orthogonal checking J by [10]

$$P_b \gtrapprox Q\left(\sqrt{\frac{2R(J+1)E_b}{N_0}}\right) \quad (4)$$

where $Q(x) \triangleq \frac{1}{\sqrt{2\pi}}\int_x^\infty e^{-\frac{y^2}{2}}dy$ and P_b is the bit error rate of the ML decoding scheme.

Figure 6 shows simulation results of CMTDF for the code with J=10, m=n=2, M=10000, R=1/2, the code length N=81600 and the minimum tap spacing 35 bits. The orthogonal checking distribution of the code is shown in Table I. The dashed line represents the lower bound of ML decoding result of the code. The error performance of CMTDF coincides with the lower bound of ML decoding performance in the error floor region. The CMTDF concatenated with PC decoding makes the BER less than 1/100 times of the lower bound of ML decoding of the SOCC without PC decoding in the error floor region. Simulation results of the 2SD are shown in Figure 7 for the codes with J=10 and 12, M=1000, R=5/10=6/12=1/2, the code length N=81600. The orthogonal checking distribution of codes are shown in Table I. The minimum tap spacing are 4 and 2 for the codes with J=10 and 12, respectively. The 2SD decoding also achieves lower bound of ML decoding performance for the codes. The 2SD with parity check decoding makes also the BER less than 1/100 times of the lower bound of ML decoding for the code without parity check decoding in the error floor region. From these observations, we expect that, the MTD based decoding with parity check decoding can achieve 1/100 times bit error rate of lower bound of ML decoding (without PC decoding) in the error floor region. This result will be applied for estimating the bit error rate of MTD based decoding with PC decoding at the BER below 10^{-12}.

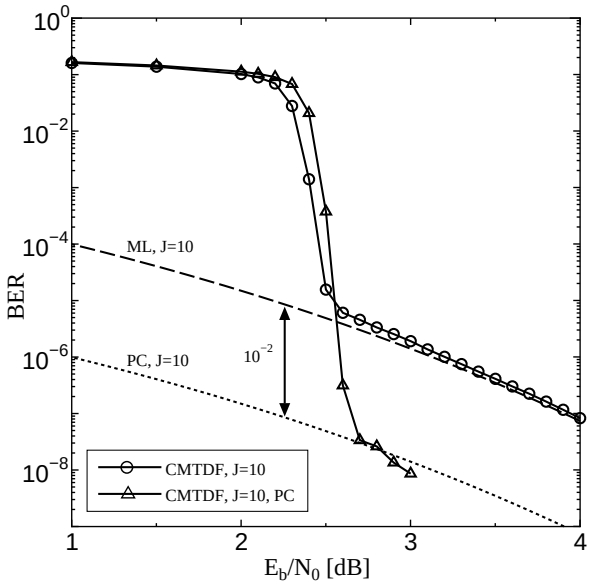

Fig. 6. Bit error performance of CMTDF for the SOCC type 2 with m=2, n=2, J=10, M=10000, R=2/4 and code length N=81600. Code is in Table I.

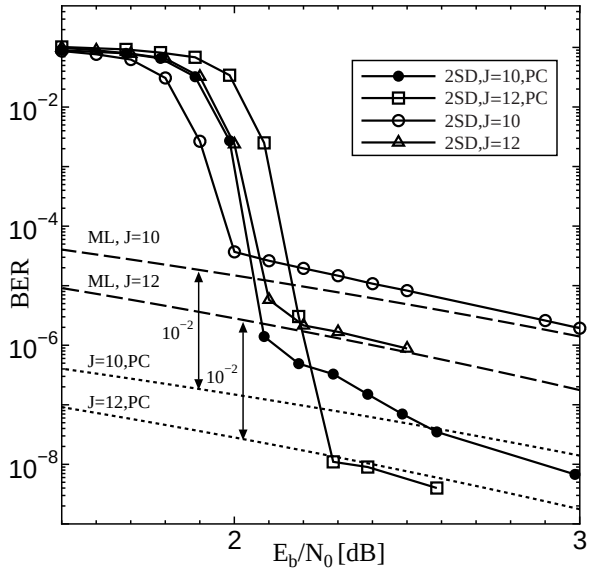

Fig. 7. Bit error performance of 2SD for the SOCC type 2 with m=n=5 for J=10 and m=n=6 for J=12, M=1000, R=5/10=6/12=1/2 and code length N=81600. Code is in Table I.

Figure 8 shows the bit error performance of CMTDF for the SOCC:TP2 with the code rate R=8/10=4/5, m=8 and n=2. The shift register length is M=5000 each. The figure shows the bit error performance for the codes with J=8, 10 and 12 and the minimum tap spacing are 2, 5 and 5, respectively. CMTDF for the codes with rate 80% also achieves the lower bound of ML decoding performance at higher E_b/N_0. The dotted line connected to the simulation result is the extrapolation of

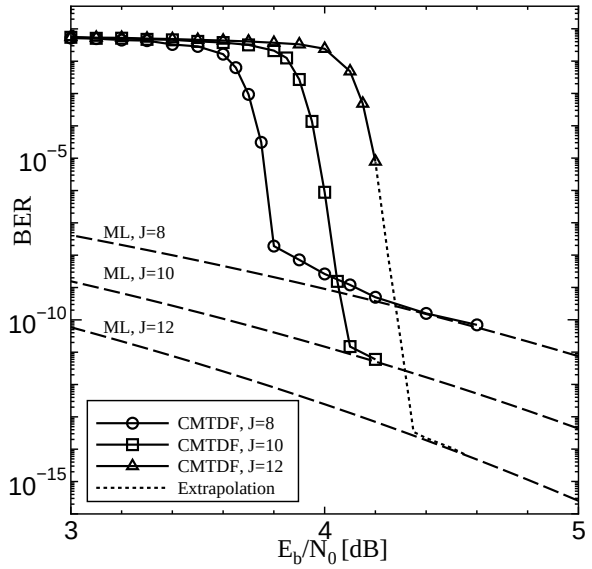

Fig. 8. Bit error performance of CMTDF for the SOCC type 2 with m=8, n=2, M=5000, R=4/5 and code length N=105060. Codes are in Table II.

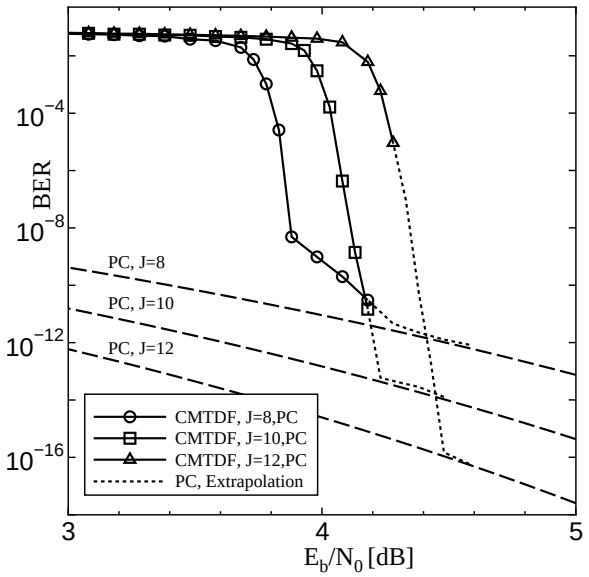

Fig. 9. Bit error performance of CMTDF with PC decoding for the SOCC type 2 of m=8, n=2, M=5000, R=4/5 and code length N=105060. Codes are in Table II.

the error performance up to lower bound line, because this performance is expected. The codes with J=8 gives better performance in the waterfall compared to the other codes, but the error floor is degraded. The 100 Gb/s OTN system demands at least 10 dB coding gain at the bit error rate less than 10^{-12}. The CMTDF for the code with J=10 achieves coding gain 9.0 dB at the BER 10^{-10}. For the code with J=12, CMTDF produces the coding gain 9.96 dB at the BER 10^{-13} and 10.20 dB at the BER 10^{-15}. In this point, the CMTDF for the SOCC:TP2 with J=12 is effective for 100 Gb/s OTN system. The decoding scheme uses average number of iterations (summation of the average iterations uses by the WMTD and by the SMTD) 23 at E_b/N_0=4.8 dB for the code with J=12.

Figure 9 shows the bit error performance of CMTDF with parity check decoding for the same codes mentioned in the Figure 8. The estimated error performance of CMTDF with PC decoding is shown by the dashed line with mark 'PC' in the figure. With the PC decoding, CMTDF for the codes with J=10 produces the bit error rate 10^{-13} and achieves the coding gain 10.10 dB. In this case, average number of iterations is 19.6 at E_b/N_0=4.8 dB. The code with J=10 with parity check decoding satisfies the requirement of 100 Gb/s OTN system. The overall code rate, in this case, is 78.43%. The same decoding scheme is used for the code with J=12. The decoding scheme achieves coding gain 10.60 dB at the BER 10^{-15} and 23 average number of iterations is used at E_b/N_0=4.8 dB.

Although CMTDF already realizes the lower bound of ML decoding performance in the error floor, we have opportunity to improve error performance in the waterfall region. The 2SD can produce some extra coding gain in the waterfall region. Figure 10 shows the bit error performance of 2SD for the codes with m=12, n=3, J=10 and shift register length M=4000. The

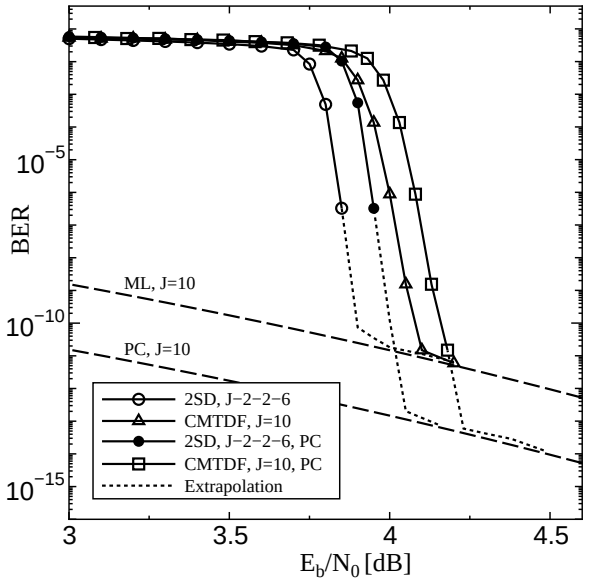

Fig. 10. Bit error performance of CMTDF and 2SD with and without PC decoding for the SOCC type 2 (m=12, n=3) in Table II. The code length is 130050.

code parameters are shown in Table II. This code provides the code rate R=12/15=4/5 and the minimum tap spacing is 4. Figure 10 also shows the comparison of the error performance between CMTDF and 2SD. Their performance with PC decoding is also given. The 2SD for the SOCC:TP2 with the code rate 80% produces additional coding gain 0.25 dB compared to CMTDF. The 2SD with PC decoding for the code achieves coding gain 10 dB at the BER 10^{-12} and 10.20 dB at the BER 10^{-13}. The 2SD uses 90 average number of iterations at E_b/N_0=4.2 dB and it is expected to decrease at

 ISBN: 978-1-61208-123-6

larger E_b/N_0. The 2SD with parity check for the code with J=10 satisfy the demands of 100 Gb/s OTN system. Moreover, the high speed decoding scheme can reduce the total decoding delay.

The Viterbi and the forward-backward (Bahl, Cocke, Jelinek, Raviv) algorithms gives the ML decoding of convolutional codes. They use trellis states of the code. The algorithms are suitable for the code with constraint length less than 20. The proposed decoding scheme handles a large constraint length (more than 1000) code. Thats why it is not comparable with them. However, min-sum decoding based iterative decoding has been shown in [9]. The CMTDF for the SOCC with rate 1/2 gives the similar decoding performance [6] of min-sum based decoding. So, it is expected that the proposed decoding scheme with high rate code also achieves similar performance with the min-sum decoding.

VII. Decoding Complexity

Table III shows the decoding complexity in terms of basic operations, e.g., modulo 2 summation, real number summation, etc. Decoding complexity is defined by the total number of operations necessary to decode an information bit. The decoding complexity of min-sum based decoding is calculated in terms of add-min operations [9] which, can be broken down to $J+1$ modulo 2 summation and J minimum weight search operations for decoding each information bit. Let, the 2SD uses (I_1, I_2) and the min-sum based decoding uses I_{tr} average number of iterations, respectively, then Table III summarizes the decoding complexity of 2SD and min-sum based decoding. Here I_1 is the average number of iterations used in 1st decoding step and I_2 is the average number of iterations used in final step of decoding for 2SD.

TABLE III
Decoding complexity of 2-step decoding and min-sum based Decoding.

Name of operations	Number of operations necessary for decoding each information bit	
	2-step decoding	min-sum based decoding [9]
Modulo 2 summation	$\leq J^2 + (I_1 + I_2)(J+2)$	$\geq I_{tr}(J^3 + 2J^2 - J - 2)/2$
Min. weight search	$J(J+1)$	$I_{tr}(J^3 + J^2 - 2J)/2$
Real number summation	$I_1(J - J_s) + I_2 J$	$I_{tr} J$

The complexity of the proposed decoding scheme depends on the J^2 operations of modulo 2 summation and minimum weight searching where the min-sum based decoding consumes J^3 operations in the same domain. Therefore, the proposed decoding method uses less number of basic operations than the decoding method given in [9].

VIII. Conclusion

This paper focuses on the forward error correction coding for the 100 Gb/s optical transport network. The optical transport network demands more than 10 dB coding gain at the BER less than 10^{-12} by allowable coding rate more than 80%. Most of the FECs proposed for the network are hard decoding based block code. This paper has presented a kind of soft decision bit flipping decoding using self-orthogonal convolutional codes. The decoding scheme is iterative threshold decoding called MTD that uses the magnitudes of received signals for making decoding decision. The combined soft decoding MTD with feedback (CMTDF) produces lower bound error performance of ML decoding. The CMTDF for the code with J=12 produces the coding gain 10.20 dB with rate R=0.8 at the BER 10^{-15}. It is effective for 100 Gb/s OTN system. When the code contains extra redundancy (not more than 1.5%) due to parity check bits, the 2SD with PC decoding makes the bit error rate 1/100 times compared to the bit error rate of 2SD for the code without extra redundancy. In this case, the code with J=12 be the best choice for the OTN, because it achieves 10.60 dB coding gain at the BER 10^{-15}. Although CMTDF already produces the lower bound of ML decoding error performance, we have possibility to acquire more coding gain in the waterfall region. The 2SD decoding can do this. The 2SD produces 0.25 dB more coding gain compared to CMTDF for the codes with rate 0.8. The 2SD with parity check decoding for the SOCC with J = 10 achieves 10 dB coding gain at the BER 10^{-12} and 10.20 dB at the BER 10^{-13}. The SOCC of J=10 concatenated with parity check code will be another candidate of FECs for the 100 Gb/s OTN system. Moreover, the proposed decoding scheme is less complex than the min-sum based decoding scheme. However, it is expected that, the 2SD for the code with larger orthogonal number produces more coding gain at the bit error rate less than 10^{-15}. Unfortunately, finding such codes with limited span of shift register is an open problem.

References

[1] ITU–T, Rec. G.975, “Forward error correction for submarine systems,” Nov. 1996.

[2] J. Justesen, K. J. Larsen and L. A. Pedersen, “Error correcting coding for OTN,” *IEEE Comm. Magazine*, vol. 48, no. 9, pp. 70–75, Sep. 2010.

[3] F. Chang, K. Onohara and T. Mizuochi, “Forward error correction for 100 G transport networks,” *IEEE Comm. Magazine*, vol. 48, no. 3, pp. s48–s55, Mar. 2010.

[4] S. J. Johnson, *Iterative Error Correction: Turbo, Low-Density Parity-Check and Repeat-Accumulate Codes*, Cambridge University Press, First Ed., 2010.

[5] J. Massey, *Threshold Decoding*, MIT Press, 1963.

[6] M. A. Ullah, K. Okada, and H. Ogiwara, “Multi-stage threshold decoding for self-orthogonal convolutional codes,” *IEICE Trans. Fundamentals*, vol. E93-A, no. 11, pp. 1932–1941, Nov. 2010.

[7] V. V. Zolotarev, G. V. Ovechkin, “An effective algorithm of noiseproof coding for digital communication systems,” *Electrosvaz*, no. 9, pp. 34–36, 2003.

[8] http://www.mtdbest.iki.rssi.ru/ (the last access date: Jan. 06, 2011).

[9] C. Cardinal, D. Haccoun, F. Gagnon, “Iterative threshold decoding without interleaving for convolutional self-doubly orthogonal codes,” *IEEE Trans. Commn.*, vol. 51, no. 8, pp. 1274–1282, Aug. 2003.

[10] M. A. Ullah and H. Ogiwara, “Performance improvement of multi-stage threshold decoding with difference register,” *IEICE Trans. Fundamentals*, unpublished.

[11] S. Lin, D.J. Costello, Jr., *Error Control Coding: Fundamentals and Applications*, Prentice-Hall, Inc. Englewood Cliffs, N. J., 1983.

[12] Y. Kou, S. Lin, and M. P. C. Fossorier, “Low-density parity-check codes based on finite geometries: a rediscovery and new results,” *IEEE Trans. Inform. Theory*, vol. 47, no. 7, pp. 2711–2736, Nov. 2001.

[13] J. P. Robinson, “Error propagation and definite decoding of convolutional codes,” *IEEE Trans. Inform. Theory*, vol. IT-14, no. 1, pp. 121–128, Jan. 1968.

 ISBN: 978-1-61208-123-6

An Invariant based Passive Testing approach for Protocol Data parts

Felipe Lalanne, Stephane Maag
Institut Telecom / TELECOM SudParis
CNRS UMR 5157
9, rue Charles Fourier
F-91011 Evry Cedex, France
{*Felipe.Lalanne, Stephane.Maag*}*@it-sudparis.eu*

***Abstract*—Conformance of implementations to protocol specifications is essential to assure interoperability between peers in network communications. Monitoring or passive testing techniques are used when no access to the communication interfaces is available or when the normal operation of the system cannot be interrupted. Most monitoring techniques only consider control portion of exchanged messages, usually ignoring the data part. However, as protocols become more complex and message exchange more data intensive, testing for data relations and constraints between exchanged messages becomes essential. In this paper we propose a novel approach for defining such relations as properties called invariants and show how they can be tested directly on traces using logic programming. Experimental results for SIP protocol traces are provided.**

***Keywords*-monitoring; invariant-based testing; data constraints; logic programming; network management**

I. INTRODUCTION

Communication standards for network protocols make it possible for different types of systems or different types of implementations to interoperate. Conformance to standards is essential to achieve communication on the Internet. *Formal methods* and *testing* techniques [1] allow to assess the conformance of implementations, usually by generating test cases from some type of specification based on the requirements of the protocol. These test cases are then provided as input to the Implementation Under Test (IUT) and the answers checked against those of the specification.

This approach, however, is not feasible when the IUT is in a production environment where its normal function cannot be disrupted. *Monitoring (or Passive testing)* techniques rely on observing the inputs/outputs provided by normal operation of the IUT, and then attempt to detect *faults*, either by comparing the observed events with the specification [2], [3], or by directly evaluating certain properties on the input/output trace [4], [5], [6]. For this last approach, called *invariant-based testing*, some properties (invariants) are defined, either by experts, directly from the protocol standard, or by extracting them from a formal specification. This techniques allows to test properties such as "*If x happens, then y MUST happen*" or "*For x to happen, then y MUST have happened before*" directly on the trace.

The current work deals with the application of such invariant-based techniques, particularly on the context of IP Multimedia Subsystem (IMS) applications. These kind of applications present interesting challenges for passive monitoring, given the distributed architecture of the IMS, and the utilization of a common protocol, the Session Initialization Protocol[7] (SIP) on most session management procedures, evaluating properties on a trace becomes non-trivial as shown by Figure 1. In [8] we defined some properties for testing on the Push-to-talk Over Cellular[9] (PoC) service traces, based on the protocol standard requirements, for instance

$$INVITE(CSeq = c0, From = u0, To = u1)/\theta, *,$$
$$\theta/OK(CSeq = c0, From = u0, To = u1)$$

indicates that a SIP *OK* response can only be received if an *INVITE* request was received first. As it can be seen in the Figure 1, the PoC trace also contains *OK* responses for *SUBSCRIBE* and *NOTIFY* requests, used by the Presence[10] service for communication. This produced *false positive* FAIL verdicts when tested on the trace, given that the property cannot distinguish between an *OK* response for an *INVITE* message from other *OK* for other type of request, or even from responses to a different *INVITE* message.

Granted, it can be argued that the defined property is rather simplistic in its definition, but shows the limitation of the expressive power of invariant properties defined this way to express data relations between messages, essential to perform more accurate testing. We believe that a more complete definition of message data and data relations for network protocol testing is necessary. This is the main motivation for the current paper.

In network protocols, communication is achieved through an exchange of messages between peers, where each peer can intermittently act as a receiver or as an emitter of the messages. As protocols evolve, messages become richer in data. Most passive testing approaches consider a small part of the message information called the *control part* (the *INVITE*, *OK* in the previous example), but very few consider the data constraints and relations for the message exchanges. A couple of examples of this are presented in [11] and [12]. In the first one, the authors use an interval refinement

 ISBN: 978-1-61208-123-6

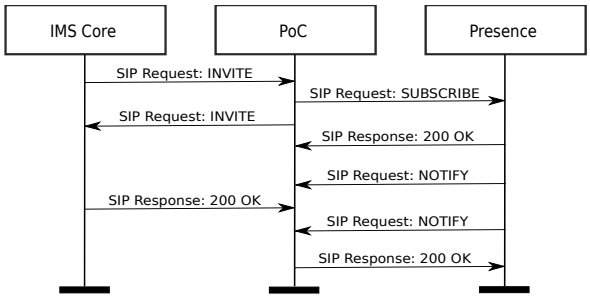

Figure 1. Interactions between applications of the IMS Subsystem. The PoC service, an IMS application, communicates with the Presence application and with the clients throught the IMS Core, all using functions of the SIP protocol.

approach to determine faults in a trace, either in data or state, by evaluation into a EEFSM (Event-driven Extended Final State Machine) formal specification. In the second one, the authors develop an algorithm to verify invariants on an EFSM specification and extract data constraints from them. However these works require a specification of the system under test, and in the industry, a complete specification is rarely available, particularly for large systems. In our work we test properties directly in the trace without the help of any formal specification.

We propose a methodology, based on first-order logic, that makes it possible to formally specify data-oriented invariants, and show how they can be tested in offline traces using a logic programming approach.

The main contributions of our work are:

- We refine the definitions of message and trace using first-order logic concepts, to better consider data domains and properties inside messages.
- With this new definition we describe how to specify data constraints and relations between messages, and define invariants as formulas in first-order logic.
- We prove the soundness of the definition to show that if an invariant verified in a formal specification does not hold in a trace, the corresponding implementation does not conform to the formal specification.
- We show how invariant formulas can be tested in real traces using logic programming and the equivalence with the first-order logic definitions.
- Finally, we present an example on the SIP protocol and show the results of testing in PoC service traces in comparison with our previous work.

II. PRELIMINARIES

In this section we describe some necessary concepts that are the basis for the introduction of data into invariants and to demonstrate the correctness of the definitions. The Event-driven Extended Finite State Machine formalism and first-order logic.

A. Event-driven Extended Finite State Machine

For the purpose of this paper, we use the Event-driven Extended Finite State Machine (EEFSM) formalism, suitable for monitoring techniques, introduced by the authors of [11] and [13].

Definition 1. An Event-driven Extended Finite State Machine (EEFSM) is a 6-tuple $M =< S, s_0, \Sigma, \vec{x}, \vec{y}, T >$ where $S = \{s_0, s_1, \ldots, s_{n-1}\}$ is a finite set of states with $s_0 \in S$ as the initial state, Σ is a finite set of events, where for each $e(\vec{y}) \in \Sigma$, e is the event name and $\vec{y} = \{y_1, \ldots, y_q\}$ is the finite set of event parameters, $\vec{x} = \{x_1, \ldots, x_p\}$ is a finite set of internal variables, and T is a finite set of transitions. For a transition $t =< s, s', e(\vec{y}), P(\vec{x}, \vec{y}), A(\vec{x}, \vec{y}) >$, $s, s' \in S$ are the starting and ending states of the transition, $e(\vec{y})$ is the triggering event, $P(\vec{x}, \vec{y})$ is a predicate and $A(\vec{x}, \vec{y})$ is an action, which is a sequence of assignments $\vec{x} := A(\vec{x}, \vec{y})$, where $\vec{x}$ and $\vec{y}$ are the current variable and event parameter values, respectively.

Example 1. The EEFSM transition $t : s \xrightarrow{?a(y_1),[y_1>x_1],x_2:=y_1+8} s'$, indicates that when the system is in state s, upon reception of event a with parameters y_1, if $[y_1 > x_1]$ then it will assign to variable x_2 the new value of $y_1 + 8$ and finally leave the system in state s'.

B. First-order Logic

Some basic concepts of first order logic are provided since they are necessary to include data for invariants. A more complete reference on first-order theory for computer science can be found in [14].

The first-order logic vocabulary is composed by two sets: a set of *predicate* symbols $\mathcal{P}$ and a set of *function* symbols $\mathcal{F}$. Each type comes with an arity, the number of parameters it expects. *Functions* of arity 0 are called *constants*. The pair $(\mathcal{F}, \mathcal{P})$ is called a logical signature.

The first-order vocabulary rules can be defined with the introduction of terms and formulas, where a term is defined in Backus-Naur form as $t ::= x|f(t, ..., t)$ where x is a variable, $f \in \mathcal{F}$ has arity n, and formula is defined as $\phi ::= P(t_1, t_2, ..., t_n)|\neg\phi|\phi \wedge \phi|\phi \vee \phi|\phi \Rightarrow \phi|\forall x\phi|\exists x\phi$ where $P \in \mathcal{P}$ is a predicate of arity n, t_i are terms and x is a variable.

In order to semantically evaluate first-order logic formulas, a *meaning* must be given to the predicate and function symbols, that is, they must be associated with real predicates and functions of a specific context or *universe*. A model $\mathfrak{M}$ is defined as a triplet $< U, (f_{\mathfrak{M}})_{f\in\mathcal{F}}, (P_{\mathfrak{M}})_{P\in\mathcal{P}} >$, where

- U is a non-empty set called universe.
- For each $f \in \mathcal{F}$ with arity n, a concrete function $f_{\mathfrak{M}}$ is defined as $f_{\mathfrak{M}} : U^n \longrightarrow U$
- For every $P \in \mathcal{P}$ with arity n, $P_{\mathfrak{M}} \subseteq U^n$

Finally, in order to evaluate formulas, variables have to be mapped to particular values in the universe. Given a set $\mathcal{X}$

 ISBN: 978-1-61208-123-6

of variables a function $l : \mathcal{X} \to U$ is called an *interpretation*. With this concept, given a model $\mathfrak{M}$ for a signature $(\mathcal{F}, \mathcal{P})$ and a formula ϕ, a *satisfaction relation* is defined as $\mathfrak{M} \models_l \phi$ meaning that the formula ϕ is *true* with respect to $\mathfrak{M}$ under interpretation l.

III. Data in Network Protocols

In a network protocol, a communication peer decides the course of action on the basis of two things: Locally stored state information (including internal data), and data contained in received messages from different peers. In passive testing, while the observed message data is available to the tester, state information and internal data are unknown. In order to test data, focus on the exchange of messages is fundamental, however, a formal definition must be provided first.

A protocol message is, in general, a collection of data fields of different domain, where each data field has a function in the data exchange. The *format* of the message, the function and domain of each field are defined in the requirements specification of the protocol.

The most basic domains of data we can find in protocols, are numeric and alphanumeric (string) values. Basic data domains can be combined in order to define more complex domains. For instance, an email data element can be defined as `mailbox ::= local-part "@" domain`, in order to distinguish the recipient from the sending address.

Traditional passive testing definitions, distinguish between a *control portion* and a *data portion* of messages, this is actually an abstraction necessary for compatibility with model-based testing. In practice, a trace is only a sequence of messages containing data. These messages are classified afterwards, according to their function in the protocol, determined by the data. This function is what constitutes the control portion. Although this is not really necessary for our approach, we will include the distinction between control and data in the definition of a message, in particular to make it compatible with the EEFSM formalism.

Definition 2. A message is a structure $m = e(\vec{x})$ where e is the message label belonging to some finite set L, and $\vec{x} = (x_1, \ldots, x_n)$ is a finite set of message parameters or *message variables*, where each $x_i \in D_j \cup \{\epsilon\}$, with D_j as its data domain (D_j's are not necessarily disjoint). The *null* value is represented by ϵ, where $\epsilon \notin D_j, \forall j \in 1 \ldots n$.

In the definition, e constitutes the control portion of the message and $\vec{x}$ is the data portion. The *null* value ϵ is used to allow messages with dynamic number of variables within the fixed-size set $\vec{x}$.

It is easy to see that this definition of a message is compatible with the one of *event* in an EEFSM and every possible message is an event, however it should be clear that not every possible EEFSM event is a message. From here on, we will denote as $\mathcal{M}$ the domain of all possible messages for a given EEFSM.

In order to reference a particular variable for a message m we will use the symbol '.' to reference it, for instance $m.email$ to reference the variable of name $email$ in message m. This should be considered only as a convention in order to ease the writing of formulas and not a formal definition.

IV. Incorporating data into invariants

In this section we describe how we incorporate data into invariants, by using the previously described logic concepts. We start by defining a new way to represent traces more suitable with a first-order model.

A. Trace representation

Using the traditional model-based approach, a trace can be defined in terms of an EEFSM: Given $M =< S, s_0, \Sigma, \vec{x}, \vec{y}, T >$, we say that the sequence $\mathfrak{T} =< e_1(\vec{y}_1), e_2(\vec{y}_2), \ldots, e_n(\vec{y}_n) >$ is a *trace* for M, if there exist states $s, s_1, \ldots, s_{n-1}, s' \in S$ such that we have the following transitions $s \xrightarrow{e_1(\vec{y}_1);P_1(\vec{x}_0,\vec{y}_1);A_1(\vec{x}_0,\vec{y}_1)} s_1$, $\ldots, s_{n-1} \xrightarrow{e_n(\vec{y}_n);P_1(\vec{x}_{n-1},\vec{y}_n);A_n(\vec{x}_{n-1},\vec{y}_n)} s'$, where $\vec{x}_0$ is t he internal variable state before the first transition, and $P_1, \ldots, P_n$ and $A_1, \ldots, A_n$ are respectively the predicates and actions for the transitions. In order to make the concept of trace more compatible with our current approach, we propose an alternative representation

Definition 3. Let $M =< S, s_0, \Sigma, \vec{x}, \vec{y}, T >$ be an EEFSM and $\mathcal{M}$ the domain of all possible messages for M, the structure $\mathfrak{T} =< R, m_0, Next >$ is defined, where

- $R \subseteq \mathcal{M}$ is a finite, non-empty set of messages.
- $m_0 \in R$ is the first message of the trace.
- $Next \subseteq R \times R$ is a relation that maps a message to its next on the trace. i.e $Next(x, y)$ indicates that x comes immediately after y on the trace. This relation must satisfy the property $Next(x, y) \wedge Next(x, z) \Leftrightarrow y = z$, to restrict to a single successor for each element.

$\mathfrak{T}$ is said to be a *trace* for M if there exist states $s, s_1, \ldots, s_{n-1}, s' \in S$ such that the following transitions exist: $s \xrightarrow{m_1=e_1(\vec{y}_1);P_1(\vec{x}_0,\vec{y}_1);A_1(\vec{x}_0,\vec{y}_1)} s_1, \ldots,$ $s_{n-1} \xrightarrow{m_n=e_n(\vec{y}_n);P_1(\vec{x}_{n-1},\vec{y}_n);A_n(\vec{x}_{n-1},\vec{y}_n)} s'$, where $m_i = e_i(\vec{y}_i) \in R$ and $Next(m_i, m_{i+1})$ holds for every $i = 1 \ldots n-1$.

For convenience we also define the following relations for the trace.

- $Prev(x, y)$ indicates that message x comes immediately before y in the trace.
- $After(x, y)$ the relation indicating that message x comes after message y in the trace.
- $Before(x, y)$ the relation indicating that message x comes before message y in the trace.

For the remainder of the paper, it should be assumed that the variables domain is the trace. That is, the expression $\exists u_1, \ldots, u_n$ is equivalent to $\exists u_1, \ldots, u_n \in \mathfrak{T}$.

 ISBN: 978-1-61208-123-6

Finally, we define $Traces(M)$ as the set of all possible traces for the EEFSM M.

B. A model for protocol traces

As our interest is to interpret invariant properties semantically, it is necessary to first define a model. We define the universe of the model as the trace, where properties are expected to hold.

Given $(\mathcal{F}, \mathcal{P})$ a logical signature, and a trace $\mathfrak{T} = (R, m_0, Next)$, we specify the sets

- $\mathcal{F}' = \mathcal{F}$
- $\mathcal{P}' = \mathcal{P} \cup \{Next, Prev, Before, After\}$.

With $(\mathcal{F}', \mathcal{P}')$ as a new signature, a model for the trace $\mathfrak{M}(\mathfrak{T})$ is constructed as follows

- The universe $U = \mathfrak{T}$.
- Each $P \in \mathcal{P}'$ is specified as a formula on the message variables for the involved messages. For instance let's suppose that each message in the trace contains a variable $index$ indicating the order where each message was collected into the trace. Then the predicate $Next$ can be stated as

$$Next(x, y) \leftarrow x.index = y.index + 1$$

- For each $f \in \mathcal{F}'$ of arity n a concrete function is defined as $f_{\mathfrak{M}(\mathfrak{T})} : \mathfrak{T}^n \rightarrow \mathfrak{T}$. We do not impose any restrictions on the kind of functions that can be defined, other than they must be within the domain of the trace, however, for the examples in this paper we will not make use of them.

C. Invariant definition

As the name implies, an invariant is a property that must be true for every trace from an implementation, formally we define

Definition 4. Let $M =< S, s_0, \Sigma, \vec{x}, \vec{y}, T >$ be an EEFSM, $\mathfrak{M}(\mathfrak{T}) =< \mathfrak{T}, (f_{\mathfrak{M}(\mathfrak{T})})_{f \in \mathcal{F}}, (P_{\mathfrak{M}(\mathfrak{T})})_{P \in \mathcal{P}} >$ be a model for a trace $\mathfrak{T}$ and $\mathcal{X}$ a set of variables, an *invariant* is any formula ϕ such that there exists *at least one* interpretation $l : \mathcal{X} \rightarrow \mathfrak{T}$ where $\mathfrak{M}(\mathfrak{T}) \models_l \phi$ for *every* trace $\mathfrak{T} \in Traces(M)$.

The fact that an invariant must hold *every* trace from the model, immediately imposes a restriction on the type of formulas that are possible, since a trace may not involve a particular property being evaluated. In particular, the definition restricts invariants to formulas of the type $\phi \Rightarrow \psi$. Due to the rules of logical implication, if the first part of the formula is *false*, the value of the formula is immediately *true*. For our approach, we will further restrict to formulas of the type: $\forall x_1, \ldots, x_p \phi \Rightarrow \exists y_1, \ldots, y_q \psi$, making it possible to describe properties such as "*Whenever x happens then y must (have) happen(ed)*".

V. Correctness of checking invariants in a trace

In this section we will first show the correctness of our approach, by using a *trace preorder* implementation relation, and then we show how to test invariants on the trace. We begin by introducing the *trace preorder* implementation relation definition as

Definition 5. Let S and I be two EEFSMs. We say that I *trace conforms* to S, denoted $I \leq_{tr} S$ if and only if $Traces(I) \subseteq Traces(S) \wedge Traces(I) \neq \emptyset$.

This definition of conformance, requires that *every* possible trace generated by the implementation, must be possible in the specification. To prove the soundness of our definitions, we also need to define correctness of an EEFSM trace with respect to an invariant as

Definition 6. Let $\mathcal{I} \stackrel{\text{def}}{=} \forall x_1, \ldots, x_p \phi \Rightarrow \exists y_1, \ldots, y_q \psi$ be an invariant and $\mathfrak{T}$ a trace from an EEFSM. We say that $\mathfrak{T}$ is *correct* with respect to $\mathcal{I}$ if there exists an interpretation $l : var(\mathcal{I}) \rightarrow \mathfrak{T}$, such that $\mathcal{I}$ holds.

Theorem 1. Let S and I be two EEFSM and $\mathcal{I}$ be an invariant verified on S. Let $\mathfrak{T}$ be a trace recorded from I. If the trace $\mathfrak{T}$ is not *correct* by Definition 6, with respect to $\mathcal{I}$, then I does not conform to S.

The proof is direct with the provided definitions.

Proof: Let $\mathcal{I}$ be a correct invariant and $\mathfrak{T} \in Traces(I)$ a trace that is not correct with respect to $\mathcal{I}$. By Definition 4, $\mathcal{I}$ holds for every trace in S, which means that $\mathfrak{T} \notin Traces(S)$, then $Traces(I) \nsubseteq Traces(S)$, therefore, by Definition 5, I does not conform to S. ■

We conclude this section by describing how we can check the correctness of invariants directly on a real trace by using logic programming. A description of logic programming is not provided, we recommend [15] as a good reference.

In logic programming, a *program* is composed by a set of *clauses* of the type $A_0 \leftarrow A_1 \wedge \ldots \wedge A_n$ where each A_i is an atomic formula (a predicate) that states a fact. Programs allow to test *goals*, or statements for which we want to obtain a truth value. The goal G is valid in the program P if $P \models G$.

In our approach, we can make the parallel between clauses and predicate definitions, and between goals and invariants. In order to test the invariants on a real trace, the trace messages have to be stated using logic programming. To solve this we define for the program the predicate $TraceMsg(index, msg)$ to state that the set of values in msg is a trace message in the position $index$. With this definition, a real trace consists of the set of statements

$$\begin{array}{c} TraceMsg(1, msg_1) \\ \vdots \\ TraceMsg(n, msg_n) \end{array}$$

where $msg_1, \ldots, msg_n$ are real message values. This way, on giving the program the goal $TraceMsg(1, x)$, it will respond

$x = msg_1$. The predicate $Next$, for instance, can be defined with the use of $TraceMsg$ as

$$\begin{array}{lll} Next(x,y) & \leftarrow & TraceMsg(i_1,x) \wedge TraceMsg(i_2,y) \\ & \wedge & i_1 = i_2 + 1 \end{array}$$

These definitions give to the program the same information as the model for the trace defined in Section IV-B, then, a trace is correct with respect to an invariant, if such invariant holds in the corresponding program.

Finally, in order to test the invariants, it is necessary to remove the quantifiers, since most logic programming languages do not support them. As in testing it is more interesting to check the traces that fail the invariant, the quantifiers can be easily removed. Let $\mathcal{I}$ be an invariant

$$\mathcal{I} = \forall x_1, \ldots, x_p \phi \Rightarrow \exists y_1, \ldots, y_q \psi$$

by the definition of logical implication this is equivalent to

$$\mathcal{I} = \exists x_1, \ldots, x_p \neg\phi \vee \exists y_1, \ldots, y_q \psi$$

Since we want to know whether a trace fails an invariant, we need to test the negation of the invariant $\mathcal{I}^{neg} = \neg\mathcal{I}$ which leaves the formula in

$$\mathcal{I}^{neg} \leftarrow \phi \wedge \neg\psi$$

easily tested using logic programming.

VI. Invariant definition for the SIP protocol

The Session Initiation Protocol (SIP) [7] is an application-layer (control) signaling protocol for creating, modifying, and terminating sessions with one or more participants. These sessions include Internet telephone calls, multimedia distribution, and multimedia conferences.

The SIP protocol is a fundamental part in the IMS framework, where the main elements in the core IMS network behave as different SIP entities (user agent server, user agent client, proxy) and communicate between them using this protocol.

In this section we apply the concepts previously explained to the SIP protocol. First, we define the message structure, then we define some predicates and their meaning in terms of variables and finally, we use them to specify some invariants.

A. SIP Messages

A SIP Message is either a request from a client to a server, or a response from a server to a client. The basic message format is the one established by RFC 3621, as follows

```
generic-message = start-line
                  *message-header
                  CRLF
                  [ message-body ]
start-line      = Request-Line | Status-Line
```

When the message is a request, it contains a Request-Line providing the **Method Request-URI** and **SIP-Version**. SIP requests contain a Status-Line as a start-line, containing the information **SIP-Version, Status-Code** and **Reason-Phrase**.

With the available information, for our approach we define the following message variables.

- $method \in RequestMethod$, where $RequestMethod$ = {'REGISTER', 'INVITE', 'ACK', 'CANCEL', 'BYE', 'OPTIONS'}. For this document we only consider the *Method* field, although a message variable could be easily defined to contain information for the request URI.
- $statusCode \in Code$, where $Code \subset \mathbb{N}$ is the set of possible status codes for the protocol.

We define a message m in SIP as at least the sequence $m = (method, statusCode)$. As it can be noticed, we are not including the control part in the message definition. Although it depends on the specification, the control part here would be a combination of the method and status code, since they define the function of the message, here we will just specify them as data variables. Along with the message definition, the following predicates will also be useful to identify a message as request or response

$$\begin{array}{l} Request(m) \leftarrow m.method \neq \epsilon \wedge m.statusCode = \epsilon \\ Response(m) \leftarrow m.method = \epsilon \wedge m.statusCode \neq \epsilon \end{array}$$

1) SIP Requests: According to the standard *"A valid SIP request formulated by a UAC MUST, at a minimum, contain the following header fields: To, From, CSeq, Call-ID, Max-Forwards, and Via; all of these header fields are mandatory in all SIP requests"*. In addition to the request line, these header fields allow the main functionality for the main SIP routing services. Adding them to the message definition, $m = (method, statusCode, to, from, cSeqNum, cSeqMethod, callId, maxForwards, via)$.

We do not detail on the on the function of this headers, but the reader is invited to refer to section 8.1.1 of [7] for further information.

2) SIP Responses: The basic procedures on how to construct a response to a request are specified in section 8.2.6.2 of the RFC. They can be translated into the following predicate

$$\begin{array}{lll} RespondsTo(x,y) & \leftarrow & Response(x) \wedge Request(y) \\ & \wedge & x.from = y.from \\ & \wedge & x.callId = y.callId \\ & \wedge & x.cSeq.seq = y.cSeq.seq \\ & \wedge & x.cSeq.method = y.cSeq.method \\ & \wedge & x.via = y.via \\ & \wedge & x.to = y.to \end{array}$$

Meaning that if the message x is a response to the message y, then the indicated variable values must be the same in both. Using this property and, given a trace $\mathfrak{T}$ for an implementation, we can define the invariant $\mathcal{I}_1 \leftarrow \forall x \in \mathfrak{T}, Request(x) \wedge x.method \neq$ 'ACK' $\Rightarrow \exists y \in \mathfrak{T}, RespondsTo(y,x) \wedge After(y,x)$, meaning that if there is a request message in the trace, there must exist a response message to it. In the same way, the invariant $\mathcal{I}_2 \leftarrow \forall x \in \mathfrak{T}, Response(x) \Rightarrow \exists y \in \mathfrak{T}, RespondsTo(x,y) \wedge Before(y,x)$, indicates that if there exists a response message in the trace,

 ISBN: 978-1-61208-123-6

then there must be a request for it at some point before it in the trace. This invariant is a more general version of the one presented in the introduction, stating the relation between `INVITE` and `OK`. This one states a relation between every request and response, allowing to test more cases than the original one.

B. SIP Registration

In SIP, registration allows a user to be located by other peers. By sending a message to a server called the registrar, the user agent client (UAC) informs the server of the location (IP address, network) where a SIP user (specified by an URI) can be located.

In terms of the protocol, in order to authenticate, the user agent client sends a `REGISTER` request to the server and the server responds with a `200 OK` response when the registration is accepted. A series of messages are sent in between, in order to perform authentication (if required by the server), determine capabilities of the server, and others. However for the purpose of this document we only consider whether a registration was successful. To achieve this, we define the following predicate

$$\begin{array}{lcl} Registration(x,y) & \leftarrow & ResponseTo(y,x) \\ & \wedge & x.method = \text{`REGISTER'} \\ & \wedge & y.statusCode = 200 \end{array}$$

C. SIP Session Establishment

In order to establish a session between two users, one of the UACs sends an `INVITE` request to the server which contacts the second UAC. An exchange of messages takes place in order to setup a session (using session description protocol), different provisional responses are sent to the first UAC to indicate the status of the process (`100 Trying`, `180 Ringing`, etc). The session is established after the negotiation where a `200 OK` message is sent to the originating UAC, and an `ACK` request is sent back to the server to acknowledge the reception.

The `ACK` message, in accordance to section 17.1.1.3 in the RFC, is constructed with the Call-ID, From and Request-URI values from the original request, and the To header from the response being acknowledged. The CSeq header in the `ACK` must contain the same sequence number as the original request, but the method parameter must be equal to "`ACK`".

Then in order to determine that the session establishment was successful we need to consider three messages as described by the following predicate.

$$\begin{array}{lcl} SessionEstabl(x,y,z) & \leftarrow & RespondsTo(y,x) \\ & \wedge & Request(z) \\ & \wedge & x.method = \text{`INVITE'} \\ & \wedge & y.statusCode = 200 \\ & \wedge & z.method = \text{`ACK'} \\ & \wedge & z.to = y.to \\ & \wedge & z.callId = x.callId \\ & \wedge & z.from = x.from \\ & \wedge & z.cSeq.seq = x.cSeq.seq \\ & \wedge & z.cSeq.method = \text{`ACK'} \end{array}$$

Again we have done some simplifications according to the previous definitions with respect to the RFC. This predicate specifies when three messages conform to a session establishment.

D. Invariant examples for the PoC service

The SIP protocol is designed for extensibility and usability in different contexts, because of that, there are not many restrictions on when a session should be established, only on the message exchange in order to establish it. However, a service using SIP can define requirements for its infrastructure. For instance, the PoC service requires that a session can be established only by registered clients. Then invariant $\mathcal{I}_3$ can verify that requirement on the trace

$$\begin{array}{r} \mathcal{I}_3 \leftarrow \forall x,y,z \in \mathfrak{T}, SessionEstabl(x,y,z) \Rightarrow \\ \exists u,v \in \mathfrak{T}, Registration(u,v) \\ \wedge\ x.from = u.from \wedge Before(v,x) \end{array}$$

indicating that whenever a session establishment is found on the trace, then a registration must previously appear on the trace from the same user. This invariant in particular is interesting for its complexity, given that it requires testing several messages in order to be checked. Such kind of property is not easy to define using similar invariant testing methodologies.

VII. Experiments and Results

In this section we briefly describe the methodology used to test the invariants defined in Section VI on real protocol traces.

We defined the predicates and invariants using the Prolog programming language. We chose this language due to its definition as an ISO standard (ISO/IEC 13211-1), portability and maturity of its implementations. In particular we used the ISO compliant SWI-Prolog implementation, because of its large library of functions. A SIP message was defined as a structure `msg(Request, StatusCode, ...)` and predicates were defined in terms of variables as described in Section VI. Invariants were specified in the negative form $\phi \wedge \neg\psi$, for instance, for invariant $\mathcal{I}_1$ the following predicate was defined

```
negInv1(X) :-
    trace_msg(_, X), request(X),
    not(msg_method('ACK',X)), trace_msg(_, Y),
    not((
        after(Y,X), responds(Y,X)
    )).
```

where `msg_method(Method, Msg)` is true if the value of the variable `Method` equals the method of the message in `Msg`. In the program, the execution of the goal `negInv1(X)` will return all request messages for which a response message is not available in the trace.

Trace files were provided by Alcatel-Lucent for a PoC service implementation, a single trace was chosen for testing, containing the establishment of an Ad-Hoc group session by 2 clients. In order to test the traces using logical programming, we implemented a prototype tool in C to convert from the XML (PDML) format exported with the tool *Wireshark*

 ISBN: 978-1-61208-123-6

into a set of statements of the form `trace_msg(index, msg)` as described in Section V.

In our tool, a configuration file defines how to relate a message variable in Prolog with a field of a respective packet, as follows

```
message: {
    Method = "sip.Method";
    StatusCode = "sip.Status-Code";
    To = "sip.to.addr";
    From = "sip.from.addr";
    ...
}
```

Using this configuration, along with the trace, the tool outputs a Prolog file containing the list of `trace_msg` statements, where each message is assigned an index according to its order in the trace, as follows

```
trace_msg(1, msg('INVITE', nil,
    'sip:user1@b.c', 'sip:user2@b.c', ... )).
trace_msg(2, msg(nil, 180,
    'sip:user1@b.c', 'sip:user2@b.c', ... )).
trace_msg(3, msg(nil, 200,
    'sip:user1@b.c', 'sip:user2@b.c', ... )).
```

If a particular field is not found in a trace message, it is replaced by the empty value *nil* (as the *Method* field in SIP response messages). However, if none of the defined fields are found, the message is ignored. This allows the tool to also act as a filter for messages of the studied protocol.

We performed experiments by manually introducing some errors on the implementation traces to evaluate the detection capabilities of our approach. The results were successful, the errors introduced were correctly detected by execution of the program, and no *false positive* results were produced, given that the definitions were specifically targeted to the PoC service, the process allowed to correctly filter out the Presence service messages. Even for a complex invariant such as invariant 3 the approach did not present any issues.

In addition to the detection of the introduced errors, the program also found some legitimate errors in the trace, that were not found by previous testing. These occurred for invariant 2, where some responses to an `INVITE` were found in the trace where the request could not be found. Upon further examination of the trace, we found that the error was due to a problem in the collection of the trace, since there were several responses from the server, indicating that the request must have been correctly received. This raises an issue about the reliability of trace collection tools and techniques, however this was an isolated case and since we only have access to the trace it is not possible to make a full assessment without further experimentation.

One issue that should be addressed is the performance of the approach. Since Prolog is a general purpose programming language and not a dedicated program, the number of evaluations performed in order to evaluate an invariant on the trace is large. For invariant 1, in a trace with only 407 messages, the program performed 5559 inferences (procedure calls) to arrive to a conclusion, however, the problem is better illustrated for invariant 3, the most complex one, where the number of inferences performed was of 583440 (although in only 0.09 seconds) to obtain a verdict. A dedicated algorithm could perform less inferences by limiting the range of comparison in the trace, instead of testing for every possible combination as Prolog does. This issue is even more critical as the number of messages involved in the property increases. Although some optimizations are possible, the creation of a dedicated program is indispensable.

VIII. Related Work

A short overview of works related to ours are given in this section, to complement the references cited throughout the paper.

Formal testing methods have been used for years to prove correctness of implementations by combining test cases evaluation with proofs of critical properties. In [16], [1] the authors present a description of the state of the art and theory behind these techniques. Within this domain, and in particular for network protocols, passive testing techniques have to be used to test already deployed platforms or when direct access to the interfaces is not available. Some examples of these techniques using FSM derivations are described in [2], [17]. Most of these techniques consider only control portions, in [11], [13], [3], data portion testing is approached by evaluation of traces in EEFSM and SEFSM (Simplified Extended Finite State Machine) models, testing correctness in the specification states and internal variable values. Our approach, although inspired by it, is different in the sense that we test critical properties directly on the trace, and using a model only for their verification. A different methodology can be found in [18], where I/O Automata and first-order logic are used to prove the correctness of the implementation w.r.t. the specification for distributed algorithms. Data relations are also taken into account. Again, this work relies on a specification to perform testing, which is not always available. There exists a considerable number of works with similar approach in literature. In [19], [4] the invariant approach was presented, and studied also in [5], [12]. A study of the application of invariants to an IMS service was also presented by us in [20], [8]. Although these invariant approaches consider in some level the data part, it is not their main objective. Some improvements have been made to invariant techniques by the authors of [6] to include temporal restrictions. Although their approach is very useful with temporal specifications, it is not extensible for testing of data. Our method improves on invariant testing by allowing to define properties with complex data relations by using a restriction on first-order logic formulas.

IX. Conclusion and Future Work

In this article we describe a new approach to invariant-based passive testing. We improve the expressiveness of invariant properties by using first-order logic, thus allowing to

 ISBN: 978-1-61208-123-6

test data constraints between messages directly into protocol traces. We also demonstrate the soundness of our approach, showing that if a trace from an implementation is not correct with respect to an invariant verified in a specification, then the implementation does not conform to such specification. We detail on how invariants defined using our definition can be tested using logic programming. We provide an example of definition of invariants for the SIP protocol directly from the protocol standard and detail on the results obtained by testing using a Prolog implementation on a real trace obtained from a PoC service implementation.

Our experiments showed that our approach makes it possible to test complex properties directly into the trace. The expressive power of invariants defined in the way described is very large, given the few limitations imposed to the definition of formulas.

However our testing approach still requires improvement. In particular, testing using logic programming showed to be very expensive in terms of the number of procedure calls required to arrive to a conclusion. One of the reasons for this is that the evaluation of the formulas does not take into account the linearity of the trace, and always tests every message in the trace, even though it is only necessary to evaluate in a single direction in the trace, forward or backward, depending on the property.

As future work, we plan to develop an algorithm to allow more efficient testing of properties by taking into account the linearity of the trace and also by optimizing the invariant formulas. This could also allow for real time passive monitoring and testing of invariants in protocol implementations.

REFERENCES

[1] R. M. Hierons, P. Krause, G. Lüttgen, A. J. H. Simons, S. Vilkomir, M. R. Woodward, H. Zedan, K. Bogdanov, J. P. Bowen, R. Cleaveland, J. Derrick, J. Dick, M. Gheorghe, M. Harman, and K. Kapoor, "Using formal specifications to support testing," *ACM Computing Surveys*, vol. 41, no. 2, pp. 1–76, 2009.

[2] D. Lee, A. Netravali, K. Sabnani, B. Sugla, and A. John, "Passive testing and applications to network management," in *Proceedings 1997 International Conference on Network Protocols*. IEEE Comput. Soc, 1997, pp. 113–122.

[3] H. Ural and Z. Xu, "An EFSM-Based Passive Fault Detection Approach," *Lecture Notes in Computer Science*, pp. 335–350, 2007.

[4] A. Cavalli, S. Prokopenko, and C. Gervy, "New approaches for passive testing using an Extended Finite State Machine specification," *Information and Software Technology*, vol. 45, no. 12, pp. 837–852, September 2003.

[5] E. Bayse, A. Cavalli, M. Núñez, and F. Zaïdi, "A passive testing approach based on invariants: application to the wap," *Computer Networks*, vol. 48, no. 2, pp. 247–266, 2005.

[6] C. Andrés, M. G. Merayo, and M. Núñez, "Formal Correctness of a Passive Testing Approach for Timed Systems," *2009 International Conference on Software Testing, Verification, and Validation Workshops*, pp. 67–76, 2009.

[7] J. Rosenberg, H. Schulzrinne, G. Camarillo, A. Johnston, J. Peterson, R. Sparks, M. Handley, and E. Schooler, "SIP: Session Initiation Protocol. RFC 3261," 2002.

[8] F. Lalanne, S. Maag, E. M. D. Oca, A. Cavalli, W. Mallouli, and A. Gonguet, "An Automated Passive Testing Approach for the IMS PoC Service," in *2009 IEEE/ACM International Conference on Automated Software Engineering*, 2009.

[9] Open Mobile Alliance, "Push to Talk over Cellular Requirements. Approved Version 1.0," Jun. 2006.

[10] Open Mobile Alliance, "Internet Messaging and Presence Service Features and Functions. Approved Version 1.2," Jan. 2005.

[11] D. Lee and R. E. Miller, "A formal approach for passive testing of protocol data portions," in *10th IEEE International Conference on Network Protocols, 2002. Proceedings.* IEEE Comput. Soc, 2002, pp. 122–131.

[12] B. Ladani, B. Alcalde, and A. Cavalli, "Passive testing: a constrained invariant checking approach," in *Proc. 17th IFIP Int. Conf. on Testing of Communicating Systems*. Springer, 2005, pp. 9–22.

[13] D. Lee, D. Chen, R. Hao, R. E. Miller, J. Wu, and X. Yin, "Network protocol system monitoring-a formal approach with passive testing," *IEEE/ACM Transactions on Networking*, vol. 14, no. 2, pp. 424–437, April 2006.

[14] M. Huth and M. Ryan, *Logic in Computer Science: Modelling and reasoning about systems*. Cambridge Univ Pr, 2004.

[15] U. Nilsson and J. Maluszynski, *Logic, programming and Prolog*, 2nd ed. Wiley, 1990. [Online]. Available: http://www.ida.liu.se/~ulfni/lpp

[16] D. Lee and M. Yannakakis, "Principles and methods of testing finite state machines: A survey," *Proceedings of the IEEE*, vol. 84, pp. 1090–1123, 1996.

[17] M. Tabourier and A. Cavalli, "Passive testing and application to the GSM-MAP protocol," *Information and Software Technology*, vol. 41, no. 11-12, pp. 813–821, September 1999.

[18] J. Sogaard-Andersen, S. Garland, J. Guttag, N. Lynch, and A. Pogosyants, "Computer-assisted simulation proofs," in *Computer Aided Verification*, vol. 124, no. 1-3. Springer, March 1984, pp. 305–319.

[19] J. Arnedo, A. Cavalli, and M. Nunez, "Fast testing of critical properties through passive testing," *Testing of Communicating Systems*, pp. 608–608, 2003.

[20] F. Lalanne and S. Maag, "From the IMS PoC service monitoring to its formal conformance testing," in *Proceedings of the 6th International Conference on Mobile Technology, Application & Systems - Mobility '09*. Nice, France: ACM Press, 2009, pp. 1–8.

 ISBN: 978-1-61208-123-6

A Reconfigurable Prototyping Platform for Modern Communication Systems

Alexander Viessmann, Christian Kocks,
Christoph Spiegel, Guido H. Bruck, Peter Jung
University of Duisburg-Essen
Department of Communication Technologies
Duisburg, Germany
E-mail: info@kommunikationstechnik.org

Jaeyoel Kim, YeonJu Lim, Hyeon Woo Lee
Samsung Electronics
Global Standards and Research Lab
Suwon, Korea

***Abstract*—The increasing number of upcoming communication systems make a reconfigurable platform concept inevitable. A strict modular, software-defined radio based concept allows to interchange several components in hardware as well as in software without affecting the residual parts of the platform in order to adapt the underlying system to various modern communication systems. In this paper, the authors describe a reconfigurable prototyping platform developed and successfully tested at the Department of Communication Technologies at University of Duisburg-Essen strictly following this software-defined radio paradigm. Using the example of the upcoming terrestrial broadcasting standard, namely DVB-T2, the necessity of a hybrid platform concept is discussed, comprising of a digital signal processor on the one hand and field-programmable gate arrays on the other hand.**

***Keywords*-DSP (Digital Signal Processor), Digital Video Broadcasting, DVB-T2, FPGA (Field Programmable Gate Array), LDPC (Low-Density Parity-Check) Codes, Prototyping Platform, Software-Defined Radio**

I. INTRODUCTION

The introduction of new communication systems, such as DVB (Digital Video Broadcasting), is mostly led by the demand for higher data rates. In order to be able to meet the various requirements, a sophisticated platform concept has to be developed. Within this paper, the authors present a reconfigurable prototyping platform based on the software-defined radio (SDR) concept [1]. Reconfigurability in radio development is not a very new technique [2]. Already during the 1980s, reconfigurable receivers were developed for radio intelligence in the short wave range. However, reconfigurability became familiar to many radio developers with the publication of the special issues on software radios of the IEEE Communication Magazine [3], [4]. The author in [2] refer to a transceiver as a software radio (SR) if its communication functions are realized as programs running on a suitable processor. Based on the same hardware, different transmitter/receiver algorithms, which usually describe transmission standards, are implemented in software in a cost effective manner [5]. An SR transceiver comprises all the layers of a communication system, in particular the physical layer, usually abbreviated by PHY layer, and the medium access control layer, denoted by MAC layer. Initially, the idea of software-defined radio was of academic interest only. However, due to the technological progress, modern hardware components are capable of making use of this concept. With the goal of implementing one of the world's first DVB-T2 (Digital Video Broadcasting - Terrestrial) receivers, a prototyping platform was developed at the Department of Communication Technologies at the University of Duisburg-Essen, strictly following the software-defined radio approach. DVB-T2 is the successor of DVB-T which has established itself as the leading specification for terrestrial television broadcasting after being introduced in the 1990s. The increasing demand for HDTV (High-Definition Television) paved the way towards a renovation of DVB-T, which does not allow the transmission of high-definition video streams. The goal of DVB-T2 was a higher spectral efficiency by using more sophisticated forward error correction techniques on the one hand and higher order modulation on the other hand. In the meantime, the standardization of DVB-T2, which began in 2006, has been completed [6].

In the following, the key parameters specified in the DVB-T2 standard [6] are mentioned. DVB-T and DVB-T2 are both based on Orthogonal Frequency Division Multiplexing (OFDM). While DVB-T uses a gross number of 8192 points, the OFDM size in DVB-T2 is 32768 points. The modulation order for each subcarrier goes up to 256 QAM (Quadrature Amplitude Modulation) in DVB-T2. Furthermore, the underlying forward error correction scheme is considerably modified. While DVB-T employs a combination of Reed-Solomon codes and convolutional codes, DVB-T2 makes use of a concatenation of BCH (Bose Chaudhuri Hocquenghem) codes and LDPC (Low-Density Parity-Check) codes with a block length of 64800 bits. LDPC codes are used in several modern and upcoming communication systems such as IEEE 802.16e (WiMAX) because of their near Shannon limit performance on the one hand and their ability for parallelized implementation on the other hand. Nevertheless, the real-time implementation of the LDPC decoder is one of the most challenging aspects when implementing DVB-T2 receivers. The modulation scheme, the channel coding parameters and the number of OFDM subcarriers have to be flexibly adaptable in the receiver [7]. Table I gives a brief comparison between

 ISBN: 978-1-61208-123-6

	DVB-T	DVB-T2
FEC	Convolutional code + Reed-Solomon code	LDPC code + BCH code
Code rates	1/2, 2/3, 3/4, 5/6, 7/8	1/2, 3/5, 2/3, 3/4, 4/5, 5/6
Modulation	QPSK, 16-QAM, 64-QAM	QPSK, 16-QAM, 64-QAM, 256-QAM
Guard intervals	1/4, 1/8, 1/16, 1/32	1/4, 19/256, 1/8, 19/128, 1/16, 1/32, 1/128
OFDM sizes	2048, 8192	1024, 2048, 4096, 8192, 16384, 32768

TABLE I
SYSTEM PARAMETERS FOR DVB-T AND DVB-T2

the system parameters of DVB-T and DVB-T2 [6] [8].

Meeting the aforementioned requirements as well as being able to adapt the system to other communication standards requires a thorough investigation of state-of-the-art hardware components. A design merely based on digital signal processors (DSPs) is not powerful enough the achieve the desired goals. Thus, authors of this paper developed a hybrid concept which relies on a digital signal processor on the one hand and on field-programmable gate arrays (FPGAs) on the other hand. Due to the consequent deployment of the software-defined radio paradigm, the developed prototyping platform is capable of implementing various modern communication standard such as DVB-T2 and is ideally suited for concept engineering in the field of wireless communications in general. This manuscript is organized as follows. After this brief introduction, Section II gives an overview over the concept of the reconfigurable prototyping platform, followed by implementation aspects of this platform in Section III. Finally, the performance of the prototyping platform is addressed in Section IV.

II. RECONFIGURABLE PROTOTYPING PLATFORM CONCEPT

Figure 1 shows the suggested reconfigurable DVB-T2 receiver architecture. It consists of a fixed-point DSP board, which does not only implement major parts of the signal processing, but is also responsible for the scheduling of all platform components, which is an essential prerequisite for a reliable real-time demonstrator functionality. A mixed-signal daughter card, which implements analog signal processing and data conversion, connects directly to the DSP. In order to fulfill even very complex forward error correction requirements, such as the LDPC codes in DVB-T2 with a block length of 64800, a Virtex-5 FPGA evaluation module (EVM) is connected to the DSP, acting as a hardware accelerator. Finally, the decoded data is transferred to a data sink. While the DSP board and the Virtex-5 evaluation module are commercially available, the mixed-signal daughter card was developed by the authors of this paper. Its concept is shown in Figure 2. It consists of a further daughter card containing the RF (Radio Frequency) front end. The mixed-signal daughter card shall be able to allow processing signals in various frequency bands. Therefore, an analog-to-digital converter with an integrated down-conversion unit and advanced filtering capabilities should be used. Using a analog-to-digital converter with an integrated down-conversion unit has the advantage that the incoming intermediate frequency signal can be down-converted digitally. In order to be suitable for several communication systems, the sampling rate of the analog-to-digital converter should be reasonably high. The output of the analog-to-digital converter is fed into a Xilinx Spartan-3 FPGA for further basic signal processing purposes, such as additional filtering and sampling rate decimation. Furthermore, it buffers the data for the DSP. For improved flexibility, the authors follow a strict modular concept. In case of technology advances in a specific field, the corresponding module - in this context the mixed-signal daughter card - can be easily replaced without affecting the residual system. The USB (Universal Serial Bus) interface shown in Figure 2 is designed for debug reasons only.

The core part of the prototyping platform shown in Figure 1 is a DSP board with a powerful Texas Instruments TMS320C6455 fixed-point DSP running at 1.2 GHz. The

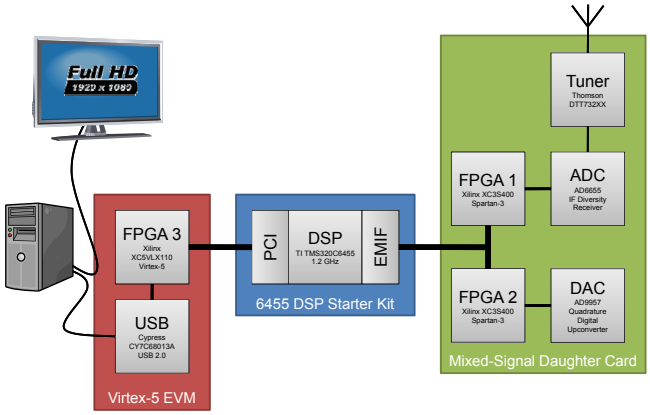

Fig. 1. Implementation concept of the SDR multimedia HDTV receiver

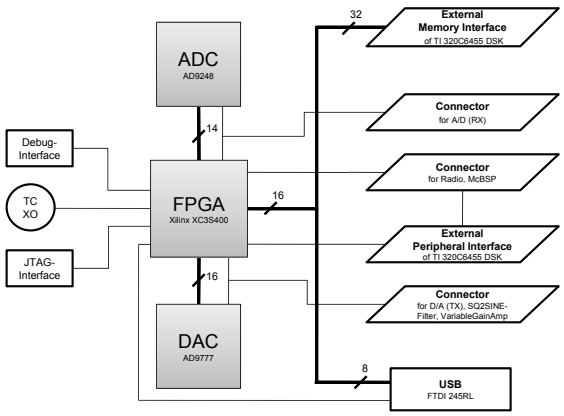

Fig. 2. Implementation concept of the mixed-signal daughter card

mixed-signal daughter card described before is connected to the DSP using a TI proprietary solution, namely the EMIF (External Memory Interface). In case of using the hardware accelerator for channel decoding, as it is done for the DVB-T2 implementation, the interface between the DSP and the Virtex-5 FPGA hardware accelerator demands for a reasonable high data rate depending on the resolution of the log-likelihood ratios representing the soft information for the channel decoder. This log-likelihood ratios are typically computed within the digital signal processor. This hardware accelerator for the DSP, which is also depicted in Figure 1, is implemented using an Avnet evaluation module hosting a Xilinx Virtex-5 LX110 FPGA. The TMS320C6455 DSP and the Xilinx Virtex-5 LX110 FPGA provide the digital signal processing capabilities required by the DVB-T2 standard as well as by further modern communication standards like IEEE 802.11n. Following this hybrid concept of a software/hardware solution has major implementation advantages. While FPGAs are ideally suited for massive parallel processing, DSPs are superior in the implementation of scheduling tasks. By combining both techniques, the proposed system architecture exhibits both advantages. The DSP is the heart of the prototyping platform, controlling and reconfiguring all further hardware components. The Virtex-5 LX110 FPGA acts as a necessary and flexibly adjustable hardware accelerator, providing, e.g., real-time error control decoding capabilities. The DSP is programmed in C++ language using the Code Composer Studio, and all FPGAs are programmed in Verilog HDL (Hardware Description Language) using the Xilinx ISE development suite. To facilitate a high-speed interconnection between DSP and Virtex-5 LX110 FPGA, the authors developed a point-to-point variant, i.e. a simplified version, of the well-known PCI (Peripheral Component Interconnect) bus, allowing a maximum transmission rate of approximately $700\,\mathrm{Mbit/s}$. For the implementation of the DVB-T2 receiver, the error control decoded bit stream is the output of the prototyping platform developed by the authors. To facilitate a low-cost and at the same time standardized interface, the authors rely on a USB 2.0 connection with a maximum achievable data rate of about $400\,\mathrm{Mbit/s}$.

After describing the concept of the underlying reconfigurable prototyping platform, within this section some implementation aspects are emphasized, focusing on the implementation of the DVB-T2 receiver. The received RF signal, prevailing either in the VHF or the UHF band, is first processed by a Thomson DTT73200 digital terrestrial tuner, generating an IF (Intermediate Frequency) receive signal at its output. To circumvent the impact of intermodulation distortions (IMD) caused by I/Q imbalancing, the authors deploy a single heterodyne analog receiver which feeds an Analog Devices AD6655 analog-to-digital converter (ADC) with a maximum sampling rate of $150\,\mathrm{MSamples/s}$. Within the AD6655, the IF received signal is sampled and digitally down-converted. This conversion scheme shows a superior robustness against analog impairments as shown in [9] especially compared to homodyne conversion. Nevertheless, in the proposed fully modular concept, the RF module can be easily replaced by a homodyne solution if necessary. The digitized received signal output by the AD6655 is decimated, digitally down-converted and low-pass filtered before being transferred to the DSP. The digital down-conversion step allows a very efficient implementation of an automatic frequency error correction (AFC) since the integrated NCO (Numerically-Controlled Oscillator) can be reconfigured very easily. Frequency offsets result from impairments in the analog signal processing branches, in particular in deviations of the local oscillator frequencies from the reference value. The Xilinx Spartan-3 FPGA acts as an interface between the parallel data output of the ADC and TIs External Memory Interface which is used to transfer the digital complex baseband signal to the TMS320C6455 DSP for synchronization and demodulation. In order to reduce the load of the digital signal processor, the data transfer between Spartan-3 FPGA and DSP is carried out by using DMA (Direct Memory Access) which allows data transfers without DSP intervention. The petri-net based scheduling of the signal processing carried out on the DSP is depicted in Figure 3. After frame synchronization, a synchronization tracking is carried out for compensating for potentially occurred synchronization mismatches. The synchronization in DVB-T2 is based on the P1 preamble. The subsequent symbol, the P2 preamble, contains signaling information required for the demodulation of the following data symbols. The channel estimation and equalization is based on pilot subcarriers and is processed in frequency domain, followed by the computation of the log-likelihood ratios (LLRs).

The LLRs are then transferred to the Xilinx Virtex-5 LX110 FPGA for LDPC decoding. Again, DMA is used to reduce the DSPs load. Finally, the error control decoded bit stream is transferred to a standard host PC (Personal Computer) via USB 2.0 carrying out the source decoding and the video displaying via an HDMI (High Definition Multimedia Interface)

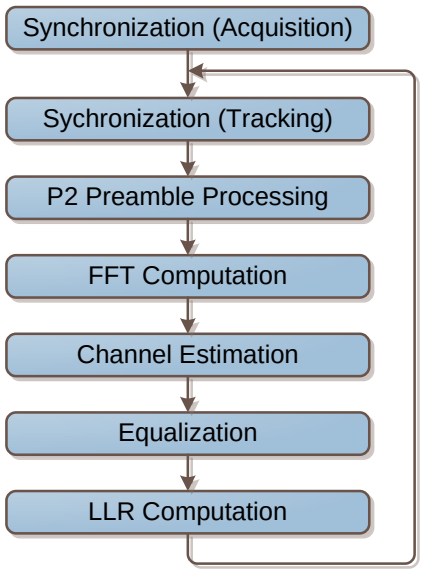

Fig. 3. Petri-net based DSP scheduling

 ISBN: 978-1-61208-123-6

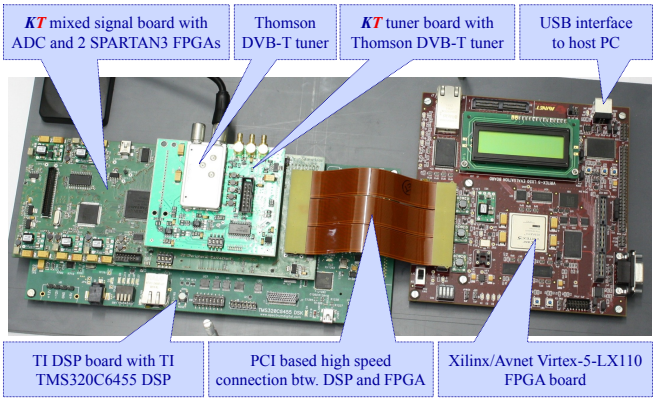

Fig. 4. Photograph of the implemented SDR based DVB-T2 receiver

connection to a full HD display.

III. Reconfigurable Prototyping Platform Implementation

Figure 4 shows a photograph of the reconfigurable prototyping platform developed by the authors, customized for the reception and demodulation of DVB-T2 signals. On the left-hand side of the photograph, a compound of three stacked printed circuit boards (PCB) can be seen. The top is the RF tuner board developed by the authors. This RF tuner board hosts the aforementioned Thomson DTT73200 digital terrestrial tuner. The RF tuner board is connected to the mixed-signal board also realized by the authors. As described before, this mixed-signal board hosts two Xilinx Spartan-3 FPGAs of which one is required for the DVB-T2 receiver. The mixed-signal board is connected to the Texas Instruments DSP board which contains the TMS320C6455 DSP. On the right-hand side of the photograph shown in Figure 4, the Virtex-5 LX110 FPGA evaluation module is located. The interconnection of the FPGA board and the mixed-signal board is a proprietary PCI solution.

IV. Performance

The resulting constellation diagram for the most challenging DVB-T2 mode with an OFDM size of 32768 points and 256-QAM subcarrier modulation is shown in Figure 5. Due to analog impairments such as local oscillator frequency and sampling clock offsets, the degradation becomes higher for increasing QAM symbol magnitudes. Nevertheless, the powerful forward error correction scheme is able to correct the occurring errors. Figure 6 depicts the obtained error performance of the demonstrator in the case of a transmission via a single path channel with additive white Gaussian noise (AWGN), assuming LDPC coding with a code rate of 3/5, a code word length of 64800 bits, 32k FFT and 256-QAM modulated data symbols transmitted over each subcarrier. This error performance was measured for benchmarking. In Figure 6, both the bit error ratio (BER) P_{bit} as well as the block error ratio (BLER) P_{block} are shown versus the signal-to-noise ratio (SNR) $10\log_{10}(E_{\mathrm{s}}/N_0)$. Both P_{bit} and P_{block} are determined at the output of the BCH decoder which follows the LDPC decoder. The LDPC decoding results was determined after a maximum of fifty decoding iterations. Both LDPC and BCH decoders are soft-input decoders. It is found that a P_{block} of 10^{-3} requires an SNR $10\log_{10}(E_{\mathrm{s}}/N_0)$ of less than $16.7\,\mathrm{dB}$. The corresponding BER is approximately 10^{-7} at the same SNR. Furthermore, it was found that the analog single heterodyne receiver allows a superb error vector magnitude (EVM) of less than $2\,\%$. The frequency offset of the RF tuner is lower than $6\,\mathrm{kHz}$ without correction, corresponding to 21.5 subcarriers. This frequency offset can be easily corrected by an automatic frequency correction (AFC) and synchronization algorithm developed and implemented by the authors. The implemented SDR based DVB-T2 receiver was tested using an RF signal which was generated and transmitted through a Rohde & Schwarz AFQ / SMIQ06 combination. The test signal was based on a 256-QAM/32k FFT variant of the DVB-T2 signal. It contained a multiplexed version of three HDTV test video streams provided by the BBC. The gross information rate was $45\,\mathrm{Mbit/s}$. The signal which is generated for the performance analysis is fed into the demonstrator and processed. The resulting bitstream is sent to a PC where the block error ratio is measured. Since the transmitter consists of calibrated measurement equipment, the power level at the antenna input can be controlled arbitrarily. Hence, the sensitivity of the demonstrator can be measured easily. In addition, the demonstrator can be put in a transparent mode which allows to measure the modulation accuracy by calculating the error vector magnitude.

Furthermore, the modular concept of the prototyping platform allows for easily implementing other communication systems beside DVB-T2. Due to the nature of the deployed hardware, the functionality can be changed to support totally

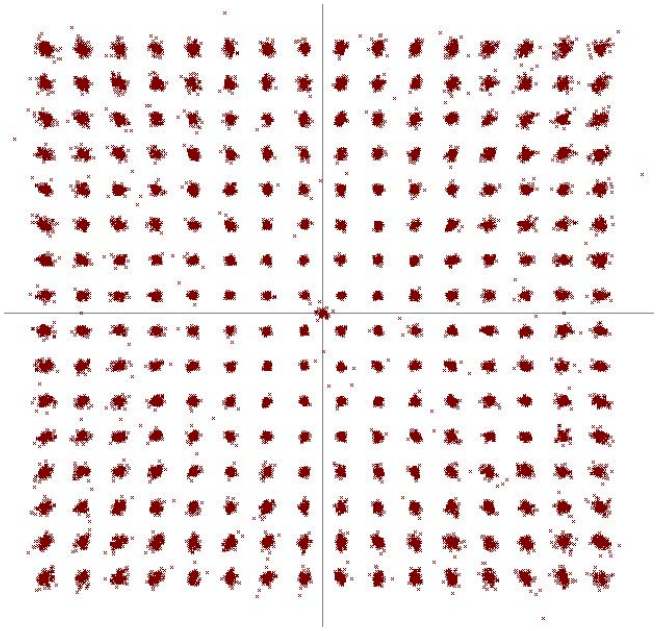

Fig. 5. Constellation diagram of a received and equalized 256-QAM signal

 ISBN: 978-1-61208-123-6

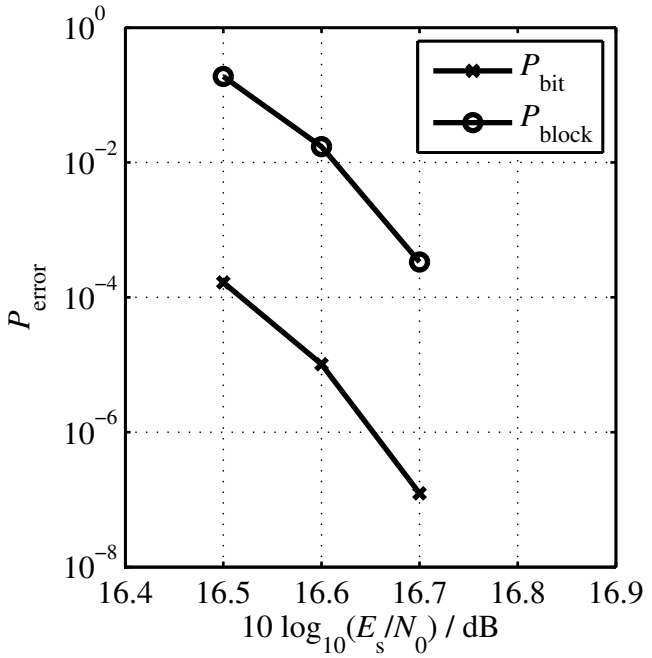

Fig. 6. Error performance

different communication standards by changing the firmware. The clock generation and distribution circuits are software controllable and can match the specification of a majority of the commercially deployed communication standards. The RF down-conversion stage is limited in the support of carrier frequencies and baseband bandwidths, but can be exchanged easily due to the modular concept.

V. Conclusion

Within this manuscript, the authors presented a system concept and setup of a reconfigurable prototyping platform using the example of DVB-T2. This platform combines the digital processing power of high-performance Texas Instruments TMS320C6455 DSP and Xilinx Virtex-5 LX110 FPGA with a single heterodyne analog receiver concept. With this system concept the authors will ease the way towards commercial and highly integrated implementations of communication systems. In addition, the presented platform is ideally suited for research and development for future wireless communication systems.

VI. Acknowledgment

The authors wish to thank their colleagues at Samsung Electronics in South Korea and at the Department of Communication Technologies of University of Duisburg-Essen for fruitful discussions during the development of the prototyping platform.

References

[1] W. Tuttlebee, *Software Defined Radio: Enabling Technologies*. New York, USA: John Wiley & Sons, 2002.

[2] F. K. Jondral, "Software-defined radio: basics and evolution to cognitive radio," *EURASIP J. Wirel. Commun. Netw.*, vol. 2005, no. 3, pp. 275–283, 2005.

[3] J. Mitola, "The software radio architecture," *IEEE Communications Magazine*, vol. 33, no. 5, pp. 26–38, 1995. [Online]. Available: http://dx.doi.org/10.1109/35.393001

[4] J. Mitola, D. Chester, S. Haruyama, T. Turletti, and W. Tuttlebee, "Globalization of software radio," *IEEE Communications Magazine*, vol. 37, no. 2, pp. 82–83, Feb 1999.

[5] R. Yates and N. Mandayam, "Challenges in low-cost wireless data transmission," *IEEE Signal Processing Magazine*, vol. 17, no. 3, pp. 93–102, May 2000.

[6] *Digital Video Broadcasting (DVB); frame structure channel coding and modulation for a second generation digital terrestrial television broadcasting system (DVB-T2)*, ETSI Std. DVB Doc. A122 Draft, June 2008.

[7] L. Vangelista, N. Benvenuto, S. Tomasin, C. Nokes, J. Stott, A. Filippi, M. Vlot, V. Mignone, and A. Morello, "Key technologies for next-generation terrestrial digital television standard dvb-t2," *IEEE Communications Magazine*, vol. 47, no. 10, pp. 146–153, October 2009.

[8] *Digital Video Broadcasting (DVB): Framing Structure, channel coding and modulation for digital terrestrial television*, ETSI Std. EN 300 744 V1.6.1, January 2009.

[9] B. Razavi, *RF Microelectronics*. Upper Saddle River, NJ, USA: Prentice-Hall, Inc., 1998.

 ISBN: 978-1-61208-123-6

EVALUATION OF FAST ALGORITHMS FOR MOTION ESTIMATION

Ionuţ Pirnog, Cristian Anghel, Andrei Alexandru Enescu, and Constantin Paleologu

Telecommunications Department, University Politehnica of Bucharest, Romania
{ionut, canghel, aenescu, pale}@comm.pub.ro

ABSTRACT

In this paper we present an evaluation of the fast algorithms used for motion estimation and compensation. The presented algorithms are classified in two categories. The first category contains the algorithms with fixed number of iterations, i.e., Three Step Search (TSS), New Three Step Search (NTSS), and Four Step Search (FSS). The second category includes motion estimation algorithms with variable number of iterations, i.e., Orthogonal Search (OS), Two Dimensional Logarithmic Search (TDLS), and Adaptive Rood Pattern Search (ARPS). It is proved that for the second category of algorithms the number of iterations depends on the dimension of the search window. The evaluation is done by comparing the peak signal-to-noise ratio (PSNR) of the compensated motion frame and the number of blocks that are used.

Keywords – Motion estimation, fast algorithms, fixed and variable iterations**.**

I. INTRODUCTION

Multimedia Information Retrieval (MIR) emerged as a branch of the Information Retrieval Domain simultaneously with the increasing interest in multimedia content analysis, characterization, and retrieval. Since by multimedia content we understand audio data, video data, textual data (and combinations of these), the Information Retrieval is defined for textual data; thus we can easily conclude that MIR means audio and video content analysis.

Motions estimation played a key role in video compression [1] and is more successfully used since the development of the Moving Pictures Experts Group (MPEG) standards. To enhance the "access to" and "retrieval of" multimedia content, MPEG has developed a standard called MPEG-7 that provides a rich set of standardized tools to describe multimedia content [2]. This set of tools includes motion descriptors that can be used for classification, indexing, comparison, and retrieval of video content [2]. For the video content compressed using the MPEG-4 standard, the motion information is contained in the form of motion vectors for the B and P frames and can be used directly for the extraction of the motion descriptors. If the video content does not include motion information, then the motion vectors can be extracted using one of the many fast motions estimation algorithms developed in the last decade.

The basic idea behind motion estimation is the block by block comparison of two consecutive frames, i.e., the current frame and the previous frame. The blocks are rectangular areas of a frame, having the dimensions chosen according to the application. Usually, the blocks are 8×8 or 16×16 pixels for compression; when high precision is needed the blocks can contain only one pixel. In this case, the motion vector has a dimension equal to the number of pixels, and is referred as "optical flow."

Fast motion estimation algorithms are used in order to minimize the computational complexity with little loss in the precision of the estimation. This is the case of video compression because the predicted frames P and B are based on a full frame I, the motion information, and the difference between the current frame and the motion compensated frame. These algorithms are simple but very efficient, so that they are extensively used in video compression.

The rest of the paper is organized as follows. In Section II we describe six of the most used motion estimation algorithms divided in two categories, i.e., fixed number of iterations and variable number of iterations. Section III contains the comparative experimental results obtained through simulations, using three different scenarios. In Section IV, we present the conclusions of the evaluation and future work.

II. BLOCK MATCHING ALGORITHMS

As stated in the first section, motion is a very important characteristic of video content and can be used for compression (e.g., MPEG-4) and retrieval (e.g., MPEG-7). Combining with image segmentation we can obtain camera motion information (using the motion vectors of the background) and object motion information (using the motion vectors of region labeled as objects).

The block matching algorithms used for motion estimation split the current frame into non overlapping blocks of size 8×8 or 16×16 pixels and, for every block, the corresponding block in the previous frame is found [3]. For a better understanding of the basic method for motion estimation, let us denote the current frame with $F_c(x,y)$, the previous frame with $F_p(x,y)$, and with $B^c_{m,j}(x,y)$ the block number j of the current frame. The parameter m is the dimension of the block and the pair (x,y) is the horizontal and vertical position of the block in the frame. In the following, in order to simplify the notation, we will omit the subscript m. For every block $B^c_j(x,y)$ of the current frame, we can define a search window $W^p_{l,j}(x,y)$ as an extension of the block in the previous frame $B^p_k(x,y)$, with the same position as the bloc in the current frame. The parameter l of the search window represents the dimension of the extension in all four directions. This means that the search window

 ISBN: 978-1-61208-123-6

$W_{l,j}^{p}(x,y)$ used for the motion estimation of a block $B_j^c(x,y)$ will have the dimension $(2l+m)\times(2l+m)$.

The corresponding block represents the best block obtained by comparing the block from the current frame, B_j^c, with all the overlapping blocks from the search window, $B_k^p, k=\overline{1,N}$, where N represents the number of blocks in the search window.

The corresponding block or the best block is found using the minimization of a cost function defined as the mean square error (MSE) or as the mean absolute error (MAE) between the current block in the current frame and the current block in the search window, i.e.,

$$MSE\left(B_j^c, B_k^p\right) = \left(B_j^c - B_k^p\right)^2 = \\ = \frac{1}{m^2}\sum_{i=1}^{m}\sum_{j=1}^{m}\left(P_c(i,j) - P_p(i,j)\right)^2 \quad (1)$$

$$MAE\left(B_j^c, B_k^p\right) = \left|B_j^c - B_k^p\right| = \\ = \frac{1}{m^2}\sum_{i=1}^{m}\sum_{j=1}^{m}\left|P_c(i,j) - P_p(i,j)\right| \quad (2)$$

where $P_c(i,j)$ and $P_p(i,j)$ represents the pixels in position (i,j) from the current and previous frames. The values of the parameters m and l determines the precision and the computational complexity of the motion estimation. If the motion of an object in a video is wide, then, for a good estimation, it is necessary a large search window, but this means that the process will be computationally expensive. This algorithm is known as the Full Search (FS) algorithm because it searches the best block from all the blocks in the search window [4]. The precision of this algorithm is very good, if the window is large enough to include the amplitude of the motion, but because it uses all the blocks in the search window it is also computationally expensive.

The class of fast block matching algorithms for motion estimation was developed with the goal of lowering the computational time without causing a high loss in precision. This is done by using for comparison only a small number of blocks in the search window. The developed fast algorithms use the same principle but with a different block selection scheme.

A. Three Step Search Algorithm

The Three Step Search (TSS) is the first fast algorithm that was developed and, as its name suggests, it uses three steps to determine the best block. The three steps are as follows [4]:

1. The current block, $B_j^c(x,y)$, is compared to the centre block in the search window, $B_j^p(x,y)$, and 8 blocks located at a distance S from the centre block. The cost function for all the blocks is computed and the best block for this step is determined as the block with the minimum cost.
2. The determined best block is selected as the new centre, the distance S is halved, and step 1 is repeated.
3. When the distance is 1, the best block is determined as the block with the minimum cost.

The values of the motion vector for the current block are obtained as de difference between the horizontal and vertical positions of the best block and the positions of the current block. Usually, the initial distance is set to $S=4$ and the search window parameter is set to $l=7$. These values where experimentally determined but lead to good enough results for estimating motion with low amplitude. Larger values of these parameters may lead, in some cases, to a better estimation, but definitely lead to an increase of the computational cost. Compared to the FS algorithm, the TSS algorithm has a nine times lower computational cost.

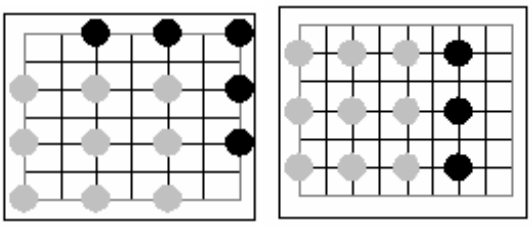

Figure 1. The neighboring blocks selected if the best block is one of the blocks with $S=1$.

B. New Three Search Algorithm

The improvement introduced by the New Three Step Search (NTSS) is a better estimation of the motion with low amplitude [5]. This is done by evaluating in the first step another 8 blocks located at a distance $S=1$ from the centre block. The best block from these initial 17 blocks is determined based on the cost functions; depending on the positions of the best block we have three situations:

1. If the best block is the one in the centre of the search window, then the algorithm stops.
2. If the best block is one of the blocks located at a distance $S=4$, then the TSS algorithm is used.
3. If the best block is one of the blocks located at a distance $S=1$, then its neighbors are compared with the current block and the best block is determined as the block with the minimum cost function.

To decrease the number of blocks compared and to eliminate the re-evaluation of some blocks, the neighbors selected in the last case depends on the position of the best block as shown in Figure 1.

C. Four Step Search Algorithm

The Four Step Search (FSS) is performed in four steps [6]:

1. The centre block and the eight block al distance $S=2$ are evaluated. If the block with the minimum cost is the centre block, then the algorithm jumps to step 4. Else it goes to step 2.
2. The block with the minimum cost is selected as the centre block and the neighboring blocks at distance

$S = 2$ are evaluated. The selection of the neighboring blocks is similar to NTSS.

3. If the best block is the centre block, then the algorithm goes to step 4, else step 2 is repeated.
4. The distance is set to $S = 1$ and the centre block and its eight neighbors are evaluated. The best block is the block with the minimum cost.

The minimum number of evaluated blocks is the same as in the case of the NTSS algorithm, but the maximum number decreases.

D. Two Dimensional Logarithmic Search Algorithm

The Two Dimensional Logarithmic Search (TDLS) algorithm is similar to the TSS algorithm, but verifies the centre block and only 4 blocks located at distance S on the horizontal and vertical axes [6]. The value of S is not fixed, as in the case of TSS and FSS algorithms, and can be chosen depending of the dimension of the search window. The steps required by this algorithm are:

1. The value of the distance parameter S is set. The centre block and the 4 blocks at distance S are evaluated, and the block with the lowest cost is selected.
2. If the selected block is the centre block, then the distance S is halved. If one of the other blocks is selected, then this block is set as the new centre and step 1 is repeated.
3. When the distance becomes equal to one, the centre block and all its neighbors are evaluated. The block with the lowest cost is the best block.

It is not always clear that the TDLS algorithm obtains better results than the other presented algorithms. But the fact that the initial value of S is not imposed can be very helpful in case of a motion with large amplitude.

E. Orthogonal Search Algorithm

The Orthogonal Search (OS) is a combination of the TSS and TDLS algorithms [3]. The algorithm involves the following steps:

1. The initial distance is chosen as half of de maximum distance of the search window. The centre block and two blocks on the horizontal axis are evaluated. The block with the minimum cost is set as the new centre.
2. The centre block and two blocks on the vertical axis are evaluated and the new centre is selected.
3. If the distance parameter S is bigger than one, then the distance is halved and the steps 1 and 2 are repeated. Else, the last centre block is the best block.

The computational cost for the OS algorithm is smaller as compared to the TDLS algorithm, but the precision decreases.

F. Adaptive Rood Pattern Search Algorithm

The Adaptive Rood Pattern Search (ARPS) algorithm uses the motion information of the neighboring block in the left. This is helpful if the current block and its neighbor on the left belong to the same object in the frame; in this case, their motion is similar [6]. The steps of the ARPS algorithm are:

Table 1. PSNR for video "Motion" with $m = 16$ and $l = 7$.

Algorithm	1-2	2-3	3-4	4-5
FS	34,06	31,93	30,28	29,27
TSS	33,98	31,81	30,15	29,25
NTSS	33,94	31,8	30,15	29,25
FSS	31,73	30,2	28,93	28,05
OS	33,86	31,44	29,56	28,41
TDLS	32,77	30,81	29,46	28,57
ARPS	33,67	31,72	30,01	29,07
5-6	**6-7**	**7-8**	**8-9**	**9-10**
30,43	29,47	29,92	27,72	27,89
30,27	29,33	29,75	27,55	27,81
30,21	29,33	29,79	27,6	27,83
28,88	28,07	28,78	27,05	27,04
29,26	27,66	28,51	25,82	27,04
29,43	28,44	28,99	27,14	27,18
30,01	29,1	29,47	27,48	27,6

1. The centre block, the block indicated by the motion vector of the neighbor, and four blocks are evaluated. The four blocks are selected on the horizontal and vertical axes at a distance S, chosen as the maximum value between the absolute values of the motion vector.
2. The block with the minimum cost is selected as the new centre block, the distance is set to 1, and the centre block together with its four axis neighbors are evaluated.
3. If the block with the minimum cost is in the centre, then the algorithm stops; consequently, this is the best block. Else, step 2 is repeated.

For the blocks in the first column, there are no left neighbors, so that the distance S is set to 2.

The major advantage of this algorithm is that after the first step the search is moved to the area where the best block is, without going through intermediary steps. Consequently, the computational cost is smaller than all the other algorithms.

III. EXPERIMENTAL RESULTS

The goal of this evaluation was to determine the performances of the fast block motion estimation algorithms, the parameters that determine the efficiency of the motion estimation, and if these algorithms can be improved.

In order to evaluate the performances, we have implemented the algorithms in Matlab using two videos for estimation of the motion. The first observation we have made based on our simulations is that the classification of the algorithms based on the efficiency and computational cost does not depend on the video selected.

We have stated in the first section that the results are presented for three scenarios. These scenarios were obtained by varying the values of the search window parameter and the block size parameter.

1. First scenario

In the first scenario, we set the blocks to 16×16 pixels and the search window parameter to 7. The results for the video "Motion" with 10 frames are shown in Table 1 and Figure 2.

 ISBN: 978-1-61208-123-6

Table 2. Number of blocks verified.

Algorithm	Nb
FS	255
TSS	25
NTSS	19
FSS	18
OS	13
TDLS	18
ARPS	11

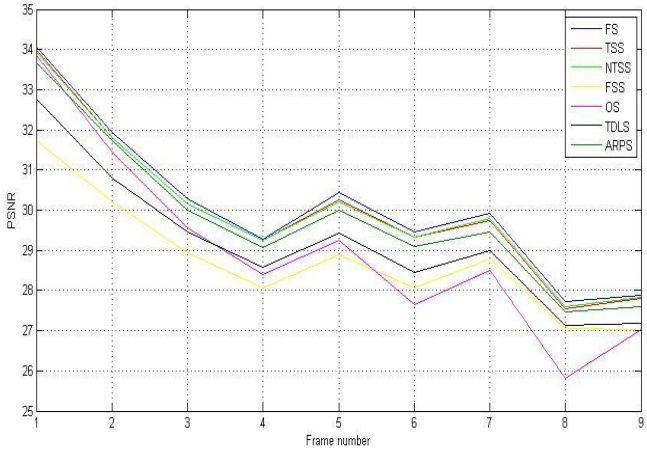

Figure 2. Motion estimation results for video "Motion" with $m = 16$ and $l = 7$.

The results in Table 1 show that the variation of the peak signal-to-noise ratio (PSNR) is not very high. The difference between these fast block matching algorithms is results in terms of the computational cost. This cost is evaluated through the number of blocks (Nb) in the verified search window for every block in the current frame. The values of the number of verified blocks are show in Table 2.

2. Second scenario

In the second scenario we set the blocks to 8×8 pixels and the search window parameter to 7. The results for the same video, "Motion", are shown in Table 3 and Figure 3.

As it can be seen, the PSNR slightly increases if we use 8×8 blocks but the increase in the computational cost is more significant. So, if the precision of estimation is not imposed it is recommended to use 16×16 blocks to obtain a smaller computational cost.

3. Third scenario

In the third scenario we set the blocks to 16×16 pixels and the search window parameter to 14 and 30. This scenario is based on the results from the first two scenarios and all of our simulations. We observed that even if we decrease the dimensions of the block, the estimation is not perfect. This happens because the motion amplitude in the videos we used is bigger than the search window. In Table 4 are presented the comparative results of the PSNR for these two values of the search window parameter and the results from the second scenario. The results are shown for frames 4 and 5 of the video "Motion."

Table 3. PSNR for video "Motion" with $m = 8$ and $l = 7$.

Algorithm	1-2	2-3	3-4	4-5
FS	34,61	32,53	31,28	30,78
TSS	34,19	32,24	30,96	30,49
NTSS	34,16	32,23	30,94	30,49
FSS	32,03	30,44	29,65	29,11
OS	34,09	31,68	29,91	28,88
TDLS	33,11	31,27	30,16	29,3
ARPS	33,27	31,76	30,46	30,02
5-6	**6-7**	**7-8**	**8-9**	**9-10**
31,91	31,21	31,94	28,71	29,06
31,57	30,85	31,54	28,46	28,9
31,54	30,92	31,69	28,56	28,97
29,83	29,21	29,87	27,82	27,82
29,97	28,78	30,03	26,53	27,76
30,29	29,83	30,49	27,9	28,09
30,75	30	30,97	28,29	28,59

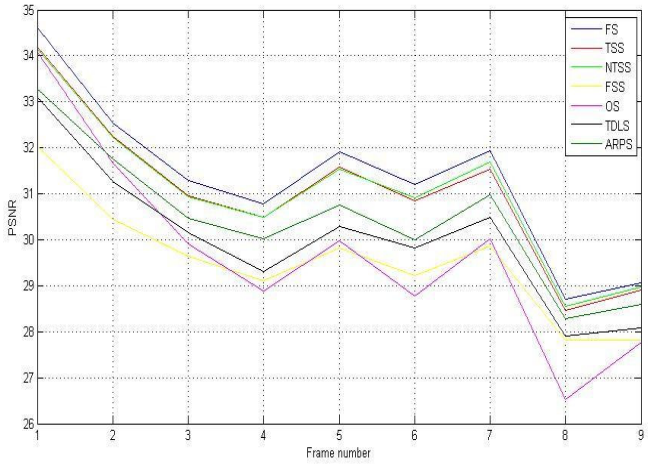

Figure 3.Motion estimation results for video "Motion" with $m = 8$ and $l = 7$.

Table 4. Comparative results of the PSNR for different search window parameters.

Algorithm	$l = 7$	$l = 14$	$l = 30$
TSS	29,25	29,25	29,25
NTSS	29,25	29,25	29,25
FSS	28,05	28,05	28,05
OS	28,41	28,41	28,41
TDLS	28,57	31,3	31,89
ARPS	29,07	30,81	31,04

The results show that the fast algorithms with fixed value of the search parameter S have the same precision even if we increase the dimensions of the search window. This was a predictable result because the search parameter of these does not depend on the search window dimension, so that the number of steps will be constant.

Significant improvement of the PSNR appears for the TDLS and ARPS algorithms, i.e., two of the algorithms that have variable search parameter and variable number of steps.

 ISBN: 978-1-61208-123-6

Table 5. Comparative results of the number of blocks verified for different search window parameters.

Algorithm	$l = 7$	$l = 14$	$l = 30$
TSS	25	25	25
NTSS	25	25	25
FSS	18	18	18
OS	13	13	13
TDLS	18	19	20
ARPS	12	14	14

As we specified in Section II, the value of the search parameter of the TDLS algorithm is not fixed and the number of steps depends on the search window. The comparative results for different dimensions of the search window are obtained for the same value of the search parameter $S = 4$.

We can see that the value of the PSNR for both the ARPS and TDLS algorithms in the case of $l = 30$ (Table 5) is higher than the PSNR for the same frames, 4 and 5, of the FS algorithm in the case of $l = 7$.

The computational complexity of the algorithms is evaluated in terms of the mean number of blocks verified for every frame. Since the evaluation of the algorithms was done using Matlab it is difficult to express the computational complexity in terms of the number of arithmetical operations. Concerning the number of blocks verified, the FS algorithm has a number of 255 blocks in the search window for every block in the current frame, and the ARPS and TDLS algorithms have blocks verified, even if we increase the search window.

IV. CONCLUSIONS AND FUTURE WORK

By evaluating a representative number of fast block matching algorithms for motion estimation, the following conclusions can be outlined.

1. There are two classes of fast algorithms for motion estimation: i) fixed search parameter and constant number of steps, and ii) variable search parameter and variable number of steps.
2. Although the differences between algorithms are not very high (in terms of both PSNR and Nb), in the case of the same search parameters and search window size, there is no room for improvement for the algorithms in the first class.
3. The dimensions of the search window determine the precision of motion estimation for the algorithms in the second class; as it was shown in Section III, the improvements brought by increasing the window size lead to a value of the PSNR higher that the value obtained for the FS algorithm.

In future work we intend to combine the two classes, meaning that we will see how the algorithms in the first class behave for different search parameters and window sizes. Another track we intend to follow is lowering the number of block verified, for a large search window, through different search schemes.

ACKNOWLEDGEMENT

This work was supported by the UEFISCSU Romania under Grant PN-II-RU-TE no. 7/05.08.2010.

V. REFERENCES

[1] Z. Chen, "Efficient block matching algorithm for motion estimation," *International Journal of Signal Processing*, vol. 5, no. 2, pp. 133–137, 2009.

[2] ISO/MPEG N4358, "Text of ISO/IEC Final Draft International Standard 15938-3 Information Technology - Multimedia Content Description Interface - Part 3 Visual," MPEG Video Group, Sydney, July 2001.

[3] A. Barjatya, "Block matching algorithms for motion estimation," Final Project Paper 2004.

[4] Y. C. Lin and S. C. Tai, "Fast full-search block-matching algorithm for motion-compensated video compression," *IEEE Trans. Communications*, vol. 45, no. 5, pp. 527–531, May 1997.

[5] R. Li, B. Zeng, and M. L. Liou, "A new three-step search algorithm for block motion estimation," *IEEE Trans. Circuits and Systems for Video Technology*, vol. 4, no. 4, pp. 438–442, Aug. 1994.

[6] S. Jamkar, S. Belhe, S. Dravid, and M. S. Sutaone, "A comparison of block-matching search algorithms in motion estimation," in *Proc. 15th International Conference on Computer Communication*, pp. 730–739, Mumbai, India, 2002.

 ISBN: 978-1-61208-123-6

Optimum QAM-TCM Schemes Using Left-Circulate Function over GF(2^N)

Călin Vlădeanu
Telecommunications Department
University Politehnica of Bucharest
Bucharest, Romania
calin@comm.pub.ro

Safwan El Assad
IREENA
École Polytechnique de l'Université de Nantes
Nantes, France
safwan.elassad@univ-nantes.fr

***Abstract*—In this paper, quadrature amplitude modulation – trellis coded modulation (QAM-TCM) schemes are designed using recursive convolutional (RC) encoders over Galois field GF(2^N). These encoders are designed using the nonlinear left-circulate (LCIRC) function. The LCIRC function performs a bit left circulation over the representation word. Different encoding rates are obtained for these encoders when using different representation wordlengths at the input and the output, denoted as N_{in} and N, respectively. A generalized 1-delay GF(2^N) RC encoder scheme using LCIRC is proposed for performance analysis and optimization, for any possible encoding rate, N_{in}/N. The minimum Euclidian distance is estimated for these QAM-TCM schemes and a general expression is found as a function of the wordlengths N_{in} and N. The symbol error rate (SER) is estimated by simulation for QAM-TCM transmissions over an additive white Gaussian noise (AWGN) channel. The proposed encoders outperform the corresponding binary encoders in terms of structural complexity and the availability of a general expression for the Euclidian distance.**

Keywords-Recursive convolutional GF(2^N) encoders; Left-circulate function; QAM-TCM.

I. INTRODUCTION

Channel encoded transmissions are used in all systems nowadays. Several types of channel encoding methods were proposed during the last decades. Almost all coding methods known in the literature use linear functions.

The nonlinear functions were used lately in chaotic sequence generators to increase the security of communications systems.

In [1], Frey proposed a chaotic digital infinite impulse response (IIR) filter for a secure communications system. The Frey filter contains a nonlinear function named left-circulate function (LCIRC), which provides the chaotic properties of the filter. In [2], Werter improved this encoder in order to increase the randomness between the output sequence samples. The performances of a pulse amplitude modulation (PAM) communication system using the Frey encoder, with additive white gaussian noise (AWGN) were analyzed in [3], by means of simulations. All previously mentioned papers considered the Frey encoder as a digital filter, operating over Galois field GF(2^N). Barbulescu and Guidi made one of the first approaches regarding the possible use of the Frey encoder in a turbo-coded communication system [4].

In [5], it was demonstrated that the Frey encoder with finite precision (wordlength of *N* bits) presented in [1] is a recursive convolutional (RC) encoder operating over GF(2^N). In [6], a new method is proposed for enhancing the performances of the chaotic PAM – trellis-coded modulation (PAM-TCM) transmission over a noisy channel. These encoders follow partially the rules proposed by Ungerboeck in [8] for defining optimum trellis-coded modulations by proper set partitioning. Using the Ungerboeck optimization procedures, GF(2^N) encoders using the LCIRC function were designed for phase shift keying – trellis-coded modulation (PSK-TCM) transmissions over a noisy channel. Two-dimensional (2D) TCM schemes using a different trellis optimization method for Frey encoder was proposed in [9]. The PSK-TCM encoders were introduced into a parallel turbo-TCM scheme in [10] and considerable coding gains were obtained. The development of optimum GF(2^N) encoders for quadrature amplitude modulation (QAM) TCM scheme is more difficult than in the case of PAM and PSK modulations, due to the larger constellations and non-uniform power per symbol.

In the present paper, a generalization of the optimum one-delay GF(4) encoder in [5] is performed, for any output wordlength *N* and for any possible encoding rate in quadrature amplitude modulation TCM (QAM-TCM) schemes.

The paper is organized as follows. Section II is presenting the LCIRC function definition and properties over GF(2^N), and its use for designing a rate 1 GF(4) RC encoder with LCIRC for a QPSK/4QAM-TCM transmission. The trellis optimization method is presented in Section III, first for a particular case, and then, for any output wordlength *N*. Therefore, in Section III, a generalized optimum GF(2^N) RC encoder scheme is proposed and an expression is provided for the minimum Euclidian distance of these encoders in a QAM-TCM transmission. The simulated symbol error rate (SER) performance is plotted in Section IV for the optimum QAM-TCM transmissions. Finally, the conclusions are drawn and some perspectives are presented in Section V.

II. DESIGN OF QAM-TCM SCHEMES WITH GF(2^N) RC ENCODERS USING LCIRC

A. Nonlinear LCIRC Function over GF(2^N)

The main component of the chaotic encoder introduced by Frey in [1] and the RC encoder presented in [5] is the

 ISBN: 978-1-61208-123-6

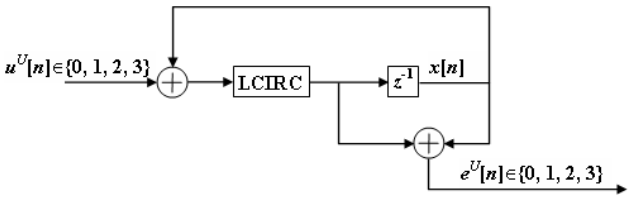

Figure 1 – Rate 1 GF(4) nonlinear encoder for 2 b/s/Hz.

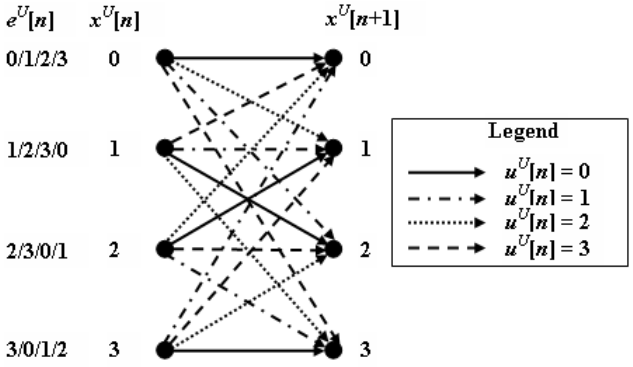

Figure 2 – Trellis for rate 1 GF(4) nonlinear encoder (2 b/s/Hz).

nonlinear LCIRC function. This function is determining both the chaotic properties of the encoder in [1], [2], and [3] and the trellis performances in [6], [7], [9], and [10]. The definition of this nonlinear function operating over finite sets and some of its properties will be presented in the sequel.

Let us denote by N the wordlength used for binary representation of each sample. The LCIRC function is used as a typical basic accumulator operation in microprocessors and performs a bit rotation by placing the most significant bit to the less significant bit, and shifting the other N-1 bits one position to a higher significance. This is the reason why the function is named left-circulate.

Considering the unsigned modulo-2^N operations for any sample moment n, the LCIRC consists in a modulo-2^N multiplication by 2 that is modulo-2^N added to the carry bit, and is given by the expression:

$$y^U[n] = LCIRC(x^U[n]) = (2 \cdot x^U[n] + s[n]) \bmod 2^N \qquad (1)$$

where the superscript U denotes that all the samples are represented in unsigned N bits wordlength, i.e. $x^U[n]$, $y^U[n] \in [0, 2^N\text{-}1]$, and the carry bit $s[n]$ is estimated as following:

$$s[n] = \begin{cases} 0, & \text{if} \quad 0 \le x^U[n] \le 2^{N-1} - 1 \\ 1, & \text{if} \quad 2^{N-1} \le x^U[n] \le 2^N - 1 \end{cases} \qquad (2)$$

We can note from (2) that besides the nonlinearity in the modulo-2^N multiplications and additions, the carry bit $s[n]$ is determining the nonlinearity of the LCIRC function.

Applying N times consecutively the LCIRC function to an N bits wordlength unsigned value x^U, it results the original value:

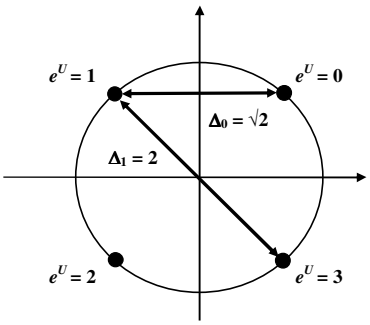

Figure 3 – Signal constellation for QPSK/4QAM-TCM.

$$LCIRC^N(x^U) \overset{\Delta}{=} \underbrace{LCIRC(LCIRC(...(LCIRC}_{N \text{ times}}(x^U)))) = x^U \qquad (3)$$

An example of a GF(4) RC encoder using LCIRC function for a QPSK-TCM scheme is presented in the next section.

B. Rate 1 GF(4) RC Encoder with LCIRC for a QPSK-TCM transmission

Let us consider a RC encoder working over GF(4) using the LCIRC function. This scheme is presented in Fig. 1. Here, all the values are represented in the unsigned form. Let us assume that N denotes the wordlength used for binary representation of each sample. This encoder is composed by one delay element with a sample interval, two modulo-2^N adders, and a LCIRC block. For each moment n, $u[n]$ represents the input data sample, $x[n]$ denotes the delay output or the encoder current state, and $e[n]$ is the output sample.

The encoding rate for the encoder in Fig. 1 is the ratio between the input wordlength N_{in} and the output wordlength N=N_{out} [5] [6], i.e., R = 1, because N_{in} = N_{out} = 2.

The trellis for the encoder in Fig. 1 is presented in Fig. 2 and does not follow the Ungerboeck rules [7], [8], [9]. This trellis has four states because the sample determining the encoder state takes four values, i.e., $x^U[n] \in \{0, 1, 2, 3\}$.

In Fig. 2, four different lines are used for representing the transitions corresponding to the input sample $u^U[n]$.

Each transition in Fig. 1 is associated to an unsigned output value $e^U[n] \in \{0, 1, 2, 3\}$. For each originating state, the values in the box, from left to right, are associated to the transitions in the descending order.

Mapping an unsigned output symbol value $e^U[n]$ into an QAM symbol value using the set partitioning (SP) map over the n-th sample interval as in [8], a 2^N levels QAM-TCM scheme is obtained.

The signal constellation for the QPSK-TCM scheme using the encoder in Fig. 1 and the SP mapping is represented in Fig. 3.

Considering the SP mapping for the constellation in Fig. 3, it results that the QPSK-TCM signal trellis in Fig. 2 presents a minimum Euclidian distance of $d^2_{E,\,N=2,\,R=1,\,\mathrm{QPSK}} = 2 \cdot \Delta_0^2 = \Delta_1^2 = 4$, offering no coding gain over the non-encoded binary PSK (BPSK) signal.

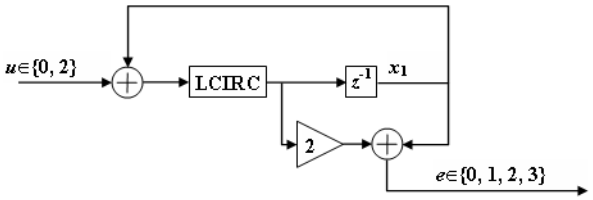

Figure 4 – Rate 1/2 optimum GF(4) RC-LCIRC encoder for 1 b/s/Hz.

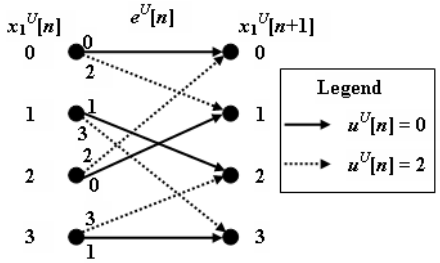

Figure 5 – Trellis for rate 1/2 optimum GF(4) RC-LCIRC encoder (1 b/s/Hz).

III. OPTIMUM QAM-TCM SCHEMES WITH GF(2^N) RC ENCODERS USING LCIRC

A. *Rate 1/2 Optimum GF(4) RC LCIRC Encoder for a QPSK-TCM transmission*

In this section, the potential of the nonlinear LCIRC function is showed, for designing efficient encoders.

Therefore, following the trellis optimization presented in [6] and [7], a simple nonlinear encoder operating over GF(4) was developed, which has a binary input. It is demonstrated that this encoder performs identically to an optimum rate 1/2 binary field RC convolutional encoder. Both encoders offer maximum coding gain for 1 b/s/Hz [8]. The scheme of the rate 1/2 optimum GF(4) encoder is presented in Fig. 4. Here, the time variable is neglected and all the values are represented in the unsigned form.

The trellis for the encoder in Fig. 4 is presented in Fig. 5 and follows all the Ungerboeck rules.

Considering the SP mapping, the QPSK-TCM signal trellis in Fig. 5 presents a minimum Euclidian distance of $d^2_{E,R=1/2,opt.,u^U \in \{0,2\},QPSK} = 2\cdot \Delta_1^2 + \Delta_0^2 = \Delta_1^2 = 10$ for a spectral efficiency of 1b/s/Hz. Hence, this rate 1/2 code for 1b/s/Hz QPSK-TCM transmission is offering a coding gain of $10\log10(2.5) \approx 4$ dB over the rate 1 QPSK-TCM in Section II.A.

B. *Generalized Optimum RC LCIRC Encoder for a QAM-TCM transmission*

Following the same design procedures as in Section III.A, we can design optimum RC encoders using LCIRC function, for any output wordlength N. In fact, for a fixed output wordlength N, an optimum RC encoder will be determined for each input wordlength $N_{in} \in \{1, 2, \ldots, N\text{-}1\}$, for which the encoding rate is $R = \{1/N, 2/N, \ldots, (N-1)/N\}$.

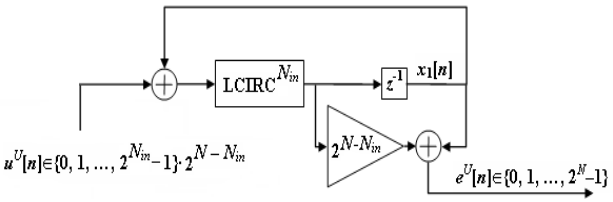

Figure 6 – Rate N_{in}/N optimum GF(2^N) RC LCIRC encoder for N_{in} b/s/Hz.

TABLE 1
MINIMUM QAM-TCM DISTANCES AS FUNCTION OF N AND N_{IN} FOR OPTIMUM GF(2^N) RC-LCIRC ENCODERS

N	N_{in}	R	d_E^2
1	1	1	8
2	1	1/2	10
2	2	1	4
4	1	1/4	9.2
4	2	1/2	3.6
4	3	3/4	2
4	4	1	0.8
6	1	1/6	≈ 9
6	2	1/3	≈ 4.47
6	5	5/6	≈ 0.48
6	6	1	≈ 0.19

The general block scheme for a rate N_{in}/N optimum QAM-TCM encoder, $N_{in} \in \{1, 2, \ldots, N\text{-}1\}$ using one delay element and the LCIRC function is presented in Fig. 6. LCIRC^{Nin} represents the LCIRC function application for N_{in} times consecutively, as it was defined in (3). Both adders and the multiplier are modulo-2^N operators.

The trellis complexity of the codes generated with the scheme in Fig. 6 increases with the wordlength, because the number of trellis states grows exponentially with the output wordlength, i.e., 2^N, while the number of transitions originating from and ending in the same state grows exponentially with the input wordlength, i.e., $2^{N_{in}}$.

It can be easily demonstrated that the minimum Euclidian distance for the QAM-TCM encoder in Fig. 6 has the following expression:

$$d^2_{E,R=N_{in}/N,2^N-QAM} = \begin{cases} \left(2^{N-N_{in}+1} + \sum_{i=0}^{N-N_{in}-1} 2^i\right)\Delta^2_{0,2^N-QAM}, & \text{for } N_{in} \in \left\{1,\ldots,\frac{N}{2}-1,\frac{N}{2}+1,\ldots,N-1\right\} \\ \left(2^{N-N_{in}+1}+1\right)\Delta^2_{0,2^N-QAM}, & \text{for } N_{in} = \frac{N}{2} \end{cases} \quad (4)$$

For example, let us consider the optimum encoders for the output wordlength equal to 4, i.e., N=4. The input wordlength may take three values $N_{in} \in \{1, 2, 3\}$, and the corresponding encoding rates are $R \in \{1/4, 1/2, 3/4\}$. For the rate 1/4 encoder the scheme in Fig. 6 is set with all the values corresponding to N_{in}=1. From (4) results that the minimum distance of this code is $d^2_{E,\ R=1/4,\ opt.,\ 16\text{-}QAM,\ u^U \in \{0,\ 8\}} = 9.2$, having a coding gain of $10\cdot\log10(d^2_{E,\ R=1/4,\ opt.,\ 16\text{-}QAM,}$

$u^U \in \{0,4,8,12\}$ / $d^2_{E,R=1,N=4,\text{ opt., 16-QAM}}$) = 10·log10(9.2/0.8) ≈ 10.6 dB over the optimum 16QAM (N=4) using a rate 1 encoder. For the rate 2/4 encoder (N_{in}=2) the minimum distance of this code is $d^2_{E,\ R=1/2,\ \text{opt., 16-QAM},\ u^U \in \{0,4,8,12\}}$ = 3.6, having a coding gain of approximately 6.53 dB over the optimum 16QAM (N=4) using a rate 1 encoder. For the rate 3/4 encoder (N_{in}=3) the minimum distance of this code is $d^2_{E,\ R=3/4,\ \text{opt., 16-QAM},\ u^U \in \{0,2,4,6,8,10,12,14\}}$ = 2, having a coding gain of approximately 3.97 dB over the optimum 16QAM (N=4) using a rate 1 encoder. The rate 1 optimum encoder is obtained for $N_{in} = N$, for any value of N, considering that $LCIRC^0(x^U) = LCIRC^N(x^U) = x^U$ assumes no bit circulation. This rate 1 optimum encoder offers a minimum distance of $d^2_{E,\ R=1,\ \text{opt. } N=4,\ \text{opt., 16-QAM}} = 0.8$.

Table 1 presents a few values of the minimum distances of the encoder shown in Fig. 6 for different values of N_{in} and N. The resulted coding rates are presented in the third column. Analyzing the values in Table 1 it can be noted that the minimum distance of a code decreases when its coding rate increases, for any value of N. This fact is well known, i.e., the code performances decrease with the rate increases. Unfortunately, these performances are related to the spectral efficiency of these PSK transmissions. For the codes presented in Table 1, having the encoder structure in Fig. 6, the spectral efficiency for the QAM transmission is equal to the input wordlength N_{in}. Hence, the code performances increase is paid by a spectral efficiency decrease.

It can be easily noticed that all the rate $(N-1)/N$, for any N value, the optimum RC-LCIRC encoders are offering the same minimum distance as the corresponding binary optimum encoders determined by Ungerboeck in [8]. However, the GF(2^N) optimum RC-LCIRC encoders are less complex than the corresponding binary encoders. The memory size of the binary encoders increases logarithmically with the number of states in the trellis, while the GF(2^N) optimum RC-LCIRC encoders include only one delay element, no matter what is the trellis complexity.

One can notice that optimum RC-LCIRC QAM-TCM encoders can be designed for any spectral efficiency value, and for any encoding rate, using the scheme in Fig. 6 with minimum distances given by (4).

IV. Simulation Results

The QAM-TCM schemes presented in Section II and Section III using all optimum encoders in Table 1 were considered for simulations. The SER performances for these encoding schemes using multilevel QAM signals and Viterbi decoding were analyzed in the presence of AWGN. The SER is plotted in Fig. 7 as a function of the SNR.

The QAM-TCM schemes using rate 1 optimum nonlinear RC encoders for the same spectral efficiencies as the three optimum encoder QAM-TCM schemes for N=4, were considered for comparison. For example, the rate 1/4 encoder for N=4 is having the same spectral efficiency as the rate 1 encoder for N=1, i.e., 1b/s/Hz, and the rate 2/4 encoder for N=4 and the rate 1 encoder for N=2 have an efficiency of 2b/s/Hz. These cases are considered in Fig. 7.

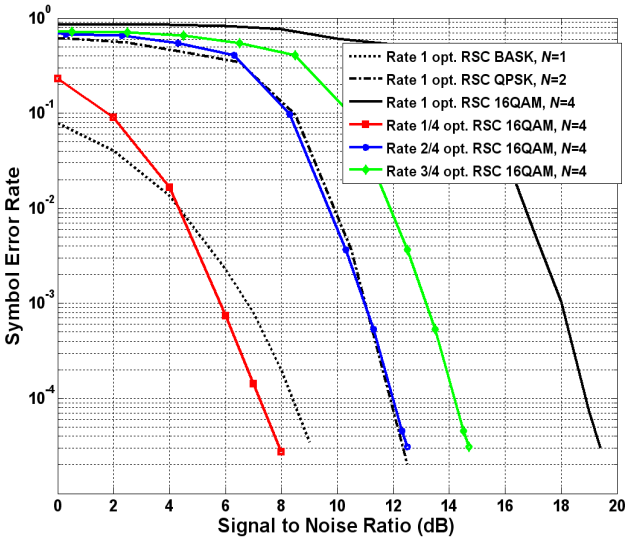

Figure 7 – SER performance for QAM-TCM schemes using optimum GF(2^N) nonlinear RC encoders.

Analyzing the SER curves it can be noticed that the rate 1/4 encoder for N=4 performs better than the rate 1 encoder for N=1 by more than 1 dB, and the rate 2/4 encoder for N=4 performs almost the same as the rate 1 encoder for N=2. The simulation results are in concordance with the theoretical results from Table 1. However, the average multiplicity of error events with the minimum distance in (4), for optimum GF(2^N) RC encoders, is smaller than multiplicity of minimum distance error events for the rate 1 encoders, for all encoders with $N_{in} < N$. This is the reason why the simulation results in Fig. 7 show slightly larger coding gains between these two encoders for a given spectral efficiency.

V. Conclusions and Future Works

It was demonstrated that optimum RC encoders over GF(2^N) can be designed using the LCIRC function. A generalized 1-delay GF(2^N) RC encoder scheme using LCIRC was defined, for any possible encoding rate. A general expression is found for the minimum Euclidian distance of QAM-TCM schemes using these optimum encoders. As advantage of this generalized encoder, we can mention its reduced complexity. Hence, using only one delay element and multiple bit circulations we designed encoders having complex trellises and large Euclidian distances. In addition, it was shown that the nonlinear encoders offer the same performances as conventional binary encoders.

In perspective, we intend to apply the presented method to other nonlinear structures and develop efficient trellis-coded modulation systems using these encoders. In addition, we will address the performances evaluation for the proposed TCM schemes over fading channels. Considering the properties of the QAM-TCM encoders presented in this paper, we also aim to analyze the turbo TCM scheme with optimum RC encoders over GF(2^N).

 ISBN: 978-1-61208-123-6

ACKNOWLEDGEMENT

This work was supported in part by the Romanian UEFISCSU PN-2 RU-TE Project no. 18/12.08.2010 and by the Romanian contract POSDRU/89/1.5/S/62557.

REFERENCES

[1] D. R. Frey, "Chaotic digital encoding: An approach to secure communication," IEEE Trans. Trans. Circ. and Syst. – II, vol. 40, Oct. 1993, pp. 660-666, doi: 10.1109/82.246168.

[2] M. J. Werter, "An improved chaotic digital encoder," IEEE Trans. Circuits and Systems – II: Analog and Digital Signal Processing, vol. 45, Feb. 1998, pp. 227–229, doi: 10.1109/82.661656.

[3] T. Aislam and J.A. Edwards, "Secure communications using chaotic digital encoding," IEE El. Letters, vol. 32, Feb. 1996, pp. 190-191, doi: 10.1049/el:19960107.

[4] S.A. Barbulescu, A. Guidi, and S.S. Pietrobon, "Chaotic turbo codes," Proc. Int. Symp. on Info. Theory, June 2000, p. 123, doi: 10.1109/ISIT.2000.866415.

[5] C. Vlădeanu, S. El Assad, J.-C. Carlach, and R. Quéré, "Improved Frey Chaotic Digital Encoder for Trellis-Coded Modulation," IEEE Trans. Circ. and Syst. – II, vol. 56, June 2009, pp. 509-513, doi: 10.1109/TCSII.2009.2020936.

[6] C. Vlădeanu, S. El Assad, J.-C. Carlach, R. Quéré, and I. Marghescu, "Optimum PAM-TCM Schemes Using Left-Circulate Function over GF(2^N)," Proc. IEEE 9th Int. Symp. on Signals, Circ. and Syst. - ISSCS 2009, July 2009, pp. 267-270, doi: 10.1109/ISSCS.2009.5206092.

[7] C. Vlădeanu, S. El Assad, J.-C. Carlach, R. Quéré, I. Marghescu, "Optimum GF(2^N) Encoders Using Left-Circulate Function for PSK-TCM Schemes," Proc. 17th European Signal Proc. Conf. - EUSIPCO 2009, Aug. 2009, pp. 1171-1175.

[8] G. Ungerboeck, "Channel coding with multilevel/phase signals," IEEE Trans. Informalion Theory, Jan. 1982, pp.55-67, doi: 10.1109/TIT.1982.1056454.

[9] C. Vlădeanu, S. El Assad, J.-C. Carlach, R. Quéré, and C. Paleologu, "Chaotic Digital Encoding for 2D Trellis-Coded Modulation," Proc. IEEE 5th Advanced Int. Conf. on Telecomm. - AICT 2009, May 2009, pp. 152-157, doi: 10.1109/AICT.2009.32.

[10] A. F. Păun, C. Vlădeanu, I. Marghescu, S. El Assad, J.-C. Carlach, and R. Quéré, "New Recursive Convolutional GF(2^N) Encoders for Parallel Turbo-TCM Schemes," IEEE 6th Advanced Int. Conf. on Telecomm. - AICT 2010, Barcelona, Spain, 9-15 May 2010, pp. 182-186, doi: 10.1109/AICT.2010.76.

 ISBN: 978-1-61208-123-6

Generic Security Services API authentication support for the Session Initiation Protocol

Lars Strand
Norwegian Computing Center
Oslo, Norway
lars.strand@nr.no

Josef Noll
UniK-University Graduate Center
Kjeller, Norway
josef.noll@unik.no

Wolfgang Leister
Norwegian Computing Center
Oslo, Norway
wolfgang.leister@nr.no

***Abstract*—The mandatory and most deployed authentication method used in the Session Initiaton Protocol, the Digest Access Authentication method, is weak. Other, more secure authentication methods have emerged, but have seen little adoption yet. In this paper, support for using a generic authentication method, the Generic Security Services API, is added to the Session Initiaton Protocol. When using this method, the Session Initation Protocol does not need to support nor implement other authentication methods, only use the provided API library. This enables the Session Initiation Protocol to transparently support and use more secure authentication methods in a unified and generic way. As the suggested method includes a modification of the Session Initiation Protocol, an initial deployment strategy towards the Generic Security Services API authentication methods is added. To negotiate an authentication service, we use the pseudo security mechanism Simple and Protected GSS-API Negotiation Mechanism.**

***Keywords*—VoIP, SIP, authentication, GSS-API, SPNEGO.**

I. Introduction

Voice over IP (VoIP) is taking over for the traditional Public Switched Telephony Network (PSTN). At the end of 2009, 29.1 % of the private market in Norway was using VoIP (not including mobile phones). There has been a steady increase in the number of VoIP users since 2002, as well as a decrease in PSTN [1]. With two billion users worldwide having access to the Internet by the end of 2010 [2], the VoIP growth potential is huge.

Several proprietary and non-proprietary VoIP protocols have been created, but the protocol pair Session Initiation Protocol (SIP) and Real-time Transport Protocol (RTP) is emerging as the industry standard. RTP transfers the media content (voice), while SIP handles the signaling, i.e., setup, modification and termination of sessions between two or more participants. SIP is an open standard developed by the Internet Engineering Task Force (IETF) and specified in RFC3261 [3]. Additional functionality is specified in numerous Request For Comments (RFC) standard documents, making the SIP standard large and complex [4].

PSTN is a mature and stable technology providing 99.999% uptime [5], and users will expect VoIP to perform at similar service level. But with an increasing number of VoIP users, VoIP will become a target for attackers looking for financial gain or mischief. A clear threat taxonomy is given by the "VoIP Security Alliance" [6] and is discussed by Keromytis [7]. Several vulnerabilities exist [8] and securing SIP based installation is far from trivial [9].

In the EUX2010sec research project [10], we revealed, in close collaboration with our project partners, that most VoIP installations only use the mandatory, but weak, Digest Access Authentication (DAA) method [11]. In two case studies, with a VoIP installation supporting 3000 and 4700 phones respectively, the public tender for those VoIP installations greatly emphasized security and authentication requirements; requirements that DAA does not cover adequately. We have replicated the project partner's VoIP installation in our VoIP lab [12]. An attack against authentication has been analyzed [13] and countered [14].

The main contribution of this paper is to present and add support for the Generic Security Services Application Program Interface (GSS-API) to SIP. Different security requirements may require different authentication mechanisms. Instead of adding support for many different authentication mechanisms in SIP, support for GSS-API will provide a generic interface that makes different authentication methods transparent to the SIP protocol. To negotiate the best available authentication service between two peers, the Simple and Protected GSS-API NEGOtiation (SPNEGO) mechanism is used on top of GSS-API.

The rest of the paper is organized as follows: a brief overview of other SIP authentication methods is given in Section II. The GSS-API and SPNEGO as a GSS-API mechanism are explained in Section III and how the GSS-API can be supported and implemented in SIP is shown in Section IV. The industry evolution uptake strategy is briefly discussed in Section V before future work and the conclusion are presented in Section VI.

II. Authentication in SIP

When SIP was designed, functionality — and not security — was the primary goal. The results today are a number of uncovered vulnerabilites and attacks [15], [16]. SIP supports a wide range of functionalities that can be utilized, ranging from mobile handsets to high-end servers, each with different security requirements. Different security requirements may use different authentication methods depending on the

 ISBN: 978-1-61208-123-6

usage and threat scenario. For example, a mobile handset may have different requirements for authentication than that authentication between SIP servers. Additional requirements like power consumption and computational power must also be considered. Thus, adding new security services to SIP to improve the security design and meet different security requirements can be challenging.

The Digest Access Authentication (DAA) method is the mandatory and most used authentication method used with SIP [17]. DAA is heavily influenced by HTTP digest authentication. It relies on a cryptographic verification of a plaintext password shared between client and server. The client computes a MD5 hash value using the password, a nonce value received from the server, and a few SIP header values. The server computes the same digest, which then is compared against the one received from the client. If these digests are identical, the client has proven its identity and is authenticated. Unfortunately, the DAA is considered weak and is vulnerable to a series of attacks [8], including registration hijacking [14].

A more secure authentication method can be achieved by using Secure MIME (S/MIME) [18]. There, the entire SIP message is encapsulated in a MIME body that is signed and optionally encrypted. When the S/MIME header is received, the receiver checks whether the sender's certificate is signed by a trusted authority. A client must support multiple root certificates since there is no consolidated root authority that is trusted by all clients. This and other certificate handling issues like revoking and renewing complicates the use of certificates. Industry support for S/MIME has been limited [19].

Two other authentication methods have emerged within the Internet Engineering Task Force (IETF):

1) The *Asserted Identity* [20] is intended to work within a trusted environment. An additional, unprotected SIP header is sent in clear that informs that the identity of the client has been checked. Since the SIP header is sent in clear rather than protected by cryptography methods, it can easily be removed by an attacker without any of the communicating peers noticing this.
2) The *SIP Strong Identity* [21] introduces a new SIP service, the "authentication service", which signs a hash over selected SIP header values, and includes the signature as a SIP header along with a URI that points to the sender's certificate. The receiver computes the same hash and compares the results. Using this method, only the client is authenticated. As above, an attacker can remove these headers without implications.

Note that both of these authentication methods rely on a successful DAA authentication to be applicable. These are also applied by the SIP servers rather than the clients themselves, and are thus only providing indirect authentication of the client since the server is authenticating on behalf of the client.

III. GSS-API WITH SPNEGO

The GSS-API [22] provides a generic interface for application layer protocols like SIP, with a layer of abstraction for different security services like authentication, integrity or confidentiality. With the GSS-API, an application does not need to support or implement every authentication method, but use the provided security API [23]. The GSS-API is developed by the IETF and has been scrutinized by security professionals over the years. It has been extensively tested, and is now classified as a mature standard by the IETF. Further extensions and improvements to GSS-API are done by IETF's "kitten" Working Group [24].

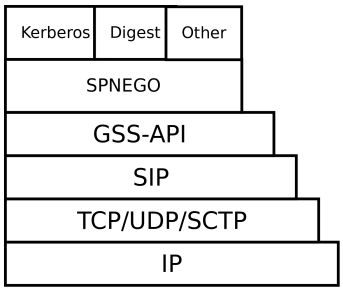

Figure 1: The GSS-API protocol stack with the SPNEGO negotiation mechanism and underlying security mechanisms.

The GSS-API is not a communication protocol in itself, but relies on the application to encapsulate, send, and extract data messages called "tokens" between the client and server. The tokens' content are opaque from the viewpoint of the calling application, and contain authentication data, or, once the authentication is complete, portion of data that the client and server want to sign or encrypt. The tokens are passed through the GSS-API to a range of underlying security mechanisms, ranging from secret-key cryptography, like Kerberos [25], to public-key cryptography, like the Simple Public-Key GSS-API Mechanism (SPKM) [26]. For an application, the use of the GSS-API becomes a standard interface to request authentication, integrity, and confidentiality services in a uniform way. However, GSS-API does not provide credentials needed by the underlying security mechanisms. Both server and client must aquire their respective credentials before GSS-API functions are called.

To establish peer entity authentication, a security context is initialized and established. After the security context has been established, additional messages can be exchanged, that are integrity and, optionally, confidentially protected. To initiate and manage a security context, the peers use the *context-level* GSS-API calls. The client calls `GSS_Init_sec_context()` that produces a "output_token" that is passed to the server. The server then calls `GSS_Accept_sec_context()` with the received token as input. Depending on the underlying security mechanism, additional token exchanges may be required in the course of context establishment. If so, `GSS_S_CONTINUE_NEEDED` status is set and additional tokens are passed between the client and server until a security context is established, as depicted in Figure 4.

After a security context has been established, *per-message* GSS-API calls can be used to protect a message by adding

 ISBN: 978-1-61208-123-6

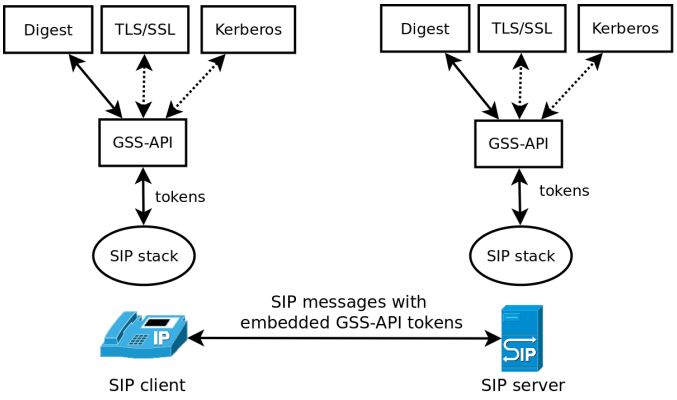

Figure 2: The GSS-API interface in SIP.

a Message Integrity Code (MIC) with `GSS_GetMIC()` and verifying the message with `GSS_VerifyMIC()`. To encrypt and decrypt messages, the peers can use `GSS_Wrap()` and `GSS_Unwrap()`. Thus, two different token types exist:

1) *Context-level tokens* are used when a context is established.
2) *Per-message tokens* are used after a context has been established, and are used to integrity or confidentiality protect data.

In addition to send and receive tokens, the application is responsible to distinguish between token types. This is necessary because different tokens types are sent by the application to different GSS-API functions. But since the tokens are opaque to the application, the application must use a method to distinguish between the token types. In our solution, we use explicit tagging of the token type that accompanies the token message.

SPNEGO [27] is a pseudo security mechanism that enables peers to negotiate a common set of one or more GSS-API security mechanisms. The GSS-API stack with SPNEGO is shown in Figure 1. The client sends a prioritized list of supported authentication mechanisms to the server. The server then chooses the preferred authentication method based on the received list from the client. The client initiates `GSS_Init_sec_context()` as with an ordinary GSS-API security mechanism, but requests that SPNEGO is used as the underlying GSS-API mechanism ("mech_type"). The SPNEGO handshake between client and server is communicated by sending and receiving tokens. After the handshake, the client and server initiate and set up a security context (authentication) using the agreed GSS-API security mechanism.

IV. GSS-API SUPPORT FOR SIP

Instead of adding numerous different authentication methods to SIP based on different security requirements, it is desirable to keep the changes to the SIP standard to a minimum. The industry might also be reluctant to adopt immature and non-standardized security services, like different authentication methods. Adding support for the GSS-API requires only one small change to the SIP standard, and will open up for a wide range of different authentication methods. In the following subsections, we outline how to include support for the GSS-API into the SIP authentication to replace the original weak DAA.

A. SIP authentication using DAA

When a SIP client is authenticated to a server using DAA, the authentication handshake data is encapsulated in the `WWW-Authenticate` header from server to client, and the `Authorization` header from client to server. We reuse these headers for GSS-API support, and instead of encapsulate DAA data, we send the GSS-API tokens. An example of both DAA `Authorization` header and the new `Authorization` header with GSS-API data is depicted in Figure 3.

During the initialization of a security context it is necessary to identify the underlying security mechanism to be used. The caller initiating the context indicates at the start of the token the security (authentication) mechanism to be used. The security mechanism is denoted by a unique Object Identifier (OID). For example, the OID for the Kerberos V5 mechanism is `1.2.840.113554.1.2.2`. However, there is no way for the initiating peer to know which security mechanism the receiving peer supports. If an unsupported "mech_type" is requested, the authentication fails. The GSS-API standard resolves this by recommending to manually standardizing on a fixed "mech_type" within a domain. Since SIP addresses are designed to be global [28], and not confined to a local domain, a GSS-API *negotiation* mechanism is required. The SPNEGO is such a GSS-API negotiation mechanism.

B. SIP authentication using GSS-API and SPNEGO

When using GSS-API with the SPNEGO mechanism, the number of SIP messages between client and server during authentication needs to be increased. During a DAA authentication, the client sends a `REGISTER` message to the server. The server, upon receiving a `REGISTER`, challenges the client with a nonce. The client then generates a digest response, a hash value computed over several SIP header values, the nonce, and a shared secret. The client then re-sends the `REGISTER` message with the digest response embedded. The message flow of a SIP DAA handshake is shown in the first four messages depicted in Figure 4.

In the following paragraphs, the numbers in parentheses refer to the numbers in Figure 4. When a client comes online and registers itself to a "location service" (SIP server), it does so by sending a SIP `REGISTER` message (1). We define the token type in the variable `ttype`. In the following messages, the `ttype` is set to "context" indicating that these tokens are *context-level tokens*. The first message (1) does not contain any `Authorization` header. The server responds with an empty `WWW-Authenticate` header (3):

```
REGISTER SIP/2.0
WWW-Authenticate: GSSAPI ttype="context"
  token=""
```

```
1.  REGISTER sip:CompanyA SIP/2.0
2.  Via: SIP/2.0/UDP 192.168.1.102;branch=z9hG4bK32F3EC44EB23347BFB0D488459C69E4E
3.  From: Alice <sip:alice@CompanyA>;tag=1234648905
4.  To: Alice <sip:alice@CompanyA>
5.  Contact: "Alice" <sip:alice@192.168.1.102:5060>
6.  Call-ID: 2B6449C74C10D4F95006A6C034E79E8E@CompanyA
7.  CSeq: 19481 REGISTER
8.  User-Agent: PolycomSoundPointIP-SPIP_550-UA/3.1.2.0392
9.  Authorization: Digest
    username="alice",realm="asterisk",nonce="3b7a1395",response="ccbde1c3c129b3dcaa14a4d5e35
    519d7",uri="sip:CompanyA",algorithm=MD5
10. Max-Forwards: 70
11. Expires: 3600
12. Content-Length: 0
```

```
1.  REGISTER sip:CompanyA SIP/2.0
2.  Via: SIP/2.0/UDP 192.168.1.102;branch=z9hG4bK32F3EC44EB23347BFB0D488459C69E4E
3.  From: Alice <sip:alice@CompanyA>;tag=1234648905
4.  To: Alice <sip:alice@CompanyA>
5.  Contact: "Alice" <sip:alice@192.168.1.102:5060>
6.  Call-ID: 2B6449C74C10D4F95006A6C034E79E8E@CompanyA
7.  CSeq: 19481 REGISTER
8.  User-Agent: PolycomSoundPointIP-SPIP_550-UA/3.1.2.0392
9.  Authorization: GSSAPI ttype="context"
    token="0401000B06092A864886F712010202DACD139402AAF44350CDE32"
10. Max-Forwards: 70
11. Expires: 3600
12. Content-Length: 0
```

Figure 3: A SIP `REGISTER` message with the original DAA `Authorization` header to the left, and the same header carrying GSS-API data to the right.

The client then calls `GSS_Init_sec_context()` with SPNEGO as underlying GSS-API mechanism to negotiate a common authentication mechanism (4). The GSS-API "mech_type" is set to SPNEGOs OID `1.3.6.1.5.5.2`. The token data might be in binary format, depending on the security mechanism used. Since the SIP headers are in ASCII string format, the token data is base64 encoded:

```
SIP/2.0 401 Unauthorized
Authorization: GSSAPI ttype="context"
  token="0401000B06092A864886F7120..."
```

The server retrieves the GSS-API data, the token, and passes this to the SPNEGO GSS-API mechanism. In this first initial token, the client embeds authentication data for its first preferred authentication mechanism. This way, should the server accept the clients preferred mechanism, we avoid an extra SIP message round trip. If the client's preferred method was accepted by the server, the server passes the relevant authentication data to the selected authentication mechanism in a `401` SIP message (5). The selected authentication method continues to pass tokens between client and server as many times as necessary to complete the authentication (6-7-N) and establish a security context. Once the security context is established, it sends a `200 OK` SIP message (N+2). Should the server have some last GSS-API data to be communicated to the client to complete the security context, it can be carried in a `WWW-Authenticate` header embedded in the `200 OK` message:

```
SIP/2.0 200 OK
WWW-Authenticate: GSSAPI ttype="context"
  token="dd02c7c2232759874e1c20558701..."
```

If the client's preferred mechanism is not the server's most preferred mechanism, the server outputs a negotiation token and sends it to the client embedded in a new `401` SIP message (5). The client processes the received SIP message and passes the authentication data to the correct authentication mechanism. The GSS-API then continues as described in the previous paragraph.

V. Evolution strategy

Industrial uptake of new ideas and protocols requires an evolution strategy, especially in the telecom world where standards are used to serve more than four billion people. TCP/IP, IPv6, and UMTS are all examples of technologies where the evolutionary path was not clearly identified, and the technological uptake was significantly delayed.

Authentication for SIP-based services will not only be limited to mobile handsets and SIP authentication servers, it will be used for sensors and devices in the future Internet of Things (IoT). Thus the basic requirement of an advanced authentication scheme is modularity and flexibility: both of these are provided by the suggested approach. Support for the GSS-API will extend the SIP protocol with an improved security mechanism that offers more flexibility in different scenarios.

An industrial uptake will first be envisaged for mobile devices such as smartphones or tabs, where SIP clients can be provided with the new functionality. Discussions with industrial actors are ongoing to ensure the compatibility on the server side. After this initial phase, an extension of the approach is envisaged including access to services in a sensor network.

VI. Conclusion and future work

Since the only mandatory and widely deployed Digest Access Authentication method in SIP is weak, other more secure authentication methods are desired. In this paper, we have added support for GSS-API in SIP, as well as for the SPNEGO mechanism that is used to negotiate the preferred GSS-API security mechanism supported by both client and server. The required change to the SIP protocol has been kept to a minimum, and the authentication header from DAA has been reused to prevent adding additional SIP headers to the standard.

Different VoIP installations have different security requirements that may require different security services. We have shown that the use of the GSS-API provides SIP with a wide range of different authentication methods in a uniform and standardized way. Different authentication methods can be used depending on the different security requirements for each SIP installation. This adds to the flexibility of SIP, like adding a new authentication method, without requiring further changes to the SIP standard, once the GSS-API is supported.

In our earlier work, we have shown that the DAA is weak [14]. Therefore, we want to replace DAA with support for a better, more robust authentication scheme that authentication methods like GSS-API supports. This implies that we *replace*

 ISBN: 978-1-61208-123-6

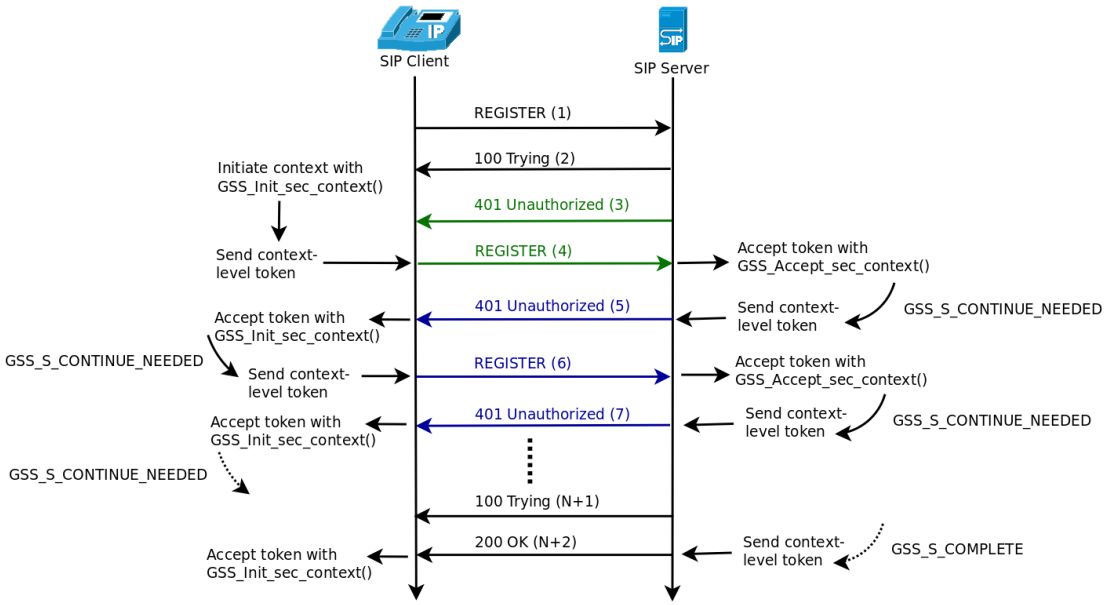

Figure 4: SIP `REGISTER` message flow with GSS-API security context establishment (authentication).

the original DAA header content with GSS-API data content. However, since the GSS-API only is an interface to underlying security mechanisms, the use of the GSS-API does not in itself provide any security service. Thus, the security of the GSS-API is no stronger than the weakest security mechanism acceptable to the client and server using the GSS-API. So, if the underlying GSS-API authentication mechanism does not protect relevant SIP headers, it might be as vulnerable to the attack shown previously with the DAA. We still need to examine what kind of SIP message integrity protection is offered by the different GSS-API authentication mechanisms.

The credential acquisition between peers must also be completed before initiating the GSS-API. Also, if the SPNEGO negotiation is not integrity-protected, the negotiation is vulnerable to a man-in-the-middle "down-grade" attack. An attacker can intercept and modify the negotiation messages so that the least favorable authentication method is used.

Future work will look into different GSS-API security mechanisms and their implications for SIP, including overhead evaluation benchmark. Implementing a proof of concept with GSS-API support for SIP is also desired. We plan to cooperate with the IETF and the "kitten" WG to further elaborate the GSS-API for SIP. Further challenges are the Simple Authentication and Security Layer (SASL) [29] for SIP, and a comparison of SASL with GSS-API, as well as the support for using GSS-API mechanisms within SASL [30].

Acknowledgment

This research is funded by the EUX2010SEC project in the VERDIKT framework of the Norwegian Research Council (Norges Forskningsråd, project 180054). The authors would like to thank Trenton Schulz and the anonymous reviewers for valuable comments on earlier drafts of this paper.

References

[1] "Det norske markedet for elektroniske kommunikasjonstjenester 2009 (The Norwegian market for electronic communication services 2009)," Post- og teletilsynet (The Norwegian Post and Telecommunications Authority), 2010. [Online]. Available: http://www.npt.no/ikbViewer/Content/119027/Ekomrapport_2009_.pdf 10. Jan 2011

[2] Telecommunication Development Sector (ITU-D), "The world in 2010," ITU-T ICT facts and figures, 2010.

[3] J. Rosenberg, H. Schulzrinne, G. Camarillo, A. Johnston, J. Peterson, R. Sparks, M. Handley, and E. Schooler, "SIP: Session Initiation Protocol," RFC 3261 (Proposed Standard), Internet Engineering Task Force, Jun. 2002, updated by RFCs 3265, 3853, 4320, 4916, 5393, 5621, 5626, 5630, 5922, 5954, 6026. [Online]. Available: http://www.ietf.org/rfc/rfc3261.txt 10. Jan 2011

[4] H. Sinnreich and A. B. Johnston, Internet communications using SIP: Delivering VoIP and multimedia services with Session Initiation Protocol, 2nd ed. New York, NY, USA: John Wiley & Sons, Inc., August 2006.

[5] D. Kuhn, "Sources of failure in the public switched telephone network," Computer, vol. 30, pp. 31–36, 1997.

[6] VoIPSA, "VoIP security and privacy threat taxonomy," Public Realease 1.0, Oct. 2005. [Online]. Available: http://voipsa.org/Activities/VOIPSA_Threat_Taxonomy_0.1.pdf 1. Nov 2011

[7] A. D. Keromytis, "Voice over IP: Risks, Threats and Vulnerabilities," in Proceedings of the Cyber Infrastructure Protection (CIP) Conference, New York, June 2009.

[8] H. Dwivedi, Hacking VoIP: Protocols, Attacks, and Countermeasures, 1st ed. No Starch Press, Mar. 2009.

[9] A. D. Keromytis, "Voice-over-IP security: Research and practice," IEEE Security & Privacy Magazine, vol. 8, no. 2, pp. 76–78, 2010.

[10] "Research project: EUX2010SEC – Enterprise Unified Exchange Security"." [Online]. Available: http://www.nr.no/pages/dart/project_flyer_eux2010sec 1. Nov 2011

[11] L. Fritsch, A.-K. Groven, L. Strand, W. Leister, and A. M. Hagalisletto, "A Holistic Approach to Open Source VoIP Security: Results from the EUX2010SEC Project," International Journal on Advances in Security, no. 2&3, pp. 129–141, 2009.

[12] L. Strand, "VoIP lab as a research tool in the EUX2010SEC project," Norwegian Computing Center, Department of Applied Research in Information Technology, Tech. Rep. DART/08/10, April 2010.

[13] A. M. Hagalisletto and L. Strand, "Formal modeling of authentication in SIP registration," in Second International Conference on Emerging

 ISBN: 978-1-61208-123-6

Security Information, Systems and Technologies SECURWARE '08. IEEE Computer Society, August 2008, pp. 16–21.

[14] L. Strand and W. Leister, "Improving SIP authentication," in Accepted for publication in The Tenth International Conference on Networks (ICN 2011), Jan 2011.

[15] A. M. Hagalisletto and L. Strand, "Designing attacks on sip call set-up," International Journal of Applied Cryptography, vol. 2, no. 1, pp. 13–22(10), July 2010. [Online]. Available: http://inderscience.metapress.com/link.asp?id=jh437k6747064307 10. Jan 2011

[16] A. D. Keromytis, "A Survey of Voice Over IP Security Research," in Proceeding of the 5th International Conference on Information Systems Security (ICISS), December 2009, pp. 1 – 17.

[17] J. Franks, P. Hallam-Baker, J. Hostetler, S. Lawrence, P. Leach, A. Luotonen, and L. Stewart, "HTTP Authentication: Basic and Digest Access Authentication," RFC 2617 (Draft Standard), Internet Engineering Task Force, Jun. 1999. [Online]. Available: http://www.ietf.org/rfc/rfc2617.txt 10. Jan 2011

[18] J. Peterson, "S/MIME Advanced Encryption Standard (AES) Requirement for the Session Initiation Protocol (SIP)," RFC 3853 (Proposed Standard), Internet Engineering Task Force, Jul. 2004. [Online]. Available: http://www.ietf.org/rfc/rfc3853.txt 10. Jan 2011

[19] D. Sisalem, J. Floroiu, J. Kuthan, U. Abend, and H. Schulzrinne, SIP Security. WileyBlackwell, Mar. 2009.

[20] C. Jennings, J. Peterson, and M. Watson, "Private Extensions to the Session Initiation Protocol (SIP) for Asserted Identity within Trusted Networks," RFC 3325 (Informational), Internet Engineering Task Force, Nov. 2002, updated by RFC 5876. [Online]. Available: http://www.ietf.org/rfc/rfc3325.txt 10. Jan 2011

[21] J. Peterson and C. Jennings, "Enhancements for Authenticated Identity Management in the Session Initiation Protocol (SIP)," RFC 4474 (Proposed Standard), Internet Engineering Task Force, Aug. 2006. [Online]. Available: http://www.ietf.org/rfc/rfc4474.txt 10. Jan 2011

[22] J. Linn, "Generic Security Service Application Program Interface Version 2, Update 1," RFC 2743 (Proposed Standard), Internet Engineering Task Force, Jan. 2000, updated by RFC 5554. [Online]. Available: http://www.ietf.org/rfc/rfc2743.txt 10. Jan 2011

[23] D. Todorov, Mechanics of User Identification and Authentication: Fundamentals of Identity Management, 1st ed. Auerbach Publication, Jun. 2007.

[24] "IETF Common Authentication Technology Next Generation (kitten)." [Online]. Available: http://datatracker.ietf.org/wg/kitten/charter/ 1. Nov 2011

[25] L. Zhu, K. Jaganathan, and S. Hartman, "The Kerberos Version 5 Generic Security Service Application Program Interface (GSS-API) Mechanism: Version 2," RFC 4121 (Proposed Standard), Internet Engineering Task Force, Jul. 2005. [Online]. Available: http://www.ietf.org/rfc/rfc4121.txt 10. Jan 2011

[26] C. Adams, "The Simple Public-Key GSS-API Mechanism (SPKM)," RFC 2025 (Proposed Standard), Internet Engineering Task Force, Oct. 1996. [Online]. Available: http://www.ietf.org/rfc/rfc2025.txt 10. Jan 2011

[27] L. Zhu, P. Leach, K. Jaganathan, and W. Ingersoll, "The Simple and Protected Generic Security Service Application Program Interface (GSS-API) Negotiation Mechanism," RFC 4178 (Proposed Standard), Internet Engineering Task Force, Oct. 2005. [Online]. Available: http://www.ietf.org/rfc/rfc4178.txt 10. Jan 2011

[28] L. Strand and W. Leister, "A Survey of SIP Peering," in NATO ASI - Architects of secure Networks (ASIGE10), May 2010.

[29] A. Melnikov and K. Zeilenga, "Simple Authentication and Security Layer (SASL)," RFC 4422 (Proposed Standard), Internet Engineering Task Force, Jun. 2006. [Online]. Available: http://www.ietf.org/rfc/rfc4422.txt 10. Jan 2011

[30] S. Josefsson and N. Williams, "Using Generic Security Service Application Program Interface (GSS-API) Mechanisms in Simple Authentication and Security Layer (SASL): The GS2 Mechanism Family," RFC 5801 (Proposed Standard), Internet Engineering Task Force, Jul. 2010. [Online]. Available: http://www.ietf.org/rfc/rfc5801.txt 10. Jan 2011

 ISBN: 978-1-61208-123-6

Technical Criteria for Value-Added Services Creation, Execution and Deployment, on Next Generation Networks

Gerardo Rojas Sierra
University of Cauca
Engineering Telematics Group
Popayán, Colombia
gerardorojas@unicauca.edu.co

Oscar M Caicedo Rendon
University of Cauca
Engineering Telematics Group
Popayán, Colombia
omcaicedo@unicauca.edu.co

Felipe Estrada Solano
University of Cauca
Engineering Telematics Group
Popayán, Colombia
cfestrada@unicauca.edu.co

Julian A Caicedo M
University of Cauca
Engineering Telematics Group
Popayán, Colombia
jacaicedo@unicauca.edu.co

***Abstract*—Create new services, in a faster way and at lower costs in order to attract new customers, keep existing ones and increase revenue, is the great target for telecom operators. This is possible with concepts like Next Generation Networks (NGNs), Service Delivery Platforms (SDPs) and Service Oriented Architecture (SOA), due to they enable the integration of the Telecommunications and Information Technologies (IT) domains. However, the telecom operators of non-developing countries have a limited knowledge about the technologies that adapt better to their needs, and how they can be used and integrated into their networks for Value-Added Services (VAS) provisioning. Therefore, a set of technical criteria that supports telecom operators in non-developing countries for VAS creation, execution and deployment, is proposed in this paper. In the same way, a general scheme for the establishment, description and definition of technical criteria is proposed under the context of NGN telecom operators with Softswitch in the control layer (without IP Multimedia Subsystem (IMS) control layer). Then, the Color/Caller Ring Back Tone (CRBT) as VAS, is developed for testing the general scheme and the technical requirements proposed. For this matter, Rhino Service Logic Execution Environment (SLEE) (Java Application Programming Interface (API) for Integrated Networks (JAIN) SLEE 1.1 specification compliance) was used. Furthermore, the results of CRBT integration into a real environment (NGN of EMCALI Colombian telecom operator) are presented. Finally, some conclusions are presented.**

Keywords- JAIN; SDP; SLEE; NGN; Technical Criteria VAS.

I. INTRODUCTION

Nowadays, telecom services providers understand their necessity to create new services in a faster way and at lower costs in order to attract new customers, as well as maintain the existing ones and increase revenue. New telecommunications services require more flexible systems with high levels of performance, large scalability and based on open standards [1]. The Next Generation Networks (NGNs) are the solution to almost all these challenges, defining a reference architecture that enables the development of new telecom services and integrates both legacy networks and Internet Protocol (IP) based ones. Today, many paradigms and technologies have emerged to develop and deploy this trend. This is the case of Service Delivery Platforms (SDPs), which was created with the idea of adapting the business model philosophy from the Information Technology context to the telecom domain.

Many research teams and communications companies look for those technologies that implement or adapt better to the SDP architecture, focusing on the solution for telecom service providers. However, a lot of telecom operators, mainly in the non-developing countries, have a lack of knowledge about how to integrate or exploit those emerging technologies for Value-Added Services (VAS) provisioning. Therefore, making technological changes is not simple and does not guarantee an optimal performance or good revenue to those telecom operators. Consequently, it is necessary to define technical criteria to be considered by telecom operators from non-developing countries in order to offer VAS on NGN. As a result this paper proposes: i) different technical criteria to be considered for VAS creation, execution and deployment on NGN with Softswitch in the control layer (non IP Multimedia Subsystem (IMS) in the control layer), and with SDP in the application layer. These criteria allow deciding the architecture and the required components to achieve a correct VAS provisioning. ii) A framework for organizing the technical criteria defined. For showing it, the reminder of this paper is organized as follows. Section 2 mentions the related work. Section 3 presents the technical criteria definition and the framework. Section 4 shows the implementation of the technical criteria under a study case. Finally, Section 5 presents the conclusions.

 ISBN: 978-1-61208-123-6

II. RELATED WORK

In [2], a SDP is proposed in order to integrate both Telecommunication and (IT) industries. This SDP is focused on creation and execution control of IMS convergent services. However, for non-developing countries, where IMS has not been totally deployed, it is not possible to adapt those technical recommendations. This paper is only focused on technologies such as Parlay-X and on the Open Mobile Alliance (OMA), but Java Application Programming Interface (API) for Integrated Networks (JAIN) is not considered.

Tselikas et al. [3] presents an efficient performance comparison between several similar middleware systems based on open APIs and service protocols. The paper describes the implementation of telecom services supported by open interfaces and standard protocols exposing call control network functions. It analyzes a middleware implementation based on a subset of technologies, such as Open Service Architecture (OSA)/Parlay APIs, JAIN APIs and SIP, regarding call control functionality.

Femminella et al. [4] describes a Session Initiation Protocol (SIP) based call control service for Internet Telephony, designed for an IP-Public Switched Telephone Network (PSTN) converged scenario. The authors work with a service based on the Back-To-Back User Agent (B2BUA) architecture. The service is deployed into a Service Logic Execution Environment (SLEE) [5] based on Mobicents [6]; an open-source platform for telecom applications, which offers a JAIN SLEE specification implementation. In this case [4] doesn't address all the technical criteria to be considered in VAS development, and deployment.

In [7], the authors present a practical deployment of a contextual service offered by a convergent telecom operator, whose functionality is to provide intelligent context-based call routing and rerouting, orchestrated from the operator service layer. Nevertheless, [7] is based on IMS control layer capabilities to properly capture the user context in a ubiquitous coverage area, and it doesn't propose a schema for organizing the technical criteria for VAS creation.

III. TECHNICAL CRITERIA FRAMEWORK

Figure 1 shows the general outline proposed structure for defining the technical criteria required for VAS provisioning.

A. VAS View

Telecom operators and third parties develop services defined in the VAS view. These new services should be defined for allowing market differentiation and the increasing of the operator revenues.

NGN Environment

NGN defines a reference architecture that enables the development of new telecom services and integrates both legacy networks and IP-based ones. Thus, it is necessary define clearly the NGN context to be used for VAS provisioning.

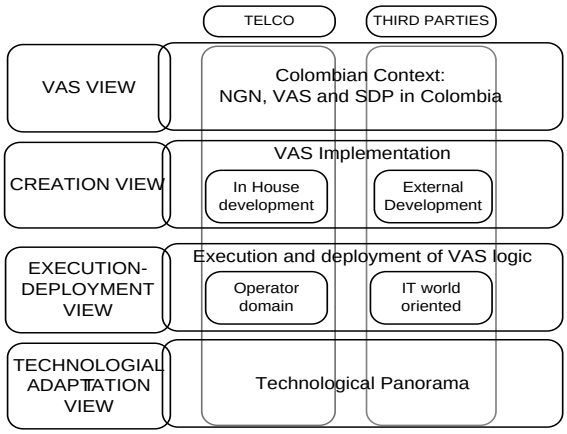

Figure 1. Framework for VAS creation, execution and deployment.

VAS Environment

There is not VAS standard definition. The VAS concept depends on the law regulations and the market context in each country. Therefore, it is extremely important to set a clear VAS definition and to establish a fully description. In order to do this, a functionality description based on states machines is recommended.

SDP Environment

It is vital for telecom operators to develop, deploy, implement, coordinate and manage new services, efficiently and effectively, generating higher incomes and maintaining low prices. These platforms enable telecom operators to have a complete environment for the creation, deployment, implementation, management and billing of a wide range of services and value-added content. Here, the main idea is to establish the environment(s) used for VAS provisioning, giving support to legacy infrastructure.

B. CreationView

In this case, the technical criteria are defined from two points of view: Third Parties and Telecom Operators.

Third Parties

Telecom operators need to increase the VAS portfolio. In order to do this, they must allow a safely interaction of third parties with their network infrastructure. Thus, in this case, open technologies, high level APIs network abstraction and solutions based on Web Services (WS), provides to IT developers, tools to develop more advanced services into telecom domain. Technologies such as OSA/Parlay [8], Parlay X [9] and Open network enablers API (OneAPI) [10], which is based on existing specifications, such as Parlay X, and has improved them to be far easier for Web developers to use, were designed with the intention of exposing network facilities to external domains through several protocols. In the other hand, Resources Adapters (RAs) from JAIN SLEE technology also enable network abstraction and third parties connection. Therefore, with these technologies a telecom operator is allowed to open its network in order to increase its services portfolio.

 ISBN: 978-1-61208-123-6

Telco

It is important to know the technical criteria on the telecom operator side in order to find the most efficient way of creating and having a short time-to market.

Programmable APIs: define software components that abstract network protocols and allow the new applications development. The abstraction level can be classified like high, medium and low. For IT developers, it is recommendable use high level APIs. The other ones require a detailed knowledge about the mechanisms, the protocols and the infrastructure.

Scripting Language: scripting languages are appropriate technologies for faster application development due to the fact that they are used to connect existing components. They are lightweight and customizable interpreted languages based on eXtensible Markup Language (XML) representing the behavior of certain applications, making it possible to change at runtime. Therefore, the XML use may offer services customization and composition.

Service Creation Environment (SCE): a SCE should be based on open technologies and standards. A service usually developed by a SCE proprietary, it only runs in the SLEE of the same ownership, whereas a service created with a standard SCE can be implemented with few changes within any SLEE that supports the respective standard. For mentioned reason, here it is recommended to use standardized tools based on Java. Thus, it is possible to get better interoperability and costs decrease.

C. Execution and Deployment View

These technical criteria are developed from two points of view: third parties and telecom operators.

Third Parties

Integrating the IT world with NGN capabilities will enable to enrich the services offered to users and most important, it will enable third parties to develop new faster applications that impact the telecom services market. Hence, the idea is working with Java Enterprise Edition (JEE) [11] technology for third parties. This will make an easier and clearer communication possible between application providers and telecom operators, due to many telecommunication servers are based on Java SIP Servlets [1] or JAIN SLEE. Besides, a lot of services platforms based on Parlay X are also supported on Java.

Telecom Operator

It is extremely important that the operator has a service execution environment that optimizes the execution and deployment of convergent applications which are meeting the telecommunications requirements.

Performance: to achieve high performance, is desirable to use technologies to ensure high throughput and low latency. The architecture used here should meet these requirements. In this sense, JAIN SLEE is recommended. JAIN SLEE is a generic application environment designed specifically for supporting carrier-grade and event-driven requirements.

High Availability: in order to achieve high availability, the cluster server mechanisms are the most appropriate. These mechanisms increase the percentage of availability in critical environments such as telecom services. Although, the cluster configuration provides redundancy, it does not mean that high availability will be achieved. The reason for this affirmation is because of the fact that one node of the array can fail and the processed information will not be transmitted to the backup node automatically. Therefore, the memory synchronization process is also an important mechanism for high availability.

Reliability: an application server must include mechanisms to control bugs as well as robust processes that give the system the ability to bounce back and face different problems. In this case, the cluster active architecture is desirable.

Portable Service: in order to decrease the services development time is important to keep on the philosophy "written once, run anywhere" through technologies with high levels of interoperability between different Operating Systems (OSs), architectures and even other technologies, like the proposed by Java. This way, the selection of an execution environment based on JAIN SLEE standard, enables services to be developed and deployed with the least effort in any runtime environment compatible with the specification.

Event Driven Applications (EDA): to meet the requirements for telecom operators, the programmers need to develop applications over event-driven states and asynchronous platforms such as JAIN SLEE. Besides, the mechanisms of events distribution (service selection) enable a way to routing requests to the most appropriate functional blocks to process them.

D. Technological Adaption Criteria

The criteria in this view are focused on building a technology landscape that enables the operator to adopt and adapt any technologies into its network infrastructure in order to achieve convergence in any services that demand the NGN structures implementation.

Network abstraction layer

Here are considered all the technologies that enable the underlying network abstraction. This type of technologies exposes the capabilities that enable the smooth functioning of services, providing access to network resources. For example, into OSA/Parlay [8], JAIN, Parlay-X [9], OneAPI [10] and OMA [12], these capabilities are encapsulated in APIs which hide the network infrastructure complexity. Due to more abstraction high level, JAIN SLEE APIs are recommended. The JAIN SLEE RAs give a network high abstraction, as well as OneAPI, but this last one is focused on Web development, while the first one is oriented to telecom services. The Parlay APIs can be considered as medium level abstraction.

 ISBN: 978-1-61208-123-6

Product support and maturity

The adoption of execution environments and tools for VAS creation should be based on standard specifications. For this reason, it is extremely important to choose a standard that clearly defines the technology path (versions of the specification), the backwards compatibility and the adaptability to future technologies.

Learning curve

If a parameter for the VAS deployment is the time spent in application development, then third parties (external services) and telecom operators (in-house services) should select a high-level API. Thus, the service creation time can be decreased. Likewise, to enrich the applications, the developers should select a high-capacity technology in order to enable the development of many applications supported by different protocols (e.g., JAIN SLEE).

Roadmap

Organizations such as European Telecommunications Standars Institute (ETSI), Parlay Group, 3GPPP and Telco companies, continually, through their working groups, study and analyze new requirements in order to further enhance the capabilities of technologies related to services provisioning. In fact, many companies have opted for existing architectures such as OSA/Parlay and JAIN SLEE. Therefore, it is important that the selected SDP for meeting telecom operator requirements also has a clear roadmap for supporting the new specifications [13]. In this sense, the support of previous specifications is essential, too.

Future permeability

The telecom operators must adopt new technologies with facility of growth [14].

Test environment

Years ago, the telecom operators of non-developing countries did not have test environments due to huge economical costs. However, technological advancement and the IT and Telco domains integration have enabled the test environment appearance. In a test environment, it is important to use simulation tools to emulate the SDP components and to test performance, traffic and latency, features, among others. In addition to performance testing, it is also possible to analyze the services behavior. Therefore, it is desirable to create a test environment for decreasing the development and deployment time.

SOA

Criteria such as the Services Buildings Blocks (SBBs), the reuse of components, the composition and the orchestration, enable a model inside the service layer, which streamlines and promotes the creation, implementation and deployment of new services [15]. These services must be defined so that they have loosely coupled and be interoperable. For achieving it, SOA is the most appropriated technology.

IV. STUDY CASE

This section will describe the way like the above criteria were applied. Promptly, in order to do it, the EMCALI study case is shown. EMCALI telecommunications is a fixed-line operator in Colombia, a non-developing country.

A. VAS View

NGN Environment

The study case was developed into the EMCALI NGN. It has two Softswitch in the control layer, and an application layer built on the Parlay X standard release three. Besides, this NGN has interoperability with PSTN, Global System for Mobile communications (GSM), TErrestrial Trunked RAdio (TETRA), among others. Due to market changes and challenges, EMCALI requires adapting new technologies that support new services for VAS provisioning, allowing positioning in the market and revenue increase.

VAS Environment

The adopted VAS concept is: "*Next Generation Services that integrate the world telecommunications and information, allowing an operator to develop and deploy a wide range of potential service according to some key futures and capabilities expected in the NGN"* [16]. The Color /Caller Ring Back Tone (CRBT) service was taken into account due to its high-host in mobile networks. The CRBT VAS allows the subscriber to replace the traditional Ring Back Tone (RBT), and even the busy-status and the not-available-status tones, by audio components that have been downloaded and defined by himself through a customized interface [17][18]. The CRBT operation process is as follows: when a call from a subscriber *A* is directed to subscriber *B* (service user), the caller (subscriber *A*) hears a sound fragment replacing the RBT. There are several audio files to configure the CRBT, such as song fragments, melodies, voice recordings, promotional messages, sound effects, among others.

SDP Environment

The EMCALI operator does not have an SDP. This makes its participation difficult on the VAS market. Thus, to meet this requirement, the OpenCloud Rhino SDP was used, which is compliant with JAIN SLEE, the open Java standard for telecommunications event-driven application servers.

Figure 2 shows the solution proposed in this work:

--JAIN SLEE server: contains the CRBT prototype service logic blocks, and the modules to adapt it to outside resources.

--Media server: exposes the module to play the audio file that replaces the call RBT. It communicates with the JAIN SLEE server through Media Gateway Control Protocol (MGCP) messages.

--Enterprise Information System (EIS): includes the module responsible for storing user information and the

 ISBN: 978-1-61208-123-6

needed data for the CRBT prototype.

--Softswitch: contains the control and signaling units that handle the information flow of the EMCALI NGN. It communicates with the JAIN SLEE server through SIP messages.

--Transport network: refers to transport nodes that belong to the EMCALI NGN infrastructure.

-- The service logic CRBT prototype architecture is based on B2BUA because it offers the flexibility to handle all SIP call signaling between two users.

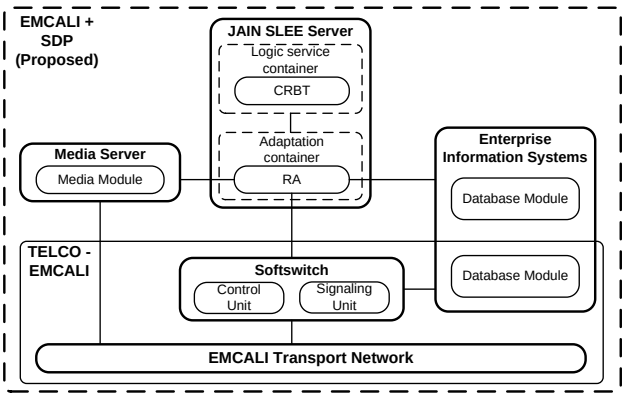

Figure 2: System solution modular architecture.

B. Creation View

The JAIN SLEE technology was selected because it allows abstraction at a high level, a not so steep learning curve for services creation and deployment. Besides, JAIN SLEE supports all SS7 protocols (including vendor variants) and all the IP/IMS protocols. As SCE, the Rhino Software Development Kit (SDK), by OpenCloud, and the Eclipse Integrated Development Environment (IDE) were used. Eclipse IDE easily integrated the libraries and plug-ins provided by OpenCloud to develop, deploy and test, the service. The SIP RA from OpenCloud (OCSIP RA) was used for binding the application layer and the control layer of the EMCALI NGN. Finally, the MGCP RA from Mobicents allowed the connection between the Rhino SLEE and the Mobicents Media Server (MMS).

C. Execution and Deployment View

Telco servers

It is extremely important to count with an execution environment geared exclusively for the telecom domain. As mention above, the JAIN SLEE technology is the most appropriate to meet the requirements of an operator like EMCALI. There are several JAIN SLEE implementations, such as Rhino SLEE [19], jNetX [20] and Mobicents JAIN SLEE [6]. In this case, Rhino SLEE by OpenCloud is highly recommended, because it is JAIN SLEE 1.1 specification fully compliant, it provides distinct licenses (open SDK, educational, commercial) and it supplies a complete set of RAs, tools, documentation and technical support.

Performance, high Availability and reliability

The technological developments made by OpenCloud, provide a robust environment to support large amounts of traffic, low latency, high availability, fault tolerance and overload. The active cluster architecture is widely used as a mechanism to resolve these high requirements.

Service Portability

The SBBs are the service basic elements that allow the development of reusable components with high performance operability [5]. The JAIN SLEE 1.1 specification defines a robust architecture that standardizes the RA, improving the interoperability and portability of its components.

EDA

Rhino SLEE is compliant with both versions 1.0 and 1.1 JAIN SLEE specification which are based on event-driven application model.

D. Technological Adaption Criteria

Rhino SLEE comprises a large number of RAs (SIP, Diameter, ISC, SOAP, SS7 family: INAP, CAP, MAP), allowing the development of applications that interact with all kind of network infrastructures.

Product support and maturity

JAIN SLEE is the only open standard for an application server designed to provide an execution environment for telecom services. Rhino SLEE, the selected JAIN SLEE implementation, is supported for a lot of companies such as Almira Labs, HP, Infocom, IBM, Motorola, Nokia Siemens, Sun (Oracle), among others.

Learning curve

This approach gathers the following three points: i) developer knowledge, where the selection of high-level APIs reduces the learning curve; ii) development and deploying time, which is decreased through high-level abstraction and service creation technology (e.g., EclipSLEE, OpenCloud JAIN SLEE plug-in); iii) high availability of tools.

Roadmap

The roadmap of JAIN SLEE technology and building services in Java is certainly promising. This community has highly distributed structured mechanisms and participation agreements for defining new recommendations.

Future Permeability

As well as JAIN SLEE achieves satisfactory scalability levels, technologies based on Java allow the constant binding and interoperability with emerging technologies to contribute to the new services enrichment [13].

E. Tests and results analysis

Signaling test

To proof that the CRBT service has been successfully integrated into the EMCALI NGN infrastructure, it has been registered the distinct messages of the different protocols present between the several equipments involved in a phone

 ISBN: 978-1-61208-123-6

call from a PSTN conventional phone to an IP domain Softphone, which has subscribed the CRBT service. Both user terminal devices are configured with numbers that are registered into the EMCALI Softswitch that has been configured to operate with the Rhino SLEE (see Figure 3).

Data recording was made using:

-- ZXNM01 ZTE Equipment Management System, which includes a signaling tool that logs the traffic sent and received by the Softswitch.

--Wireshark, a protocol analyzer that logs all the traffic that passes through the network which is connected to the computer where it has been installed.

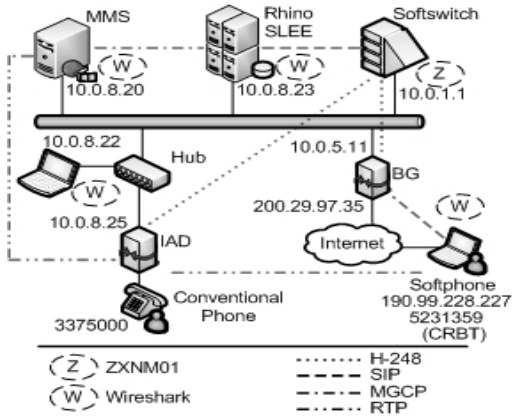

Figure 3: Network topology and test-design tools

F. Performance Test Description

The reference scenario used for the performance test was entirely independent from the EMCALI NGN. The Rhino SLEE Server 2.1 was deployed on a HP desktop PC with Intel Core 2 Duo E8300 @ 2.83 GHz; 2 GB RAM; OS Debian 5.0.4; Java Virtual Machine (JVM) 1.6.0_18 64 bit. The MMS 2.0.0.CR1 was deployed on a Gateway laptop PC with AMD Turion X2 TL-60 @ 2.0 GHz; 4 GB RAM; OS Debian 5.0.4; JVM 1.6.0_18 64 bit. The SIPp traffic generator was deployed on a HP laptop PC with Intel Core 2 Duo T9400 @ 2.53 GHz; 4 GB RAM; OS Linux Ubuntu 9.10. All computers were connected using a dedicated switch ZTE ZXR10 2826S Local Area Network, Ethernet 100 Based-TX.

Taking into account the MMS hardware features, it was configured to support 500 simultaneously multimedia sessions. Furthermore, the MMS source code was modified to solve an implementation failure. Moreover, the open files limit on OS Linux was incremented to 65535 due to the number of simultaneous calls to test.

Two different services were tested: the Traditional Call Service (TCS) and the CRBT service. Both services were configured in a SIPp scenario with 10 seconds call answer time and 3.5 minutes call duration. In the TCS, the MMS component doesn't operate.

The SIPp UAC and UAS were used to generate SIP traffic with an average rate equal to λ ranging: i) for TCS, from 10 to 110 calls per second (cps) in 10 cps steps; ii) for CRBT, from 10 to 50 cps in 10 cps steps. This last one has a smaller range due to MMS capacity limitations.

Each test was done with a constant λ value for 30 minutes. Before starting to collect statistics, a warm-up session of 15 minutes was performed to allow the Java Garbage Collector to be executed at least once and avoid JVM and JAIN SLEE transient effects [4].

G. Performance Test Metrics and Results

Throughput, obtained as the percentage of successful calls, and Session Request Delay (SRD) are used as performance metrics. SRD [21] is measured on the caller side and it is defined as the time interval from the initial INVITE to the first non-100 provisional response. It is used to measure the latency experienced by the caller when initiating the call session. Also, the CPU utilization was measured, which is extremely important to define hardware requirements.

Figure 4 shows that for up to 50 cps almost all call attempts were successful. Besides, taking into account that the operator handles 45 cps so during peak hours, this indicates that the development of CRBT using the technical criteria is appropriate.

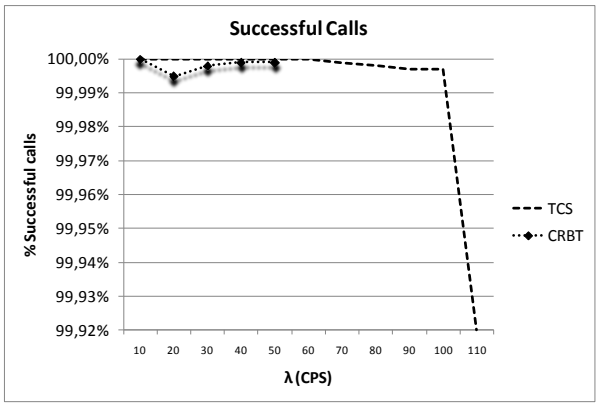

Figure 4: Throughput vs. cps

Figure 5 shows less than 100 ms between 0 and 50 cps, presenting a great performance and low latency in the response message.

The Creation View criteria were evaluated through two service implementation development time cases: while in this project the CRBT prototype service was built in four months, other project developers created a similar one in eight months [22], demonstrating the reduced development time with the JAIN SLEE use. Besides, after documentation, the components service (SBBs) building started soon and they were developed faster each time, exposing a slow learning curve of this technology. These SBBs were successfully deployed and tested in another JAIN SLEE implementation (Mobicents JAIN SLEE),

 ISBN: 978-1-61208-123-6

evaluating the service portability capacity provided by the standard release 1.1. On the other hand, high availability and reliability criteria were reached through the Rhino SLEE technological tool, due to its exclusive cluster architecture design.

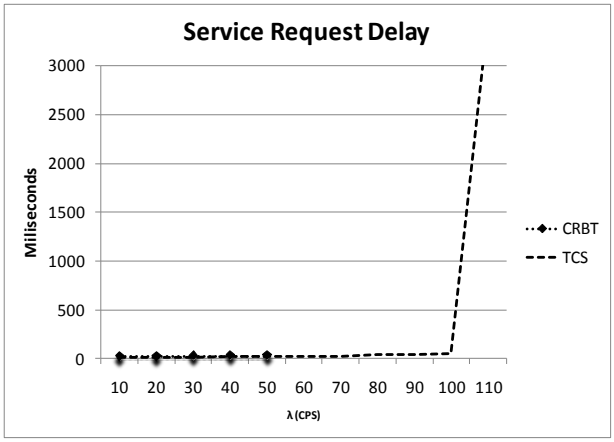

Figure 5: Average setup delay vs. cps

V. CONCLUSION

This paper presents technical criteria necessary for the creation, execution and development of VAS in NGN with Softswitch in the control layer. It also shows the technologies and tools for the creation, execution and development of VAS.

Within the development, implementation and deployment of VAS, the service execution environment is the key element in a NGSDP. This component must meet the high requirements in the Telco domain.

JAIN SLEE is the only open standard agreement for a telecom application server designed for high performance event-driven applications with reuse of components and high levels of growth.

The JAIN SLEE technology enables to make through its RA architecture, an abstraction of the transport layer of the NGN architecture, achieving rapid development and deployment of new applications and services.

The development of NGN applications is similar in many aspects to developing applications on the Internet, mostly because the main skills required for application development in this context are based on the use of Java and XML technologies. This makes creating applications more accessible to a broad community of developers, as it is easier, more productive and more creative.

The technical criteria defined allowed to decrease the development time, an outstanding achievement in the market context.

The technical criteria defined above, allowed meet the requirements for VAS provisioning on non-developing countries. This was demonstrated in the EMCALI operator study case.

REFERENCES

[1] N. Kryvinska, C. Strauss, L. Auer, and P. Zinterhof, "Conceptual Framework for Services Creation/Development Environment in Telecom Domain," 10th International Conferene on Information Integration and Web-based Applications & Services (iiWAS2008), Procedings ACM, pp. 324-33, November 2008, 978-1-60558-349-5/08/0011.

[2] S. Hiroshi, et. al., "Service Delivery Platform Architecture for the Next-Generation Network," [Online] [Cited: February 25, 2011.] http://www.icin.biz/files/2008papers/Session9A-2.pdf.

[3] N. Tselikas, G. Tselikis, and N. Sagias, "Software and Middleware Technologies based on Open APIs and Protocols for modern Service Provision in Telecoms," 14th Panhellenic Conference on Informartics (PCI 2010), pp. 33-37, September 2010, 978-1-4244-7838-5.

[4] M. Femminella, et al., "Design, Implementation, and Performance Evaluation of an Advanced SIP-based Call Control for VoIP Services" Dresden : s.n., 2009. Communications, 2009. ICC'09. On, pp. 1-5, August 2009, 978-1-4244-3435-0.

[5] D. Ferry, JSR 240 JAIN SLEE v1.1, [Online] [Cited: February 25, 2011.] http://jcp.org/en/jsr/detail?id=240.

[6] Mobicents Web Site, [Online] [Cited: February 25, 2011.] http://www.mobicents.org.

[7] A. Cadenas, A. Sanchez, and B. Carro, "Deployment of Contextual Corporate Telco Services Based on Protocol Adaptation in the NGN Environment.," Procedings IEE Communications Magazine, vol. 48, pp. 34-40, April 2010, 0163-6804.

[8] ETSI TISPAN., Open Service Access (OSA);Application Programming Interface (API);Part 1: Overview (Parlay 6). ETSI. 2008. Standar. ETSI ES 204 915-1 V1.1.1.

[9] M. Unmehopa, K. Vemuri, and A. Bennet, Parlay/OSA From Standards to Reality, Wiley, 2006, 296 p.

[10] D. Wang, M. Song, and Y. Li, "OneAPI Services and Java Implementation," Advanced Materials Research. Beijin, China, vol. 143 – 144, pp. 1159-1163, October 2010.

[11] Oracle, Java EE 6 Technologies, [Online] [Cited: February 25, 2011.] http://www.oracle.com/technetwork/java/javaee/tech/index.html.

[12] ITU NGN-GSI., ITU-T NGN FG Proceedings Part II. Ginebra : ITU, 2005.

[13] M. Femminella, et al., "Scalability and performance evaluation of a JAIN SLEE-based platform for VoIP services," 21st International Teletraffic Congress (ITC2009), pp. 1-8, October 2009, 978-1-4244-4744-2.

[14] J. Zuidweg, "Middleware en Telecomunicaciones." Tecsidel Tic. [Online] [Cited: February 25, 2011.] http://www.tecsidel.es/tecsidel/index.php?id=896&L=2.

[15] T. Van de Velde, Value-Added Services for Next Generation Networks. Boca Ratón : Auerbach Publications, 2008.

[16] J. Crimi, Next Generation Network (NGN) Services. Telcordia Technologies.

[17] Blogspot., "Ring Back Tone." Blogspot. [Online].[Cited: February 25, 2011.] http://rbt-review.blogspot.com.

[18] Dialogic., "Mobile CRBT." Dialogic. [Online] [Cited: February 25, 2011.] http://www.dialogic.com/solutions/mobile-vas/mobile-crbt.htm.

[19] OpenCloud Web Site, [Cited: February 25, 2011.] http://www.opencloud.com

[20] jNetX Web Site, [Cited: February 23, 2010.] http://www.jnetx.com.

[21] D. Malas, "SIP End-to-End Performance Metrics," IETF Internet Draft, draft-ietf-pmol-sip-perf-metrics-01.txt, [Online] [Cited: February 25, 2011.] http://tools.ietf.org/html/draft-malas-performance-metrics-08.

[22] O. Mondragon and Z. Solarte, Propuesta de un modelo arquitectonico para la implementación de nuevos servicios telematicos sobre la red multiservicios de EMCALI, 1st ed., Autonoma University, September 2010, 80p, 1692-2832.

 ISBN: 978-1-61208-123-6

Design of Network Resource Federation towards Future Open Access Networking

Michiaki Hayashi, Nobutaka Matsumoto, Kosuke Nishimura and Hideaki Tanaka
KDDI R&D Laboratories Inc.
Saitama, Japan
{mc-hayashi, nb-matsumoto, nish, hide}@kddilabs.jp

***Abstract*—Various network applications, such as virtual private network, cloud computing and Internet protocol television, are often provided across multiple network operators. One difficulty in managing quality of service across operator domains is the barrier for adoption especially to service level agreement-sensitive and mission-critical cases. Federating network resources among operators is necessary to manage quality of service across operators. To manage network resources of other operator domains, network operator's federation mechanisms aiming at future of open access network model is designed. Mechanisms of the signaling process as well as the capability of the bandwidth broker are proposed for the open access networking, where multiple operators are connected via a common access network operator. Considering both next generation network and non-next generation network architectures coexist in the open access network, the design identifies functional extensions to existing bandwidth broker implementations for the federation signaling. The proposed design is prototyped and the demonstration results show that the federation mechanism can assure the bandwidth of targeted live data stream on demand across trunk and access network operators even under congestion.**

Keywords- QoS; federation; NGN; open access.

I. INTRODUCTION

Network applications, such as virtual private network (VPN), cloud computing and Internet protocol television (IPTV) are often provided across multiple networks operators, such as telecom operators or ISPs. Those applications sometimes have difficulty in ensuring the quality of service (QoS) because of uncertainty condition of networks. Therefore, adoptions of the network applications to SLA-sensitive or mission-critical cases are difficult, which may also block the growth of future network applications. To ensure QoS across operators, network resources across multiple domains must be managed, which requires the capability of federating network resources among operators. The network resource federation denotes the mechanism to negotiate and coordinate network resources, such as bandwidth for a typical example, among operators for inter-operator connections. The bandwidth broker (BB) concept [1] and several solutions for Internet applications [2, 3] and also mobile applications [4] have been proposed as the federation enabler. However, rolling out the federation mechanism to the whole Internet is not likely because of the huge meshed structure inducing also complicated pricing model [5, 6]. Another possible scenario is an open access network (OAN) [7, 8] where the access network operator (i.e., typically incumbent telecom operator) provides access infrastructure to the trunk network operator (i.e., typically competitive telecom operator). Since the OAN has a relatively simple structure, the QoS-managed federation is more feasible than the Internet. Indeed, telecommunication standardization organizations, such as ETSI and ITU-T, have established the architectural framework of the next generation network (NGN) [9], where the capability of the OAN is incorporated in its network to network interface (NNI). A bandwidth broker called the resource and admission control function (RACF) can have NNI for the inter-operator network resource federation. Based on the QoS requests from adjacent NGN, RACF controls an NGN edge router called the border gateway function (BGF) to ensure QoS within the NGN domain. This means that a QoS-managed federation in NGN architecture requires BGFs to be installed in the transport network. Hence, the NGN-based approach cannot be simply applied to the OAN, since BGF has not been widely rolled out yet. Even in the case of inter-NGN domain federation, the signaling procedure has not been discussed yet.

To design a network resource federation for future OAN, this paper proposes a design of signaling mechanisms for QoS-managed multi-domain networks where both NGN and non-NGN operators can coexist. Non-NGN operator assumes to be conventional IP-based transport network, or the other architectures having the BB that is different from the RACF. The design identifies functional extensions to existing BB implementations for the federation signaling. The design is prototyped and the demonstration results show the feasibility of bandwidth-assured services for QoS sensitive cases in the OANs.

Section II describes structures of the network resource federation using the open access network model. Section III introduces existing technical approaches related to the network resource federation. Considering the remaining issues of the related works, Section IV proposes design of network resource federation. Based on the proposed framework, Section V demonstrates basic signaling procedure of the network resource federation.

II. SERVICE MODEL OF NETWORK FEDERATION

As an example, users of VPN, cloud computing and IPTV services connect to remote offices, data centers and application servers, respectively. In the OAN-based

 ISBN: 978-1-61208-123-6

service model, ethose services are provided via a common access network operator and multiple trunk network operators, as shown in Fig. 1.

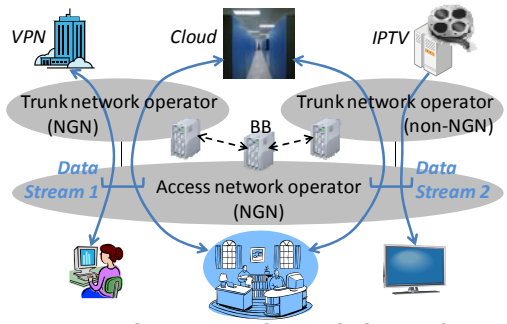

Figure 1. An example scenario involving multiple network operators based on the open access network (OAN) model.

In those scenarios, data streams passes across multiple network operators, as shown in data stream 1 and 2 in Fig. 1. To ensure QoS of those network applications, the BB of each network operator needs to cooperate with each other for managing end-to-end bandwidth resources of the relevant data streams. Several cases must be considered to address network resource federation. Aiming at future OAN scenarios, we focus on two federation cases, that are the federation between NGN operators and the federation between NGN and non-NGN operators. The latter case is indispensable to migrate into the future OAN environment. In Fig. 1, data Stream 1 requires the federation between two NGN operators, while Data Stream 2 requires the federation between NGN and non-NGN operators.

III. Related Works

Several BB implementations have been proposed for the Internet architectures as we discussed in Section I. On the other hand, BB solutions recently developed for NGN [10] and future Internet architectures [11] may also be applicable to the OAN. In the NGN architecture defined by ETSI TISPAN and ITU-T, BB called RACF has a standard inter-NGN federation interface, shown as "Ri" interface, as shown in Fig. 2. NGN architecture has been developed especially for telecom operators, and thus is suitable for the OAN. Policy decision functional entity (PD-FE) is responsible for federating resources with other NGN, as well as resource reservation based on the availability information residing in the transport resource control functional entity (TRC-FE). Although the Ri federation interface has been defined, the resource reservation procedure (i.e., signaling mechanism) has not been defined yet. Moreover, interworking with a non-NGN domain or resource reservation of a non-NGN by RACF is currently beyond the scope of standardizations.

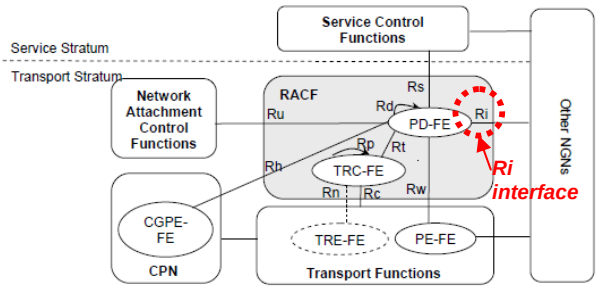

Figure 2. RACF as a BB for inter-NGN resource federation via "Ri" signaling interface [10].

While in the current Internet architecture it is difficult to ensure end-to-end network resources, research testbeds towards the future Internet architecture are developing several control frameworks incorporating a BB mechanism called as "clearinghouse" for resource reservations of both intra- and inter-domains [11]. Although the architectural design of the clearing house is based on the existing BB, the clearing house handles both network and computing resources. However, there are a few demonstrations showing its feasibility of multi-domain resource federation [12]. Since the standardization of the federation interface has not been sufficiently discussed, the control framework often requires complicated interface wrappers (i.e., converters of interface protocols) as shown in Fig. 3. Hence, the applicability of standardized resource federation interfaces needs to be assessed to simplify the signaling design. Especially for the OAN case, the applicability of the telecom federation standard (i.e., "Ri" interface) is attractive not only for the NGN operator but also for the non-NGN operator.

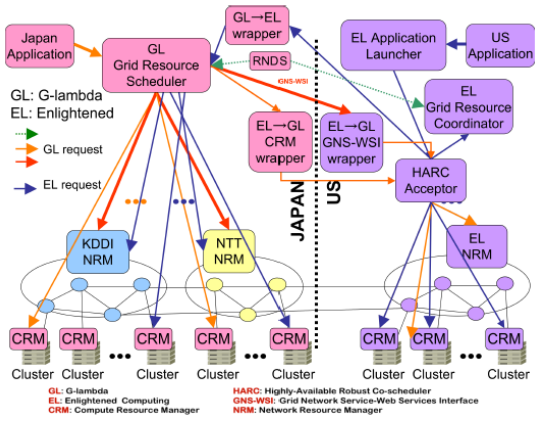

Figure 3. Inter-domain resource federation involving interface wrappers (i.e., protocol converters) [12].

IV. Design of Resource Management Framework

A universal BB implementation both for NGN and non-NGN domains has been proposed [13]. That concept extends the standardized RACF architecture to scope not only NGN resource (i.e., BGF in transport network) but also non-NGN resources (e.g., PON, MPLS, etc.), and

 ISBN: 978-1-61208-123-6

such the implementation can be an enabler of the federated signaling operation proposed in this Section. However, to find resources residing in other domains, two functional extensions are required in addition to the existing works.

As the first extension, the capability of finding BB for the federating domain must be added. For inter-domain operation, the function that judges whether the request can be processed within own domain or the request needs federation with other domains is defined, but such functionality has not been defined in the current RACF [10] and BB [13]. To identify an appropriate federating BB requires address resolution capability, such as domain name system (DNS) function, when receiving incoming requests. In the NGN control framework, addressing information is incorporated in the network attachment control function (NACF). However, the standard NACF has only knowledge of its own domain.

As the second extension, the capability of resolving hidden addresses must be added. Considering inter-operator federation scenarios, a connection termination point specified by an IP address in other domains may be hidden by the peer BB (e.g., using NAPT) for concealing its topology. Therefore, termination points of the service may be specified using terminal ID, which is a relative value specifying a termination point rather than specifying an absolute IP address value. Ri protocol [14] has introduced "user identifier" to describe media flow, and the parameter can be identical to the terminal ID. Using the terminal ID, the BB must resolve the IP address inside own domain in order to control relevant resource accordingly. The resolution may be done by the user profile database such as NACF, and thus NACF is required to have a table of correspondence between terminal ID and IP address.

Considering the aforementioned extensions with the basis of the Ri interface, the federation signaling is designed using Diameter protocol [15], which provides authentication, authorization and accounting framework for roaming, network access and IP mobility applications. To cover scenarios based on Fig. 1, both cases are discussed. The first case is federating inter-NGN domains, and the second case is federating NGN and non-NGN domains. As for the interface between the service control function (SCF) and BB, standardized "Rs" interface, which is depicted in Fig. 2, is used as a candidate of the common interface. SCF may be a cloud provisioning system, application server, and so forth.

Fig. 4 shows the proposed signaling procedure of the first case (i.e., federation between NGN domains), and the procedure describes the BB of Domain 1 receives a resource request from SCF and negotiates with BB of Domain 2 to reserve resources between two terminals. Two domains are inter-connected by border BGFs, and two end terminals are connected to access BGFs in each domain. In the reservation phase, based on the standard procedure of Rs interface, SCF sends Diameter AA request (AAR) for two ends of the stream with upstream and downstream, and thus totally 4 AAR messages are sent from SCF to BB. In accordance with the AAR sent from SCF, 4 AAR messages are sent from BB of Domain 1 to BB of Domain 2. This AAR messaging process plays the role of reserving the TCP/UDP port resource as well as bandwidth resources at the termination point of BGF. AA answer (AAA) message informs the result of resource assignment with the information of the assigned TCP/UDP port resource at BGF. Since the standard Rs procedure is designed for one domain and SCF has no knowledge of other domains, the inter-NGN process must be masked by BB of Domain 1, whose process is not defined in standards. BB of Domain 1 conceals the existence of TCP/UDP port termination points at two BGFs in Domain 2. From the SCF's perspective, terminal in Domain 2 can be understood as the one accommodated to the border BGF of Domain 1. When receiving AAR, the BB of Domain 1 needs to perform the capability of finding BB of the federating domain, and the process is depicted as (1). The capability of resolving hidden address also needs to be performed by the BB of Domain 2 when controlling BGF, as depicted (2). BBs also reserve resources of standard BGFs using the Megaco protocol [16], which is designed to control transport equipment for managing gateway of each media stream. To finalize the federation, the BB of Domain 1 sends AAR messages to indicate the commitment of the federation. Extending the signaling procedure only of the BB with Ri interface, SCF and BGF do not have to be aware of the existence of the inter-NGN operation.

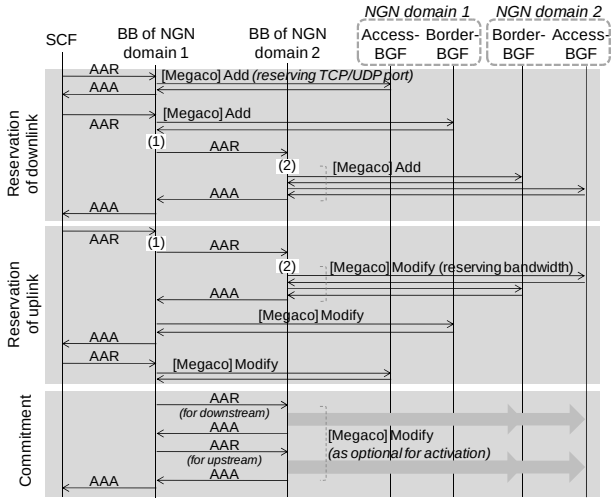

Figure 4. Signaling procedure of resource federation between NGN-domains.

Next, Fig. 5 shows the proposed signaling procedure of the second case (i.e., federation between non-NGN and NGN domains). Although the base procedure for SCF and Ri interface are not dramatically changed, the internal process of BB needs to be modified deriving from non-NGN does not have the TCP/UDP port reservation mechanism. BB operation within the non-NGN domain follows the existing procedure [13] using SOAP protocol message "NetResourceReservation" to reserve bandwidth

 ISBN: 978-1-61208-123-6

resources of logical links at passive optical network (PON) and MPLS segments, etc. SOAP [17] is a protocol for exchanging extensible makeup language (XML)-structured information of Web services. To manage multiple segment resources, the non-NGN domain has multiple network resource managers (NRMs) that locally manage the resources of each segment. For the purpose of synchronizing reservation states of the resource segments, two-phased commitment is effective for the reservation. In addition, since non-NGN equipment does not have the capability of reserving any TCP/UDP port resource at the equipment. The BB of the non-NGN domain proxies BGF's role supplying terminal port values of the stream since any network address port translation (NAPT) [18] is performed within the non-NGN domain. The port proxy function is performed at Diameter AAA messages marked as (3). Hence, the two-phased SOAP operation and the port proxy function is the third additional extension to BB. Based on those mechanisms, SCF, BB in the NGN domain and BGF do not have to be aware of inter-domain operation.

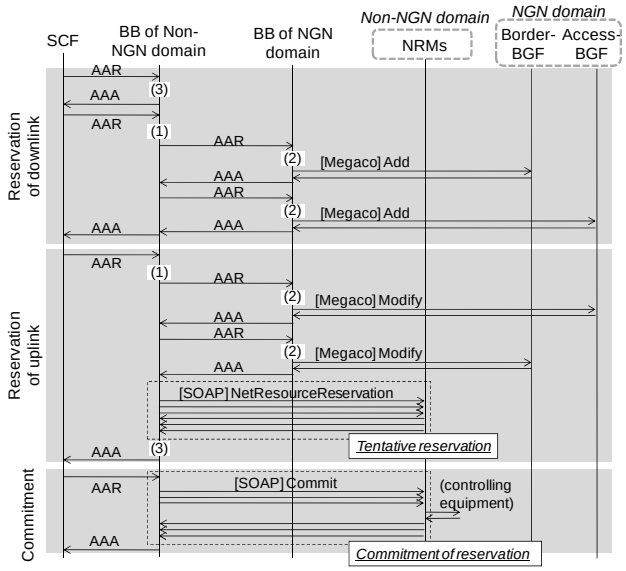

Figure 5. Signaling procedure of resource federation between non-NGN and NGN domains.

V. DEMONSTRATION OF FEDERATION SIGNALING

As a proof of concept of the signaling design described in Section IV, federation-capable BBs for NGN and non-NGN are developed, respectively. The prototype BBs are installed to the OAN testbed, and QoS-managed federation service across trunk operator (i.e., non-NGN) and access operator (i.e., NGN) is demonstrated. Bandwidth-assured content transfer across domains is evaluated using the testbed configuration shown in Fig. 6. A contents server is located in an non-NGN domain, and identical 30 Mbps unicast contents are sent to Terminal X and Y in the NGN domain, respectively. Based on the Rs protocol-based request from a content server, the BB in each domain communicates with each other using the Ri signaling procedure. The BB in the NGN domain controls BGFs using the Megaco protocol, and the BB in the non-NGN domain control NRM for the MPLS router using the SOAP protocol, as described in Fig. 5. NRM performed the call admission control to ensure the bandwidth reservation of the MPLS network. The link capacity of each link is 1 Gbps. Using the federation signaling between the BBs, the bandwidth of only the content stream to Terminal X is reserved, while a bandwidth of the stream to Terminal Y is not reserved. In addition, for both content streams, the background stream of 1.5 Gbps is periodically generated between traffic generator ports within the access operator domain. The background traffic shares an outgoing link of BGF with the content streams, and induces the congestion.

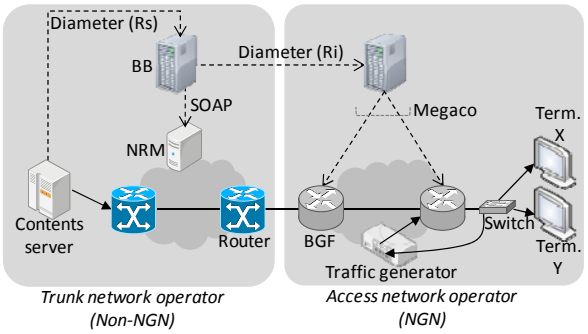

Figure 6. Configuration of concept-proof demonstration for the network federation using proposed signaling method.

Fig. 7 shows the throughput of the content streams and the amount of the generated background traffic. Before activating the federation process, the throughputs of two streams were both affected by the background traffic. Next, the federation signaling was activated to reserve 35 Mbps only for the stream to Terminal X, and then the throughput was stably maintained at 30 Mbps after the federation process. This signaling mechanism assured the targeted live stream on demand without any significant disruption to the targeted traffic.

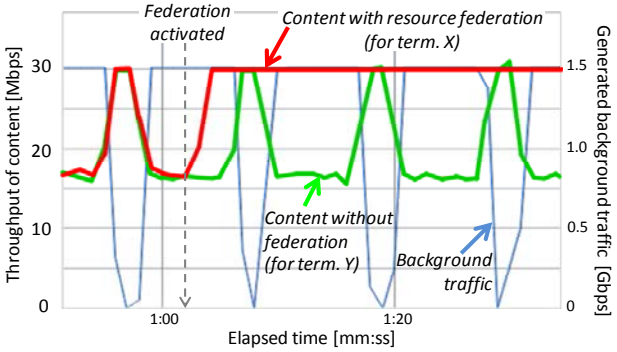

Figure 7. Throughput of contents and generated background traffic.

 ISBN: 978-1-61208-123-6

The signaling operation was captured as Fig. 8. The completion time was about 2.46 sec including configuration of the network equipment.

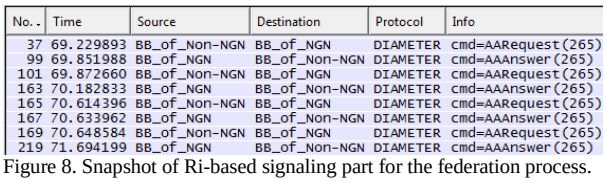

No.	Time	Source	Destination	Protocol	Info
37	69.229893	BB_of_Non-NGN	BB_of_NGN	DIAMETER	cmd=AARequest(265)
99	69.851988	BB_of_NGN	BB_of_Non-NGN	DIAMETER	cmd=AAAnswer(265)
101	69.872660	BB_of_Non-NGN	BB_of_NGN	DIAMETER	cmd=AARequest(265)
163	70.182833	BB_of_NGN	BB_of_Non-NGN	DIAMETER	cmd=AAAnswer(265)
165	70.614396	BB_of_Non-NGN	BB_of_NGN	DIAMETER	cmd=AARequest(265)
167	70.633962	BB_of_NGN	BB_of_Non-NGN	DIAMETER	cmd=AAAnswer(265)
169	70.648584	BB_of_Non-NGN	BB_of_NGN	DIAMETER	cmd=AARequest(265)
219	71.694199	BB_of_NGN	BB_of_Non-NGN	DIAMETER	cmd=AAAnswer(265)

Figure 8. Snapshot of Ri-based signaling part for the federation process.

VI. CONCLUSION

To design the network resource federation for future open access networking, signaling mechanisms are proposed for multi-domain networks where both NGN and non-NGN operators coexist. The design has been identified functional extensions to existing BB implementations for the federation signaling. The design is prototyped and the demonstration has shown that the federation mechanism can assure bandwidth of targeted live stream on demand across trunk and access network operators even under congestion. With the proposed federation mechanisms, QoS sensitive services are expected to be provided across multiple domains in future open access environments.

In the next steps of this study, our BB prototype needs to be extended considering scalability of network resources and transaction volume. For the future roll out of the federated OAN model, the federation operations simulating various operators' policies, such as usage of terminal ID, notifying event, and charging, must be examined in the testbed. The proposed OAN model also needs to be discussed in the future Internet communities for the better compatibility with the access infrastructure providers.

ACKNOWLEDGMENT

This research is partially supported by National Institute of Information and Communications Technology (NICT) under the Research and Development of Dynamic Network Technology Project.

REFERENCES

[1] K. Nichols, V. Jacobson, and L. Zhang, "A Two-bit Differentiated Services Architecture for the Internet," RFC 2638, July, 1999.

[2] X. Xiao and L. M. Ni, "Internet QoS: A Big Picture," IEEE Network, pp. 8-18, March/April, 1999.

[3] M. Günter, T Braun, and I. Khalil, "An Architecture for Managing QoS-enabled VPNs over the Internet," in Proceedings of LCN '99, pp. 122-131, Oct., 1999.

[4] R. Aguiar, D. Bijwaard, B. A. Farshchian, K. Jonas, and A. Sarma, "Pervasive Services for Next Generation Heterogeneous Networks," in Proceedings of WTC '06, May 2006.

[5] K. R. Vemu, D. T Daniel, and Y. Nagappa, "Optimal Multiclass Internet Pricing with Game Theoretical Approach," in Proceedings of ICOIN 2009, pp. 1-5, Jan., 2009.

[6] S. Shelford, E. G. Manning, and G. C. Shoja, "A framework for quality of service control through pricing mechanisms," in Proceedings of NOMS 2006, pp. 24-32, Apr., 2006.

[7] M. Forzati, C. P. Larsen, and C. Mattsson, "Open Access Networks, the Swedish Experience," in Proceedings of ICTON 2010, pp. 1-4, Jul., 2010.

[8] R. Battiti, R. L. Cigno, F. Orava, and B. Pehrson, "Global Growth of Open Access Networks: from WarChalking and Connection Sharing to Sustainable Business," in Proceedings of WMASH 2003, 2003.

[9] ITU-T Recommendation Y.2012, "Functional requirements and architecture of the NGN," Apr., 2010.

[10] ITU-T Recommendation Y.2111, "Resource and admission control functions in next generation networks," Nov., 2008.

[11] GENI project office, "GENI control framework requirements," GENI-SE-CF-RQ-01.3, Jan., 2009.

[12] S. R. Thorpe et al., "G-lambda and EnLIGHTened: wrapped in middleware co-allocating compute and network resources across Japan and the US," in Proceedings of GridNets 2007, October, 2007.

[13] N. Matsumoto, M. Hayashi, and H. Tanaka, "Network Middleware Design for Bridging Legacy Infrastructures and NGN," in Proceedings of NGI 2009, pp. 1-9, Jul., 2009.

[14] ITU-T Recommendation Q.3307.1, "Resource Control Protocol No. 7 – Protocol at the Interface Between Inter-Domain Policy Decision Physical Entities (Ri interface)," Jun., 2009.

[15] P. Calhoun, J. Loughney, E. Guttman, G. Zorn, and J. Arkko, "Diameter Base Protocol," RFC3588, Sep., 2003.

[16] ITU-T Recommendation H.248.1, "Gateway control protocol: Version 3," Sep., 2005.

[17] M. Gudgin et al., "SOAP Version 1.2 Part 1: Messaging Framework (Second Edition)," W3C recommendation, Apr., 2007.

[18] P. Srisuresh and M. Holdrege, "IP Network Address Translator (NAT) Terminology and Considerations," RFC2663, Aug., 1999.

 ISBN: 978-1-61208-123-6

Switching Networks with Hysteresis Mechanism

Mariusz Głąbowski, Maciej Sobieraj, Maciej Stasiak, and Joanna Weissenberg
Chair of Communication and Computer Networks, Poznan University of Technology
ul. Polanka 3, 60-965 Poznan, Poland
Email: mglabows@et.put.poznan.pl, maciej.sobieraj@put.poznan.pl, stasiak@et.put.poznan.pl, joanna@weissenberg.pl

***Abstract*—The paper proposes a new analytical method for determining traffic characteristics of multi-stage switching networks implementing threshold mechanism with hysteresis. The proposed method makes it possible to calculate point-to-group blocking probability in switching networks with multi-rate traffic streams. The basis of the presented method is the effective availability concept. The results of analytical calculations in two switching networks are compared with simulation data.**

***Keywords*-switching networks; multi-rate traffic; threshold mechanism with hysteresis;**

I. INTRODUCTION

Due to an enormous increase in the amount of information that the public has access to in an open communications network, attributed to the increasing popularity of multimedia services, the Internet is on the verge of collapse from congestion of available resources (bit rates) [1]. This situation has been triggered by an ever-increasing number of demanded network resources by services that can be differentiated into three traffic classes – considered in traffic theory, i.e. streaming, adaptive and elastic traffic classes [2]. In the streaming service, a demanded amount of resources is fixed and cannot undergo any changes with an increase of the load of the system. The adaptive class allows for decreasing admitted resources to accommodate new calls, with their service time unchanged. As far as the elastic class is concerned, the primary task – regardless of the available resources – is to execute a given service call. Therefore, along with an increase in the load of the system, it is possible to decrease the amount of the resources allocated to new calls with a simultaneous lengthening of the service time.

Any network load balancing solutions adopted by telecommunications operators to counteract the growing congestion require performing appropriate traffic analyses of the operating network systems and their optimal shaping and dimensioning. Until recently, the main emphasis has been put on the traffic analysis of links between telecommunications nodes. Increased capacity of these links and the introduction of technically advanced traffic control mechanisms have effected, however, in a situation in which switching structures of network nodes have again become topical and relevant. One of the most frequently used switching structures, in networks with electronic and optical switching alike, are multi-stage Clos networks. The literature considers Clos networks both within the context of applicable transmission techniques [1], algorithms for the selection of connection paths [3] and a modification to the structure itself [4]. Nowadays, in order to fully determine the influence of elastic and adaptive services on the effectiveness of a telecommunications network it is thus necessary to work out analytical methods that would enable us to model traffic characteristics of switching networks that perform and execute this type of service.

The present article proposes an analytical method for a determination of point-to-group blocking probability in switching networks carrying multi-rate traffic streams generated by streaming, adaptive and elastic services. For this purpose, a threshold mechanism with hysteresis is proposed, i.e. a system in which the decompression limit ("decompression limit" – the occupancy state below which the amount of assigned resources is equal to the initial values) is lower (often considerably) than the compression limit ("compression limit" – the occupancy state above which the amount of assigned resources decreases). This type of threshold mechanism allows to limit the number of changes in the amount of the assigned resources and improves the operation stability of the switching nodes. In the work on threshold systems hitherto reported and published, the focus is mainly on single resources (links).

The first attempt of elaborating the method devoted to determining blocking probability in switching networks with threshold mechanism was taken in [5]. In [5] only the basic model of threshold mechanism was considered – the threshold mechanism without hysteresis – it is the model assuming that the upper limit (compression limit) is equal to the lower limit (decompression limit). However, such an operation of the threshold mechanism causes frequent changes in the amount of assigned resources for calls, especially when the average load of the system is closed to the threshold state (the upper limit is equal to the lower limit) of the system.

The remaining part of the paper is organized as follows. In Section II the basic assumptions related to switching networks are presented. In Section III the implementation of the threshold mechanisms with hysteresis in the switching networks is proposed. The models of inter-stage links and outgoing links are described in Section IV. The proposed method of determining the blocking probability in

 ISBN: 978-1-61208-123-6

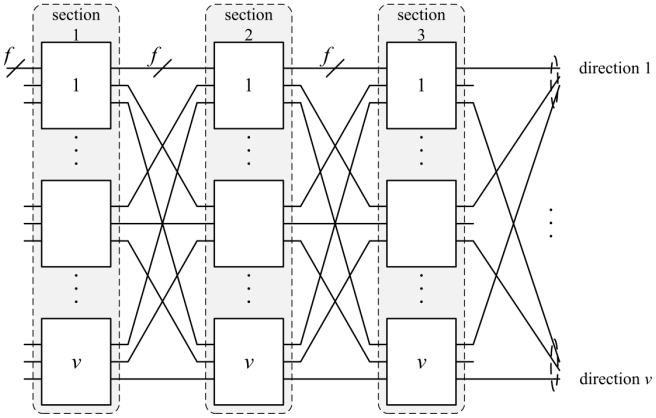

Figure 1. 3-stage switching network

the switching networks implementing threshold mechanism with hysteresis is presented in Section V. The results of analytical modeling of the considered switching networks are compared with simulation data in Section VI. Section VII concludes the paper.

II. Basic Assumptions

In the paper the switching networks with Clos structure are considered. The model of 3-stage switching network with multi-rate traffic is presented on Fig. 1. Each of inter-stage links has the capacity equal to f BBUs (Basic Bandwidth Units) and outgoing transmission links create link groups called directions. One of typical methods for realization outgoing directions is presented is Fig. 1; each direction v has one outgoing link v from each the last-stage switch. Each switch has v inputs and v outputs.

The switching network is offered m Erlang traffic streams generated by Poisson call streams. Poisson call streams are described by the arrival rates $\lambda_1, \ldots, \lambda_i, \ldots, \lambda_m$ of calls of particular traffic classes. A class i call requires t_i BBUs to set up a connection. The holding (service) time for the calls of particular classes has an exponential distribution with the parameters: $\mu_1, \ldots, \mu_i, \ldots, \mu_m$. The intensity λ_i of Poisson call stream of class i does not depend on the occupancy state of the system. Thus, the mean traffic A_i offered to the system by Poisson calls of class i is equal to λ_i/μ_i.

The considered switching network works with point-to-group selection. Following the control algorithm of this selection, the control device of the switching network determines the first stage switch, on the incoming link of which a class i call appears. Then, the control system finds the last-stage switch having an outgoing link with at least t_i free BBUs in the required direction. Next, the control device tries to find the connection path between the first-stage and the last-stage switch. Existence of the connection path causes realization of the connection. In opposite case, the control system begins the second attempt to set up a connection. If the connection path cannot be found during the last try v (the number of possible tries equals the number of links in the required direction), the call is lost as the result of the internal blocking. If each last-stage switch does not have t_i free BBUs in the required direction, the call is lost because of the external blocking.

III. Switching Networks with Hysteresis

The losses in the switching networks occur as the result of the internal blocking or the external blocking. In order to shape the dependencies between the blocking probabilities of various traffic classes it is possible to apply the threshold mechanism with hysteresis to the considered switching networks. The threshold mechanism with hysteresis can be considered as a realization of the Call Admission Control (CAC) function.

In the paper the threshold mechanism with hysteresis is applied only to the outgoing links forming the outgoing directions of the switching network. The application of this mechanism allows to adapt the traffic parameters of carried traffic classes to the occupancy state of a system. It should be noticed that the introduction of threshold mechanism to the outgoing links has an indirect impact on traffic characteristics of the internal links due to the decrease of the number of assigned BBUs for calls accepted in pre-threshold area and post-threshold area.

According to the adopted method of switching networks modeling, in the paper it is assumed that the interstage links can be modeled by the full-availability group [6] while the outgoing links (outgoing directions) can be modeled by the limited-availability group [6], presented in the next section of the paper.

IV. Switching Network's Links with Hysteresis

A. Model of Inter-stage Links

Let us consider a threshold model with hysteresis of the full-availability group with multi-rate traffic, the so-called FAGTH model (Full-availability Group Threshold with Hysteresis). The capacity of the system is equal to V BBUs. Let us assume that set $\mathbb{T}$ contains the traffic classes, selected from all m traffic classes offered to the switching network, to which the threshold mechanism with hysteresis has been applied. Let us assume further that two thresholds Q_1 and Q_2 are introduced ($Q_2 < Q_1$) for calls in set $\mathbb{T}$ (the threshold is the defined occupancy state of the system, determined by the number of busy BBUs). In the instance of an increase in the load of the system above the pre-defined first threshold Q_1 a decrease in the number of assigned BBUs to calls of belonging to set $\mathbb{T}$ ensues, and the average holding time of the calls may be increased (the holding time changes in the case of elastic services and remains unchanged in the case of adaptive services). However, when the load of the system decreases below the second threshold Q_2, an increase to the default values of the number of demanded BBUs by calls belonging to set $\mathbb{T}$ ensues, and

 ISBN: 978-1-61208-123-6

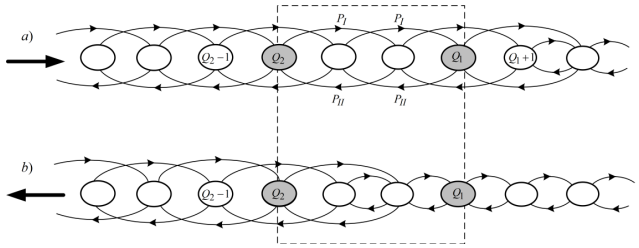

Figure 2. Fragment of two Markov chains

the average holding time of the call may be decreased. The service processes of the considered system can be presented as two Markov chains presented in Figure 2. Analyzing both the Markov chains of the service process occurring in the considered system, one in each direction, we can observe that the occupancy distribution in the inter-threshold area can be approximated by the following weight distribution:

$$[P_n]_{Q,V} = P_I\,[P_n]_{Q_1,V} + P_{II}\,[P_n]_{Q_2,V}\,, \qquad (1)$$

where P_I and P_{II} are weights which describe the probabilities that the system is in the occupancy states belonging to inter-threshold area as well as the passage direction in inter-threshold area, while the distributions $[P_n]_{Q_1,V}$ and $[P_n]_{Q_2,V}$ are the occupancy distributions determined for the systems in which single threshold Q_1 and Q_2 are introduced, respectively (i.e., in the systems with thresholds without hysteresis). P_n determines the probability of occupancy state n, i.e., the probability of n BBUs being busy.

Probabilities P_I and P_{II} can be determined on the basis of passage probabilities described for state n of the Markov chain (Fig. 2):

$$P_I = \frac{\sum_{i=1}^{m} A_i t_{i,0}}{\sum_{i=1}^{m} A_i t_{i,0} + w}, \qquad (2)$$

$$P_{II} = \frac{n}{\sum_{i=1}^{m} A_i t_{i,0} + w}, \qquad (3)$$

where $t_{i,0}$ is the number of BBUs assigned to class i calls in the first threshold area (in the occupancy states lower than Q_1 when the load of the system increases – Fig. 2a) and w is determined by (4).

In Equations (2) and (3) it is assumed that the probability that the system is being in the given occupancy state depends on the sum of effective traffics ($\sum_{i=1}^{m} A_i t_{i,0}$) offered to the system and on the occupancy state of the system ($\sum_{i=1}^{m} y_i(n + t_{i,0})t_{i,0}$), where y_i determines the average number of class i calls being serviced in state n. It means, that the probability P_I – the increase in the load of the system to the state of n BBUs being busy – is directly proportional to the sum of effective traffics offered to the system. However, probability P_{II} – the decrease in the load of the system to the state of n BBUs being busy – is directly proportional to the sum of effective traffics serviced in state n (Fig. 3). The values of these probabilities, determined for

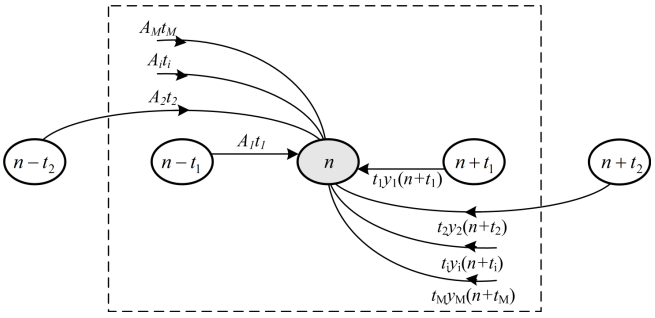

Figure 3. Fragment of Markov chain for state n

the states belonging to inter-threshold area, differ from each other slightly. Consequently, in order to determine the values P_I and P_{II} state w between states Q_1 and Q_2 has been selected:

$$w = \lfloor (Q_1 - Q_2)/2 \rfloor + 1. \qquad (4)$$

In order to determine the weighted threshold distribution let us determine the occupancy distributions in single-threshold (without hysteresis) systems, i.e., the distributions $[P_n]_{Q_1,V}$ and $[P_n]_{Q_2,V}$. First, let us consider the system with single threshold equal to Q_1 introduced for traffic classes from set $\mathbb{T}$. According to [2], [7]:

$$n[P_n]_{Q_1,V} = \sum_{i=1}^{m}\sum_{q=0}^{1} \sigma_{i,q}^{I}(n - t_{i,q}) A_{i,q} t_{i,q} \left[P_{n-t_{i,q}}\right]_{Q_1,V}\,, \qquad (5)$$

where:

$$\sigma_{i,0}^{I}(n) = \begin{cases} 1 & \text{for} \quad i \notin \mathbb{T}, \\ 1 & \text{for} \quad i \in \mathbb{T} \ \wedge \ n \le Q_1, \\ 0 & \text{for} \quad i \in \mathbb{T} \ \wedge \ n > Q_1, \end{cases} \qquad (6)$$

$$\sigma_{i,1}^{I}(n) = \begin{cases} 0 & \text{for} \quad i \notin \mathbb{T}, \\ 0 & \text{for} \quad i \in \mathbb{T} \ \wedge \ n \le Q_1, \\ 1 & \text{for} \quad i \in \mathbb{T} \ \wedge \ n > Q_1. \end{cases} \qquad (7)$$

For all states higher than Q_1 (Fig. 2a), the number of assigned BBUs for class i calls decreases from $t_{i,0}$ to $t_{i,1}$.

The mean number of given class calls being serviced in particular occupancy states (threshold area q) of the system (the so-called reverse transition rates) can be determined on the basis of the local equilibrium equations:

$$n_{i,q}^{I}(n) = \begin{cases} A_{i,0}\sigma_{i,0}^{I}(n - t_{i,0}) \left[P_{n-t_{i,0}}\right]_V / [P_n]_V \\ \qquad \text{for} \quad q = 0 \ \wedge \ n \le Q_1 + t_{i,0}, \\ A_{i,1}\sigma_{i,1}^{I}(n - t_{i,1}) \left[P_{n-t_{i,1}}\right]_V / [P_n]_V \\ \qquad \text{for} \quad q = 1 \ \wedge \ n > Q_1 + t_{i,1}. \end{cases} \qquad (8)$$

Subsequently, let us consider now the other system in which for classes from set $\mathbb{T}$ also a single threshold, equal to Q_2 has been introduced. Analogously as in the case of

the first system:

$$n[P_n]_{Q_1,V} = \sum_{i=1}^{m} \sum_{q=0}^{1} \sigma_{i,q}^{II}(n - t_{i,q}) A_{i,q} t_{i,q} \left[P_{n-t_{i,q}}\right]_{Q_1,V}, \tag{9}$$

where:

$$\sigma_{i,0}^{II}(n) = \begin{cases} 1 & \text{for} \quad i \notin \mathbb{T}, \\ 1 & \text{for} \quad i \in \mathbb{T} \ \wedge \ n \leq Q_2, \\ 0 & \text{for} \quad i \in \mathbb{T} \ \wedge \ n > Q_2, \end{cases} \tag{10}$$

$$\sigma_{i,1}^{II}(n) = \begin{cases} 0 & \text{for} \quad i \notin \mathbb{T}, \\ 0 & \text{for} \quad i \in \mathbb{T} \ \wedge \ n \leq Q_2, \\ 1 & \text{for} \quad i \in \mathbb{T} \ \wedge \ n > Q_2. \end{cases} \tag{11}$$

When the load of the system decreases (the system in occupancy states below state Q_2) (Fig. 2b), the assigned number of BBUs for calls from set $\mathbb{T}$ increases from $t_{i,1}$ to the initial value $t_{i,0}$.

The mean number of class i calls being serviced in particular states of the system with threshold Q_2 can be determined analogously to the system with threshold Q_1:

$$n_{i,q}^{II}(n) = \begin{cases} A_{i,0}\sigma_{i,0}^{II}(n - t_{i,0}) \left[P_{n-t_{i,0}}\right]_V / [P_n]_V \\ \qquad \text{for} \quad q = 0 \wedge n \leq Q_2 + t_{i,0}, \\ A_{i,1}\sigma_{i,1}^{II}(n - t_{i,1}) \left[P_{n-t_{i,1}}\right]_V / [P_n]_V \\ \qquad \text{for} \quad q = 1 \wedge n > Q_2 + t_{i,1}. \end{cases} \tag{12}$$

The blocking probability for class i calls can be determined as the sum of the probabilities of the states in which the system cannot admit a new class i call:

$$E_i = \begin{cases} \sum\limits_{n=V-t_{i,0}+1}^{V} [P_n]_{Q,V} & \text{for } i \notin \mathbb{T}, \\ \sum\limits_{n=V-t_{i,1}+1}^{V} [P_n]_{Q,V} & \text{for } i \in \mathbb{T}, \end{cases} \tag{13}$$

where the occupancy distribution $[P_n]_{Q,V}$ is calculated on the basis of (1).

B. Model of Outgoing Links

Since the outgoing directions of the considered switching networks are modeled as the limited availability groups let us consider now the so-called threshold model of limited-availability group with hysteresis, i.e., LAGTH (Limited Availability Group Threshold with Hysteresis) model. Let us remind that the limited availability group is the model of systems consisting of υ identical separated transmission links. Each link has the capacity equal to f BBUs [6]. Thus, the total capacity of the system V is equal to $V = \upsilon f$ BBUs. The system services a call – only when this call can be entirely carried by the resources of an arbitrary single link.

In the paper it is assumed the occupancy distribution in the limited-availability group with the threshold mechanism with hysteresis can be calculated on the basis of the appropriately modified generalized Kaufman-Roberts recursion [8]. For taking into consideration the influence of the specific structure of the limited-availability group on the process of determination of occupancy distribution using the generalized Kaufman-Roberts recursion the using of conditional coefficients of passing $\sigma_{i,\text{LAG}}(n)$, was proposed. The value of parameter $\sigma_{i,\text{LAG}}(n)$ can be determined as follows [6]:

$$\sigma_{i,\text{LAG}}(n) = \frac{F(V-n,\upsilon,f,0) - F(V-n,\upsilon,t_i-1,0)}{F(V-n,\upsilon,f,0)}, \tag{14}$$

where $F(x,\upsilon,f,t)$ is the number of arrangement of x free BBUs in υ links, calculated with the assumption that the capacity of each link is equal to f BBUs and each link has at least t free BBUs:

$$F(x,\upsilon,f,t) = \sum_{r=0}^{\lfloor \frac{x-\upsilon t}{f-t+1} \rfloor} (-1)^r \binom{\upsilon}{r} \binom{x-\upsilon(t-1)-1-r(f-t+1)}{\upsilon-1}. \tag{15}$$

Let us observe that in the case of the considered LAGTH model the operation of the threshold mechanism introduces additional dependence between the traffic stream in the system and the current state of the system. This dependence can be taken into consideration by the introduction of the threshold coefficient of passing $\sigma_{i,q}(n)$ to each of the thresholds q. The threshold mechanism is introduced to the group regardless of its structure, what allows us to carry on with a product-form determination of the total coefficient of passing in the limited-availability group $\sigma_{i,q,\text{Total}}(n)$:

$$\sigma_{i,q,\text{Total}}^{I}(n) = \sigma_{i,q}^{I}(n) \cdot \sigma_{i,q,\text{LAG}}^{I}(n), \tag{16}$$

$$\sigma_{i,q,\text{Total}}^{II}(n) = \sigma_{i,q}^{II}(n) \cdot \sigma_{i,q,\text{LAG}}^{II}(n). \tag{17}$$

For determining basic traffic characteristics in considered system we can used, appropriately adapted, FAGTH method. The modification of FAGTH method consists in regarding the coefficients of passing defined by (16) and (17) during the occupancy distribution calculation.

V. Analytical Model of Switching Networks with Hysteresis

A. Effective availability in switching networks

Multi-service switching networks were the subject of many analysis [6], [9]–[11]. At present, for blocking probability determination in the considered switching networks the well-proven methods of the so-called effective availability [6], [11], [12] are usually applied. According to the main idea of the effective availability methods [6], the calculation of blocking probability in switching networks with multi-rate traffic comes down to the calculation of the blocking in an equivalent network carrying a single-rate traffic. Each link of equivalent network is treated as a single-channel link with a fictitious load $e_l(i)$ equal to blocking probability for a class i stream in a link of real switching network between section l and $l+1$. This probability can be calculated on

the basis of the blocking probability in the full-availability group implementing threshold algorithm with hysteresis (Formula (13)).

The effective availability in a real z-stage switching network is equal to the effective availability in an equivalent switching network and can be determined by the formula derived in [6]:

$$d(i) = [1 - \pi_z(i)]\upsilon + \pi_z(i)\eta Y_1(i) + \\ + \pi_z(i)[\upsilon - \eta Y_1(i)]w_z(i)\sigma_z(i), \quad (18)$$

where:
$d(i)$ – the effective availability for the class i traffic stream in an equivalent network,
$\pi_z(i)$ – the probability of non availability of a given last stage switch for the class i connection. $\pi_z(i)$ is the probability of an event where the class i connection path cannot be set up between a given first-stage switch and a given last-stage switch. Evaluation of this parameter is based on the channel graph of the equivalent switching network,
υ – the number of outgoing links from the first stage switch,
$Y_1(i)$ – the average value of the fictitious traffic served by the switch of the first stage:

$$Y_1(i) = \upsilon e_1(i), \quad (19)$$

η – a portion of the average fictitious traffic from the switch of the first stage which is carried by the direction in question; if the traffic is uniformly distributed between all h directions, we obtain $\eta = 1/h$,
$w_z(i)$ – the fictitious traffic carried by a single input of the equaivalent switching network, equal to the blocking probablity $e_z(i)$ of class i calls in the corresponding link in the real switching network, calculated according to FAGTH method,
$\sigma_z(i)$ – the so-called *secondary availability coefficient* [6] which is the probability of an event in which the connection path of the class i connection passes through directly available switches of intermediate stages:

$$\sigma_z(i) = 1 - \prod_{r=2}^{z-1} \pi_r(i). \quad (20)$$

B. Distribution of available links

In effective availability methods, the second element essential for determining blocking probability in switching networks is so-called distribution of available links [6]. This distribution determines the probability $P(i, s)$ of an event in which each of arbitrarily chosen s links can carry the class i calls:

$$P(i, s) = \sum_{n=0}^{V} [P_n]_V P(i, s|V - n), \quad (21)$$

where $[P_n]_V$ is the occupancy distribution in limited-availability group with hysteresis (LAGTH method) and $P(i, s|x)$ is the conditional distribution of available links, which determines the probability of such an arrangement of $x = V - n$ free BBUs in s links that each of s arbitrarily chosen links has at least t_i free BBUs required for set up a connection for class i call, while in each of the remaining $\upsilon - s$ links the number of free BBUs is lower than t_i [6]:

$$P(i, s|x) = \frac{\binom{\upsilon}{s} \sum_{w=st_i}^{\Psi} F(w, s, f, t_i) F(x - w, \upsilon - s, t_i - 1, 0)}{F(x, \upsilon, f, 0)}. \quad (22)$$

In Equation (22) $\Psi = sf$, if $x \geq sf$, $\Psi = x$, if $x < sf$, $F(x, \upsilon, f, t)$ is the number of arrangement of x free BBUs in υ links, calculated with the assumption that capacity of each link is equal to f BBUs and each link has at least t free BBUs.

C. Point-to-Group Blocking Probability

Total blocking probability $E(i)$ for the class i call is a sum of external $E_{\text{ex}}(i)$ and internal $E_{\text{in}}(i)$ blocking probabilities. Assuming the independence of internal and external blocking events, we obtain:

$$E(i) = E_{\text{ex}}(i) + E_{\text{in}}(i)\left[1 - E_{\text{ex}}(i)\right]. \quad (23)$$

The phenomenon of the external blocking occurs when none of outgoing links of the demanded direction of the switching network can service the class i call (i.e., does not have t_i free BBUs). The external blocking probability is equal to the blocking probability in the limited-availability group modeling the outgoing direction of the switching network and can be determined on the basis of LAGTH method.

The internal blocking probability in the considered method is determined under the following conditions:

- there are s links in the require direction which can carry a class i call
- there are $d(i)$ last-stage switches available for the given first-stage switch on the incoming links of which a class i call appears.

For the switching network in the state described by the listed assumptions the internal point-to-group blocking phenomenon appears when all links (of the considered direction) belonging to the $d(i)$ available last-stage switches have not sufficient number of free BBUs for the class i call:

$$E_{\text{in}}(i) = \sum_{s=1}^{\upsilon - d(i)} \frac{P(i, s)}{1 - P(i, 0)} \left[\binom{\upsilon - s}{d(i)} \Big/ \binom{\upsilon}{d(i)} \right], \quad (24)$$

where υ is the number of links in the given direction.

VI. Numerical results

In order to evaluate the accuracy of the proposed analytical method of point-to-group calculation in switching networks implementing threshold mechanism with hysteresis, the results of analytical modeling has been compared with data of simulation experiments. The simulations were carried out for a typical three-stage Clos switching network considered both in electronic and optical switching (Figure 1).

 ISBN: 978-1-61208-123-6

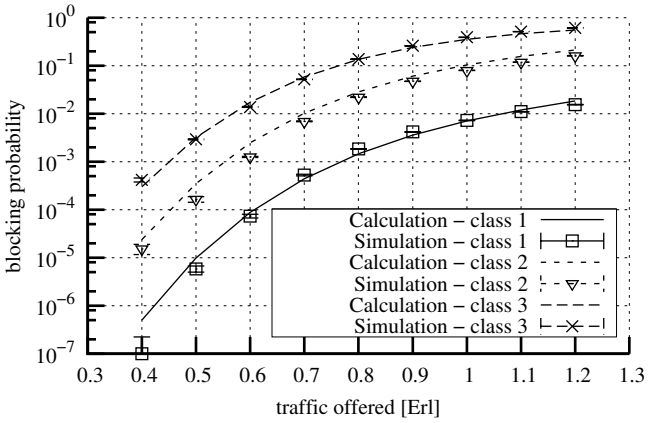

Figure 4. Point-to-group blocking probability; switching network structure: $\upsilon = 4$, $f = 30$ BBUs, $V = 120$ BBUs; traffic structure: class 1: $t_{1,0} = 1$ BBU, $\mu_{1,0}^{-1} = 1$, class 2: $t_{2,0} = 6$ BBUs, $\mu_{2,0}^{-1} = 1$, $t_{2,1} = 3$ BBUs, $\mu_{2,1}^{-1} = 2$, class 3: $t_{3,0} = 10$ BBUs, $\mu_{3,0}^{-1} = 1$, $t_{3,1} = 6$ BBUs, $\mu_{3,1}^{-1} = 1.667$; $Q_1 = 90$ BBUs, $Q_2 = 60$ BBUs; $\mathbb{T} = \{2, 3\}$.

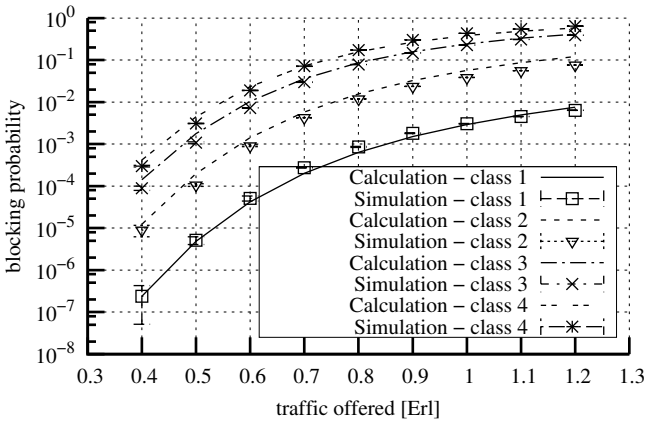

Figure 5. Point-to-group blocking probability; switching network structure: $\upsilon = 4$, $f = 35$ BBUs, $V = 140$ BBUs. traffic structure: class 1: $t_{1,0} = 1$ BBU, $\mu_{1,0}^{-1} = 1$, class 2: $t_{2,0} = 5$ BBUs, $\mu_{2,0}^{-1} = 1$, $t_{2,1} = 3$ BBUs, $\mu_{2,1}^{-1} = 1.667$, class 3: $t_{3,0} = 8$ BBUs, $\mu_{3,0}^{-1} = 1$, $t_{3,1} = 6$ BBUs, $\mu_{3,1}^{-1} = 1.33$, class 4: $t_{4,0} = 10$ BBUs, $\mu_{4,0}^{-1} = 1$, $t_{4,1} = 8$ BBUs, $\mu_{4,1}^{-1} = 1.25$, $Q_1 = 105$ BBUs, $Q_2 = 70$ BBUs; $\mathbb{T} = \{2, 3, 4\}$

The research was conducted for the multi-service switching networks to which independent classes of Erlang traffic streams were offered. The result of simulation are shown in the charts with 95% confidence intervals that have been calculated according to the t-Student distribution for the five series with 1,000,000 calls of each class. The research was carried out for two different structures of switching networks servicing three (Figure 4) and four (Figure 5) traffic classes.

VII. Conclusion

In the paper, the threshold mechanism with hysteresis for switching networks servicing a multi-rate traffic was proposed. The proposed mechanism ensures a substantial decrease in blocking probabilities of certain traffic classes in the access to switching network resources. The analytical methods of calculations of the point-to-group blocking probabilities in the multi-service switching networks with threshold mechanism with hysteresis is also presented. The method is based on the concept of the effective availability and ensure fair accuracy of calculations.

References

[1] M. Casoni and A. Sacchi, "System design and evaluation of a large photonic switch based on optical codes for optical burst switched networks," *IEEE 3rd Intl Symposium on Advanced Networks and Telecommunication Systems*, pp. 1–3, 2009.

[2] V. G. Vassilakis, I. D. Moscholios, and M. D. Logothetis, "Call-level performance modelling of elastic and adaptive service-classes with finite population," *IEICE Transactions on Communications*, vol. E91-B, no. 1, pp. 151–163, 2008.

[3] S. Jiang, G. Hu, S. Liew, and H. Chao, "Scheduling algorithms for shared fiber-delay-line optical packet switches: the three-stage clos-network case," *Journal of Lightwave Technology*, vol. 23, pp. 1601–1609, April 2005.

[4] Y. Liu, "A new model of nonblocking multicast WDM optical switching network with reduced complexity," *IEEE Intl Conf. on Network Infrastr. and Digital Content*, pp. 508–512, 2009.

[5] M. Głąbowski and M. Sobieraj, "Point-to-group blocking probability in switching networks with threshold mechanisms," in *Proc. A-ICT 2009*. Venezia, 2009, pp. 95–100.

[6] M. Stasiak, "Combinatorial considerations for switching systems carrying multi-channel traffic streams," *Annales des Télécommunications*, vol. 51, no. 11–12, pp. 611–625, 1996.

[7] M. Głąbowski, "Continuous threshold model for multi-service wireless systems with PCT1 and PCT2 traffic," in *Proceedings of 7th International Symposium on Communications and Information Technologies*, Sydney, Oct. 2007, pp. 427–432.

[8] M. Głąbowski, A. Kaliszan, and M. Stasiak, "Modeling product-form state-dependent systems with BPP traffic," *Journal of Perf. Eval.*, vol. 2010, no. 67, pp. 174–197, 2010.

[9] J. Conradt and A. Buchheister, "Considerations on loss probability of multi-slot connections," in *Proceedings of 11th International Teletraffic Congress*, Kyoto, 1985, pp. 4.4B–2.1.

[10] M. Beshai and D. Manfield, "Multichannel services performance of switching networks," in *Proc. 12th Intl Teletraffic Congress*. Torino, 1988, pp. 857–864.

[11] M. Głąbowski, "Recurrent method for blocking probability calculation in multi-service switching networks with BPP traffic," LNCS 5261. Springer, 2008, pp. 152–167.

[12] V. A. Ershov, "Some further studies on effective accessibility: Fundamentals of teletraffic theory," in *Proc. 3rd Intl Seminar on Teletraffic Theory*, Moscow, 1984, pp. 193–196.

 ISBN: 978-1-61208-123-6

Performance Study in Multi-rate Switching Networks with Additional Inter-stage Links

Michał Stasiak
Chair of Communications and Computer Networks
Poznan University of Technology
ul. Polanka 3, room 110, 60-965 Poznan, Poland
E-mail: michal.m.stasiak@doctorate.put.poznan.pl

Piotr Zwierzykowski
Chair of Communications and Computer Networks
Poznan University of Technology
ul. Polanka 3, room 231, 60-965 Poznan, Poland
E-mail: piotr.zwierzykowski@put.poznan.pl

***Abstract*—The paper presents the results of a simulation study on multi-rate three-stage Clos switching networks with additional inter-stage links. Switching networks in which a system of overflow links was provided for the first, second and the third stage are investigated. Additionally, different structures of connections between inter-stage links are discussed. The investigation has proved that an application of overflow systems is followed by a substantial decrease in the internal blocking probability in the switching network. An appropriate capacity of overflow links can even result in a virtually complete elimination of internal blocking. This paper proves that the best results are obtained with the introduction of overflow links to the first stage of the network, both in the case of point-to-point and point-to-group selection.**

***Keywords*-switching networks, inter-stage links**

I. INTRODUCTION

Switching networks form a base for the operation of many systems and devices, including that of exchanges or routers that constitute nodes in telecommunications networks. It is their effectiveness in performance that is decisive in enabling the maximum amount of traffic that a network can carry. Most of switching networks used in network nodes are blocking networks. This means a loss to performance with regard to part of traffic offered to network nodes. Constructions that eliminate the phenomenon of blocking in the switching network (the so-called non-blocking networks) are also known [1], [2], [3], [4], [5]. These networks, however, require a large number of switches, which translates directly into a substantial increase in the financial outlays for the construction of such switching networks. There exist techniques for reducing blocking states in switching networks. The three fundamental techniques include: the application of additional inter-stage (overflow) links [6], call rearrangement or repacking and re-switching [5]. Call repacking and re-switching do not interfere with the actual architecture of a switching network. These are based on the introduction of special algorithms for executing procedures related to setting up connections in a required way. Due to computational complexity, solutions of this type tend to overload controlling devices while setting up connections to a much higher degree that the most commonly used random algorithms and sequential algorithms, which is a drawback and a considerable limitation. The application of overflow links is accompanied with a slight interference into the physical architecture of a switching network and is based on an application of switches with an appropriately higher number of inputs and outputs. In the past, switching networks with overflow links were used on an industrial scale in analogue telephone exchanges manufactured by Pentaconta [6]. The exchange of the Pentaconta system was composed of two-stage switching networks in which switching devices of the first stage were connected with one another by special inter-stage links. The application of overflow links made it possible to reduce substantially (by several percent) the internal blocking probability of the exchange [7]. Later, a possibility of introducing overflow links in electronic exchanges was also considered [8], [9]. No analysis of the effectiveness of the introduction of overflow traffic has been carried out so far for multi-stage switching networks with multi-rate traffic. This paper presents the results of a simulation study of multi-rate three-stage Clos networks to which different architectures of overflow systems were applied.

The paper has been divided into 5 sections. Section 2 introduces the reader to the issues of modelling blocking and non-blocking switching networks. Section 3 discusses the architecture and the routing algorithms in the proposed switching structures with inter-stage links, while Section 4 presents the obtained results of the study. A conclusion follows in Section 5 of the paper.

II. BLOCKING AND NON-BLOCKING SWITCHING NETWORKS

Consider the Clos three-stage switching network presented in Figure 1. The switching network is composed of n symmetrical switches $n \times n$ of links in every stage. Each link has the capacity of f BBUs (Basic Bandwidth Units [10]). The switching network is offered multi-rate traffic composed of a number of traffic streams called traffic classes. Each traffic class is defined by parameters: call intensity, service intensity and the number of BBUs required

 ISBN: 978-1-61208-123-6

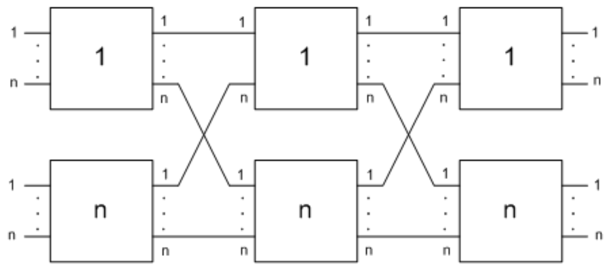

Figure 1. Three-stage Clos network v(m,n,r)

to set-up a connection. Our further assumption is that a stream of offered traffic of each class can be either an Erlang or Engset stream [11]. The Basic Bandwidth Unit is defined as the greatest common divisor of all bit rates allocated to calls of particular classes:

$$R_{BBU} = GCD\lfloor R_1, ..., R_M \rfloor, \quad (1)$$

where R_i is the bit rate allocated to each call of class i. The number of BBUs corresponding to a call of class i is defined by the following formula:

$$t_i = \left\lceil \frac{R_i}{R_{BBU}} \right\rceil, \quad (2)$$

The capacity of one free link of a switch can be also determined in BBUs:

$$f = \left\lfloor \frac{C}{R_{BBU}} \right\rfloor, \quad (3)$$

where C is the total bitrate in one link. The process of a determination of the parameters of individual call classes and the capacity of the component elements of the system in BBUs, on the basis of Equations (1)–(3), is called *bandwith discretization* [10]. The process makes the analysis and modelling of multi-stage switching networks and many other switching systems much more easy [14], [15].

Two basic types of selections are commonly used in switching networks: point-to-point selection and point-to group selection [12], [13]. With the point-to-point selection, the controlling algorithm determines the input stage switch at which a call of class i appeared. Then, the controlling algorithm defines a switch for the output stage that has at least one free outputs, i.e. an output link that has at least t_i free BBUs. In the next step, the algorithm tries to find a free connection path between these switches. If this is not possible, then the call is lost due to internal blocking. If the controlling algorithm indicates the absence of just one switch in the last stage with a free output, then the call is lost as well due to internal blocking. With the application of the point-to-group selection, the outputs of the switches of the last stage are divided into link groups called directions. The controlling algorithm for the network first determines the input switch at which a call of a given class appears. Then, the controlling algorithm chooses an output switch that has a free output in the required direction. In the next step, the controlling algorithm tries to set up a connection between a given switch of the first stage and a selected switch of the outgoing stage. If there is no possibility of setting up a connection path between these switches, then the controlling algorithm determines another switch of the last stage of the network that has a free output in the demanded direction. If, again, the connection between the switches of the first and the last stages cannot be set up, then the controlling algorithm determines next switch with free outputs in the direction and another attempt at setting up a connection is made. If, during one of such attempts, a connection can be successfully set up, then the controlling algorithm proceeds to execute the connection. If, in turn, all possible attempts fail to set up a connection, then the connection is lost due to internal blocking. The occupancy of all links in a given direction is followed by a loss of a call due to external blocking.

There are two basic methods for dividing outputs of the last stage in direction [12], [14]. The first method assumes that all outputs for a given switch represent just one direction. The other method is based on a selection of one (or more) output links with the same number in each of the switches of the last stage. This paper considers the latter method for the execution of the output direction.

A measure for the number of events of blocking is the blocking probability, which can be defined as a ratio of the number of blocked connections to the total number of demands for setting up connections in the switching network. The total blocking probability E_T is the sum of the internal blocking probability E_{in} and the external blocking probability E_{ex}:

$$E_T = E_{in} + E_{ex}. \quad (4)$$

In non-blocking networks, internal blocking probabilities are equal to zero. Thus, in non-blocking networks, the following equality takes place:

$$E_T = E_{ex}. \quad (5)$$

Equation (5) means that in non-blocking networks the blocking event occurs solely in output groups of the network and depends exclusively on their capacity and offered traffic. Hence, the internal structure of a non-blocking network is "transparent" for offered traffic and the whole network can be treated - from the traffic engineering perspective - as a single-stage system, i.e. as an output group of the network. Structures of non-blocking networks are constructed based on strictly defined rules and theorems [1], [2], [3], [5]. A transformation of a given structure of a blocking network into a structure of a non-blocking network may be based on an increase in the number of switches of appropriate stages or, additionally, an increase in the number of stages in a

 ISBN: 978-1-61208-123-6

switching network. Special control algorithms that manage the procedures of setting up connections are also known. These algorithms lead eventually to a non-blocking property of the network [5]. From the economic point of view, non-blocking networks are far more expensive than blocking networks. Therefore, in engineering practice most solutions employ much cheaper blocking networks in which the phenomenon of internal blocking is handled in such a way as to guarantee its maximum limitation. Switching networks with a low value of the internal blocking probability (that deliver at least one order of magnitude lower than the external blocking probability) are called quasi-non-blocking networks. One of the most effective ways of diminishing the internal blocking in the switching network is the application of overflow links. Switching networks with overflow links are described in the following section.

III. Switching Networks with Additional Inter-stage Links

Consider any example of a stage of the switching network shown in Figure 1, in which additional inter-stage links have been introduced. Figure 2 presents two ways of setting up overflow connections in a given stage of the switching network. In the first case (Figure 2a), the presented system of overflow links (called system I) is based on an application of switches with one additional input and one additional output in a given stage. An overflow link connects a given switch with another switch, whereas the last switch is connected with the first switch. The second example (Figure 2b) shows a system of overflow links (further on called system II). In this system, switches with two additional inputs and outputs are used. Each switch is connected by one inter-stage link with a neighbouring switch. The second overflow link leads to the next switch in a row. Thus, i-switch of a given stage is connected with $i+1$ switch and $i+2$ switch of the same stage. Each of the presented two overflow systems can be applied in each stages of a three-stage Clos network. If System I is applied to the second stage of the network, then thus obtained structure will be labelled as System 1.2 (the number of system, the number of the stages).

The algorithm for setting up a connection always tries to set up a connection without overflow links first. When the connection cannot be executed, an attempt is made to effect the connection with the help of overflow links. Assume that the 1.3 structure is introduced to the switching network with point-to-point selection, i.e. a system with overflows in the third stage. If in a given state of the network a point-to-point connection with a given output of the second switch of the third stage cannot be set up, then the controlling algorithm tries to set up this connection with the first switch of the third stage that has a connection (through the overflow link) with the second switch of the third stage.

The following general algorithm for setting up connections is applied to the considered switching networks with inter-

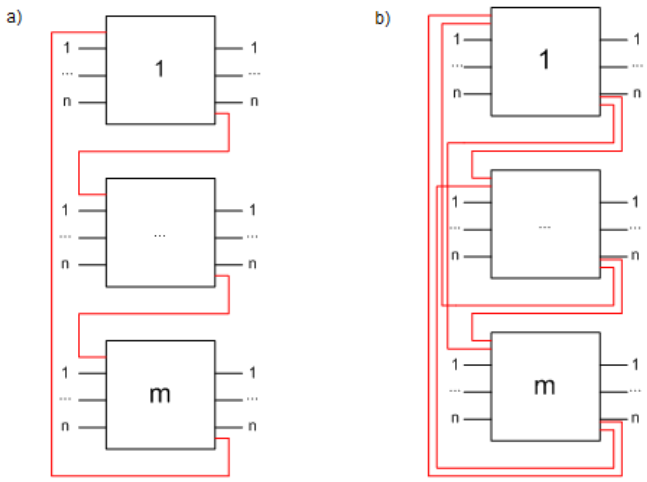

Figure 2. Overflow systems in a selected stage of the Clos network.

stage links. In the first step, the controlling device determines the input on which a new call appeared, as well as a required output in a given direction (point-to-point selection), or a demanded direction (point-to-group selection). In the next step an attempt is made to set up a point-to-point connection (or, alternatively, a point-to-group connection) without the application of overflow links. If setting up of a connection without overflow links fails to be executed, the controlling device proceeds to step three, in which all possible connection paths executed by the switches of a given stage to which the considered switch has access to through free overflow links are checked. If there are any free connection paths that use overflow links, then, on the basis of the random algorithm, one path is chosen and a connection of given type (point-to-point or point-to-group) is set up. Otherwise, a call is rejected. In order to diminish the amount of the volume of occupied resources and the complexity of the controlling algorithm for setting up a connection, one overflow link is used at the maximum. This means that if an attempt at setting up a connection with the use of overflow links is failed, then no attempts with the application of next overflow links will be made. It is assumed then, that in each attempt to set up a connection only one overflow link can be used.

IV. Numerical Results

To determine traffic effectiveness of switching networks with additional inter-stage links, a simulation tool that enables to determine traffic characteristics of the networks with the required confidence interval was developed for the purposes of the study. An event planning method was used to construct the simulator [16]. Thus constructed simulator allows you to study three-stage Clos switching networks with point-to-point selection and point-to-group selection. Either of the overflow links systems described in Section 2 can be introduced to each of the stages. The network is

 ISBN: 978-1-61208-123-6

offered a mixture of Erlang traffic of various classes (a call stream of each of the traffic classes is a Poisson stream, whereas the service time of each class of calls is described by an exponential distribution).

The investigation involved a simulation of a three-stage Clos switching network composed of symmetrical switches 4×4 links, each with the capacity of f=30 BBUs. The number of switches of each of the stages is equal to 4 switches. A network is offered three classes of calls that demand respectively t_1=9 BBUs, t_2=6 BBUs, and t_3=2 BBUs. It is assumed that appropriate traffic classes are offered in the following proportions: $a_1 : a_2 : a_3 = 2 : 3 : 6$. The simulations were carried out for such a number of series (each series includes 100,000 calls of the class with the highest demands) that guarantees 99% confidence interval defined on the basis of the *t*-Student distribution. This interval in the simulation experiments in question is lower by at least one order of magnitude than the average value of the simulation result. The results of the simulation are presented in relation to the volume of traffic offered to one BBU of an output link (a). Figure 3 shows a comparison of the internal point-to-point blocking probabilities for the calls of class i in the networks 0.0 (without overflow links) and 1.1 (overflow system I in the first stage of the network).

An introduction of a simple system of overflow links leads to a decrease in the internal blocking probability in a switching network.

Figure 4 shows the changes in the internal blocking probability of a call of class 1 in the network 1.1 in relation to the changes in the capacity of the overflow link for a=1 Erl/BBU. The figure indicates the exponential nature of these changes. With the capacity of the overflow link equal to the capacity of a link used in the switching network (f=*30*), the internal blocking probability does not continue to decrease. It emerges from the study that for $a < 1$ Erl/BBU, the internal blocking probability stabilizes earlier $f < 30$. These results are of practical significance since the conclusion that follows indicates that an application of overflow links with identical capacity as the remaining links of a switching network are sufficient for constructing effective quasi-non-blocking switching network.

Figure 4 presents the changes in the internal, external and the total blocking probability for calls of class 1 in relation to the capacity of overflow links in the network 1.1. Along with the increase of the capacity of overflow links, the internal blocking probability decreases. A decrease in the probability leads to an increase in the external blocking probability. This phenomenon can be explained in the following way. A decrease in the internal probability blocking is equivalent to an increase in call access of a given class to output groups (directions) of the switching network. Increased traffic at the outputs of the switching network results in an increase in the external blocking probability. Since the decrease in the internal blocking probability is higher than the increase in the external blocking probability, then, as a result, we obtain a decrease in the total blocking probability.

A system of overflow links can be applied in any stage of the three-stage Clos network. A choice of a stage of the network and an overflow system in the switching network has a substantial influence on the internal blocking probability. Hence, the study included an analysis of System I and System II used in each of the stages of the switching network. Relevant investigations were carried out for the point-to-point selection and the point-to-group selection. Figure 5 shows exemplary juxtaposition and comparison of the point-to-point internal blocking probability for different structures of switching networks with overflow in line with the notation adopted in Section 2. The probability is expressed as a percentage of the value of the internal blocking probability in a network without overflow links, with the assumption that the average traffic for a BBU is equal to a=1 Erl. Figure 5 presents the results ordered according to the level of the decrease in the blocking probability.

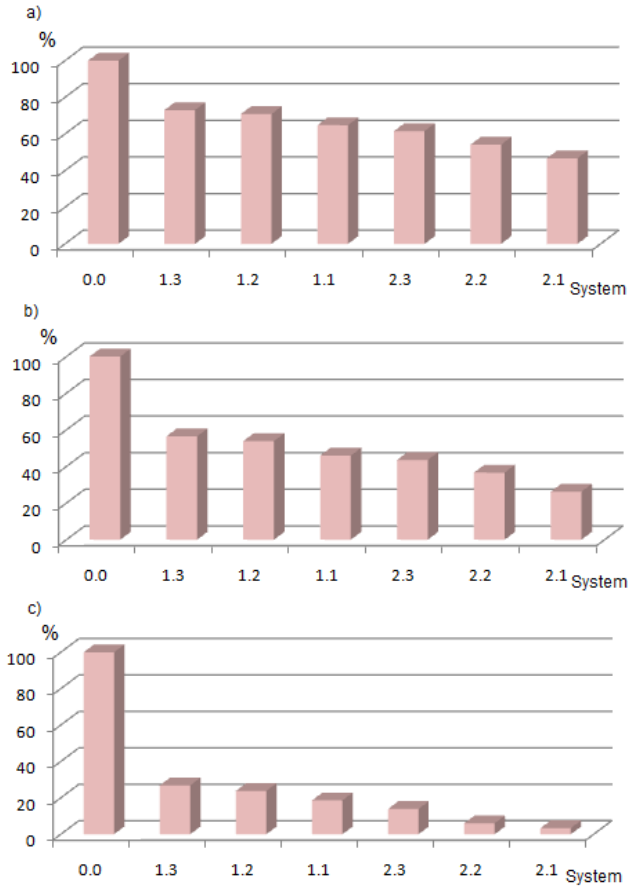

Figure 5. Internal blocking probability in a three-stage Clos network for the point-to-point selection: a) class 1, b) class 2, c) class 3

As the results of the study show, the introduction of overflow links in the first stage of the switching network

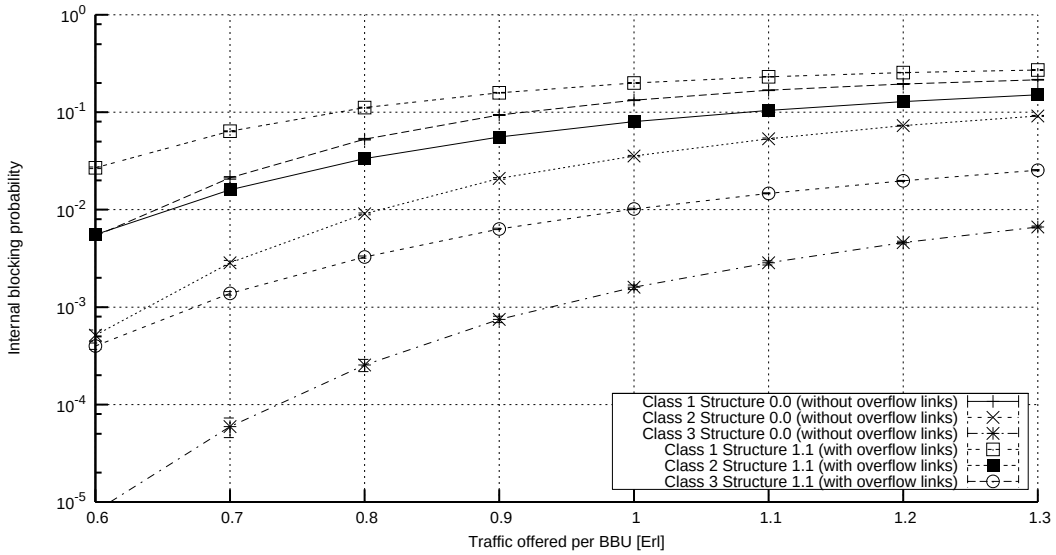

Figure 3. Internal blocking probability in a three-stage Clos network for the point-to-point selection with and without overflow links

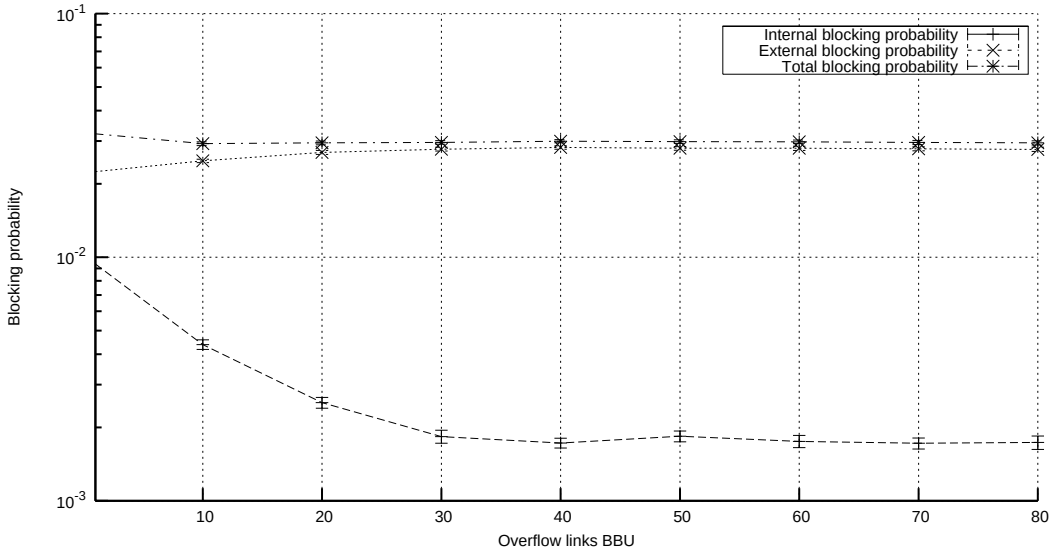

Figure 4. Dependence between internal, external and the total blocking probability and the capacity of overflow links in the network of System 1 for the first traffic class (t_1 = 10 BBUs), point-to-point selection

is the most effective. This phenomenon can be described and interpreted combinatorially. The application of overflow links in the first stage is followed by the highest number of potentially possible connection paths for connections, whereas an increase in the number of potentially possible connection paths in the third stage, resulting from the application of overflow links, is the lowest. The presented results constitute only a small fragment of the more complex study carried out by the authors. Due to the limited space of the paper, the figures show only the results yielded for the point-to-point selection. With the case of the point-to-group selection, however, similar changes occur in the blocking probability and can be compared to those obtained for the point-to-point selection, though the extent of these changes is slightly lower. The phenomenon is related to the particular way of operation of the point-to-point selection, in which there are more potential connection paths for a point-to-direction (a number of points) to be set up than in the case of setting up a point-to-point connection.

The results presented in the paper were limited to switching networks 4×4. The authors also examined switching networks with a much larger size, i.e. 16×16. The obtained results confirm that an introduction of overflow links in the first stage of the switching network also in that case is the most effective.

 ISBN: 978-1-61208-123-6

V. CONCLUSIONS

The paper discusses the results of a simulation study of Clos networks with the application of inter-stage links. On the basis of the obtained results it can be unequivocally stated that the most optimal solution is the application of overflow structures in the first stage of the network. All the simulations carried out by the authors confirm the highest percentage decrease in the blocking probability recorded in this particular configuration.

The paper also includes the results of an investigation into the dependencies between the internal blocking probability and the capacity of overflow links. It is then proved that the value of the capacity of an overflow link that is equal to the capacities of links in a switch of the switching network can virtually eliminate internal blocking. It emerges from the studies carried out by the authors that in switching networks with higher capacities the actual operation of the system of overflow links is even more effective, i.e. a lower number of overflow links (with lower capacities) appears to be sufficient to eliminate the phenomenon of internal blocking in the network. Given the low cost of constructing a system of overflow links, i.e. first stage switches with an increased number of input and output links, the application of the solution in practice (in construction of quasi-non-blocking networks) seems to be justified and well-grounded.

REFERENCES

[1] C. Clos, A study of non- blocking switching networks, *Bell System Technical Journal*, vol. 32, No. 2, 1953, pp.406-424.

[2] F.K. Hwang, Three-stage multiconnection network which are nonblocking in the wide sense. *Bell System Technical Journal*, vol. 58, No. 10, 1979, pp. 2183-2187.

[3] A. Jajszczyk ,On nonblocking switching networks composed of digital symmetrical matrices. *IEEE Transactions on Communications*, vol. 31, No. 1, 1983, pp. 2-9.

[4] W. Kabaciński, On nonblocking switching networks for multi-channel connections. *IEEE Transactions on Communications*, vol. 43, No. 2/3/4, 1995, pp. 222-224.

[5] W. Kabaciński, Nonblocking Electronic and Photonic Switching Fabrics, Springer, 2005.

[6] R. Fortet Ed. ,Calcul d'organe, Systeme Pentaconta, L.M.T Paris, 1961.

[7] M. Stasiak, Computation of the probabilisty of losses in commutation systems with mutual aid selectors. *Rozprawy Elektrotechniczne*, Journal of the Polish Academy of Science, Vol. XXXII, No. 3, 1986, pp. 961-977 (in polish)

[8] H. Inose, T. Saito, M. Kato, Three-stage time-division switching junctor as alternate route. *Electronics letters*, vol 2, No. 5, 1966, pp.78-84

[9] L. Katzschner, W. Lorcher, H. Weisschuh, On a experimental Local PCM Switching Network, *Proc. International Seminar on Integrated System for Speech, Video and Data Communication*, Zurich, 1972, pp. 61-68.

[10] J. Roberts, V. Mocci, and I. Virtamo, Eds., Broadband Network Teletraffic, *Final Report of Action COST 242*, Berlin: Commission of the European Communities, Springer, 1996.

[11] V.B. Iversen, Engineering Handbook, *ITU-D, SG-2*, Geneva, 2002.

[12] A. Eldin, Automatic telephone exchanges based on the link connection principle, *L. M. Ericsson*, Stockholm, 1969.

[13] A. Lotze, A. Roder, G. Thierer, PCM- charts, *Published by Institute of Switching and Data Technics*, University of Stuttgart, 1979.

[14] M. Stasiak, Combinatorial considerations for switching systems carrying multi-channel traffic streams. *Annals of Telecommunications*, vol. 51, No. 11-12, 1996, pp. 611-625.

[15] M. Stasiak, Effective availability models for switching networks. Published by Poznań Universty of Technology, Poznań, 2005, pp. 1-260 (in polish)

[16] J. Tyszer, *Object-Oriented Computer Simulation of Discrete-Event Systems*, Springer, 1999.

 ISBN: 978-1-61208-123-6